Uniwersytet Wrocławski
Instytut Fizyki Teoretycznej

Grzegorz Kondrat

Perkolacja i zablokowanie w procesach adsorpcji obiektów rozciągłych na płaszczyźnie

rozprawa habilitacyjna

Wrocław 2010

Spis treści

Wprowadzenie

Nieustanny rozwój nauki i technologii powoduje, że pewne dawno rozpatrywane zagadnienia stają się na nowo interesujące. Dobrze znane konstrukcje teoretyczne w nowym kontekście zyskują nowego wymiaru, co pozwala na stawianie nowych pytań i potwierdza zasadność wielu uprzednich, często czysto teoretycznych poszukiwań. Istotny postęp w dziedzinie nanotechnologii, który obserwujemy w ostatnich latach, sprawił, że na nowo wzrosło zainteresowanie perkolacją i zablokowaniem, rozważanymi m.in. w kontekście własności nowoczesnych kompozytów.

Właśnie tym zagadnieniom, modelowanym za pomocą ciągle nośnego podejścia adsorpcji sekwencyjnej, poświęcona jest niniejsza rozprawa. Rozważam w niej różnorodne aspekty perkolacji i zablokowania oraz ich wzajemnych relacji w przypadku, gdy obiekty przyłączające się do badanej powierzchni są relatywnie duże, tzn. mają pewną strukturę przestrzenną. Pozwala to opisywać procesy z udziałem włókien węglowych, nanorurek czy też innych cząsteczek o bardziej złożonych kształtach.

Część I

Autoreferat

Rozdział 1

Kontekst

Niniejszy rozdział stanowi krótkie wprowadzenie w tematykę rozprawy habilitacyjnej. Omówię tutaj pojęcia i zagadnienia dotyczące procesów adsorpcji sekwencyjnej.

Często z pozoru zupełnie niezwiązane ze sobą zjawiska można opisać stosując podobne schematy teoretyczne, gdyż istnieją podobnego typu zależności między poszczególnymi elementami układu. Wiele procesów zachodzących w przyrodzie charakteryzuje się nieodwracalnością w badanych skalach czasowych, a ich dynamika jest ograniczona przez niedostępne dla procesu obszary, które powiększają się na skutek adsorpcji, czyli trwałego wiązania się obiektów (cząsteczek, makromolekuł, kryształów itp.) z podłożem. Mimo bardzo dużej złożoności wielu procesów okazuje się, że istnieją stosunkowo proste modele teoretyczne, które są w stanie wytłumaczyć rzeczywistość z dużą dokładnością. Punktem wyjścia dla wyżej wspomnianej klasy zjawisk jest model losowej adsorpcji sekwencyjnej (ang. RSA — *Random Sequential Adsorption*), który odpowiednio modyfikowany znajduje zastosowanie w bardzo wielu sytuacjach.

W podstawowej wersji mamy do czynienia z obiektami, które zajmują określoną ilość miejsca i mogą się wiązać z podłożem. W jednym momencie dopuszcza się możliwość adsorpcji tylko jednego obiektu, a jego położenie i orientację ustala się w sposób losowy za pomocą określonego rozkładu prawdopodobieństwa (zwykle używa się rozkładu jednostajnego). W przypadku gdy wylosowana pozycja nie koliduje z obiektami uprzednio zaadsorbowanymi, obiekt zostaje tam unieruchomiony, powiększając tzw. adsorbat. W przeciwnym wypadku (gdy obiekty nachodzą na siebie) próba adsorpcji jest odrzucana i generowana jest nowa pozycja, która nie jest skorelowana ze starą. Tak skonstruowany model odtwarza szereg istotnych charakterystyk powierzchni, takich jak stopień zapełnienia czy wzajemne korelacje. Dodatkowo otrzymuje się zależność tych wielkości od czasu.

Aby możliwie wiernie opisać rzeczywistość, wprowadza się różne modyfikacje do podstawowego modelu [1]. W zależności od sytuacji podłoże może być jednowymiarowe (np. łańcuch polimeru, do którego w różnych punktach przyłączają się odpowiednie grupy[1]),

[1]Właśnie z reakcji łączenia się sąsiednich podstawników w łańcuchu poliwinylowym wywodzą się pierwsze tego typu modele [2].

dwuwymiarowe (np. błony biologiczne, powierzchnie kryształów) albo nawet fraktalne. Sama struktura podłoża może być ciągła albo dyskretna, przy czym dynamika obu typów modelu bardzo się od siebie różni. Pewnym rozszerzeniem modelu jest ograniczenie losowości kolejnych prób adsorpcji na rzecz wprowadzenia rozkładu pozycji zależnego od stanu otoczenia (taka modyfikacja uwzględnia np. oddziaływania cząsteczek z adsorbatem jeszcze przed przyłączeniem się). Aby uwzględnić wpływ mechanizmu transportu cząsteczek na badane procesy, modyfikuje się model, włączając do niego dyfuzję adsorbowanych cząsteczek (dominujące siły typu brownowskiego) albo zakładając ruch balistyczny (obiekt adsorbowany trafiając na zajęte już miejsce próbuje ześlizgnąć się w linii największego spadku w kierunku podłoża: jeśli na nie upadnie — zostaje, jeśli nie — wraca do roztworu; odpowiada to sytuacji zdominowanej siłami grawitacji). W niektórych modelach dopuszcza się także możliwość desorpcji, tzn. spontanicznego odłączenia się cząsteczek z powrotem do roztworu. Zupełnie odrębną podklasę stanowią modele adsorpcji, w których rozpatruje się różne rodzaje cząsteczek (od mieszaniny dwóch typów cząsteczek do ciągłego rozkładu wielkości charakteryzującej cząsteczki). Wówczas zachowanie układu istotnie zależy od przyjętych parametrów mieszaniny, takich jak wielkość cząsteczek, ich względna ilość itp. Można także rozpatrywać adsorpcję cząsteczek jednego rodzaju na podłoże uprzednio zanieczyszczone, tzn. pokryte do pewnego stopnia innego rodzaju cząsteczkami. Aby modelować procesy wzrostu za pomocą adsorpcji sekwencyjnej, można wprowadzić do modelu możliwość układania się jednych cząsteczek na drugich, otrzymując wielowarstwowy adsorbat. Wreszcie na charakterystykę układu zasadniczy wpływ ma wielkość i kształt obiektów, które podlegają adsorpcji. W przypadku ciągłym bada się adsorpcję m.in. dysków, kwadratów, prostokątów, elips, a dla sieci dyskretnych — dimerów, trimerów, liniowych łańcuchów, a także polimerów o bardziej złożonych kształtach.

Jednowymiarowy ciągły model adsorpcji odcinków na prostej (tzw. problem parkowania samochodów) daje się rozwiązać ściśle [3]. Otrzymana gęstość adsorbatu $\theta(t)$ w granicy długich czasów zmierza do progu zablokowania $\theta(\infty) \approx 0,7476$ w sposób potęgowy: $\theta(t) - \theta(\infty) \propto t^{-1}$. Funkcja rozkładu G przerw o długości h między odcinkami w granicy długich czasów wykazuje logarytmiczną rozbieżność wokół $h = 0$: $G(h, t = \infty) \propto -\ln h$. Otrzymana w tym modelu dwupunktowa funkcja korelacyjna zanika na dużych odległościach dużo szybciej niż wykładniczo (w przeciwieństwie do wykładniczego zaniku w typowych układach równowagowych).

W większej liczbie wymiarów modele nie dają się rozwiązać ściśle i stosuje się metody przybliżone (analityczne i numeryczne). Okazuje się, że charakterystyki modelu jednowymiarowego są również typowe dla wyższych wymiarów — mamy także do czynienia z nietrywialnym progiem zablokowania (np. $\theta(\infty) \approx 0,547$ dla dysków), wolną kinetyką ($\theta(t) - \theta(\infty) \propto t^{-1/2}$ dla dwóch wymiarów), logarytmiczną rozbieżnością funkcji korelacyjnej dla $h = 0$ i nierównowagowością osiągniętego stanu granicznego. Sytuacja jest tu inna niż w przypadku równowagowej mechaniki statystycznej, dla której modele jednowymiarowe istotnie różnią się od 2- i 3-wymiarowych odpowiedników (w jednym wymiarze nie ma termodynamicznych przejść fazowych).

Ponieważ w wielu zastosowaniach mamy do czynienia z adsorpcją obiektów anizotropowych (np. silnie wydłużonych w jednym kierunku), w wielu pracach analizuje się adsorpcję takich obiektów jak elipsy, prostokąty (zwykłe i zaokrąglone) albo nawet nieskończenie cienkie igły. Okazuje się, że z reguły: a) maksymalne zapełnienie otrzymuje się dla obiektów o stosunku rozmiarów (długość/szerokość) rzędu 2; b) dla bardzo wydłużonych obiektów granica zapełnienia jest bliska zeru; c) dla obiektów anizotropowych graniczna wartość zapełnienia jest osiągana wolniej niż dla dysków.

W przypadku sieci dyskretnej dla klasycznego jednowymiarowego modelu adsorpcji dimerów [2] z granicznym zapełnieniem $\theta(\infty) = 1 - e^2 \approx 0,8647$ korelacje przestrzenne zanikają z odległością szybciej niż wykładniczo, podobnie jak ma to miejsce w przypadku ciągłym. W jednym wymiarze przejście między przypadkiem dyskretnym i ciągłym otrzymuje się w granicy wielkości cząsteczek $k \to \infty$ (dla dużych k słuszne jest rozwinięcie $\theta(k) = \theta(\infty) + 0,216181/k + 0,362559/k^2 + ...$). Na dyskretnej sieci inna jest jednak dynamika dochodzenia do stanu zapełnienia — od pewnego momentu różnica między gęstością adsorbatu a progiem zablokowania maleje wykładniczo z czasem: $\theta(\infty) - \theta(t) \propto \exp(-t/const)$ [4] (w przeciwieństwie do zaniku potęgowego dla przypadku ciągłego). Słynna hipoteza Palastiego mówi o tym, że próg zablokowania dla adsorpcji n-wymiarowych kostek o boku k na sieci hiperkubicznej jest n-tą potęgą progu zablokowania dla problemu adsorpcji k-meru w jednym wymiarze[2].

Dla adsorpcji liniowych k-merów na sieci kwadratowej otrzymano [5] analitycznie przybliżony związek granicznego zapełnienia $\theta(k) = 0,664 + 0,827/k - 0,699/k^2$ (co pozostaje w zgodności z wynikami Monte Carlo z dokładnością do 2%). Badania procesu adsorpcji liniowych k-merów na dyskretnym substracie były prowadzone tylko w przypadku sieci węzłów, natomiast ujęcie sieci wiązań nie było wcześniej badane (co jest przedmiotem pracy [H2]).

Oprócz analizy kinetyki adsorpcji i stanu zablokowanego w procesach adsorpcji sekwencyjnej często zwraca się szczególną uwagę na zagadnienia perkolacji. Bada się warunki, w jakich powstaje klaster rozpinający (tzn. zbiór bezpośrednio sąsiadujących ze sobą obiektów sięgający brzegów układu). Jest to jeden z prostszych i równocześnie fundamentalnych modeli przejść fazowych, który znajduje szerokie zastosowanie w fizyce statystycznej. Przypadek perkolacji jest klasycznym przykładem jednej z podstawowych klas uniwersalności zjawisk krytycznych (tzw. klasy uniwersalności perkolacji). Wykładniki krytyczne, decydujące o przynależności do klas, opisują zachowanie się szeregu wielkości charakteryzujących układ (korelacje przestrzenne, wielkość klastra maksymalnego itp.) przy zbliżaniu się do punktu krytycznego. Od początków zainteresowania perkolacją [6], kiedy autorzy badali perkolację nieskorelowanych monomerów na sieci, do chwili obecnej tematyka pozostaje ciągle interesująca i ukazuje się wiele prac jej poświęconych (patrz np. przeglądy [7, 8, 9, 10]).

[2]Chociaż hipoteza nie jest ściśle prawdziwa, daje zaskakująco dobre wyniki liczbowe, np. $\theta(2 \times 2) \approx 0,74788$, a $\theta(2)^2 \approx 0,74765$, $\theta(3 \times 3 \times 3) \approx 0,5595$, a $\theta(3)^3 \approx 0,5588$.

Modele perkolacji w procesach adsorpcji sekwencyjnej można podzielić na dwie grupy: ciągłe i dyskretne. W ramach podejścia ciągłego rozważa się obiekty sztywne (np. twarde dyski, kule), ze sztywnym jądrem (ang. *hard core soft shell*), a także z możliwością nawet całkowitego nakładania się (model typu sera szwajcarskiego, w którym w jednolitym bloku materiału wycina się dziury odpowiedniego kształtu). Ponadto rozważa się adsorpcję nieskończenie cienkich linii, które modelują pęknięcia materiału (to podejście wykorzystuje się m.in. w petrologii do opisu ośrodków porowatych) bądź odpowiadają włóknom tworzącym kompozyt. Modele rozszerza się, podając zamiast jednej wielkości charakteryzującej adsorbowane obiekty cały ich rozkład (w rzeczywistości często mamy do czynienia ze zbiorem obiektów podobnych, ale jednak różniących się rozmiarami). W różny sposób zadaje się kryterium łączenia obiektów w klastry — od bezpośredniego styku (zachodzenia na siebie), przez minimalną odległość, aż do losowania spośród bliskich sąsiadów. W jeszcze innym podejściu modeluje się proces wzrostu domen przez umieszczenie punktowych zarodków domen, które następnie się powiększają (puchną), aż zetkną się z sąsiednimi domenami. W ramach teorii perkolacji bada się także bardziej skomplikowane ciągłe modele polimerów, które będąc w roztworze podlegają wielu siłom wewnątrz- i międzycząsteczkowym, w efekcie których następują zmiany konformacyjne i przejścia fazowe typu np. zol-żel. We wszystkich wyżej wymienionych modelach bada się wykładniki krytyczne, progi perkolacji, funkcje korelacyjne itp. Okazuje się, że wiele różnych modeli — m.in. ciągła perkolacja sztywnych dysków, dysków ze sztywnym jądrem, nieskończenie cienkich igieł, a nawet dyskretna perkolacja dimerów, trimerów itp. na sieciach jednorodnych i niejednorodnych — należy do jednej klasy uniwersalności perkolacji (wykładniki krytyczne zależą tutaj raczej od wymiaru przestrzennego modelu niż od szczegółów samej dynamiki).

Odrębną klasę tworzą modele sieciowe, dla których położenia i orientacje obiektów mogą przyjmować wartości ze zbioru dyskretnego. Ograniczenie to, z jednej strony, stanowi pewne uproszczenie ułatwiające dalszą analizę, a z drugiej — lepiej pasuje do rzeczywistości fizycznej w przypadkach, w których np. substrat ma strukturę periodyczną i tylko w niektórych miejscach cząsteczki mogą się do niego przyłączyć. Ponieważ kształt cząsteczek może mieć istotny wpływ na ich zachowanie się, obecnie bada się modele perkolacji w układzie prostokątów, igieł oraz, w ogólności, k-merów, utworzonych z pojedynczych atomów na różne sposoby. Pomiędzy liniowym kształtem łańcucha z jednej strony a kształtem otrzymanym przez losowe błądzenie z samounikaniem z drugiej istnieje całe spektrum możliwości, którego zbadaniu poświęcone są m.in. prace [H3] i [H6]. Analizuje się także wpływ składu na perkolację dla mieszanin różnych typów cząsteczek. Aby opisać sytuacje bardziej skomplikowane (i często bliższe rzeczywistości), wprowadza się niejednorodność sieci przez modyfikacje dostępnych wiązań (tzw. *site-bond problem*) albo nawet tworząc sieć zupełnie od nowa (do tej szerokiej klasy problemów należy np. zagadnienie odporności sieci na atak z zewnątrz). Odrębną sprawą jest związek perkolacji z zablokowaniem — czy np. klaster perkolujący jest szkieletem dla fazy zablokowanej (temu poświęcona jest m.in. praca [H1]).

Jeśli chodzi o badanie adsorpcji obiektów rozciągłych, okazuje się, że jedynie mo-

dele jednowymiarowe dają się w niektórych przypadkach rozwiązać ściśle do końca [3]. Zwykle pozostają metody przybliżone, które można podzielić na dwie grupy. W pierwszej grupie metod analitycznych znajdują się m.in.: podejście bazujące na użyciu argumentów geometrycznych i rozwinięcia funkcji korelacyjnych na wzór teorii równowagowej (równania typu Mayera-Montrolla, Kirkwooda-Salsburga, Ornsteina-Zernike'a). Drugą grupę stanowią metody numeryczne, m.in. symulacje Monte Carlo, które w wielu przypadkach wnoszą najwięcej informacji o badanym procesie, gdyż napotykane trudności techniczne często znacznie ograniczają stosowalność metod z grupy pierwszej.

Istnieje wiele prac eksperymentalnych weryfikujących modele adsorpcji sekwencyjnej. Już w latach osiemdziesiątych XX wieku mierzono progi zablokowania dla lateksowych kulek wytrącających się z roztworu koloidalnego [11] i wykorzystywano perkolację do wyjaśnienia charakterystyki przewodnictwa kompozytów z włókien węglowych [12]. Badano eksperymentalnie adsorpcję sferycznych cząsteczek koloidów podlegających dyfuzji oraz grawitacji, otrzymując dobrą zgodność z modelem teoretycznym [13]. Ciekawym przykładem doświadczalnego badania związku nadprzewodnictwa z orientacją ziaren Nb_3Sn na gruncie perkolacji jest niedawna praca [14]. Również pewne własności elektryczne ostatnio tak popularnych kompozytów utworzonych z nanorurek węglowych próbuje się tłumaczyć za pomocą opisanego wyżej schematu teoretycznego [15, 16]. Niektóre niedawne eksperymenty sugerują wykorzystanie modeli adsorpcji na sieciach dyskretnych [17]. W części doświadczeń substrat jest poddawany naturalnym procesom, ograniczającym wolną przestrzeń, na której może występować adsorpcja [17] — do opisu tego typu sytuacji odpowiedni jest model adsorpcji na uprzednio zanieczyszczonej powierzchni [H4, H5].

Bibliografia

[1] J. Talbot, G. Tarjus, P.R. Van Tassel, P. Viot, *From car parking to protein adsorption: an overview of sequential adsorption processes*, Colloid Surf. A **165** (2000), 287.

[2] P. Flory, *Intramolecular Reaction between Neighboring Substituents of Vinyl Polymers*, J. Am. Chem. Soc. **61** (1939), 1518.

[3] A. Renyi, *Egy egydimenziós véletlen térkitöltési problémáró*, Publ. Math. Inst. Hung. Acad. Sci. **3** (1958), 109; A. Renyi, *On a One-Dimensional Problem Concerning Random Space-Filling*, Sel. Trans. Math. Stat. Prob. **4** (1963), 205.

[4] V. Privman, J.-S. Wang, P. Nielaba, *Continuum limit in random sequential adsorption*, Phys. Rev. B **43** (1991), 3366.

[5] B. Bonnier, M. Hontebeyrie, Y. Leroyer, C. Meyrers, E. Pommiers, *Adsorption of line segments on a square lattice*, Phys. Rev. E **49** (1994), 305.

[6] S.R. Broadbent, J.M. Hammersley, *Percolation Processes I. Crystals and Mazes*, Cambridge Philos. Soc. **53** (1957), 629.

[7] D. Stauffer, A. Aharony, *Introduction to Percolation Theory*, wyd. 2, Taylor and Francis, Londyn 1994.

[8] J.W. Evans, *Random and cooperative sequential adsorption*, Rev. Mod. Phys. **65** (1993), 1281.

[9] M.B. Isichenko, *Percolation, statistical topography, and transport in random media*, Rev. Mod. Phys. **64** (1992), 961.

[10] W. Bauhofer, J.Z. Kovacs, *A review and analysis of electrical percolation in carbon nanotube polymer composites*, Composites Science and Technology **69** (2009), 1486.

[11] G.Y. Onoda, E.G. Liniger, *Experimental determination of the random-parking limit in two dimensions*, Phys. Rev. A **33** (1986), 715.

[12] F. Carmona, F. Barreau, P. Delhaes, R. Canet, *An experimental model for studying the effect of anisotropy on percolative conduction*, J. Physique Lett. **41** (1980), L531.

[13] P. Lavalle, P. Schaaf, M. Ostafin, J.-C. Voegel, B. Senger, *Extended random sequential adsorption model of irreversible deposition processes: From simulations to experiments*, Proc. Natl. Acad. Sci. USA **96** (1999), 11100.

[14] W.D. Markiewicz, J. Toth, *Percolation and the resistive transition of the critical temperature T_c of Nb_3Sn*, Cryogenics **46** (2006), 468.

[15] J.K.W. Sandler, J.E. Kirk, I.A. Kinloch, M.S.P. Shaffer, A.H. Windle, *Ultra-low electrical percolation threshold in carbon-nanotube-epoxy composites*, Polymer **44** (2003), 5893.

[16] M. Moniruzzaman, K.I. Winey, *Polymer Nanocomposites Containing Carbon Nanotubes*, Macromolecules **39** (2006), 5194.

[17] A. Cadilhe, N.A.M. Araújo, V. Privman, *Random sequential adsorption: from continuum to lattice and pre-paterned surfaces*, J. Phys.: Condens. Matter **19** (2007), 065124, oraz prace tam cytowane.

[18] W.H. Press, S.A. Teukolsky, W.T. Vetterling, B.P. Flannery, *Numerical Recipes in C*, wyd. 2, Cambridge University Press 1992.

[19] N. Vandevalle, S. Galam, M. Kramer, *A new universality for random sequential deposition of needles*, Eur. Phys. J. B **14** (2000), 407.

[20] E.S. Loscar, R.A. Borzi, E.V. Albano, *Fluctuations of jamming coverage upon random sequential adsorption on homogeneous and heterogeneous media*, Phys. Rev. E **68** (2003), 041106.

[21] Y. Leroyer, E. Pommiers, *Monte Carlo analysis of percolation of line segments on a square lattice*, Phys. Rev. B **50** (1994), 2795.

Rozdział 2

Cel i tezy rozprawy

2.1 Cel rozprawy

Celem rozprawy jest analiza procesów adsorpcji sekwencyjnej na dwuwymiarowych substratach ze szczególnym naciskiem położonym na własności związane z perkolacją (tworzeniem się globalnego klastra złożonego z sąsiadujących cząsteczek danego typu) oraz z zablokowaniem (ang. *jamming*), które ma miejsce, gdy bieżąca konfiguracja przyłączonych czasteczek (adsorbat) nie pozwala na adsorpcję kolejnej cząsteczki. Moje podejście bazuje na stosunkowo prostych modelach teoretycznych, które jednak nie dają się rozwiązać analitycznie. Właściwym narzędziem do realizacji tego zadania są numeryczne symulacje Monte Carlo wzbogacone o odpowiednią obróbkę statystyczną i argumenty natury fizycznej. Punktem wyjścia jest uzyskanie zależności odpowiednich progów (perkolacji, zablokowania) w funkcji parametrów modelu (np. wielkości cząsteczek, ich sztywności, wielkości substratu). Dalszy krok w analizie to wyeliminowanie efektów brzegowych związanych ze skończonością próbki, na którą adsorbują cząsteczki – używam tutaj m.in. skalowania skończonych rozmiarów (ang. *finite size scaling*). Tak przygotowane dane podlegają dalszej analizie w celu głębszego zrozumienia dynamiki modelu i przyczyn obserwowanego zachowania. W moich badaniach zajmuję się istniejącymi modelami, które analizuję w nowy sposób ([H1]), oraz – w przeważającej części – tworzę nowe modele, będące rozszerzeniem już istniejących (prace [H2-H6]).

W cyklu prac [H1-H6] wchodzących w skład rozprawy rozważam różne sytuacje modelowe, które można podzielić na grupy ze względu na cztery następujące kryteria:

- **typ badanego zjawiska:**
  - perkolacja
  - zablokowanie
- **jakość substratu:**
  - czysty

  - uprzednio zanieczyszczony

- **struktura cząsteczek:**
  - sztywne igły
  - giętkie łańcuchy
- **typ sieci substratu:**
  - kwadratowa sieć punktów (KP)
  - kwadratowa sieć wiązań (KW)
  - trójkątna sieć punktów (TP).

Poniższa tabela pokazuje w graficzny sposób obszar badań będący przedmiotem poszczególnych prac wchodzących w skład rozprawy:

		PERKOLACJA		ZABLOKOWANIE	
		czysty	zanieczyszczony	czysty	zanieczyszczony
sztywne igły	KP	H1		H1	
	KW	H2		H2	
	TP		H4		H5
giętkie łańcuchy	KP	H3, H6			
	KW				
	TP	H3, H6			

Zanim przejdę do szczegółowego omówienia tez rozprawy, chciałbym najpierw opisać wykorzystany we wszystkich pracach wchodzących w jej skład mechanizm symulacji Monte Carlo, za pomocą którego otrzymuje się dane podlegające dalszej analizie.

2.2 Losowa adsorpcja sekwencyjna i symulacje Monte Carlo

Punktem wyjścia jest substrat – pewien skończony podzbiór dwuwymiarowej regularnej sieci (w rozprawie będą to sieci kwadratowe punktów [węzłów], sieci kwadratowe wiązań oraz sieci trójkątne punktów). Modeluje on skończoną powierzchnię rzeczywistej próbki, na której osiadają cząsteczki (drobinki, kryształy itp.). W praktyce wybieram kwadrat o boku L bądź sześciokąt (dla sieci trójkątnej) także o boku L jednostek[1]. Wielkość L jest parametrem, którgo wartości zawierają się w przedziale od 30 do 3000. Przyjmuję sztywne warunki brzegowe (*hard wall b.c.*), które mają naśladować zachowanie prawdziwych próbek (cykliczne warunki brzegowe zmniejszają wprawdzie wpływ skończonego rozmiaru próbki na wynik, ale są w tym kontekście niefizyczne). Sprawdziłem również ([H1, H2]), że przyjęcie otwartych warunków brzegowych nie zmienia zachowania modelu. W zależności od wariantu modelu pierwotnie substrat jest czysty (sieć jest pusta) bądź zanieczyszczony (pokryty częściowo cząsteczkami zanieczyszczenia).

Zasadniczym elementem modelu są cząsteczki[2], które mogą ulegać nieodwracalnej adsorpcji na powierzchni substratu. Adsorbujące cząsteczki obowiązuje reguła niezachodzenia na siebie, a adsorbat (tj. wszystkie zaadsorbowane do tej pory cząsteczki) przez cały czas mieści się w warstwie jednoatomowej. Rozważam tutaj dwa rodzaje cząsteczek: sztywne igły, które składają się z kolejno po sobie następujących atomów wzdłuż linii prostej, a odległość między kolejnymi atomami jest równa stałej sieci, oraz giętkie łańcuchy tworzące linię łamaną łączącą kolejne punkty (wiązania) sieci. Podstawowym parametrem opisującym wielkość cząsteczki jest liczba atomów, z których się ona składa (oznaczenie: a). Wartość a zawiera się zwykle między 1 a 50 (choć w [H1] używam również większych wartości, ale w celu zilustrowania wpływu skończonych rozmiarów układu na wynik). W przypadku giętkich łańcuchów wprowadzam dodatkowy parametr pośrednio opisujący ich sztywność. W pracy [H3] jest nim temperatura, wchodząca do czynnika Boltzmanna $\exp(-\Delta E/kT)$, który bezpośrednio reguluje prawdopodobieństwo uzyskania w cząsteczce odpowiednio wygiętego fragmentu łańcucha (dla temperatur bardzo niskich dozwolone są jedynie proste łańcuchy, natomiast dla bardzo wysokich temperatur rozkład otrzymanych kształtów odpowiada błądzeniu losowemu z samounikaniem [*self avoiding random walk*]). W pracy [H6], która opiera się na rozszerzonej wersji modelu, parametrem opisującym kształt jest wprost procentowa zawartość odpowiednich typów wiązań (zgięć) w łańcuchu — dla sieci kwadratowej p_0 opisuje odsetek wiązań prostych (typu $S0$, zob. rys. 1), a $p_1 = 1 - p_0$ wiązań pod kątem prostym (typu $S1$). Dla sieci trójkątnej mamy trzy sumujące się do jedynki parametry opisujące kształt:

[1] Jednostką długości jest tutaj stała sieci.

[2] Pojęcie *cząsteczka* jest tu użyte nie tylko w dosłownym tego słowa znaczeniu, ale także do opisu większych struktur, które jako całość podlegają adsorpcji, np. metalowe igły, włókna itp.

p_0, p_1 i p_2, dotyczące typów, odpowiednio, $T0$, $T1$ i $T2$.

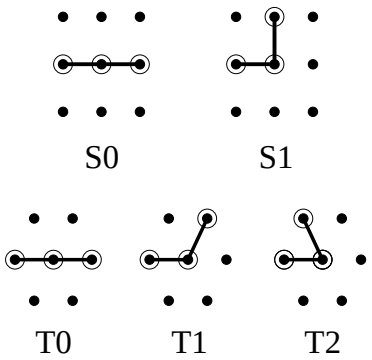

Rys. 1. Typy wiązań występujących w giętkich łańcuchach.

Adsorpcja cząsteczek jest losowa – położenie i orientacja cząsteczki, która ma być zaadsorbowana, są wybierane losowo z rozkładu jednostajnego. Próba adsorpcji jest zakończona sukcesem, jeśli cząsteczka o wybranym położeniu i orientacji nie nakłada się na żadną inną cząsteczkę uprzednio zaadsorbowaną. W przeciwnym razie wybiera się nową konfigurację cząsteczki i ponawia próbę aż do skutku. Adsorpcja jest też sekwencyjna – podejmuje się próbę adsorpcji kolejnej cząsteczki po zakończeniu poprzedniej próby. W trakcie adsorpcji coraz to nowych cząsteczek tworzy się na substracie adsorbat, którego pewne charakterystyki są na bieżąco monitorowane. W przypadku badania perkolacji sprawdzam wielkość adsorbatu (stopień zapełnienia sieci zaadsorbowanymi atomami) w momencie, w którym pojawiła się perkolacja (powstał klaster łączący przeciwległe brzegi układu). W przypadku badania zablokowania w układzie sprawdzam wielkość adsorbatu w takim momencie, w którym nie ma już możliwości dodania do adsorbatu nowych cząsteczek ze względu na brak wolnego miejsca.

Dla zapewnienia statystycznej wiarygodności powtarzam pojedyncze symulacje, zapisując otrzymane progi (perkolacji, zablokowania). Do dalszej analizy biorę wartość średnią progu z serii N symulacji, a szerokość rozkładu mierzę za pomocą odchylenia standardowego σ. Zwykle wybór $N = 100$ daje dobrą statystykę wyników, choć w niektórych przypadkach (np. w badaniu rozkładu masy wszystkich klastrów w układzie w pracy [H2]) przyjąłem $N = 10\ 000$.

W pracach do generowania liczb pseudolosowych używam znanego [18] generatora ran2, który charakteryzuje się dobrymi parametrami.

2.3 Szczegółowe omówienie tez rozprawy

2.3.1 Perkolacja i zablokowanie na sieci punktów (sztywne igły)

W pracy [H1] dokonałem analizy zależności progów perkolacji i zablokowania dla adsorpcji liniowych cząsteczek (sztywnych igieł) o rozmiarze $1 \times a$ na czystym substracie. Rozważane były sieci o wielkości $L = 30, ..., 2500$ i igły o długości $a = 1, ..., 2000$; duże wartości a były analizowane w pracy głównie pod kątem ilustracji efektu skończonego rozmiaru układu. Otrzymałem niemonotoniczną zależność progu perkolacji $c_p(a)$ w funkcji wielkości igieł. Zauważyłem, że wzrost progu dla $a > a_{min} = 13$ (rys. 2) można powiązać z faktem, iż dla dłuższych cząsteczek łatwiej tworzą się zwarte domeny złożone z wielu sąsiednich cząsteczek ułożonych równolegle do siebie. Otrzymałem zależność progu zablokowania $c_j(a)$, którą dało się dobrze opisać prawem potęgowym $c_j(a) = 0,66 + 0,44a^{-0,77}$ dla $a = 5, ..., 45$ (rys. 3).

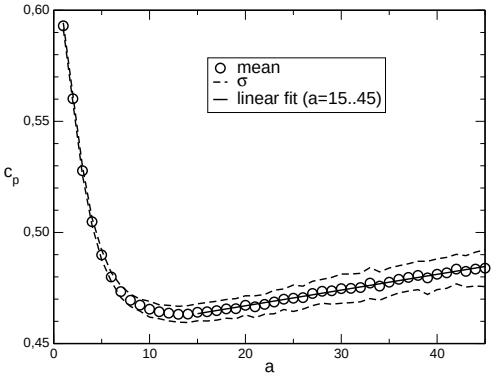

Rys. 2. Próg perkolacji w funkcji długości igły.

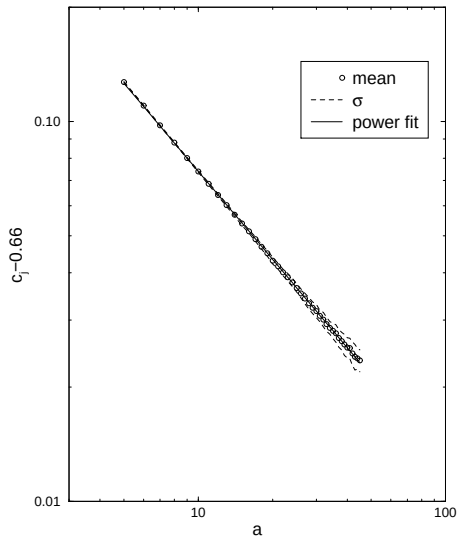

Rys. 3. Próg zablokowania w funkcji długości igły.

Po przeanalizowaniu wartości stosunku progów c_p/c_j wykazałem, że nie jest on stały, jak wcześniej sądzono [19], ale po osiągnięciu plateau dla $a = 3, ..., 7$ następuje dalszy wzrost jego wartości (rys. 4). Zatem trzeba odrzucić sugerowany w [19] związek struktury klastra perkolującego z fazą pełnego zablokowania (postulowano, że ten pierwszy jest klastrem fundamentalnym [szkieletem] dla fazy zablokowanej).

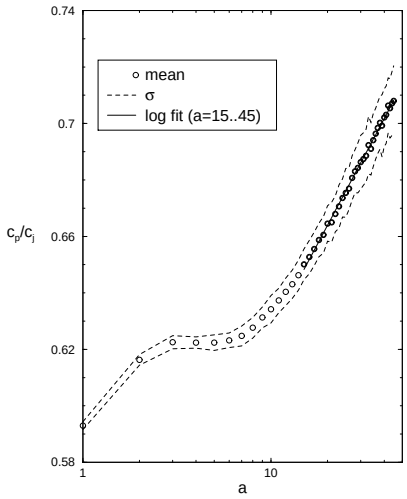

Rys. 4. Iloraz progów c_p/c_j w funkcji długości igły.

Analizując skalowanie szerokości przejścia (mierzonego odchyleniem standardowym σ) z wielkością układu L, potwierdziłem zgodność wykładnika krytycznego ν_p z wartością znaną dla standardowej nieskorelowanej perkolacji punktów $\nu_0 = 4/3$ [7]. Podobnie dla zablokowania otrzymałem wartość $\nu_j = 1$ zgodną z innymi danymi dla tego typu procesów.

Istotną sprawą jest wykazanie, że istnienie minimum progu perkolacji nie jest artefaktem związanym z małymi rozmiarami sieci, ale że jest to własność uniwersalna, również dla dużych wartości L — dane prezentowane w pracy [H1], poszerzone dodatkowo o wyniki symulacji dla sieci o rozmiarach aż do $L = 5000$, stanowią tego potwierdzenie (rys. 5).

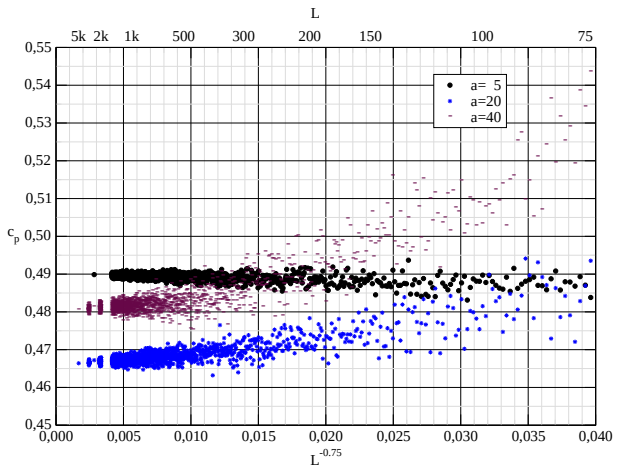

Rys. 5. Próg perkolacji w funkcji rozmiarów sieci dla igieł o długości $a = 5$, 20 i 40. Z wykresu jasno wynika, że niemonotoniczność progu perkolacji w funkcji długości igły ma miejsce również dla bardzo dużych sieci.

Przystępując do pracy nad perkolacją i zablokowaniem sztywnych igieł na sieci nie dotarłem do żadnych źródeł, w których rozważano by taki układ, poza pracą [19], która

stanowiła bezpośredni przyczynek do zajęcia się tą tematyką. W trakcie dalszych moich badań nad zagadnieniami adsorpcji (już po opublikowaniu pracy [H1]) odkryłem, że podobny problem (ale dla cyklicznych warunków brzegowych i dla innego wyboru długości igieł) był wcześniej rozważany w literaturze [21]. Moje podejście dotyczy sztywnych warunków brzegowych, pokazuje dla szerszego zbioru długości igieł prawidłowości w przebiegu funkcji $c_p(a)$ i $c_j(a)$ oraz dokonuje analizy w innym kontekście (wzajemne powiązanie perkolacji i zablokowania).

2.3.2 Perkolacja i zablokowanie na sieci wiązań (sztywne igły)

W pracy [H2] rozważyłem progi perkolacji i zablokowania pojawiające się w procesie adsorpcji sztywnych igieł w przypadku modelowania substratu na kwadratowej sieci wiązań, a nie punktów. Odkryłem, że dla igieł o długości $a > a^* = 6$ perkolacja w ogóle nie zachodzi w dostatecznie dużych układach. Dokładniejsza analiza doprowadziła mnie do zaobserwowania zmiany charakteru rozkładu masy w klastrach (w momencie zablokowania) przy przechodzeniu przez wartość a^* (rys. 6). Dla igieł krótkich ($a < a^*$) większa część masy jest skupiona w dużym klastrze (istnieje duży klaster perkolujący). Dla igieł długich ($a > a^*$) mamy do czynienia głównie z małymi klastrami, a duże klastry występują sporadycznie. Dla wartości przejściowej ($a = a^*$) zależność średniej masy zawartej w klastrach nie większych od s w funkcji s jest zbliżona do liniowej. Dla igieł perkolujących ($a \leq a^*$) zbadałem wykładnik Fishera opisujący potęgową zależność gęstości rozkładu masy w momencie perkolacji [7]. Uzyskana wartość $\tau = 2,02 \pm 0,04$ jest zgodna z wartością teoretyczną $\tau_0 = 187/91 \approx 2,055$, uniwersalną dla wielu dwuwymiarowych modeli perkolacji (w tym klasycznej perkolacji nieskorelowanych punktów).

Zaobserwowałem, że, podobnie jak w przypadku adsorpcji igieł na sieci punktów, próg zablokowania zależy potęgowo od długości igły: $c_j(a) - c_j^* \propto a^{-1,05}$, z tym że wartość graniczna $a \to \infty$ dla sieci wiązań ($c_j^* = 0,3350$) jest połową wartości granicznej dla adsorpcji na sieci punktów. Mając zależności progu perkolacji i zablokowania od długości igły, zauważyłem, że ich stosunek jest z dobrą dokładnością funkcją liniową (rys. 7).

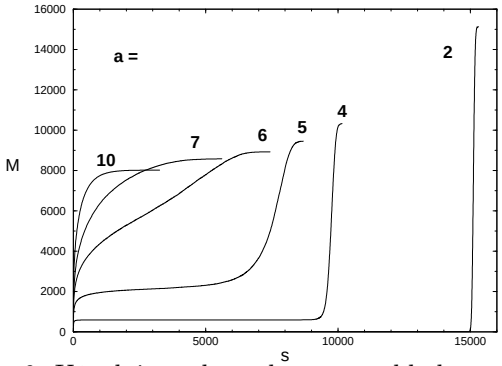

Rys. 6. Uśredniona dystrybuanta rozkładu masy w klastrach różnej wielkości w momencie zablokowania dla różnych długości igieł.

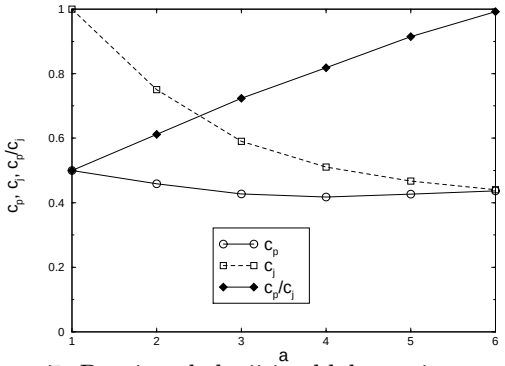

Rys. 7. Progi perkolacji i zablokowania oraz ich stosunek w funkcji długości igły.

2.3.3 Perkolacja giętkich łańcuchów

W pracach [H3] i [H6] zbadałem dwa warianty modelu adsorpcji giętkich łańcuchów pod kątem perkolacji. W pierwszym przypadku ([H3]) giętkość łańcuchów jest pośrednio związana z temperaturą roztworu T, z którego cząsteczki pochodzą. Dla dowolnego łańcucha liczona jest energia konformacji, określona przez sumę energii potencjalnych związanych z oddziaływaniem poszczególnych atomów ze sobą — poszczególnym kątom zgięcia łańcucha (dla przypadku rozważanej sieci trójkątnej) dla $T0$, $T1$ i $T2$ z rys. 1 odpowiadają energie $E0 = 0$, $E1 = 15$ oraz $E2 = 100$ wyrażone w pewnych, bliżej nieokreślonych jednostkach (ich wybór jest rzeczą wtórną: wartości $E0$ oraz $E2$ są przyjęte arbitralnie, a ich zmiana odpowiada przeskalowaniu osi energii, wartość $E1$ wynika z przyjęcia odpychającego coulombowskiego typu oddziaływania). Prawdopodobieństwo wyboru odpowiedniego kształtu cząsteczki podlegającej adsorpcji określone jest za pomocą czynnika Boltzmanna $\exp(-E/T)$ opisującego szansę trafienia na konformację o całkowietj energii E w równowadze; temperatura T jest mierzona w tych samych jednostkach co energia. Badając zależność progu perkolacji c_p w funkcji temperatury T i długości igieł a (rys. 8) wyróżniłem i przeanalizowałem różne typy zachowania ograniczone trzema charakterystycznymi temperaturami: granicą sztywności $T_1 = 2,0$, poniżej której cząsteczki perkolują tak jak sztywne igły; temperaturą $T_2 = 2,65$, dla której próg perkolacji nie zależy od długości łańcucha (dla $a > 10$); oraz $T_3 = 7,5$ — temperaturą, w której perkolacja zachodzi najłatwiej (minimum ze względu na T wspólne dla różnych a). Zauważyłem też, że dla bardzo wysokich temperatur próg perkolacji wysyca się jak $1/T$.

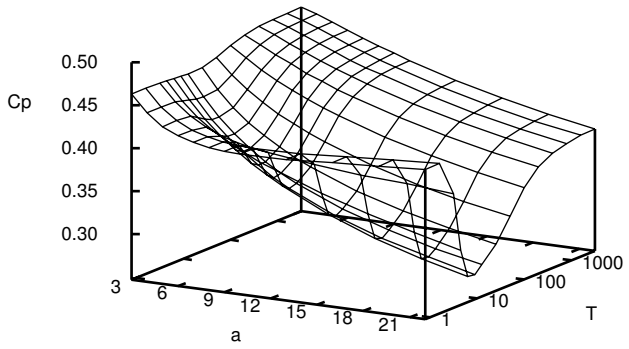

Rys. 8. Perkolacja giętkich łańcuchów.

Zaobserwowałem ciekawe zjawisko zachodzące w stosunkowo niskiej temperaturze ($T < 6$): energie konformacji adsorbowanych cząsteczek są istotnie niższe (w niektórych przypadkach nawet o 40%) niż średnia energia konformacji cząsteczki swobodnej w danej temperaturze (tzn. o kształcie wynikającym z czynnika Boltzmanna). Jest to efekt filtrowania z roztworu cząsteczek o kształcie pasującym do pozostałych pustych miejsc.

Potwierdziłem uniwersalność otrzymanych efektów — na sieci kwadratowej zależność $c_p(a, T)$ jest podobna, a otrzymane temperatury charakterystyczne pozostają w takiej

samej proporcji na obu sieciach: $T_1(TRI) : T_2(TRI) : T_3(TRI) = T_1(SQR) : T_2(SQR) : T_3(SQR)$.

Ponadto sprawdziłem, że próg zablokowania nie jest tak czuły na temperaturę jak próg perkolacji i właściwie od niej nie zależy.

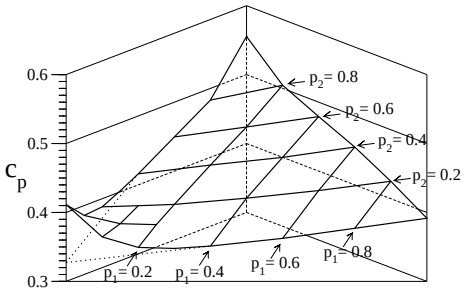

Rys. 9. Próg perkolacji $c_p(p_0, p_1, p_2)$.

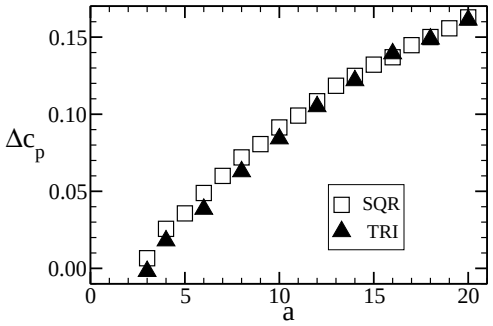

Rys. 10. Wielkość maksimum drugiego składnika.

W drugim, uogólnionym wariancie modelu, opisanym w pracy [H6], badam wpływ występowania różnych zgięć łańcucha na perkolację. Podstawowymi parametrami modelu są udziały procentowe p_0, p_1, p_2 odpowiednich typów zgięć w cząsteczkach (odpowiednio dla $T0$, $T1$ i $T2$ na sieci trójkątnej oraz p_0 i p_1 dla $S0$ i $S1$ na sieci kwadratowej, zob. rys. 1). Dla obu przypadków sieci próg perkolacji w funkcji $\{p_i\}_{i=0,1,2}$ można przedstawić jako sumę liniowego składnika oraz funkcji przyjmującej ostre maksimum w zerze[3] i szybko znikającej poza nim (na rys. 9 przedstawiona jest zależność $c_p(\{p_i\})$ dla sieci trójkątnej). Wartość samego maksimum jest wielkością uniwersalną — nie zależy od typu sieci, ale tylko od długości łańcucha (rys. 10). Wielkość ta opisuje, na ile sztywne igły różnią się pod względem perkolacji od giętkich łańcuchów.

Zaobserwowałem, że w rozszerzonym modelu występuje zjawisko braku perkolacji w przypadku długich łańcuchów ($a > 23$) i wysokiej zawartości zgięć typu $T2$ bądź $S1$ (w zależności od rodzaju sieci). Dokonałem analizy skalowania wielkości NoP opisującej względną liczbę pojedynczych symulacji w serii, które nie zakończyły się perkolacją. Przejście między obszarami z $NoP = 0$ a $NoP = 1$ ma cechy przejścia fazowego (wraz ze wzrostem rozmiaru sieci obszar parametrów $(a, \{p_i\})$ z wartością $0 < NoP < 1$ zawęża się).

Z dokonanej przeze mnie analizy związku między progiem perkolacji a średnim promieniem bezwładności (żyracji) adsorbowanych cząsteczek i średnią odległością między końcami łańcucha wynika, że nie istnieje bezpośrednie powiązanie tych wielkości. Natomiast zauważyłem istnienie znaczących korelacji między wartością progu perkolacji a ilością atomów w adsorbacie, które w chwili perkolacji mają dokładnie dwóch sąsiadów (na sieci kwadratowej).

Analiza skalowania progu perkolacji z rozmiarem układu pozwoliła ustalić, że dla tego

[3]Wartość zero przyjmują parametry p_1 i (dla sieci trójkątnej) p_2.

modelu wykładnik krytyczny ν jest zgodny z wartością 4/3 uniwersalną dla wielu modeli w dwóch wymiarach.

2.3.4 Perkolacja na zanieczyszczonym substracie (sztywne igły)

W pracy [H4] rozważyłem wpływ zanieczyszczeń na perkolację w układzie. Bardzo często dzieje się tak, że substrat, na który adsorbują cząstki, nie jest czysty, ale już od samego początku pokrywa go pewna ilość zanieczyszczeń. Ich poziom oraz właściwości cząsteczek zanieczyszczenia mają istotny wpływ na procesy przebiegające na powierzchni substratu. W pracy [H4] badam sytuację następującą: substrat jest początkowo pokrywany (w procesie losowej adsorpcji sekwencyjnej) cząsteczkami zanieczyszczeń do poziomu zapełnienia id; cząsteczki te mają postać sztywnych igieł o długości ad stałych sieci (w pracy rozważam wartości $ad = 1, ..., 24$). Na tak przygotowany substrat następuje adsorpcja punktowych[4] cząsteczek przewodnika[5]. Jedną z podstawowych wielkości badanych w tym modelu jest próg perkolacji cząsteczek przewodnika w funkcji wielkości cząsteczek zanieczyszczenia i całkowitego poziomu zanieczyszczeń. Zauważyłem, że można wyróżnić dwie całkowicie odmienne sytuacje: układ zachowuje się inaczej dla zanieczyszczeń punktowych ($ad = 1$) niż dla wszystkich innych przypadków ($ad > 1$).

W sytuacji $ad = 1$ (punktowe zanieczyszczenia) otrzymany próg perkolacji w ogóle nie zależy od poziomu zanieczyszczeń, pod warunkiem jednak, że poziom zanieczyszczeń $id < 0,5$. W pracy [H4] podałem prosty argument kombinatoryczny wyjaśniający to, skądinąd zaskakujące, zachowanie. To, że perkolacja nie występuje dla $id \geq 0,5$, można wyjaśnić faktem, że właśnie wartość 0,5 jest progiem perkolacji dla punktowych cząsteczek zanieczyszczenia; wówczas cząsteczki przewodnika nie mogą już perkolować.

Zbadałem, że dla większych cząsteczek zanieczyszczeń również perkolacja cząsteczek przewodnika jest ograniczona do pewnego obszaru zmienności poziomu zanieczyszczeń — dla skończonych rozmiarów sieci L istnieje przedział $id \in [id^-(ad), id^+(ad)]$, dla którego liczba symulacji zakończonych brakiem perkolacji zwiększa się od 0 do 100%. Przedział ten kurczy się dla $L \to \infty$, osiągając punkt $id^*(ad)$, będący dopełnieniem progu perkolacji zanieczyszczeń: $id^*(ad) = 1 - c_p^*(ad)$, gdzie $c_p^*(ad)$ jest graniczną wartością poziomu zanieczyszczeń o wielkości cząsteczek ad, dla której pojawia się perkolacja tychże zanieczyszczeń.

[4] To znaczy zajmujących pojedynczy węzeł sieci.

[5] Terminu *cząsteczki przewodnika* używam tu w sensie cząsteczek, których perkolacja jest badana. W praktyce perkolacja może nie tylko oznaczać przejście typu izolator-przewodnik, ale także, w wielu przypadkach, chodzi np. o pewne globalne własności mechaniczne (powstanie fazy żelu).

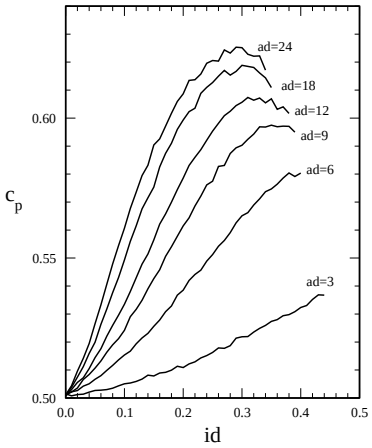

Rys. 11. Próg perkolacji przy większych cząsteczkach zanieczyszczeń.

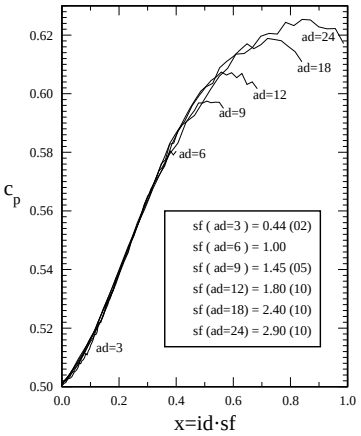

Rys. 12. Nakładanie się odpowiednio przeskalowanych zależności.

Dla większych cząsteczek zanieczyszczeń ($ad > 1$) próg perkolacji cząsteczek przewodnika zależy nietrywialnie od poziomu zanieczyszczeń (rys. 11), gdyż korelacje miejsc zajętych przez zanieczyszczenia są niezerowe. Po systematycznym wzroście progu c_p na dużym przedziale zmienności id funkcja przestaje być monotoniczna dla argumentów zbliżających się do granicznej wartości id^*, dla której perkolacja znika. Dokładniejsza analiza zależności $c_p(ad, id)$ pozwoliła mi zauważyć pewną uniwersalność zachowania. Przy ograniczeniu się do obszarów odległych od id^* i odpowiednim przeskalowaniu argumentów wszystkie wykresy dla różnych wartości ad nakładają się na siebie (rys. 12). Z kolei obszar bliski id^* jest ciekawy ze względu na pojawienie się maksimum: powyżej pewnej wartości uprzednie zwiększenie poziomu zanieczyszczeń daje efekt obniżenia się progu perkolacji. Zaproponowałem wyjaśnienie tej sytuacji, biorąc pod uwagę dwa czynniki: a) obszar wolny od zanieczyszczeń dla $id \lesssim id^*$ ma strukturę podobną do struktury klastra perkolującego nieco powyżej progu perkolacji, tzn. składa się z kropel (*blobs*), łączników (*links*) i ślepych końców (*dead ends*) [7]; oraz b) pierwotny rozkład zanieczyszczeń jest modyfikowany warunkiem *a posteriori* występowania perkolacji przewodników w układzie (tylko symulacje kończące się perkolacją są wykorzystywane przy obliczaniu średniej c_p). Blisko granicy id^* zwiększenie poziomu zanieczyszczeń częściej następuje w ślepych końcach, gdyż: po pierwsze, stanowią one znaczący odsetek pozostałej wolnej przestrzeni, po drugie, cząsteczki zanieczyszczeń nie mogą być zaadsorbowane w łącznikach, gdyż wtedy blokowana jest perkolacja przewodników, i w rezultacie symulacja nie jest liczona do średniej. Ostatecznie daje to względne zmniejszenie gęstości ślepych końców dostępnych dla adsorpcji cząsteczek przewodnika i prowadzi do obniżenia progu perkolacji. W pracy zaproponowałem także użycie względnego progu perkolacji $c_p^{rel}(id) = c_p(id)/(1-id)$, który określa ile procent powierzchni wolnej od zanieczyszczeń jest zajęte przez cząsteczki przewodnika w momencie perkolacji. Tak wprowadzona wielkość pozostaje rosnąca w całym zakresie zmienności parametru id.

2.3.5 Zablokowanie na zanieczyszczonym substracie (sztywne igły)

W pracy [H5] zbadałem wpływ zanieczyszczeń na zablokowanie w układzie. Substrat podlega najpierw adsorpcji cząsteczek zanieczyszczenia, które, będąc sztywnymi igłami o długości b, zapełniają czystą początkowo powierzchnię do poziomu c_i. Na tak przygotowane podłoże następnie adsorbowane są cząsteczki drugiego typu (też sztywne igły, ale o długości a). Po dojściu układu do stanu zablokowania (żadna cząsteczka drugiego typu nie jest w stanie zmieścić się w pozostałej wolnej przestrzeni) sprawdzam poziom pokrycia substratu cząsteczkami drugiego typu. Po wykonaniu odpowiedniej liczby symulacji otrzymuję wiarygodną wartość średnią progu zablokowania c_j, która jest przedmiotem dalszej analizy. Badając zależność progu zablokowania w funkcji wielkości poszczególnych rodzajów cząsteczek oraz poziomu zanieczyszczenia układu $c_j(a, b, c_i)$, zauważam, że należy rozgraniczyć dwa jakościowo różne przypadki: kiedy $a < b$ (większe są cząsteczki zanieczyszczeń) oraz kiedy $a > b$ (większe są cząsteczki drugiego rodzaju). Przypadek graniczny $a = b$ okazuje się trywialny ($c_j(a, a, c_i) = c_j(a, a, 0) - c_i$). Dla sytuacji, gdy $a > b$, odkryłem, że odpowiednio przeskalowany próg zablokowania y spełnia z dobrą dokładnością proste równanie $x + y^\beta = 1$, gdzie x jest odpowiednio przeskalowanym poziomem zanieczyszczeń, a wykładnik β zależy tylko od różnicy długości igieł obu typów (rys. 13). W drugim przypadku $a < b$ (większe są cząsteczki zanieczyszczeń) wyznaczyłem wykładnik krytyczny ν oraz wydzielając z fluktuacji część odpowiedzialną za niejednorodność zanieczyszczonego substratu [20], otrzymałem fraktalny wymiar przestrzeni wolnej od zanieczyszczeń równy 2.

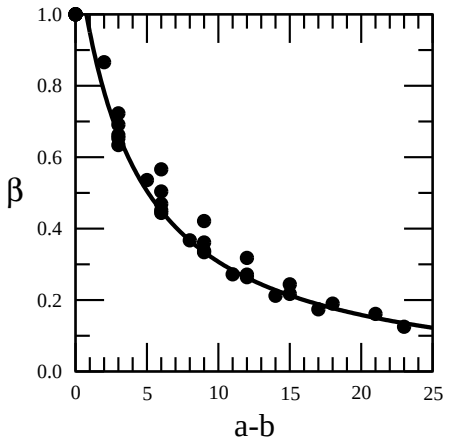

Rys. 13. Wykładnik β w funkcji różnicy długości igieł obu typów.

Rozdział 3

Podsumowanie wyników

W niniejszym rozdziale znajduje się zbiorcze zestawienie nowych wyników uzyskanych przeze mnie i opublikowanych w pracach wchodzących w skład rozprawy.

[H1] G. Kondrat, A. Pękalski,
Percolation and jamming in random sequential adsorption of linear segments on a square lattice,
Phys. Rev. E 63 (2001), 051108.

- Zaproponowałem jakościowe wyjaśnienie przyczyn istnienia minimum progu perkolacji dla przypadku adsorpcji prostych łańcuchów (igieł) na sieci kwadratowej.
- Odkryłem brak wysycenia dla wartości ilorazu progu perkolacji do progu zablokowania dla przypadku adsorpcji prostych łańcuchów (igieł) na sieci kwadratowej — po lokalnym wypłaszczeniu dla długości igieł $a = 3$–7 ów iloraz dalej rośnie ze wzrostem wartości a.

[H2] G. Kondrat, A. Pękalski,
Percolation and jamming in random bond deposition,
Phys. Rev. E 64 (2001), 056118.

- Odkryłem, że dla adsorpcji prostych łańcuchów na kwadratowej sieci wiązań perkolacja zachodzi tylko dla łańcuchów o długości co najwyżej $a^* = 6$.
- Odkryłem niemonotoniczne zachowanie progu perkolacji w funkcji długości łańcucha (minimum dla $a = 4$).
- Zbadałem strukturę rozkładu masy klastrów w momencie zablokowania — funkcja opisująca tę strukturę zmienia charakter przy przejściu przez wartość charakterystyczną a^*.
- Wyznaczyłem wykładnik Fishera dla tego modelu $\tau = 2,02(4)$.
- Wyznaczyłem próg zablokowania w funkcji długości łańcucha i znalazłem prostą postać tej zależności: $c_j(a) - c_j^* \propto a^{\Delta}$ z $c_j^* = 0,3350(25)$ i $\Delta = -1,05(10)$.

- Odkryłem liniowość ilorazu progu perkolacji do progu zablokowania w zakresie dopuszczonym przez istnienie perkolacji.

- Dokonałem analizy zbieżności progów perkolacji i zablokowania w granicy bardzo dużych sieci.

[H3] G. Kondrat,
Influence of temperature on percolation in a simple model of flexible chains adsorption,
J. Chem. Phys. 117 (2002), 6662-6666.

- Zaproponowałem prosty model giętkich polimerów podlegających adsorpcji, w którym jeden parametr (temperatura) charakteryzuje stopień ich sztywności i zarazem determinuje kształt cząsteczek.

- Przeanalizowałem wartość progu perkolacji w zależności od wielkości łańcuchów i temperatury (istnieje kilka reżimów temperaturowych, dla każdego zachowanie układu jest inne) oraz zaproponowałem wyjaśnienie otrzymanych wyników.

- Zaobserwowałem dla pewnych sytuacji efekt filtrowania, który polega na dopasowywaniu się adsorbowanych cząsteczek do kształtu wolnych obszarów, co powoduje dla tych cząsteczek obniżenie średniej energii związanej z ich kształtem.

- Wykazałem uniwersalność zachowania modelu — otrzymane temperatury charakterystyczne (oddzielające różne reżimy temperaturowe) pozostają w stałym stosunku dla różnych sieci.

- Zbadałem, że próg zablokowania nie zależy od temperatury.

[H4] G. Kondrat,
The study of percolation with the presence of impurities,
J. Chem. Phys. 122 (2005), 184718.

- Zbadałem wpływ kształtu cząsteczek i poziomu zanieczyszczeń na próg perkolacji w procesie adsorpcji na uprzednio zanieczyszczoną powierzchnię.

- Dla przypadku punktowych zanieczyszczeń uzyskałem niezależność progu perkolacji od poziomu zanieczyszczeń (poniżej pewnej granicznej wartości) i uzasadniłem tę nieoczekiwaną własność modelu w sposób ścisły.

- Dla przypadku wydłużonych cząsteczek zanieczyszczeń uzyskaną zależność progu perkolacji od parametrów udało mi się przedstawić w postaci zwartej funkcji.

- Wyjaśniłem istnienie otrzymanego maksimum progu perkolacji za pomocą argumentów odwołujących się do struktury adsorbatu.

[H5] G. Kondrat,
The effect of impurities on jamming in random sequential adsorption of elongated objects,
J. Chem. Phys. 124 (2006), 054713.

- Dla procesu adsorpcji jednych cząsteczek (P) na powierzchni zanieczyszczonej uprzednio innymi cząsteczkami (I) zbadałem próg zablokowania cząsteczek typu P w zależności od parametrów (wielkości obu rodzajów cząsteczek, poziom zanieczyszczenia cząsteczkami typu I) i opisałem go za pomocą zwartej funkcji.

[H6] G. Kondrat,
Impact of composition of extended objects on percolation on a lattice,
Phys. Rev. E 78 (2008), 011101.

- W zaproponowanym przeze mnie modelu giętkich łańcuchów (rozszerzenie modelu z [H3]) zbadałem próg perkolacji w zależności od wielkości oraz składu cząsteczek (dokładniej — od częstości występowania odpowiednich typów wiązań między kolejnymi atomami).

- Zbadałem wielkość odchylenia od liniowej zależności dla prostych cząsteczek o dużej sztywności dla dwóch różnych sieci (trójkątnej i kwadratowej).

- Zbadałem przejście „perkolacja" → „brak perkolacji", które występuje przy pewnych wartościach parametrów modelu.

- Odkryłem wysoką korelację między progiem perkolacji a gęstością atomów mających dokładnie dwóch sąsiadów.

Część II

Opis publikacji

Rozdział 1

Wykaz publikacji wchodzących w skład rozprawy

[H1] G. Kondrat, A. Pękalski,
Percolation and jamming in random sequential adsorption of linear segments on a square lattice,
Phys. Rev. E **63** (2001), 051108.

[H2] G. Kondrat, A. Pękalski,
Percolation and jamming in random bond deposition,
Phys. Rev. E **64** (2001), 056118.

[H3] G. Kondrat,
Influence of temperature on percolation in a simple model of flexible chains adsorption,
J. Chem. Phys. **117** (2002), 6662-6666.

[H4] G. Kondrat,
The study of percolation with the presence of impurities,
J. Chem. Phys. **122** (2005), 184718.

[H5] G. Kondrat,
The effect of impurities on jamming in random sequential adsorption of elongated objects,
J. Chem. Phys. **124** (2006), 054713.

[H6] G. Kondrat,
Impact of composition of extended objects on percolation on a lattice,
Phys. Rev. E **78** (2008), 011101.

Rozdział 2

Wykaz wszystkich publikacji

Do dnia 23.08.2010 lista moich publikacji w czasopismach naukowych składała się z 16 pozycji, z czego:

- 14 prac to prace niekonferencyjne, a 2 [P4, P5] konferencyjne
- 4 prace [P1, P3-P5] wchodziły w skład doktoratu
- 11 prac to prace po doktoracie [P6-P16]
- 6 prac wchodzi w skład rozprawy habilitacyjnej [P7-P11, P13].

Opublikowałem je w następujących czasopismach:

- 6 prac w Phys. Rev. E
- 3 prace w J. Chem. Phys.
- 2 prace w J. Phys. A: Math. Gen.
- 1 pracę w Phys. Rev. Lett.
- 1 pracę w J. Stat. Mech. Theory and Experiment
- 1 pracę w Int. J. Mod. Phys. C
- 1 pracę w Chaos, Solitons and Fractals
- 1 pracę w Acta Phys. Polon. B.

LISTA PUBLIKACJI[1]:

[P1] P. Garbaczewski, G. Kondrat,
Burgers Velocity Fields and Dynamical Transport Processes,
Phys. Rev. Lett. **77** (1996), 2608-2611.

[P2] A. Jadczyk, G. Kondrat, R. Olkiewicz,
On uniqueness of the jump process in event enhanced quantum theory,
J. Phys. A: Math. Gen. **30** (1997), 1863-1880.

[P3] P. Garbaczewski, G. Kondrat, R. Olkiewicz,
Burgers' flows as Markovian diffusion processes,
Phys. Rev. E **55** (1997), 1401-1412.

[P4] P. Garbaczewski, G. Kondrat, R. Olkiewicz,
Burgers Velocity Fields and Electromagnetic Forcing in Diffusive (Markovian) Matter Transport,
Acta Phys. Polon. B **28** (1997), 1731-1746.
Praca zaprezentowana na konferencji IX Symposium on Statistical Physics (Zakopane, 23-28.09.1996).

[P5] P. Garbaczewski, G. Kondrat, R. Olkiewicz,
Schrödinger's Interpolating Dynamics and Burgers' Flows,
Chaos, Solitons and Fractals **9** (1998), 29-41.
Praca zaprezentowana na konferencji International Conference on Applied Chaotic Systems (Inowłódz, 26-30.09.1996).

[P6] G. Kondrat, S. Peszat, B. Zegarliński,
Ergodicity for generalized Kawasaki dynamics,
J. Phys. A: Math. Gen. **33** (2000), 5901-5912.

[P7=H1] G. Kondrat, A. Pękalski,
Percolation and jamming in random sequential adsorption of linear segments on a square lattice,
Phys. Rev. E 63 (2001), 051108.

[P8=H2] G. Kondrat, A. Pękalski,
Percolation and jamming in random bond deposition,
Phys. Rev. E 64 (2001), 056118.

[1]Pozycje wyróżnione pogrubioną czcionką wchodzą w skład rozprawy habilitacyjnej.

[P9=H3] G. Kondrat,
Influence of temperature on percolation in a simple model of flexible chains adsorption,
J. Chem. Phys. 117 (2002), 6662-6666.

[P10=H4] G. Kondrat,
The study of percolation with the presence of impurities,
J. Chem. Phys. 122 (2005), 184718.

[P11=H5] G. Kondrat,
The effect of impurities on jamming in random sequential adsorption of elongated objects,
J. Chem. Phys. 124 (2006), 054713.

[P12] G. Kondrat, K. Sznajd-Weron,
Three types of outflow dynamics on square and triangular lattices and universal scaling,
Phys. Rev. E **77** (2008), 021127.

[P13=H6] G. Kondrat,
Impact of composition of extended objects on percolation on a lattice,
Phys. Rev. E 78 (2008), 011101.

[P14] G. Kondrat, K. Sznajd-Weron,
Percolation framework in Ising-spin relaxation,
Phys. Rev. E **79** (2009), 011119.

[P15] G. Kondrat, M. Gorzelańczyk,
On phase transitions in quantum continuous gases in the Maxwell-Boltzmann statistics,
J. Stat. Mech.: Theory and Experiment (2010), P01022.

[P16] G. Kondrat, K. Sznajd-Weron,
Spontaneous reorientations in a model of opinion dynamics with anticonformists,
Int. J. of Mod. Phys. C **21** (2010), 559-566.

Rozdział 3

Cytowania prac wchodzących w skład rozprawy

Prace wchodzące w skład rozprawy habilitacyjnej były cytowane **40** razy (z pominięciem samocytowań) [**39** razy bez cytowań współautorów][1].

[H1] G. Kondrat, A. Pękalski,
Percolation and jamming in random sequential adsorption of linear segments on a square lattice;
Phys. Rev. E 63 (2001), 051108.
Praca była cytowana **17** razy:

1. Cherkasova VA, Tarasevich YY, Lebovka NI, et al., *Percolation of aligned dimers on a square lattice,* EUR PHYS J B 74 (2): 205-209 MAR 2010.

2. Adamczyk P, Polanowski P, Sikorski A, *Percolation in polymer-solvent systems: A Monte Carlo study,* J CHEM PHYS 131 (23): art. no. 234901 DEC 21 2009.

3. Cornette V, Ramirez-Pastor AJ, Nieto F, *Adsorption of interacting monomers on spanning clusters of polyatomic species,* PHYSICA A 388 (20): 4387-4396 OCT 15 2009.

4. Adamczyk P, Romiszowski P, Sikorski A, *A simple model of stiff and flexible polymer chain adsorption: The influence of the internal chain architecture,* J CHEM PHYS 128 (15): art. no. 154911 APR 21 2008.

5. Tarasevich YY, Cherkasova VA, *Dimer percolation and jamming on simple cubic lattice,* EUR PHYS J B 60 (1): 97-100 NOV 2007.

6. Vygornitskii NV, Lisetskii LN, Lebovka NI, *Percolation in the model of random successive adhesion of anisotropic particles,* COLLOID J+ 69 (5): 557-562 OCT 2007.

[1] Dane na dzień 23.08.2010 według Science Citation Index Expanded, Scopus i Google scholar.

7. Cornette V, Ramirez-Pastor AJ, Nieto F, *Percolation of polyatomic species with the presence of impurities,* J CHEM PHYS 125 (20): art. no. 204702 NOV 28 2006.

8. Loscar ES, Borzi RA, Albano EV, *Interplay between thermal percolation and jamming upon dimer adsorption on binary alloys,* PHYS REV E 74 (5): art. no. 051601 Part 1 NOV 2006.

9. Bea AE, Irurzun IM, Mola EE, *Scaling properties in the average number of attempts until saturation in random sequential adsorption processes,* PHYS REV E 73 (5): art. no. 051604 Part 1 MAY 2006.

10. Cornette V, Ramirez-Pastor AJ, Nieto F, *Percolation of polyatomic species on site diluted lattices,* PHYS LETT A 353 (6): 452-458 MAY 15 2006.

11. Quintana M, Kornhauser I, Lopez R, et al., *Monte Carlo simulation of the percolation process caused by the random sequential adsorption of k-mers on heterogeneous triangular lattices,* PHYSICA A 361 (1): 195-208 FEB 15 2006.

12. Dolz M, Nieto F, Ramirez-Pastor AJ, *Site-bond percolation of polyatomic species,* PHYS REV E 72 (6): art. no. 066129 Part 2 DEC 2005.

13. Trojan K, Ausloos M, *Effects of relaxation processes during deposition of anisotropic grains on a flat substrate,* PHYSICA A 351 (2-4): 332-346 JUN 15 2005.

14. Loscar ES, Borzi RA, Albano EV, *Scaling behavior of jamming fluctuations upon random sequential adsorption,* EUR PHYS J B 36 (2): 157-160 NOV 2003.

15. Loscar ES, Borzi RA, Albano EV, *Fluctuations of jamming coverage upon random sequential adsorption on homogeneous and heterogeneous media,* PHYS REV E 68 (4): art. no. 041106 Part 1 OCT 2003.

16. Rampf F, Albano EV, *Interplay between jamming and percolation upon random sequential adsorption of competing dimers and monomers,* PHYS REV E 66 (6): art. no. 061106 Part 1 DEC 2002.

17. Tan ZJ, Zou XW, Zhang W, et al., *Pattern formation on nonuniform surfaces by correlated random sequential absorptions,* PHYS REV E 65 (5): art. no. 057201 Part 2 MAY 2002.

[H2] G. Kondrat, A. Pękalski,
Percolation and jamming in random bond deposition,
Phys. Rev. E 64 (2001), 056118.
Praca była cytowana **9** razy [**8** razy bez cytowań współautorów]:

1. Adamczyk P, Polanowski P, Sikorski A, *Percolation in polymer-solvent systems: A Monte Carlo study,* J CHEM PHYS 131 (23): art. no. 234901 DEC 21 2009.

2. Adamczyk P, Romiszowski P, Sikorski A, *A simple model of stiff and flexible polymer chain adsorption: The influence of the internal chain architecture,* J CHEM PHYS 128 (15): art. no. 154911 APR 21 2008.

3. Tarasevich YY, Cherkasova VA, *Dimer percolation and jamming on simple cubic lattice,* EUR PHYS J B 60 (1): 97-100 NOV 2007.

4. Cornette V, Ramirez-Pastor AJ, Nieto F, *Percolation of polyatomic species with the presence of impurities,* J CHEM PHYS 125 (20): art. no. 204702 NOV 28 2006.

5. Loscar ES, Borzi RA, Albano EV, *Interplay between thermal percolation and jamming upon dimer adsorption on binary alloys,* PHYS REV E 74 (5): art. no. 051601 Part 1 NOV 2006.

6. Cornette V, Ramirez-Pastor AJ, Nieto F, *Percolation of polyatomic species on site diluted lattices,* PHYS LETT A 353 (6): 452-458 MAY 15 2006.

7. Quintana M, Kornhauser I, Lopez R, et al., *Monte Carlo simulation of the percolation process caused by the random sequential adsorption of k-mers on heterogeneous triangular lattices,* PHYSICA A 361 (1): 195-208 FEB 15 2006.

8. Dolz M, Nieto F, Ramirez-Pastor AJ, *Site-bond percolation of polyatomic species,* PHYS REV E 72 (6): art. no. 066129 Part 2 DEC 2005.

9. Pękalski A, *Microreview of some non-solid state two-dimensional models,* PROG SURF SCI 74 (1-8): 415-421 DEC 2003.

[H3] G. Kondrat,
Influence of temperature on percolation in a simple model of flexible chains adsorption,
J. Chem. Phys. 117 (2002), 6662-6666.
Praca była cytowana **2** razy:

1. Adamczyk P, Polanowski P, Sikorski A, *Percolation in polymer-solvent systems: A Monte Carlo study,* J CHEM PHYS 131 (23): art. no. 234901 DEC 21 2009.

2. Adamczyk P, Romiszowski P, Sikorski A, *A simple model of stiff and flexible polymer chain adsorption: The influence of the internal chain architecture,* J CHEM PHYS 128 (15): art. no. 154911 APR 21 2008.

[H4] G. Kondrat, *The study of percolation with the presence of impurities,*
J. Chem. Phys. 122 (2005), 184718.
Praca była cytowana **6** razy:

1. Barcenas M, Duda Y, *Irreversible colloidal agglomeration in presence of associative inhibitors: Computer simulation study,* PHYS LETT A 365 (5-6): 454-457 JUN 11 2007.

2. Starke TKH, Johnston C, Grant PS, *Evolution of percolation properties in nanocomposite films during particle clustering,* SCRIPTA MATER 56 (5): 425-428 MAR 2007.

3. del Moral FG, O'Valle F, del Moral RG, *„Permeability and mass transfer as a function of the cooking temperature during the frying of beefburgers" by Oroszvari B.K., Rocha C.S., Sjoholm I. and Tornberg E. [Journal of Food Engineering 74 (2006) 1-12],* J FOOD ENG 80 (1): 374-376 MAY 2007.

4. Loscar ES, Borzi RA, Albano EV, *Interplay between thermal percolation and jamming upon dimer adsorption on binary alloys,* PHYS REV E 74 (5): art. no. 051601 Part 1 NOV 2006.

5. Cornette V, Ramirez-Pastor AJ, Nieto F, *Percolation of polyatomic species with the presence of impurities,* J CHEM PHYS 125 (20): art. no. 204702 NOV 28 2006.

6. Cornette V, Ramirez-Pastor AJ, Nieto F, *Percolation of polyatomic species on site diluted lattices,* PHYS LETT A 353 (6): 452-458 MAY 15 2006.

[H5] G. Kondrat,
The effect of impurities on jamming in random sequential adsorption of elongated objects,
J. Chem. Phys. 124 (2006), 054713.
Praca była cytowana **5** razy:

1. Araujo NAM, Cadilhe A, *Jammed state characterization of the random sequential adsorption of segments of two lengths on a line,* J STAT MECH-THEORY EXP : art. no. P02019 FEB 2010.

2. Matoz-Fernandez DA, Linares DH, Ramirez-Pastor AJ, *Critical behavior of long straight rigid rods on two-dimensional lattices: Theory and Monte Carlo simulations,* J CHEM PHYS 128 (21): art. no. 214902 JUN 7 2008.

3. Matoz-Fernandez DA, Linares DH, Ramirez-Pastor AJ, *Determination of the critical exponents for the isotropic-nematic phase transition in a system of long rods on two-dimensional lattices: Universality of the transition,* EPL-EUROPHYS LETT 82 (5): art. no. 50007 JUN 2008.

4. Loscar ES, Borzi RA, Albano EV, *Interplay between thermal percolation and jamming upon dimer adsorption on binary alloys,* PHYS REV E 74 (5): art. no. 051601 Part 1 NOV 2006.

5. Cornette V, Ramirez-Pastor AJ, Nieto F, *Percolation of polyatomic species with the presence of impurities,* J CHEM PHYS 125 (20): art. no. 204702 NOV 28 2006.

[H6] G. Kondrat,
Impact of composition of extended objects on percolation on a lattice,
Phys. Rev. E 78 (2008), 011101.
Praca była cytowana **1** raz:

1. Ziff RM, Gu H, *Universal condition for critical percolation thresholds of kagome-like lattices,* PHYS REV E 79 (2): art. no. 020102 Part 1 FEB 2009.

Rozdział 4

Cytowania wszystkich prac

Wszystkie moje prace były cytowane łącznie **72** razy (z pominięciem samocytowań) [**56** razy bez cytowań współautorów]. W tym prace wchodzące w skład rozprawy były cytowane **40** razy [**39** razy bez cytowań współautorów], a prace niewchodzące w skład rozprawy **32** razy [**17** razy bez cytowań współautorów][1].

[P1] P. Garbaczewski, G. Kondrat,
Burgers Velocity Fields and Dynamical Transport Processes,
Phys. Rev. Lett. **77** (1996), 2608-2611.
Praca była cytowana **7** razy [**2** razy bez cytowań współautorów].

[P2] A. Jadczyk, G. Kondrat, R. Olkiewicz,
On uniqueness of the jump process in event enhanced quantum theory,
J. Phys. A: Math. Gen. **30** (1997), 1863-1880.
Praca była cytowana **9** razy [**4** razy bez cytowań współautorów].

[P3] P. Garbaczewski, G. Kondrat, R. Olkiewicz,
Burgers' flows as Markovian diffusion processes,
Phys. Rev. E **55** (1997), 1401-1412.
Praca była cytowana **12** razy [**7** razy bez cytowań współautorów].

[P4] P. Garbaczewski, G. Kondrat, R. Olkiewicz,
Burgers Velocity Fields and Electromagnetic Forcing in Diffusive (Markovian) Matter Transport,
Acta Phys. Polon. B **28** (1997), 1731-1746.

[P5] P. Garbaczewski, G. Kondrat, R. Olkiewicz,
Schrödinger's Interpolating Dynamics and Burgers' Flows,
Chaos, Solitons and Fractals **9** (1998), 29-41.
Praca była cytowana **2** razy [**2** razy bez cytowań współautorów].

[1] Wszystkie dane na dzień 23.08.2010 za Science Citation Index Expanded, Scopus i Google scholar.

[P6] G. Kondrat, S. Peszat, B. Zegarliński,
Ergodicity for generalized Kawasaki dynamics,
J. Phys. A: Math. Gen. **33** (2000), 5901-5912.

[P7=H1] G. Kondrat, A. Pękalski,
Percolation and jamming in random sequential adsorption of linear segments on a square lattice,
Phys. Rev. E 63 (2001), 051108.
Praca była cytowana 17 razy [17 razy bez cytowań współautorów].

[P8=H2] G. Kondrat, A. Pękalski,
Percolation and jamming in random bond deposition,
Phys. Rev. E 64 (2001), 056118.
Praca była cytowana 9 razy [8 razy bez cytowań współautorów].

[P9=H3] G. Kondrat,
Influence of temperature on percolation in a simple model of flexible chains adsorption,
J. Chem. Phys. 117 (2002), 6662-6666.
Praca była cytowana 2 razy.

[P10=H4] G. Kondrat,
The study of percolation with the presence of impurities,
J. Chem. Phys. 122 (2005), 184718.
Praca była cytowana 6 razy.

[P11=H5] G. Kondrat,
The effect of impurities on jamming in random sequential adsorption of elongated objects,
J. Chem. Phys. 124 (2006), 054713.
Praca była cytowana 5 razy.

[P12] G. Kondrat, K. Sznajd-Weron,
Three types of outflow dynamics on square and triangular lattices and universal scaling,
Phys. Rev. E **77** (2008), 021127.
Praca była cytowana **2** razy [**2** razy bez cytowań współautorów].

[P13=H6] G. Kondrat,
Impact of composition of extended objects on percolation on a lattice,
Phys. Rev. E 78 (2008), 011101.
Praca była cytowana 1 raz.

[P14] G. Kondrat, K. Sznajd-Weron,
Percolation framework in Ising-spin relxation,
Phys. Rev. E **79** (2009), 011119.

[P15] G. Kondrat, M. Gorzelańczyk,
On phase transitions in quantum continuous gases in the Maxwell–Boltzmann statistics,
J. Stat. Mech.: Theory and Experiment (2010), P01022.

[P16] G. Kondrat, K. Sznajd-Weron,
Spontaneous reorientations in a model of opinion dynamics with anticonformists,
Int. J. of Mod. Phys. C **21** (2010), 559-566.

Rozdział 5

Opis prac niewchodzących w skład rozprawy

[P1] **P. Garbaczewski, G. Kondrat,** ***Burgers Velocity Fields and Dynamical Transport Processes,*** **Phys. Rev. Lett. 77 (1996), 2608-2611.**
W pracy rozważaliśmy transport cząstek znaczonych w polach prędkości spełniających równanie Burgersa z uwzględnieniem deterministycznych sił zewnętrznych. Scharakteryzowaliśmy proces dyfuzyjny opisujący pole gęstości cząstek znaczonych i szczegółowo przeanalizowaliśmy jego stochastyczne własności, używając do tego celu tzw. schematu Schrödingera interpolacji między wartościami brzegowymi.

[P2] **A. Jadczyk, G. Kondrat, R. Olkiewicz,** ***On uniqueness of the jump process in event enhanced quantum theory,*** **J. Phys. A: Math. Gen. 30 (1997), 1863-1880.**
W pracy rozważaliśmy matematyczne podstawy rozszerzonej mechaniki kwantowej w ramach modelu EEQT (ang. *Event Enhanced Quantum Theory*), w którym oddziaływanie układów klasycznego i kwantowego opisywane jest półgrupą dynamiczną z generatorem typu Lindblada. Wychodząc z dynamiki układu na poziomie macierzy gęstości, wykazaliśmy istnienie procesu stochastycznego odtwarzającego dynamikę układu oraz jego jednoznaczność i pokazaliśmy explicite jego postać.

[P3] **P. Garbaczewski, G. Kondrat, R. Olkiewicz,** ***Burgers' flows as Markovian diffusion processes,*** **Phys. Rev. E 55 (1997), 1401-1412.**
W ramach podejścia przedstawionego w pracy [P1] przeprowadziliśmy szczegółową analizę sytuacji, gdy człon sił zewnętrznych w równaniu Burgersa jest niezachowawczy. Wykorzystując jądra Feynmana-Kaca, otrzymaliśmy postać procesu stochastycznego dla przypadku zewnętrznego pola magnetycznego. Dla najprostszej nietrywialnej sytuacji stałego i jednorodnego pola magnetycznego przedstawiliśmy postać rozwiązania fundamentalnego.

[P4] **P. Garbaczewski, G. Kondrat, R. Olkiewicz,** ***Burgers Velocity Fields and Electromagnetic Forcing in Diffusive (Markovian) Matter Transport,*** **Acta Phys.**

Polon. B 28 (1997), 1731-1746.
Jest to praca konferencyjna opisująca wyniki z prac [P3] i [P5].

[P5] **P. Garbaczewski, G. Kondrat, R. Olkiewicz, *Schrödinger's Interpolating Dynamics and Burgers' Flows,* Chaos, Solitons and Fractals 9 (1998), 29-41.**
Przedmiotem pracy jest analiza związków równania Burgersa (w ogólności z członem sił zewnętrznych) z dyfuzjami i problemem interpolacji między wartościami brzegowymi (tzw. problem Schrödingera). Rozważane przez nas przykłady ilustrują szczegółowo subtelności, które napotyka się przy rozwiązywaniu tego typu zagadnień. Jest to praca konferencyjna.

[P6] **G. Kondrat, S. Peszat, B. Zegarliński, *Ergodicity for generalized Kawasaki dynamics,* J. Phys. A: Math. Gen. 33 (2000), 5901-5912.**
Dla uogólnionej dynamiki typu Kawasaki z potencjałem skończonego zasięgu podaliśmy warunki dostateczne i konieczne na miarę Gibbsa, żeby spełniony był warunek przerwy masowej oraz logarytmiczna nierówność Sobolewa. Dla odpowiednio małych gładkich potencjałów o skończonym zasięgu pokazaliśmy istnienie miary Gibbsa, która ponadto spełnia logarytmiczną nierówność Sobolewa. Omówiliśmy konstrukcję półgrupy Markowa w nieskończonej objętości dla ogólnego przypadku, gdy jednocząstkową przestrzenią stanów jest zwarta i spójna rozmaitość Riemanna.

[P12] **G. Kondrat, K. Sznajd-Weron, *Three types of outflow dynamics on square and triangular lattices and universal scaling,* Phys. Rev. E 77 (2008), 021127.**
W pracy zaproponowaliśmy proste uogólnienie jednowymiarowej dynamiki wypływu na sieciach dwuwymiarowych i zbadaliśmy je, a także dwa inne, znane wcześniej uogólnienia pod kątem rozkładu czasów relaksacji, wrażliwości na typ sieci (trójkątna, kwadratowa) i warunki początkowe. Przedmiotem pracy były również odpowiednie skalowania wielkości takich jak czasy relaksacji wraz z rozmiarem układu. Odkryliśmy dwa reżimy czasowe w rozkładzie czasów relaksacji, w których obowiązują wykładnicze zależności ogonu dystrybuanty od czasu z różnymi współczynnikami w wykładniku.

[P14] **G. Kondrat, K. Sznajd-Weron, *Percolation framework in Ising-spin relaxation,* Phys. Rev. E 79 (2009), 011119.**
W pracy badaliśmy zerotemperaturowe dynamiki Glaubera i dynamiki wypływu na sieciach pod kątem zrozumienia pojawiających się tam dwóch reżimów czasowych w rozkładzie czasów relaksacji. Zaproponowaliśmy schemat tłumaczący te zjawiska, oparty na pojęciu perkolacji. Odkryliśmy, że szybka relaksacja związana jest z przechodzeniem układu przez stany typu kropla, a relaksacja wolna jest związana z przechodzeniem przez stany typu pasy.

[P15] **G. Kondrat, M. Gorzelańczyk, *On phase transitions in quantum continuous gases in the Maxwell-Boltzmann statistics,* J. Stat. Mech.: Theory and Experiment (2010), P01022.**
W pracy rozważaliśmy własności stanu Gibbsa w granicy termodynamicznej. Dla gazu

Maxwella-Boltzmanna z nieujemnym, regularnym i ograniczonym potencjałem wykazaliśmy brak przejścia fazowego dla istotnie większych obszarów gęstości, niż te dotychczas badane. W dowodzie wykorzystaliśmy podejście J. Ginibre'a i teorię dodatnich operatorów na stożkach w przestrzeniach Banacha. W efekcie udało nam się zbadać własności spektralne operatora Kirkwooda-Salsburga prowadzące do analityczności odpowiednich funkcji korelacyjnych i braku przejść fazowych.

[P16] G. Kondrat, K. Sznajd-Weron, *Spontaneous reorientations in a model of opinion dynamics with anticonformists,* Int. J. of Mod. Phys. C 21(2010), 559-566.

W pracy rozważyliśmy zmodyfikowany model wypływu, w którym oprócz zachowań konformistycznych dopuszczone są także zachowania nonkonformistyczne. Przy odpowiednich wartościach parametrów zaobserwowaliśmy w modelu spontaniczne przeorganizowania całego układu i zbadaliśmy, w jakich warunkach takie przejścia zachodzą najszybciej.

Część III

Materiały uzupełniające

Rozdział 1

Działalność naukowa, dydaktyczna i organizacyjna

1.1 Życiorys naukowy

- **Imię i nazwisko:** Grzegorz Kondrat
- **Stopień i tytuł naukowy:** doktor nauk fizycznych
- **Data i miejsce urodzenia:** 21.03.1970 Wrocław
- **Miejsce pracy:** Uniwersytet Wrocławski, Instytut Fizyki Teoretycznej (od 01.10.1997)
- **Stanowisko:** adiunkt
- **Wykształcenie:**
  - **szkoła średnia:** 1984-1988 XIV L.O. im. Polonii Belgijskiej we Wrocławiu
  - **studia wyższe:** 1988-1993 fizyka (Uniwersytet Wrocławski, Instytut Fizyki Teoretycznej)
  - **praca magisterska:** 17.06.1993 *Stochastyczne i nieliniowe modele redukcji wektora stanu w kwantowej teorii pomiaru*, pod opieką prof. Arkadiusza Jadczyka
  - **studia doktoranckie:** 1993-1997, fizyka teoretyczna (Uniwersytet Wrocławski, Instytut Fizyki Teoretycznej)
  - **doktorat:** 18.04.1997 *Niestacjonarne procesy losowe w zewnętrznie zaburzanych układach klasycznych i kwantowych*, promotor prof. Piotr Garbaczewski
- **Wyróżnienia, granty, nagrody i stypendia:**
  - 1985-88 stypendium Krajowego Funduszu na Rzecz Dzieci

- 1986-88 laureat Olimpiad: Astronomicznej (3 razy, w tym dwukrotne zajęcie I miejsca) i Fizycznej (3 razy)
- 1987, 1988 wyróżnienia na Międzynarodowej Olimpiadzie Fizycznej
- 1991-93 stypendium Ministra Edukacji Narodowej
- 14.11.1997 nagroda Rektora Uniwersytetu Wrocławskiego za osiągnięcia naukowe (nagroda zespołowa)
- 01.10.1998 nagroda Ministra Edukacji Narodowej (nagroda zespołowa)
- 01.01.1999-31.12.1999 grant badawczy Uniwersytetu Wrocławskiego *Niestacjonarne procesy losowe na rozmaitościach Riemanna*
- 01.08.2001-30.06.2002 grant badawczy KBN *Badania modelu losowej adsorpcji sekwencyjnej obiektów rozciągłych* (jako kierownik)
- 01.10.2002 nagroda Ministra Edukacji Narodowej i Sportu (nagroda zespołowa)

1.2 Działalność naukowa

- **Główne zainteresowania naukowe:**
  - Problem rozszerzenia mechaniki kwantowej o stochastyczny opis oddziaływania z klasycznym układem pomiarowym, zagadnienia teorii pomiaru kwantowego (praca magisterska, [P2]).
  - Zagadnienie procesu dyfuzji w polach zewnętrznych, związek pól prędkości procesu z równaniem Burgersa, problem Schrödingera odtwarzania procesu stochastycznego z rozkładów początkowych i końcowych (praca doktorska, [P1, P3-P5]).
  - Pola wektorowe na rozmaitościach Riemanna, procesy dyfuzji na rozmaitościach z hipoeliptycznym generatorem zadanym przez pola wektorowe w kontekście uogólnionej dynamiki typu Kawasaki ([P6]).
  - Procesy adsorpcji obiektów rozciągłych, perkolacja, zablokowanie ([P7-P11, P13]).
  - Matematyczne podstawy przejść fazowych — podejście wywodzące się z prac Ginibre'a ([P15]).
  - Uogólnienia modeli wypływu — ich dynamika, rozkłady czasów relaksacji i zastosowania ([P12, P14, P16]).
- **Wyjazdy naukowe:**
  - Universität Bielefeld 17-29.07.1995 (na zaproszenie prof. Phillipe'a Blancharda)
  - ICTP Triest 17-31.08.1997 (w ramach programu Federation Scheme)

  - Imperial College Londyn 27.06-20.12.1998 (staż naukowy u prof. Bogusława Zegarlińskiego)
  - ICTP Triest 29.07-19.08.2001 (w ramach programu Federation Scheme)
  - Katholieke Universiteit Leuven 13-20.01.2002 (na zaproszenie prof. Josepha Indekeu)

- **Recenzowanie prac w czasopismach naukowych:**
  - Physical Review E (8 prac)
  - Physica A (1 praca)
  - Physics Letters A (1 praca)
  - Chemical Engineering Communications (1 praca)

- **Uczestnictwo w konferencjach:**
  - High-T_C thin films and single crystals (Ustroń 1989)
  - 31 Zimowa Szkoła Fizyki Teoretycznej: Chaos, The Interplay Between Stochastic and Deterministic Behaviour (Karpacz 1995)
  - Quantum Theory Without Observers (Bielefeld 1995)
  - Quantum Structures (Berlin 1996)
  - The Dynamics of Complexity (Triest 1997)
  - Nonlinear Cooperative Phenomena in Biological Systems (Triest 1997)
  - Workshop on Statistical Physics of Frustrated Systems (Triest 1997)
  - 34 Zjazd Fizyków Polskich (Katowice 1997)
  - 10 Sympozjum Maksa Borna: Quantum future (Przesieka 1997)
  - 11 Sympozjum Maksa Borna: Anomalous Diffusion: from Basis to Applications (Lądek Zdr. 1998)
  - The Future of Stochastic Analysis II – referat (Sztokholm 1998)
  - 13 Sympozjum Maksa Borna: Statistical Physics in Biology (Wrocław 1999)
  - 36 Zimowa Szkoła Fizyki Teoretycznej: Exotic Statistical Physics (Lądek Zdr. 2000)
  - 26 MECO – poster (Praga 2001)
  - School and Workshop on Dynamical Systems (Triest 2001)
  - Challenges in Granular Physics (Triest 2001)
  - 27 MECO – poster (Sopron 2002)
  - 28 MECO – poster (Saarbrücken 2003)

  - 18 Sympozjum Maksa Borna: Statistical Physics Outside Physics (Lądek Zdr. 2003)
  - 41 Zimowa Szkoła Fizyki Teoretycznej: Diffusion and Soft Matter Physics – referat (Lądek Zdr. 2005)
  - 23 Sympozjum Maksa Borna: Critical Phenomena in Complex Systems (Polanica Zdr. 2007)

1.3 Działalność dydaktyczna

- **Prowadzenie zajęć dydaktycznych:**
  - na Uniwersytecie Wrocławskim (1.10.1994-30.09.1997 jako doktorant, od 1.10.1997 jako adiunkt w Instytucie Fizyki Teoretycznej)
  - w Wyższej Szkole Informatyki i Zarządzania „Copernicus" we Wrocławiu (1.03.2002-30.09.2002 jako starszy wykładowca, 1.10.2002-30.09.2006 jako adiunkt, od 1.10.2006 na umowę o dzieło)
- **Prowadzenie wykładów:**
  - metody komputerowe I
  - programowanie graficznego interfejsu użytkownika
  - wstęp do programowania
  - algebra liniowa
  - analiza matematyczna
  - matematyka dyskretna
  - fizyka
- **Prowadzenie konwersatoriów:**
  - algebra
  - analiza matematyczna
  - rachunek różniczkowo-całkowy
  - elementy probabilistyki
  - elektrodynamika
  - matematyka i statystyka
  - fizyka
- **Prowadzenie laboratoriów komputerowych:**
  - metody komputerowe I

  - metody komputerowe II
  - programowanie obiektowe
  - zastosowanie komputerów w fizyce teoretycznej
  - programowanie graficznego interfejsu użytkownika
  - wstęp do programowania
  - grafika komputerowa

- **Prace dyplomowe:**
  - opieka nad pracami licencjackimi: 3
  - opieka nad pracami magisterskimi: 5
  - opieka nad pracami inżynierskimi: 3
  - recenzje prac dyplomowych: 4

1.4 Działalność organizacyjna

- **Organizacja konferencji (skarbnik):**
  - 36 Zimowa Szkoła Fizyki Teoretycznej (2000)
  - 18 Sympozjum Maksa Borna (2003)
  - 23 Sympozjum Maksa Borna (2007)
  - 47 Zimowa Szkoła Fizyki Teoretycznej (2011)
- Członek Komitetu Głównego Olimpiady Astronomicznej (od 1990)
- Członek International Board of International Olympiad on Astronomy and Astrophysics (2008/9)
- Lider (opiekun) polskiej reprezentacji na 2nd International Olympiad on Astronomy and Astrophysics (Bandung 2008)
- Koordynator Wydziału Fizyki i Astronomii ds. Dolnośląskiego Festiwalu Nauki (od 2008)
- Członek Polskiego Towarzystwa Fizycznego (2001-2009)
- Sekretarz seminarium Zakładu Dynamiki Nieliniowej i Układów Złożonych IFT (od 1996)
- Prezentacje z fizyki w szkołach ponadpodstawowych w ramach kółek fizycznych (2010)

Rozdział 2

Odpis dyplomu doktorskiego

Rozdział 3

Oświadczenia współautorów

Mój udział w powstaniu prac [H1] (G. Kondrat, A. Pękalski, *Percolation and jamming in random sequential adsorption of linear segments on a square lattice,* Phys. Rev. E **63** [2001], 051108) oraz [H2] (G. Kondrat, A. Pękalski, *Percolation and jamming in random bond deposition,* Phys. Rev. E **64** [2001], 056118) był podobny i polegał na dyskusji założeń, otrzymanych wyników (programy pisał samodzielnie dr Grzegorz Kondrat) oraz na współtworzeniu ostatecznej wersji tekstu.

prof. dr hab. Andrzej Pękalski

Część IV

Publikacje wchodzące w skład rozprawy

Część V

Publikacje po doktoracie niewchodzące w skład rozprawy

Burgers Velocity Fields and Dynamical Transport Processes

Piotr Garbaczewski and Grzegorz Kondrat
Institute of Theoretical Physics, University of Wrocław, pl. M. Borna 9, PL-50 204 Wrocław, Poland
(Received 13 March 1996)

We explore a connection of the forced Burgers equation with the Schrödinger (diffusive) interpolating dynamics in the presence of deterministic external forces. This entails an exploration of the consistency conditions interpreting the dispersion of passive contaminants in the Burgers flow as a Markovian diffusion process. In general, the usage of the continuity equation $\partial_t \rho = -\nabla(\vec{v}\rho)$, with $\vec{v} = \vec{v}(\vec{x}, t)$ the Burgers field and ρ the density of transported matter, is at variance with the explicit diffusion scenario. We give a complete characterization of diffusive matter transport governed by Burgers velocity fields. This extends both to the approximate description of the transport driven by an incompressible fluid and to motions in an infinitely compressible medium. [S0031-9007(96)01263-X]

PACS numbers: 47.10.+g, 05.40.+j, 05.60.+w, 47.20.Ky

The Burgers equation [1,2] recently has acquired a considerable popularity in a variety of physical contexts. They range from an astrophysical issue of the stratified large-scale distribution of matter in the early Universe [3–5], through acoustic turbulence dealing with intense noise in compressible liquids and gases [6], to primitive fluid turbulence modeling in terms of the statistics of Burgers shocks in the low viscosity regime (enhanced by random initial data) [1,3,7,8], eventually ending with the analysis of a fully developed Burgers turbulence that is regarded as a result of random forcing (stirring) of respective velocity fields [9,10]. It also pertains to the turbulence-without-pressure models [11], description of directed polymers in a random potential [10], random interface growth problem governed by the related Kardar-Parisi equation [12], and fluctuations or dispersion in deterministic or random flows [12,13]. An exhaustive discussion of its role in acoustic turbulence and gravitational contexts, where the emergence of shock pressure fronts is crucial, can be found in Ref. [14].

The Burgers equation usually is considered without any forcing term, and its solutions are known under the gradient form assumption. We shall preserve the latter restriction, but consider a more general form of the Burgers equation that accounts for an external force field $\vec{F}(\vec{x}, t)$,

$$\partial_t \vec{v} + (\vec{v}\nabla)\vec{v} = \nu\triangle\vec{v} + \vec{F}(\vec{x}, t)\,. \tag{1}$$

Many recent investigations are devoted to the statistically relevant curl $\vec{v} = 0$ solutions implemented by random initial data and/or random forcing term (the random potential in the above-mentioned Parisis-Kardar equation), and Burgers velocity fields (or their potentials) are analyzed on their own. However, an issue of matter transport driven by those nonlinear velocity fields requires knowledge of an exact evolution of concentration and/or density fields, much in the spirit of early hydrodynamical studies of advection and diffusion of passive tracers [15,16]; see also [17]. This particular issue is addressed in the present paper, under a simplifying assumption of nonrandom initial data and deterministic force fields, by regarding the stochastic diffusion process as a primary phenomenon responsible for the emergence of (1).

Knowing the Burgers fields, we may consistently ask what is the particular matter transport dynamics (of density fields) that is consistent with the chosen (Burgers) velocity field evolution. Then, the passive scalar (tracer or contaminant) advection-in-a-flow problem [10,13] naturally appears through the parabolic dynamics,

$$\partial_t T + (\vec{v}\nabla)T = \nu\triangle T\,; \tag{2}$$

see, e.g., also [15–17]. For incompressible fluids, (2) coincides with the conventional Fokker-Planck equation for the diffusion process. This feature does not persist in the compressible case.

While looking for the stochastic implementation of the microscopic (molecular) dynamics (2) [10,13,17], it is assumed that the "diffusing scalar" (contaminant in the lore of early statistical turbulence models) obeys the Itô equation,

$$d\vec{X}(t) = \vec{v}(\vec{x}, t)dt + \sqrt{2\nu}\, d\vec{W}(t)\,, \tag{3}$$
$$\vec{X}(0) = \vec{x}_0 \longrightarrow \vec{X}(t) = \vec{x}\,,$$

where the given forced Burgers velocity field is perturbed by the noise term representing a molecular diffusion. In the, by now conventional, Itô representation of diffusion-type random variable $\vec{X}(t)$ one explicitly refers to the standard Brownian motion (e.g., the Wiener process) $\sqrt{2\nu}\,\vec{W}(t)$, instead of the usually adopted formal white noise integral $\int_0^t \vec{\eta}(s)\,ds$, coming from the Langevin-type version of (3).

Under these premises, we cannot view Eqs. (1)–(3) as completely independent (disjoint) problems: The velocity field $\vec{v}$ cannot be arbitrarily inferred from (1) or any other velocity-defining equation without verifying the *consistency* conditions, which would allow one to associate (2) and (3) with a well defined random dynamics (stochastic process), and Markovian diffusion, in particular [18].

In connection with the usage of Burgers velocity fields (with or without external forcing) which in (3) clearly are

 0031-9007/96/77(13)/2608(4)$10.00

intended to replace the standard *forward drift* of the would-be-involved Markov diffusion process, we have not found in the literature any attempt to resolve apparent contradictions arising if (2) and/or (3) are defined by means of (1). Also, an issue of the necessary *correlation* (cf. [13], Chap. 7.3, devoted to the turbulent transport and the related dispersion of contaminants) between the probabilistic Fokker-Planck dynamics of the diffusing tracer and this of the passive tracer (contaminant) concentration (2) has been left aside in the literature.

Moreover, rather obvious hesitation could have been observed in attempts to establish the most appropriate matter transport rule, if (1)–(3) are adopted. Depending on the particular phenomenological departure point, one adopts the standard continuity equation [3,4] that is valid to a high degree of accuracy in the low viscosity limit $\nu \downarrow 0$ of (1)–(3), but incorrect on mathematical grounds *if* there is a diffusion involved *and* simultaneously a solution of (1) stands for the respective *current* velocity of the flow: $\partial_t \rho(\vec{x},t) = -\nabla[\vec{v}(\vec{x},t)\rho(\vec{x},t)]$. Alternatively, following the white noise calculus tradition stating that the stochastic integral $\vec{X}(t) = \int_0^t \vec{v}[\vec{X}(s),s]\,ds + \int_0^t \vec{\eta}(s)\,ds$ necessarily implies the Fokker-Planck equation, one adopts $\partial_t \rho(\vec{x},t) = \nu\triangle\rho(\vec{x},t) - \nabla[\vec{v}(\vec{x},t)\rho(\vec{x},t)]$ which is clearly problematic in view of the classic McKean's discussion of the propagation of chaos for the Burgers equation [19,20] and deriving the stochastic "Burgers process" in the following: "The fun begins in trying to describe this Burgers motion as the path of a tagged molecule in an infinite bath of like molecules" [19].

To put things on solid ground, let us consider a Markovian diffusion process, which is characterized by the transition probability density (generally inhomogeneous in space and time law of random displacements) $p(\vec{y},s,\vec{x},t), 0 \le s < t \le T$, and the probability density $\rho(\vec{x},t)$ of its random variable $\vec{X}(t), 0 \le t \le T$. The process is completely determined by these data. For clarity of discussion, we do not impose any spatial boundary restrictions, nor fix any concrete limiting value of T which, in principle, can be moved to infinity.

The following conditions valid for any $\epsilon < 0$: (a) there holds $\lim_{t\downarrow s}(1/t-s)\int_{|\vec{y}-\vec{x}|>\epsilon} p(\vec{y},s,\vec{x},t)\,d^3x = 0$, (b) there exists a (forward) drift $\vec{b}(\vec{x},s) = \lim_{t\downarrow s}(1/t-s)\int_{|\vec{y}-x|\le\epsilon}(\vec{y}-\vec{x})p(\vec{x},s,\vec{y},t)\,d^3y$, and (c) there exists a diffusion function (in our case it is simply a diffusion coefficient ν) $a(\vec{x},s) = \lim_{t\downarrow s}(1/t-s)\int_{|\vec{y}-\vec{x}|\le\epsilon}(\vec{y}-\vec{x})^2 p(\vec{x},s,\vec{y},t)\,d^3y$, are conventionally interpreted to define a diffusion process [18]. Under suitable restrictions (boundedness of involved functions, their continuous differentiability) the function

$$g(\vec{x},s) = \int p(\vec{x},s,\vec{y},T)g(\vec{y},T)\,d^3y \tag{4}$$

satisfies the backward diffusion equation [notice that the minus sign appears, in comparison with (2)]

$$-\partial_s g(\vec{x},s) = \nu\triangle g(\vec{x},s) + [\vec{b}(\vec{x},s)\nabla]g(\vec{x},s)\,. \tag{5}$$

Let us point out that the validity of (5) is known to be a *necessary* condition for the existence of a Markov diffusion process, whose probability density $\rho(\vec{x},t)$ is to obey the Fokker-Planck equation [the forward drift $\vec{b}(\vec{x},t)$ replaces the previously utilized Burgers field $\vec{v}(\vec{x},t)$]:

$$\partial_t \rho(\vec{x},t) = \nu\triangle\rho(\vec{x},t) - \nabla[\vec{b}(\vec{x},t)\rho(\vec{x},t)]\,. \tag{6}$$

The case of particular interest in the nonequilibrium statistical physics literature appears when $p(\vec{y},s,\vec{x},t)$ is a *fundamental solution* of (5) with respect to variables $\vec{y},s$ [18]; see, however, [21] for an alternative situation. Then, the transition probability density *also* satisfies the second Kolmogorov (e.g., the Fokker-Planck) equation in the remaining $\vec{x},t$ pair of variables. Let us emphasize that these two equations form an *adjoint pair,* referring to the slightly counterintuitive for physicists, although transparent for mathematicians [23–26], issue of time reversal of diffusions.

After adjusting (3) to the present context, $\vec{X}(t) = \int_0^t \vec{b}(\vec{X}(s),s)\,ds + \sqrt{2\nu}\,\vec{W}(t)$ we can utilize standard rules of the Itô stochastic calculus [24–27], to realize that for any smooth function $f(\vec{x},t)$ of the random variable $\vec{X}(t)$ the conditional expectation value

$$\lim_{\triangle t\downarrow 0}\frac{1}{\triangle t}\left[\int p(\vec{x},t,\vec{y},t+\triangle t)f(\vec{y},t+\triangle t)\,d^3y - f(\vec{x},t)\right]$$
$$= (D_+ f)(\vec{X}(t),t) = [\partial_t + (\vec{b}\nabla) + \nu\triangle]f(\vec{x},t)\,, \tag{7}$$
$$\vec{X}(t) = \vec{x}\,,$$

determines the forward drift $\vec{b}(\vec{x},t)$ (if we set components of $\vec{X}$ instead of f) and introduces the local field of forward accelerations associated with the diffusion process, which we constrain by demanding (see, e.g., Refs. [24–27] for prototypes of such dynamical constraints)

$$(D_+^2\vec{X})(t) = (D_+\vec{b})(\vec{X}(t),t)$$
$$= [\partial_t\vec{b} + (\vec{b}\nabla)\vec{b} + \nu\triangle\vec{b}](\vec{X}(t),t) = \vec{F}(\vec{X}(t),t)\,, \tag{8}$$

where, at the moment arbitrary, the function $\vec{F}(\vec{x},t)$ may be interpreted as the external forcing applied to the diffusing system [22]. In particular, if we assume that drifts remain gradient fields, curl $\vec{b} = 0$, under the forcing, then those that are allowed by the prescribed choice of $\vec{F}(\vec{x},t)$ *must* fulfill the compatibility condition (notice the conspicuous absence of the standard Newtonian minus sign in this analog of the second Newton law)

$$\vec{F}(\vec{x},t) = \nabla\Omega(\vec{x},t)\,, \tag{9}$$

$$\Omega(\vec{x},t) = 2\nu\left[\partial_t\Phi + \frac{1}{2}\left(\frac{b^2}{2\nu} + \nabla b\right)\right].$$

This establishes the connection of the forward drift $\vec{b}(\vec{x},t) = 2\nu\nabla\Phi(\vec{x},t)$ with the (Feynman-Kac, cf. [21,22]) potential $\Omega(\vec{x},t)$ of the chosen external force field.

One of the distinctive features of Markovian diffusion processes with the positive density $\rho(\vec{x},t)$ is that the notion of the *backward* transition probability density $p_*(\vec{y},s,\vec{x},t)$ can be consistently introduced on each finite time interval, say $0 \le s < t \le T$,

$$\rho(\vec{x},t)p_*(\vec{y},s,\vec{x},t) = p(\vec{y},s,\vec{x},t)\rho(\vec{y},s)\,, \tag{10}$$

so that $\int \rho(\vec{y},s)p(\vec{y},s,\vec{x},t)\,d^3y = \rho(\vec{x},t)$ and $\rho(\vec{y},s) = \int p_*(\vec{y},s,\vec{x},t)\rho(\vec{x},t)\,d^3x$. This allows us to define the backward derivative of the process in the conditional mean (cf. [22,27–29] for a discussion of these concepts in the case of the most traditional Brownian motion and Smoluchowski-type diffusion processes)

$$\lim_{\triangle t\downarrow 0}\frac{1}{\triangle t}\left[\vec{x} - \int p_*(\vec{y},t-\triangle t,\vec{x},t)\vec{y}\,d^3y\right] = (D_-\vec{X})(t) = \vec{b}_*(\vec{X}(t),t),$$
$$(D_-f)(\vec{X}(t),t) = [\partial_t + (\vec{b}_*\nabla) - \nu\triangle]f(\vec{X}(t),t)\,. \tag{11}$$

Accordingly, the backward version of the dynamical constraint imposed on the acceleration field reads

$$(D_-^2\vec{X})(t) = (D_+^2\vec{X})(t) = \vec{F}(\vec{X}(t),t)\,, \tag{12}$$

where under the gradient-drift field assumption, curl $\vec{b}_* = 0$, we have explicitly fulfilled the forced Burgers equation [cf. (1)],

$$\partial_t\vec{b}_* + (\vec{b}_*\nabla)\vec{b}_* - \nu\triangle\vec{b}_* = \vec{F}\,, \tag{13}$$

where [22,24,25], in view of $\vec{b}_* = \vec{b} - 2\nu\nabla\ln\rho$, we deal with $\vec{F}(\vec{x},t)$ previously introduced in (9). A notable consequence of the involved backward Itô calculus is that the Fokker-Planck equation (6) can be transformed to an *equivalent* form of

$$\partial_t\rho(\vec{x},t) = -\nu\triangle\rho(\vec{x},t) - \nabla[\vec{b}_*(\vec{x},t)\rho(\vec{x},t)]\,, \tag{14}$$

which, however, describes a density evolution in the reverse sense of time. Let us recall that a time inversion of the probabilistic evolution $\rho(\vec{x},0)\to\rho(\vec{x},t)\to\rho(\vec{x},T)$, with $0\le t\le T$, read $\rho(\vec{x},T)\to\rho(\vec{x},T-t)\to\rho(\vec{x},0)$.

At this point let us recall that Eqs. (5) and (6) form a natural adjoint pair of equations that determine the Markovian diffusion process in the chosen time interval $[0,T]$. Clearly, an adjoint of (14) reads

$$\partial_s f(\vec{x},s) = \nu\triangle f(\vec{x},s) - [\vec{b}_*(\vec{x},s)\nabla]f(\vec{x},s)\,, \tag{15}$$

where

$$f(\vec{x},s) = \int p_*(\vec{y},0,\vec{x},s)f(\vec{y},0)\,d^3y\,, \tag{16}$$

to be compared with (4) and (5) and the previously mentioned passive scalar dynamics (2). Here, manifestly, the time evolution of the backward drift is governed by the Burgers equation, and the diffusion equation (15) is correlated [via the definition (10)] with the probability density evolution rule (14).

This pair *only* can be consistently utilized if the diffusion process is to be driven by forced (or unforced) Burgers velocity fields.

Let us notice that the familiar logarithmic Hopf-Cole transformation [2] of the Burgers equation into the generalized diffusion equation (yielding explicit solutions in the unforced case) has received a generalization in the framework of the so-called Schrödinger boundary-data (interpolation) problem [21,22,25,26,29,30]; see also [31,32]. In particular, in its recent reformulation [21,22], the problem of defining a suitable Markovian diffusion process was reduced to investigating the adjoint pairs of parabolic partial differential equations, as, e.g., (5) and (6) or (14) and (15). For gradient drift fields this amounts to checking (imposing limitations on the admissible force field potential) whether the Feynman-Kac kernel

$$k(\vec{y},s,\vec{x},t) = \int \exp\left[-\int_s^t c(\omega(\tau),\tau)\,d\tau\right]d\mu_{(x,t)}^{(y,s)}(\omega) \tag{17}$$

is positive and continuous in the open space-time area of interest, and whether it gives rise to positive solutions of the adjoint pair of generalized heat equations,

$$\partial_t u(\vec{x},t) = \nu\triangle u(\vec{x},t) - c(\vec{x},t)u(\vec{x},t)\,,$$
$$\partial_t v(\vec{x},t) = -\nu\triangle v(\vec{x},t) + c(\vec{x},t)v(\vec{x},t)\,, \tag{18}$$

where $c(\vec{x},t) = (1/2\nu)\Omega(\vec{x},t)$ follows from the previous formulas. In the above, $d\mu_{(\vec{x},t)}^{(\vec{y},s)}(\omega)$ is the conditional Wiener measure over sample paths of the standard Brownian motion.

Solutions of (18) upon suitable normalization give rise to the Markovian diffusion process with the factorized probability density $\rho(\vec{x},t) = u(\vec{x},t)v(\vec{x},t)$ which interpolates between the boundary density data $\rho(\vec{x},0)$ and $\rho(\vec{x},T)$, with the forward and backward drifts of the process defined as follows:

$$\vec{b}(\vec{x},t) = 2\nu\,\nabla v(\vec{x},t)/v(\vec{x},t)\,,$$
$$\vec{b}_*(\vec{x},t) = -2\nu\,\nabla u(\vec{x},t)/u(\vec{x},t)\,, \tag{19}$$

in the prescribed time interval $[0,T]$. The transition probability density of this process reads

$$p(\vec{y},s,\vec{x},t) = k(\vec{y},s,\vec{x},t)\,v(\vec{x},t)/v(\vec{y},s)\,. \tag{20}$$

Here, neither k (17) nor p (20) needs to be the fundamental solutions of appropriate parabolic equations; see, e.g., Ref. [21] where an issue of differentiability is analyzed.

The corresponding [since $\rho(\vec{x},t)$ is given] transition probability density (10) of the backward process has the form

$$p_*(\vec{y},s,\vec{x},t) = k(\vec{y},s,\vec{x},t)\,u(\vec{y},s)/u(\vec{x},t)\,. \qquad (21)$$

Obviously [21,25], in the time interval $0 \le s < t \le T$ there holds $u(\vec{x},t) = \int u_0(\vec{y})k(\vec{y},s,\vec{x},t)\,d^3y$ and $v(\vec{y},s) = \int k(\vec{y},s,\vec{x},T)v_T(\vec{x})\,d^3x$.

By defining $\Phi_* = \ln u$, we immediately recover the traditional form of the Hopf-Cole transformation for Burgers velocity fields $\vec{b}_* = -2\nu\nabla\Phi_*$. In the special case of the standard free Brownian motion, there holds $\vec{b}(\vec{x},t) = 0$ while $\vec{b}_*(\vec{x},t) = -2\nu\nabla \ln \rho(\vec{x},t)$.

Our discussion provides a complete identification of the stochastic diffusion process underlying *both* the deterministically forced Burgers velocity dynamics and the related matter transport (14), in terms of suitable density fields. The generalization of the Hopf-Cole procedure to this case involves a powerful methodology of Feynman-Kac kernel functions. Let us stress that the connection between the Burgers equation and the generalization (forward) heat equation is not merely a formal trick that generates solutions to the nonlinear problem. The forward equation (18), in fact, carriers complete information about the implicit *backward stochastic evolution*, that is, a Markov diffusion process. Indeed, the transition probability density (21) obeys the familiar Chapman-Kolmogorov formula. If we wish to analyze a concrete density field governed by this process, any two boundary density data $\rho(\vec{x},0)$ and $\rho(\vec{x},T)$ allow us to deduce the ultimate form of the (more traditional, forward) diffusion process (20), by means of the Schrödinger boundary data problem [21,25]. Then, the adjoint pair of equations (18) gives all details of the dynamics, with (19)–(21) as a necessary consequence. On the other hand, the presented discussion implies a direct import of the shock-type (generally compressible) matter density profiles to the general nonequilibrium statistical physics of random phenomena.

One of the authors (P. G.) received financial support from KBN research Grant No. 2 P302 057 07.

[1] J. M. Burgers, *The Nonlinear Diffusion Equation* (Reidel, Dordrecht, 1974).
[2] E. Hopf, Pure Appl. Math. **3**, 201 (1950).
[3] S. F. Shandarin and B. Z. Zeldovich, Rev. Mod. Phys. **61**, 185 (1989).
[4] S. Albeverio, A. A. Molchanov, and D. Surgailis, Prob. Theory Relat. Fields **100**, 457 (1994).
[5] Y. Hu and W. A. Woyczynski, in *Chaos—The Interplay Between Stochastic and Deterministic Behavior*, edited by P. Garbaczewski, M. Wolf, and A. Weron, Lecture Notes in Physics Vol. 457 (Springer-Verlag, Berlin, 1995), p. 135.
[6] S. N. Gurbatov and A. I. Saichev, Zh. Eksp. Teor. Fiz. **80**, 689 (1981).
[7] Z. She, E. Aurell, and U. Frisch, Commun. Math. Phys. **148**, 623 (1992).
[8] Ya. G. Sinai, Commun. Math. Phys. **148**, 601 (1992).
[9] J. D. Fournier and U. Frisch, J. Mec. Theor. Appl. **2**, 699 (1983).
[10] J. P. Bouchaud, M. Mézard, and G. Parisi, Phys. Rev. E **52**, 3656 (1995).
[11] A. M. Polyakov, Phys. Rev. E **52**, 6183 (1995).
[12] M. Kardar, G. Parisi, and Y. C. Zhang, Phys. Rev. Lett. **56**, 889 (1986).
[13] A. S. Monin and A. M. Yaglom, *Statistical Fluid Mechanics* (The MIT Press, Cambridge, MA, 1973).
[14] S. N. Gurbatov, A. N. Malakhov, and A. I. Saichev, *Nonlinear Random Waves and Turbulence in Nondispersive Media: Waves, Rays, Particles* (Manchester University Press, Manchester, 1991).
[15] P. G. Saffman, J. Fluid Mech. **8**, 273 (1960).
[16] A. A. Towsend, Proc. R. Soc. London A **209**, 418 (1951).
[17] A. I. Saichev and W. A. Woyczynski, Physica (Amsterdam) D (to be published).
[18] A. Friedman, Partial Differential Equations of Parabolic Type (Prentice-Hall, Englewood, NJ, 1964).
[19] H. P. Mc Kean, in *Lecture Series in Differential Equations*, edited by A. K. Aziz (Van Nostrand, Amsterdam, 1969), Vol. II, p. 177.
[20] P. Calderoni and M. Pulvirenti, Ann. Inst. Henri Poincaré **39**, 85 (1983).
[21] P. Garbaczewski and R. Olkiewicz, J. Math. Phys. (N.Y.) **37**, 730 (1996).
[22] Ph. Blanchard and P. Garbaczewski, Phys. Rev. E **49**, 3815 (1994).
[23] U. G. Haussmann and E. Pardoux, Ann. Prob. **14**, 1188 (1986).
[24] E. Nelson, *Quantum Fluctuations* (Princeton University Press, Princeton, 1985).
[25] J. C. Zambrini, J. Math. Phys. (N.Y.) **27**, 3207 (1986).
[26] J. C. Zambrini, in *Chaos—The Interplay Between Stochastic and Deterministic Behavior* (Ref. [5]), p. 393.
[27] E. Nelson, *Dynamical Theories of the Brownian Motion* (Princeton University Press, Princeton, 1967).
[28] P. Garbaczewski and J. P. Vigier, Phys. Rev. A **46**, 4634 (1992).
[29] P. Garbaczewski and R. Olkiewicz, Phys. Rev. A **51**, 3445 (1995).
[30] P. Garbaczewski, J. R. Klauder, and R. Olkiewicz, Phys. Rev. E **51**, 4114 (1995).
[31] S. Albeverio, Ph. Blanchard, and R. Høegh-Krohn, in *Stochastic Aspects of Classical Quantum Systems*, edited by S. Albeverio *et al.*, Lecture Notes in Mathematics Vol. 1109 (Springer-Verlag, Berlin, 1985), p. 189.
[32] M. Freidlin, *Functional Integration and Partial Differential Equations* (Princeton University Press, Princeton, 1985).

J. Phys. A: Math. Gen. **30** (1997) 1863–1880. Printed in the UK PII: S0305-4470(97)74843-1

On uniqueness of the jump process in event enhanced quantum theory

A Jadczyk†, G Kondrat and R Olkiewicz

Institute of Theoretical Physics, University of Wrocław, Pl Maxa Borna 9, PL-50 204 Wrocław, Poland

Received 23 May 1996, in final form 8 November 1996

Abstract. We prove that, in constrast to the theories of continuous observation, in the formalism of event enhanced quantum theory the stochastic process generating sample histories of pairs (observed quantum system, observing classical apparatus) is unique. This result gives a rigorous basis to the previous heuristic argument of Blanchard and Jadczyk.

1. Introduction

Effective time evolution of a quantum system is usually described by a dynamical semigroup: a semigroup of completely positive, unit preserving transformations acting on the algebra of observables of the system. A general form of generator of a norm-continuous semigroup was published in 1976 independently by Gorini *et al* [1] (for matrix algebras) on the one hand, and by Lindblad [2] (for the more general, norm-continuous case) on the other. It is usually referred to as the Lindblad form; it reads

$$\dot{A} = \mathrm{i}[H, A] + \sum_{\alpha} V_{\alpha}^{*} A V_{\alpha} - \tfrac{1}{2}\{\Lambda, A\} \tag{1}$$

where $H = H^{*}$ is the Hamiltonian, $\{\,,\,\}$ stands for anticommutator, and

$$\Lambda = \sum_{\alpha} V_{\alpha}^{*} V_{\alpha}. \tag{2}$$

In contrast to a pure unitary evolution that describes closed systems and which is time-reversible, the second dissipative part of the generator makes the evolution of an open system irreversible. This irreversibility is not evident from the very form of the equation, it is connected with the positivity property of the evolution. Formally we can often solve the evolution equation backward in time, but positivity of the reversed evolution will be lost.

We can also look at the dual time evolution of states rather than of observables. For states, described by density matrices, we get

$$\dot{\rho} = -\mathrm{i}[H, A] + \sum_{\alpha} V_{\alpha} \rho V_{\alpha}^{*} - \tfrac{1}{2}\{\rho, \Lambda\} \tag{3}$$

where the duality is defined by $\mathrm{Tr}(\dot{A}\rho) = \mathrm{Tr}(A\dot{\rho})$.

Here again only propagation forward in time is possible, when we try to propagate backward we will have to deal with negative probabilities. This irreversibility is reflected in the fact that pure states evolve into mixed states. How do mixed states arise? In quantum

† E-mail address: ajad@ift.uni.wroc.pl

0305-4470/97/061863+18$19.50

theory, similarly as in classical theory, they arise when we go from individual description to ensemble description, from maximal available information to partial information. Or simply, they arise by mixing of pure states. Pure states are represented by one-dimensional projection operators P. If $\mathrm{d}\mu(P)$ is a probabilistic measure on pure states, then the density matrix ρ defined by $\rho = \int P\,\mathrm{d}\mu(P)$ is a mixed state, unless $\mathrm{d}\mu(P)$ is a Dirac measure. In contrast to classical theory, however, in quantum theory decomposition of a mixed state into pure ones is non-unique. So, for instance, the identity operator can be decomposed into *any* complete orthonormal basis: $I = \sum_i |i\rangle\langle i|$, thus in indenumerably many ways. This mysterious and annoying non-uniqueness of decomposition into pure states in quantum theory can be simply taken as an unavoidable price for our progress from classical to quantum—as a fact of life. And so it was. Yet it has started to cause problems in quantum measurement theory.

The first attempt to give a precise mathematical formulation of quantum measurement theory must be ascribed to John von Neumann. In his monograph [3] he introduced two kinds of evolution: a continuous, unitary evolution U of an 'unobserved' system, and discontinuous 'projections' that accompany 'observations' or 'measurements.' His projection postulate, later reformulated by Lüders for mixed states, is expressed as follows: 'if we measure a property E of the quantum system, and if the property E holds, then as the result of this measurement the system which was previously described by a density matrix ρ switches to the new state described by the density matrix $E\rho E/\operatorname{Tr} E\rho E$.'

A whole generation of physicists has been influenced by this apparently precise formulation. Few dared to ask: who are 'we' in the phrase 'if we measure' [4], what is 'measurement' [5, 6], at which particular instant of time does the reduction take place? How long does it take [7], if ever [8], to reduce? Can it be observed? Can it be verified experimentally [9–11]? Nobody could satisfactorily answer these questions. And so it was taken for granted that quantum theory cannot really be understood in physical terms, that it is a peculiar mixture of objective and subjective. That it is about 'observations,' and so it makes little or no sense without 'observers,' and without 'mind'. There were many who started to believe that it is the sign of a new age and the sign of progress. A few opponents did not believe the completeness of a physical theory that could not even define what constitutes 'observation' [5–6]—but they could not change the overall feeling of satisfaction with the successes of quantum theory.

This situation started to change rapidly when technological progress made it possible to make prolonged experiments with individual quantum systems. The standard 'interpretation' did not suffice. Experimenters were seeing with their own eyes not the 'averages' but individual sample histories. In particular, experiments in quantum optics allowed one to almost 'see' the quantum jumps. In 1988 Cook [12] discussed photon counting statistics in fluorescence experiments and revived the question 'what are quantum jumps?' Another reason to pay more attention to the notion of quantum jumps came from the several groups of physicists working on effective numerical solutions of quantum optics master equations. The works of Carmichael [13], Dalibard *et al* [14, 15], Dum *et al* [16], Gardiner *et al* [17], developed the method of quantum trajectories, or the quantum Monte Carlo (QMC) algorithm for simulating solutions of master equations. It was soon realized (cf e.g. [18–22]) that the same master equations can be simulated either by the quantum Monte Carlo method based on quantum jumps, or by a continuous quantum state diffusion. Wiseman and Milburn [23] discussed the question of how different experimental detection schemes relate to continuous diffusions or to discontinuous jump simulations. The two approaches were recently also put to comparison by Garraway and Knight [24]. There are, at present, two schools of simulations. Gisin *et al* [25] tried to reconcile the two arguing that '*the*

quantum jumps can be clearly seen' also in the quantum state diffusion plots. On the other hand, already in 1986 Diosi [26] proposed a pure state, piecewise deterministic process that reproduces a given master equation. In spite of the title of his paper that suggests uniqueness of his scheme, his process, although mathematically canonical for a given master equation, is not unique. This problem of non-uniqueness is especially important in theories of gravity-induced spontaneous localization (see [27], also [28, 29] and references therein) and in the recent attempts to merge mind-brain science with quantum theory [30–32], where quantum collapse plays an important role.

In the next section we shall see how the situation changes completely with the new approach to quantum measurement developed by Ph Blanchard and one of us (AJ) (see [33] and references there)†. In section 2 we will sketch the main idea of the new approach. We will also indicate infinitesimal proof of uniqueness of the stochastic process that reproduces the master equation for the total system, i.e. quantum system + classical apparatus. In section 3 we give concrete examples of non-unicity when only a pure quantum system is involved—as it is typical in quantum optics. In section 4 we give a rigorous, global proof of unicity of the process, when classical apparatus is coupled in an appropriate way to the quantum system. The technical part of the proof can be found in the appendix. Conclusions are given in section 5. There we also comment upon the most natural question: we all know that every apparatus consists of atoms—then how can it be classical?

2. The formalism

Let us sketch the mathematical framework of the 'event-enhanced quantum theory'. Details can be found in [33]. To describe events, one needs a classical system C, then possible events are identified with changes of a (pure) state of C. One can think of events as 'clicks' of a particle counter, changes of the pointer position, or changing readings on an apparatus LCD display. The concept of an event is of course an idealization, like all concepts in a physical theory. Let us consider the simplest situation corresponding to a finite set of possible events. The space of pure states of C, denoted by $\mathcal{S}_c$, has m states, labelled by $\alpha = 1, \ldots, m$. Statistical states of C are probability measures on $\mathcal{S}_c$—in our case just sequences $p_\alpha \geqslant 0, \sum_\alpha p_\alpha = 1$.

The algebra of observables of C is the algebra $\mathcal{A}_c$ of complex functions on $\mathcal{S}_c$—in our case just sequences $f_\alpha, \alpha = 1, \ldots, m$ of complex numbers.

We use Hilbert space language even for the description of the classical system. Thus we introduce an m-dimensional Hilbert space $\mathcal{H}_c$ with a fixed basis, and we realize $\mathcal{A}_c$ as the algebra of diagonal matrices $F = \mathrm{diag}(f_1, \ldots, f_m)$. Statistical states of C are then diagonal density matrices $\mathrm{diag}(p_1, \ldots, p_m)$, and pure states of C are vectors of the fixed basis of $\mathcal{H}_c$. Events are ordered pairs of pure states $\alpha \to \beta, \alpha \neq \beta$. Each event can thus be represented by an $m \times m$ matrix with 1 at the (α, β) entry, zero otherwise. There are $m^2 - m$ possible events.

We now come to the quantum system. Let Q be the quantum system whose bounded observables are from the algebra $\mathcal{A}_q$ of bounded operators on a Hilbert space $\mathcal{H}_q$. In this paper we will assume $\mathcal{H}_q$ to be *finite dimensional*. Pure states of Q are unit vectors in $\mathcal{H}_q$; proportional vectors describe the same quantum state. Statistical states of Q are given by non-negative density matrices $\hat{\rho}$, with $\mathrm{Tr}(\hat{\rho}) = 1$.

Let us now consider the total system $T = Q \times C$. For the algebra $\mathcal{A}_t$ of observables

† Complete, actual bibliography of the quantum future project is always available under URL: http://www.ift.uni.wroc.pl/~ajad/qf-pub.htm

of T we take the tensor product of algebras of observables of Q and C: $\mathcal{A}_t = \mathcal{A}_q \otimes \mathcal{A}_c$. It acts on the tensor product $\mathcal{H}_q \otimes \mathcal{H}_c = \oplus_{\alpha=1}^{m} \mathcal{H}_\alpha$, where $\mathcal{H}_\alpha \approx \mathcal{H}_q$. Thus $\mathcal{A}_t$ can be thought of as algebra of *diagonal* $m \times m$ matrices $A = (a_{\alpha\beta})$, whose entries are quantum operators: $a_{\alpha\alpha} \in \mathcal{A}_q$, $a_{\alpha\beta} = 0$ for $\alpha \neq \beta$.

Statistical states of $Q \times C$ are given by $m \times m$ diagonal matrices $\rho = \mathrm{diag}(\rho_1, \ldots, \rho_m)$ whose entries are positive operators on $\mathcal{H}_q$, with the normalization $\mathrm{Tr}(\rho) = \sum_\alpha \mathrm{Tr}(\rho_\alpha) = 1$. Duality between observables and states is provided by the expectation value $\langle A \rangle_\rho = \sum_\alpha \mathrm{Tr}(A_\alpha \rho_\alpha)$.

We will now generalize slightly our framework. Indeed, there is no need for the quantum Hilbert spaces $\mathcal{H}_\alpha$, corresponding to different states of the classical system, to coincide. We will allow them to be different in the rest of this paper. We denote $n_\alpha = \dim(\mathcal{H}\alpha)$.

We now consider dynamics. It is normal in quantum theory for classical parameters to enter the quantum Hamiltonian. Thus we assume that quantum dynamics, when no information is transferred from Q to C, is described by Hamiltonians $H_\alpha : \mathcal{H}_\alpha \longrightarrow \mathcal{H}_\alpha$, that may depend on the actual state of C (as indicated by the index α). We will use matrix notation and write $H = \mathrm{diag}(H_\alpha)$. Now take the classical system. It is discrete here. Thus it cannot have continuous time dynamics of its own.

As in [33] the *coupling* of Q to C is specified by a matrix $V = (g_{\alpha\beta})$, where $g_{\alpha\beta}$ are linear operators: $g_{\alpha\beta} : \mathcal{H}_\beta \longrightarrow \mathcal{H}_\alpha$. We put $g_{\alpha\alpha} = 0$. This condition expresses the simple fact: we do not need dissipation without receiving information (i.e. without an event). To transfer information from Q to C we need a non-Hamiltonian term which provides a completely positive (CP) coupling. As in [33] we consider couplings for which the evolution equation for observables and for states is given by the Lindblad form

$$\dot{A}_\alpha = \mathrm{i}[H_\alpha, A_\alpha] + \sum_\beta g^\star_{\beta\alpha} A_\beta g_{\beta\alpha} - \tfrac{1}{2}\{\Lambda_\alpha, A_\alpha\} \tag{4}$$

or equivalently:

$$\dot{\rho}_\alpha = -\mathrm{i}[H_\alpha, \rho_\alpha] + \sum_\beta g_{\alpha\beta} \rho_\beta g^\star_{\alpha\beta} - \tfrac{1}{2}\{\Lambda_\alpha, \rho_\alpha\} \tag{5}$$

where

$$\Lambda_\alpha = \sum_\beta g^\star_{\beta\alpha} g_{\beta\alpha}. \tag{6}$$

The above equations describe the statistical behaviour of ensembles. Individual sample histories are described by a Markov process with values in pure states of the total system. In [33] this process was argued to be infinitesimally unique. For the sake of completeness we repeat here the arguments. First, we use equation (5) to compute $\rho_\alpha(\mathrm{d}t)$ when the initial state $\rho_\alpha(0)$ is pure:

$$\rho_\alpha(0) = \delta_{\alpha\alpha_0} |\psi_0\rangle\langle\psi_0|. \tag{7}$$

In the equations below we will discard terms that are higher than linear order in $\mathrm{d}t$. For $\alpha = \alpha_0$ we obtain

$$\rho_{\alpha_0}(\mathrm{d}t) = |\psi_0\rangle\langle\psi_0| - \mathrm{i}[H_{\alpha_0}, |\psi_0><\psi_0|]\,\mathrm{d}t - \tfrac{1}{2}\{\Lambda_{\alpha_0}, |\psi_0\rangle\langle\psi_0|\}\,\mathrm{d}t \tag{8}$$

while for $\alpha \neq \alpha_0$

$$\rho_{\alpha_0}(\mathrm{d}t) = g_{\alpha\alpha_0} |\psi_0\rangle\langle\psi_0| g^\star_{\alpha\alpha_0}\,\mathrm{d}t. \tag{9}$$

The term for $\alpha = \alpha_0$ can be written as

$$\rho_{\alpha_0}(\mathrm{d}t) = p_{\alpha_0} |\psi_{\alpha_0}\rangle\langle\psi_{\alpha_0}| \tag{10}$$

where

$$\psi_{\alpha_0} = \frac{\exp(-\mathrm{i}H_{\alpha_0}\,\mathrm{d}t - \frac{1}{2}\Lambda_{\alpha_0}\,\mathrm{d}t)\psi_0}{\|\exp(-\mathrm{i}H_{\alpha_0}\,\mathrm{d}t - \frac{1}{2}\Lambda_{\alpha_0}\,\mathrm{d}t)\psi_0\|} \tag{11}$$

and

$$p_{\alpha_0} = 1 - \lambda(\psi_0, \Lambda_{\alpha_0}\psi_0)\,\mathrm{d}t. \tag{12}$$

The term with $\alpha \neq \alpha_0$ can be written as

$$\rho_\alpha(\mathrm{d}t) = p_\alpha|\psi_\alpha\rangle\langle\psi_\alpha| \tag{13}$$

where

$$p_\alpha = \|g_{\alpha\alpha_0}\psi_0\|^2\,\mathrm{d}t \tag{14}$$

and

$$\psi_\alpha = \frac{g_{\alpha\alpha_0}\psi_0}{\|g_{\alpha\alpha_0}\psi_0\|}. \tag{15}$$

This representation is unique and it defines the infinitesimal version of a piecewise deterministic Markov process. The process is defined by the following piecewise deterministic algorithm (cf [33]).

Let us assume a fixed, sufficiently small, time step $\mathrm{d}t$. Suppose that at time t the system is described by a quantum state vector ψ_0 and a classical state α_0. Compute the scalar product $\lambda(\psi_0, \alpha_0) = \langle\psi_0, \Lambda_{\alpha_0}, \psi_0\rangle$. Choose a uniform random number $p \in [0, 1]$. Jump if $p < \lambda(\psi_0, \alpha_0)\,\mathrm{d}t$. Otherwise do not jump. When jumping, change $\alpha_0 \to \alpha$ with probability $p_{\alpha_0\to\alpha} = \|g_{\alpha\alpha_0}\psi_0\|^2/\lambda(\psi_0, \alpha_0)$, and change $\psi_0 \to g_{\alpha\alpha_0}\psi_0/\|g_{\alpha\alpha_0}\psi_0\|$. If not jumping, change

$$\psi \to \frac{\exp\{-\mathrm{i}H_{\alpha_0}\,\mathrm{d}t - \frac{1}{2}\Lambda_{\alpha_0}\,\mathrm{d}t\}\psi_0}{\|\exp\{-\mathrm{i}H_{\alpha_0}\,\mathrm{d}t - \frac{1}{2}\Lambda_{\alpha_0}\,\mathrm{d}t\}\psi_0\|} \qquad t \to t + \mathrm{d}t.$$

Repeat the steps.

3. Non-uniqueness in the pure quantum case

In this section we will show on simple examples the nature of non-uniqueness in the pure quantum case. At first let us note that so-called 'canonical decomposition' of a dynamical generator L is not unique. To see this suppose that

$$L(\rho) = -\mathrm{i}[H,\ \rho] + \sum_{k=1}^{n} a_k\rho a_k^* - \frac{1}{2}\left\{\sum_{k=1}^{n} a_k^* a_k,\ \rho\right\}$$

where $H = H^*$ is the Hamiltonian and a_k are arbitrary bounded operators. Let us define

$$\tilde{H} = H + \frac{1}{2\mathrm{i}}(S - S^*) \qquad \tilde{a_k} = \sum_{l=1}^{n} \lambda_{kl}a_l + z_k$$

where $z_k \in \mathbb{C}$, (λ_{kl}) is a unitary matrix and $S = \sum_{k,l} \overline{z_k}\lambda_{kl}a_l$. Then $\tilde{L}(\rho)$ given by

$$\tilde{L}(\rho) = -\mathrm{i}[\tilde{H},\ \rho] + \sum_{k=1}^{n} \tilde{a_k}\rho\tilde{a_k}^* - \frac{1}{2}\left\{\sum_{k=1}^{n} \tilde{a_k}^*\tilde{a_k},\ \rho\right\}$$

coincides with $L(\rho)$. For more details see [34].

Now we show that the nature of the non-uniqueness is much deeper than that described above. For simplicity let us consider a two-state quantum system whose algebra of observables is equal to $M_{2\times 2}$. Let T_t be a dynamical semigroup with a generator L given by

$$L(\rho) = a\rho a^* - \tfrac{1}{2}\{a^*a, \rho\}$$

where $a \in M_{2\times 2}$.

3.1. Pure diffusion process

First let us show that the time evolution determined by L can be described by a diffusion process with values in $\mathbb{C}P^1$ [35]. Let a two-component complex valued process $\psi_t = (\psi_t^1, \psi_t^2)'$ (prime denotes the transposition) be given by the following stochastic differential equation,

$$\mathrm{d}\psi_t^i = f_i(\psi_t)\,\mathrm{d}B_t + g_i(\psi_t)\,\mathrm{d}t \qquad i = 1, 2$$

where B_t is a one-dimensional real Brownian motion and

$$g_i(\psi_t) = \sum_j (\langle a^*\rangle_t a_{ij} - \tfrac{1}{2}(a^*a)_{ij})\psi_t^j - \tfrac{1}{2}\langle a^*\rangle_t\langle a\rangle_t\psi_t^i$$

$$f_i(\psi_t) = \sum_j a_{ij}\psi_t^j - \langle a\rangle_t\psi_t^i$$

$$\langle a\rangle_t = \frac{\langle\psi_t|a|\psi_t\rangle}{\langle\psi_t|\psi_t\rangle} \qquad \langle a^*\rangle_t = \frac{\langle\psi_t|a^*|\psi_t\rangle}{\langle\psi_t|\psi_t\rangle}.$$

Moreover, let us choose an initial condition $\psi_0 = (z_0^1, z_0^2)'$ such that $|z_0^1|^2 + |z_0^2|^2 = 1$. Because f_i and g_i are continuously differentiable (in the real sense) on $\mathbb{C}^2 \setminus \{0\}$ so there exists a local solution with a random explosion time T (see, for example, [36]). But

$$\mathrm{d}|\psi_t^i|^2 = \psi_t^i\,\mathrm{d}\bar\psi_t^i + \bar\psi_t^i\,\mathrm{d}\psi_t^i + \mathrm{d}[\psi_t^i, \bar\psi_t^i]_t$$

where $[\psi_t^i, \bar\psi_t^i]_t$ is the quadratic covariation of ψ_t^i and $\bar\psi_t^i$. Thus

$$\mathrm{d}[\psi_t^i, \bar\psi_t^i]_t = |f_i(\psi_t)|^2\,\mathrm{d}t$$

and so

$$\mathrm{d}\|\psi_t\|^2 = \sum_i(\psi_t^i\,\mathrm{d}\bar\psi_t^i + \bar\psi_t^i\,\mathrm{d}\psi_t^i) + \|f(\psi_t)\|^2\,\mathrm{d}t = 0.$$

It implies that $T = \infty$ with probability one and so our process is a diffusion with values in a sphere S^3. Let us define a process P_t with values in one-dimensional projectors by

$$P_t = |\psi_t\rangle\langle\psi_t| = \sum_{i,j}\psi_t^i\bar\psi_t^j e_{ij}$$

where e_{ij} form the standard basis in $M_{2\times 2}$. Then, using the equation

$$\mathrm{d}(\psi_t^i\bar\psi_t^j) = (\bar f_j\psi_t^i + f_i\bar\psi_t^j)\,\mathrm{d}B_t + (\bar g_j\psi_t^i + g_i\bar\psi_t^j + f_i\bar f_j)\,\mathrm{d}t$$

we obtain that

$$\mathrm{d}P_t = [(a - \langle a\rangle_t)P_t + P_t(a^* - \langle a^*\rangle_t)]\,\mathrm{d}B_t - \tfrac{1}{2}\{a^*a, P_t\}\,\mathrm{d}t + aP_ta^*\,\mathrm{d}t.$$

Since B_t is a martingale then after taking the average we get

$$\mathrm{d}E[P_t] = aE[P_t]a^*\,\mathrm{d}t - \tfrac{1}{2}\{a^*a, E[P_t]\}\,\mathrm{d}t.$$

Let us define a density matrix $\rho_t = E[P_t]$. Then

$$\dot{\rho}_t = a\rho_t a^* - \tfrac{1}{2}\{a^*a, \rho_t\}$$

and so the average of the diffusion gives the quantum dynamical evolution.

Finally, we show that $\rho_t = \int P(t, x_0, \mathrm{d}y)P_y$, where $P_y = |y\rangle\langle y|$, $x_0 = |\psi_0\rangle\langle\psi_0|$ and $P(t, x, \mathrm{d}y)$ is the transition probability of the described diffusion. By the definition, $P(t, x_0, \Gamma)$ is the distribution of the random variable $P_t^{x_0}$ such that $P_0^{x_0} = x_0$. It implies that for every bounded and measurable function f defined on $\mathbb{C}P^1$ we have

$$E[f(P_t^{x_0})] = \int f(y)P(t, x_0, \mathrm{d}y).$$

Let us consider a function given by $f(y) = \mathrm{Tr}(AP_y)$, where $A \in M_{2\times 2}$. Then

$$\int \mathrm{Tr}(AP_y)P(t, x_0, \mathrm{d}y) = E[\mathrm{Tr}(AP_t^{x_0})] = \mathrm{Tr}(A\rho_t).$$

So $\mathrm{Tr}(A\int P(t, x_0, \mathrm{d}y)P_y)) = \mathrm{Tr}(A\rho_t)$ for every A and thus $\rho_t = \int P(t, x_0, \mathrm{d}y)P_y$ with $\rho_0 = x_0$.

3.2. Piecewise deterministic solution

On the other hand, it is possible to associate with the same quantum dynamics a piecewise deterministic process, as in the method of quantum trajectories [13]. Now the situation is more complicated, because, in general, we cannot replace the Brownian motion by the Poisson process. We have to solve a stochastic differential equation for an unknown process $(\tilde{N}_t, \psi_t)$.

$$\mathrm{d}\psi_t^i = f_i(\psi_{t^-})\,\mathrm{d}\tilde{N}_t + g_i(\psi_t)\,\mathrm{d}t$$

where f_i and g_i are prescribed functions, together with the following constrain: $\tilde{N}_t$ is a semimartingale such that

(a) $[\tilde{N}, \tilde{N}]_t = \tilde{N}_t$, $\tilde{N}_0 = 0$, $E[\tilde{N}_t] < \infty$ for all $t \geqslant 0$;

(b) for a given non-negative function $\lambda : \mathbb{C}^2 \to \mathbb{R}$ the process $M_t := \tilde{N}_t - \int_0^t \lambda(\psi_s)\,\mathrm{d}s$ is a martingale.

It is clear that M_t will be a purely discontinuous martingale. A continuous, increasing and with paths of finite variation on compacts process $\int_0^t \lambda(\psi_t)\,\mathrm{d}s$ is called the compensator of $\tilde{N}_t$. In our case due to assumption (a) it is also the conditional quadratic variation of $\tilde{N}_t$ [36]. The functional $\lambda(\psi_t)$ is called the stochastic intensity and plays the role of the intensity of jumps. Let us recall that for the (homogeneous) Poisson process $N_t - \int_0^t \lambda\,\mathrm{d}s = N_t - \lambda t$ is a martingale. From the assumption (a) above we obtain that $\tilde{N}_t$ is quadratic pure jump, its continuous part is equal zero and $\triangle\tilde{N}_s = (\triangle\tilde{N}_s)^2$, where $\triangle\tilde{N}_s = \tilde{N}_s - \tilde{N}_s$—so it is a point process. Let us emphasize that in general it is not an inhomogeneous Poisson process since its compensator would be a deterministic function equal to $E[\tilde{N}_t]$ [37]. So it will be the case only when the stochastic intensity is a deterministic function depending on t.

Moreover, $[\tilde{N}, t]_t = 0$ as $\tilde{N}_t$ is of finite variation on compacts. This implies the following symbolic rules:

$$(\mathrm{d}\tilde{N})^2 = \mathrm{d}\tilde{N} \qquad \mathrm{d}\tilde{N}\,\mathrm{d}t = \mathrm{d}t\,\mathrm{d}\tilde{N} = 0.$$

From assumption (b) we get $\mathrm{d}M_t = \mathrm{d}\tilde{N}_t - \lambda(\psi_t)\,\mathrm{d}t$. Let $\mathcal{F}_t$ be a σ-algebra of all events up to time t. Because M_t is a martingale, so $E[\mathrm{d}M_t|\mathcal{F}_t] = 0$ which implies

$$E[\mathrm{d}\tilde{N}_t|\mathcal{F}_t] = \lambda(\psi_t)\,\mathrm{d}t$$

see [39].

Up until now the operator $a \in M_{2\times 2}$ was arbitrary. A particular simple case is if we take

$$a^* = a = \begin{pmatrix} 0 & 1 \\ 1 & 0 \end{pmatrix}.$$

Then $L(\rho_t) = a\rho_t a - \rho_t$ and so the intensity

$$\lambda(\psi_t) = \langle a^* a\rangle_t = \frac{\langle\psi_t|a^*a|\psi_t\rangle}{\langle\psi_t|\psi_t\rangle} = 1$$

which implies that $\tilde{N}_t = N_t$. Because there is no deterministic evolution (we do not have the Hamiltonian part and the jump rate is constant) so in this case we can put $g_1 = g_2 = 0$ and $f_1(\psi_t) = \psi_t^2 - \psi_t^1$, $f_2(\psi_t) = \psi_t^1 - \psi_t^2$ as the probability of a particular jump depends on the difference between ψ_t^1 and ψ_t^2. Thus we arrive at

$$\mathrm{d}\psi_t^i = f_i(\psi_{t^-})\,\mathrm{d}N_t.$$

Using the identity $\mathrm{d}[\psi^i, \psi^j]_t = f_i \bar{f}_j\,\mathrm{d}N_t$ we find that $\mathrm{d}\|\psi\|^2 = 0$ and $\mathrm{d}P_t = (aP_t a - P_t)\,\mathrm{d}N_t$. Taking the average we obtain $\dot{\rho}_t = a\rho_t a - \rho_t$, since $N_t - \lambda t$ is a martingale. The above stochastic differential equation admits the following solution:

$$\psi_t^1 = z_0^1 \frac{1+(-1)^{N_t}}{2} + z_0^2 \frac{1-(-1)^{N_t}}{2}$$
$$\psi_t^2 = z_0^1 \frac{1-(-1)^{N_t}}{2} + z_0^2 \frac{1+(-1)^{N_t}}{2}.$$

This implies that

$$P_t = x_0 \frac{1+(-1)^{N_t}}{2} + y_0 \frac{1-(-1)^{N_t}}{2}$$

where $x_0 = |\psi_0\rangle\langle\psi_0|$ and $y_0 = |\phi_0\rangle\langle\phi_0|$, $\phi_0 = (a + a^*)\psi_0 = (z_0^2,\ z_0^1)\prime$.

If we take

$$a = \begin{pmatrix} 0 & 1 \\ 0 & 0 \end{pmatrix}$$

as is usual in quantum optics problems, then we have

$$\lambda(\psi_t) = \frac{|\psi_t^2|^2}{\|\psi_t\|^2}.$$

So we need a point process whose rate function is random and the situation is slightly more complicated. We have to use the more general method described at the beginning of this paragraph.

Let us start with calculating functions g_i, which are responsible for the deterministic flow. They are obtained by taking the derivative of

$$\psi_s = \frac{\exp(-\frac{1}{2}sa^*a)\psi_t}{\|\exp(-\frac{1}{2}sa^*a)\psi_t\|}\|\psi_t\|$$

with respect to s and at the instant $s = 0$. So we get

$$g(\psi_t) = \tfrac{1}{2}(-a^*a + \langle a^*a\rangle_t)\psi_t.$$

It can be checked that the only functions f_i which lead to the Lindblad equation are of the following type,

$$f_1(\psi_t) = -\psi_t^1 + \sqrt{\langle\psi_t|\psi_t\rangle}\,\mathrm{e}^{\mathrm{i}h(\psi_t)} \qquad f_2(\psi_t) = -\psi_t^2$$

where $h : \mathbb{C}^2 \to \mathbb{R}$ is an arbitrary Lipschitz function. Let us point out that if we put $e^{ih} = \psi_t^2/|\psi_t^2|$ then we can write f in a compact form

$$f(\psi_t) = \left(\frac{a}{\sqrt{\langle a^* a\rangle_t}} - \mathbf{1}\right)\psi_t$$

see [39], but it needs a careful interpretation because zero can appear in the denominator. Again by simple calculations we find that $\mathrm{d}\|\psi_t\|^2 = 0$ and

$$\mathrm{d}P_t = \begin{pmatrix} |\psi_t^2|^2 & -\psi_t^1\bar{\psi}_t^2 \\ -\bar{\psi}_t^1\psi_t^2 & -|\psi_t^2|^2 \end{pmatrix}_- \mathrm{d}\tilde{N}_t + \frac{1}{2\langle\psi_t|\psi_t\rangle}\begin{pmatrix} 2|\psi_t^1|^2|\psi_t^2|^2 & \psi_t^1\bar{\psi}_t^2(|\psi_t^2|^2 - |\psi_t^1|^2) \\ \bar{\psi}_t^1\psi_t^2(|\psi_t^2|^2 - |\psi_t^1|^2) & -2|\psi_t^1|^2|\psi_t^2|^2 \end{pmatrix}\mathrm{d}t.$$

However, $\mathrm{d}\tilde{N}_t = \mathrm{d}M_t + \lambda(\psi_t)\,\mathrm{d}t$ so after averaging we get the quantum evolution equation for $\rho_t = E[P_t]$.

4. Global existence and uniqueness

After analysing a typical example of non-uniqueness in the pure quantum case, here we will return to the general EEQT scheme as described in section 2. Let T_t be a norm-continuous dynamical semigroup on states of the total algebra $\mathcal{A}_T$ corresponding to equation (5). We extend T_t by linearity to the whole predual space $\mathcal{A}_{T*}$, which is equal to $\mathcal{A}_T$, because the total algebra is finite-dimensional. Let E denote a space of all one-dimensional projectors in $\mathcal{A}_T$. Because $\mathcal{A}_T = \oplus_{\alpha=1}^{\alpha=m} M(n_\alpha \times n_\alpha)$ we obtain that $E = \dot{\cup}_\alpha \mathbb{C}P_\alpha$ and so E is a disjoint sum of compact differentiable manifolds (complex projective spaces in $\mathcal{H}_\alpha$). We would like to associate with T_t a homogeneous Markov–Feller process with values in E such that for every $x \in E$

$$T_t(P_x) = \int_E P(t, x, \mathrm{d}y)\,P_y \tag{16}$$

where $P(t, x, \mathrm{d}y)$ is the transition probability function for the process ξ_t and $y \to P_y$ is the tautological map, which assigns to every point $y \in E$ a one-dimensional projector P_y. This leads us to the following definition.

Definition. Let $\mathcal{M}(E)$ denote a Banach space of all complex, finite, Borel measures on E. We say that a positive and contractive semigroup $U_t : \mathcal{M}(E) \to \mathcal{M}(E)$ with a Feller transition function $P(t, x, \Gamma)$ is *associated* with T_t iff equation (16) is satisfied.

Let us describe this notion more precisely. Let π be a map between the two Banach spaces $\mathcal{M}(E)$ and $\mathcal{A}_{T*}$ given by

$$\pi(\mu) = \int_E \mu(\mathrm{d}x)\,P_x.$$

It is clear that π is linear, surjective, preserves positive cones and $\|\pi\| = 1$. An intuitive meaning of the map π is clear: every measure on one-dimensional projections of the total algebra defines an operator and every operator in the algebra decomposes into one-dimensional projections. This decomposition is non-unique, because of the non-uniqueness of the quantum decomposition of the unit, and $\ker\pi$ measures this non-uniqueness.

Proposition 1. U_t is associated with T_t iff $\ker\pi$ is U_t invariant and $\hat{U}_t = T_t$, where $\hat{U}_t$ is the quotient group of U_t by $\ker\pi$.

Proof. Let U_t be associated with T_t. It implies that

$$\int_E P(t,x,\mathrm{d}y)\,P_y = T_t(P_x)$$

thus for any $\mu_0 \in \ker\pi$ we have

$$\int_E (U_t\mu_0)(\mathrm{d}x)\,P_x = \int_E\int_E P(t,y,\mathrm{d}x)\,\mu_0(\mathrm{d}y)\,P_x = \int_E T_t(P_y)\mu_0(\mathrm{d}y)$$
$$= T_t\left[\int_E \mu_0(\mathrm{d}y)\,P_y\right] = 0$$

and so $U_t\mu_0 \in \ker\pi$. Moreover, $\forall\mu \in \mathcal{M}(E)$

$$\hat{U}_t\pi(\mu) = \pi(U_t\mu) = \int_E (U_t\mu)(\mathrm{d}y)P_y = \int_E\int_E P(t,x,\mathrm{d}y)\mu(\mathrm{d}x)P_y$$
$$= T_t\left[\int_E \mu(\mathrm{d}x)P_x\right] = T_t\pi(\mu).$$

Now let us assume that $\hat{U}_t = T_t$, i.e. $\forall\mu \in \mathcal{M}(E)$ we have $\hat{U}_t\pi(\mu) = T_t\pi(\mu)$. Let us take $\mu = \delta_x$. Then

$$\hat{U}_t\pi(\delta_x) = \pi(U_t\delta_x) = \int_E (U_t\delta_x)(\mathrm{d}y)\,P_y = \int_E\int_E P(t,z,\mathrm{d}y)\delta_x(\mathrm{d}z)P_y$$
$$= \int_E P(t,x,\mathrm{d}y)P_y$$

and $T_t\pi(\mu) = T_t(P_x)$ so $T_t(P_x) = \int_E P(t,x,\mathrm{d}y)P_y$. □

This means that to find U_t is to extend the semigroup T_t from $\mathcal{M}(E)/\ker\pi$ to $\mathcal{M}(E)$ in an invariant way. It should be emphasized that, in general, such an 'extension' may not exist or, if it exists, need not be unique. We show that in our case, under mild assumptions, the existence and the uniqueness can be proved.

Let us write the evolution equation for states in the Lindblad form

$$\dot{\rho} = -\mathrm{i}[H,\rho] + \sum_k V_k^*\rho V_k - \frac{1}{2}\left\{\rho, \sum_k V_k V_k^*\right\}$$

where $H = \mathrm{diag}(H_1,\ldots,H_m)$, $H_\alpha = H_\alpha^* \in M(n_\alpha \times n_\alpha)$ and V_k satisfy the following assumptions:

(a) $(V_k)_{\alpha\alpha} = 0$ for every k and α;

(b) if for some k,l,α,β $(V_k)_{\alpha\beta} \neq 0$ and $(V_l)_{\alpha\beta} \neq 0$ then $k = l$†.

We will now construct a Markov process on pure states of the total system, associated with the above master equation, and then prove its uniqueness. Because we can already guess the process from the infinitesimal argument of section 2, we start with the description of the generator of the semigroup U_t that describes the process.

Let A be a densely defined linear operator on $C(E)$ with $D(A) = C^1(E)$ given by

$$(Af)(x) = \sum_{\alpha\neq\alpha_0} c_\alpha(x)f(x_\alpha) - c(x)f(x) + v(x)f$$

† In general, we can allow for a weaker version: $(V_k)_{\alpha\beta} \neq 0$ and $(V_l)_{\alpha\beta} \neq 0 \Rightarrow \exists c \in \mathbb{C} : (V_k)_{\alpha\beta} = c(V_l)_{\alpha\beta}$, but this simply reduces to (b) above by the substitution $(\tilde{V}_k)_{\alpha\beta} := \sqrt{1+|c|^2}(V_k)_{\alpha\beta}$ and $(\tilde{V}_l)_{\alpha\beta} = 0$ for $k \neq l$.

where $x \in \mathbb{C}P_{\alpha_0}$, $c_\alpha(x) = \mathrm{Tr}(P_x W_{\alpha_0\alpha} W^*_{\alpha_0\alpha})$, $W_{\alpha_0\alpha} = \sum_k (V_k)_{\alpha_0\alpha} \in L(H_\alpha, \mathcal{H}_{\alpha_0})$, $W^*_{\alpha_0\alpha} = \sum_k (V_k)^*_{\alpha_0\alpha} \in L(\mathcal{H}_{\alpha_0}, H_\alpha)$, $c(x) = \sum_{\alpha\neq\alpha_0} c_\alpha(x)$, $P_{x_\alpha} = W^*_{\alpha_0\alpha} P_x W_{\alpha_0\alpha} / \mathrm{Tr}(P_x W_{\alpha 0\alpha} W^*_{\alpha_0\alpha}) \in \mathbb{C}P_\alpha$ and $x \to v(x)$ is a vector field on E given by

$$v(x) = -\mathrm{i}[H_{\alpha_0}, P_x] - \frac{1}{2}\left\{P_x, \sum_{\alpha\neq\alpha_0} W_{\alpha_0\alpha} W^*_{\alpha_0\alpha}\right\} + P_x \,\mathrm{Tr}\left(P_x \sum_{\alpha\neq\alpha_0} W_{\alpha_0\alpha} W^*_{\alpha_0\alpha}\right).$$

It may be easily checked that $v(x) \in T_x \mathbb{C}P_\alpha = T_x E$. Because

$$g_t(P_x) = \frac{\exp[t(-\mathrm{i}H_{\alpha_0} - \frac{1}{2}\sum_{\alpha\neq\alpha_0} W_{\alpha_0\alpha} W^*_{\alpha_0\alpha})] P_x \exp[t(\mathrm{i}H_{\alpha_0} - \frac{1}{2}\sum_{\alpha\neq\alpha_0} W_{\alpha_0\alpha} W^*_{\alpha_0\alpha})]}{\mathrm{Tr}(P_x \exp[-t\sum_{\alpha\neq\alpha_0} W_{\alpha_0\alpha} W^*_{\alpha_0\alpha}])}$$

is an integral curve for v, we have that v is a complete vector field.

Theorem 2. A is a generator of a strongly continuous positive semigroup of contractions S_t on $C(E)$.

Proof. $A = A_1 + A_2$, where $(A_1 f)(x) = \sum_{\alpha\neq\alpha_0} c_\alpha(x)\delta_{x_\alpha} f - c(x)\delta_x f$ and $A_2 = v$. It is clear that A_1 is a bounded and dissipative operator. It is also a dissipation, i.e. $A_1(f^2) \geqslant 2f A_1(f)$ for $f = \bar{f}$. Because A_2 generates a flow on E given by $f(x) \to f(g_t(x))$, where $g_t(x)$ is the integral curve of v starting at the point x, it follows that $A = A_1 + A_2$ is the generator of a strongly continuous semigroup of contractions (see, for example, [40]). Positivity follows from the Trotter product formula, since both A_1 and A_2 generate positive semigroups. □

Let $P(t, x, \Gamma)$ denote the transition function of S_t. It is clear that this is a Feller transition function [41].

Now prove that our process reproduces T_t.

Theorem 3. Let $(U_t\mu)(\Gamma) := \int_E P(t, x, \Gamma)\mu(\mathrm{d}x)$ for $\mu \in \mathcal{M}(E)$. Then U_t is associated with T_t.

The proof is given in the appendix. We can pass to the uniqueness problem. Let us consider a Markov pregenerator B_0 given by

$$(B_0 u)(x) = \sum_{ij} T^{ij}(x)(\partial_i\partial_j u)(x) + \sum_i V^i(x)(\partial_i u)(x) + \int_E \mu_0(x, \mathrm{d}y)u(y) - \mu_0(x, E)u(x) \tag{17}$$

where $(T^{ij}(x))$ form a positive matrix and $\mu_0(x, \mathrm{d}y)$ is a positive measure such that $\mu_0(x, \{x\}) = 0$ for every $x \in E$. Its domain $D(B_0)$ consists of C^∞-functions. It follows from the theory of Dirichlet forms that this is the most general form of a pregenerator of a Markov semigroup (see [42]).

Theorem 4. Let B be the operator closure of B_0. If B generates a Markov–Feller semigroup associated with T_t then $D(A) = D(B)$ and $A = B$.

The proof is given in the appendix. Thus we have the uniqueness. In the proof we used repeatedly the fact that our Hilbert spaces were finite-dimensional. In an infinite-dimensional case the problem is much harder and we have no rigorous result. Our intuition is shaped here only by the infinitesimal argument of section 3.

5. Conclusions

We have seen that the special class of couplings between a classical and a quantum system leads to a unique piecewise deterministic process on pure states of the total system that, after averaging, recovers the original master Liouville equation for statistical states. Irreversibility of the master equation describing time evolution of ensembles is reflected by going from potential to actual in the course of quantum jumps that accompany classical events. Why is this uniqueness result so interesting? During the roundtable discussions at the conference *Quantum Theory Without Observers*, held in Bielefeld in August 1995, the following wish was repeatedly expressed: 'in a complete quantum theory all should be in the equations, nothing relegated to the background.' Although this statement was made in particular reference to the consistent histories approach to quantum measurement theory, it applied as well to the problem of quantum mechanical descriptions of individual quantum systems. The necessity of having such a description became increasingly apparent as progress in technology enabled us to perform continuous observations of individual atoms. Quantum opticians were among the first to propose and to look for the philosophical consequences of stochastic algorithms reproducing a given master equation (ME). It soon became apparent that not all is in the equations. As we have illustrated in section 3 there are infinitely many different algorithms that, after averaging, lead to the same ME. Yet, in each case, Nature chooses only one of them. Our position is that the only way to have all in the equation is by admitting explicitly the classical nature of part of the experimental set-up—according to Bohr's philosophy. We interpret the results of the present paper as confirming that this is, indeed, the case.

One may ask what are the possible implications of EEQT in general, and of the uniqueness theorem in particular? One of the simplest applications that is already worked out is in the solution of Mielnik's 'waiting screen problem' [43]. As shown in [11] the long standing problem of the time of arrival observable in quantum theory (cf [44] for a recent review) finds a simple solution within EEQT. Moreover, in [45] a relativistic formulation of the event generating algorithm has been given. The uniqueness theorem of the present paper applies also to this relativistic generalization—provided time is replaced by proper time.

Our results may be compared to those obtained by Diosi [26]. As noted in the introduction his 'ortho-process', using only the quantum master equation, although canonical (in cases where there is no infinite-dimensional degeneracy) is *not* unique. It is, however, interesting to observe that if the method by Diosi is generalized and extended to a hybrid classical + quantum system then his prescription coincides with our process. This is not a surprise because, as we have proven in this paper, our process *is* a unique one for the total system.

That is all fine and good, but the natural question arises: what *is* classical? There are several options possible when answering this question. First of all the theory may be considered as phenomenological—then we choose as classical that part of the measurement apparatus (or observer) whose quantum nature is simply irrelevant for the given problem. Second, we may think of superselection quantities [46, 47] as truly classical variables. Some of them may play an important role in the dynamics of the measurement process—this remains for a while just a hypothesis. It is to be noted that Jibu and Yasue (cf [48], especially the last section 'Quantum measurement by quantum brain' puts forward a similar hypothesis in relation to the possible role of microtubules in the quantum dynamics of consciousness.

Finally, a careful reader certainly noticed that in the formalism of EEQT one never really needs C to be a *classical* system. It can be a quantum system as well. What is important

is that the the Liouville evolution preserves the diagonal of C. Thus the end product of the decoherence program [49–51] can be directly fed into the EEQT event engine. The uniqueness result above will be immediately relevant in this case also.

Acknowledgments

The early version of this paper was written when one of us (AJ) was visiting RIMS, Kyoto University. Thanks are due to Professor H Araki and for his kind hospitality and to the Japanese Ministry of Education for the extended support. RO acknowledges support of the Polish KBN grant No 2P30205707. AJ is also grateful for the support of the A von Humboldt Foundation. He also thanks L Knight for reading parts of the manuscript. We thank Professor Ph Blanchard for many discussions, encouragement and hospitality at BiBoS. Last but not least we thank to the anonymous referee for his criticism which allowed us to improve the presentation and to make more clear several points.

Appendix

A.1. Proof of theorem 3

At first we show that $\forall x \in E$

$$L(P_x) = [A(P)](x) \tag{18}$$

where L is the generator of T_t, A is the generator of S_t and $P : x \to P_x$.

Let $x \in \mathbb{C}P_{\alpha_0}$. In $\mathcal{H} = \oplus_{\alpha=1}^{m}\mathcal{H}_\alpha$ let us choose any orthonormal basis $\{e_{\alpha,i_\alpha}\}_{i_\alpha=1,\ldots,n_\alpha}^{\alpha=1,\ldots,m}$, for which $e_{\alpha,i_\alpha} \in \mathcal{H}_\alpha$. Obviously, for any $P_x \in \mathcal{A}_{T*}\langle e_{\alpha,i_\alpha}|L(\rho)|e_{\beta,i_\beta}\rangle = 0$ for $\alpha \neq \beta$ and the same is true for $[A(P)](x)$. So it is enough to evaluate the $(\beta, i_\beta, j_\beta)$th matrix elements of both sides of equation (18):

$$\begin{aligned}
\langle e_{\beta,i_\beta}|[A(P)](x)|e_{\beta,j_\beta}\rangle &= \sum_{\alpha\neq\alpha_0} \mathrm{Tr}(P_x W_{\alpha_0\alpha} W^*_{\alpha_0\alpha}) \frac{\langle e_{\beta,i_\beta}|W^*_{\alpha_0\alpha} P_x W_{\alpha_0\alpha}|e_{\beta,j_\beta}\rangle}{\mathrm{Tr}(P_x W_{\alpha_0\alpha} W^*_{\alpha_0\alpha})} \\
&\quad - \sum_{\alpha\neq\alpha_0} \mathrm{Tr}(P_x W_{\alpha_0\alpha} W^*_{\alpha_0\alpha})\langle e_{\beta,i_\beta}|P_x|e_{\beta,j_\beta}\rangle \\
&\quad + \langle e_{\beta,i_\beta}|\Bigg(-\mathrm{i}[H_{\alpha_0}, P_x] - \frac{1}{2}\Bigg\{P_x, \sum_{\alpha\neq\alpha_0} W_{\alpha_0\alpha} W^*_{\alpha_0\alpha}\Bigg\} \\
&\quad + P_x\,\mathrm{Tr}\Bigg(P_x \sum_{\alpha\neq\alpha_0} W_{\alpha_0\alpha} W^*_{\alpha_0\alpha}\Bigg)\Bigg)|e_{\beta,j_\beta}\rangle = \langle e_{\beta,i_\beta}|W^*_{\alpha_0\beta} P_x W_{\alpha_0\beta}|e_{\beta,j_\beta}\rangle \\
&\quad + \delta_{\alpha_0\beta}\langle e_{\beta,i_\beta}|\Bigg(-\mathrm{i}[H_{\alpha_0}, P_x] - \frac{1}{2}\Bigg\{P_x, \sum_{\alpha\neq\alpha_0} W_{\alpha_0\alpha} W^*_{\alpha_0\alpha}\Bigg\}\Bigg)|e_{\beta,j_\beta}\rangle.
\end{aligned} \tag{19}$$

On the other hand, the βth component of $L(P_x)$

$$\begin{aligned}
(L(P_x))_\beta &= \sum_k (V_k)^*_{\alpha_0\beta} P_x (V_k)_{\alpha_0\beta} + \delta_{\alpha_0\beta} - \Bigg(\mathrm{i}[H_{\alpha_0}, P_x] + \frac{1}{2}\Bigg\{P_x, \sum_{k,\alpha}(V_k)_{\beta\alpha}(V_k)^*_{\beta\alpha}\Bigg\}\Bigg) \\
&= W^*_{\alpha_0\beta} P_x W_{\alpha_0\beta} + \delta_{\alpha_0\beta}\Bigg(-\mathrm{i}[H_{\alpha_0}, P_x] - \frac{1}{2}\Bigg\{P_x, \sum_{\alpha\neq\alpha_0} W_{\alpha_0\alpha} W^*_{\alpha_0\alpha}\Bigg\}\Bigg)
\end{aligned} \tag{20}$$

where the last equality holds owing to assumptions (a) and (b) above. Taking the $(\beta, i_\beta, j_\beta)$th matrix element of (20) we see that it coincides with (19), thus, due to arbitrariness of $(\beta, i_\beta, j_\beta)$, we have proved equation (18).

Let F denote the finite-dimensional space of functions generated by $x \to \langle\psi|P_x|\phi\rangle$. It is clear that $F = \{f : f(x) = \mathrm{Tr}(AP_x), A \in \mathcal{A}_T\}$. So $\dim F = \dim \mathcal{A}_T$. We show that F is the null space for $\ker \pi$. Let $f(x) = \sum_{i,j}\langle\psi_i|P_x|\psi_j\rangle$ and let $\mu_0 \in \ker \pi$. Then

$$\mu_0(f) = \int \mu_0(\mathrm{d}x)\, f(x) = \sum_{i,j}\langle\psi_i| \int \mu_0(\mathrm{d}x)\, P_x|\psi_j\rangle = 0.$$

Moreover, because $(A\langle\psi_i|P|\psi_j\rangle)(x) = \langle\psi_i|L(P_x)|\psi_j\rangle$ we have that $A : F \to F$ and so $S_t : F \to F$. This implies that $U_t : \ker\pi \to \ker\pi$ since $U_t\mu(f) = \mu(S_t f)$. Let $\hat{U}_t$ be the quotient semigroup. Then

$$\lim_{t\to 0}\frac{1}{t}[\hat{U}_t(P_x) - P_x] = \lim_{t\to 0}\frac{1}{t}[\pi(U_t\delta_x) - P_x]$$
$$= \lim_{t\to 0}\frac{1}{t}\left(\int\int P(t,z,\mathrm{d}y)\,\delta_x(\mathrm{d}z)\,P_y - P_x\right) = (AP)(x) = L(P_x)$$

so $\hat{U}_t$ and T_t have the same generator and thus coincide. By proposition 1 U_t is associated with T_t. □

A.2. Proof of theorem 4

At first we show the following lemma.

Lemma 1. $(V_k)_{\alpha\alpha} = 0 \Rightarrow \forall\alpha \in \{1,\ldots,m\}\,\forall x, y \in \mathbb{C}P_\alpha$ such that $P_x \perp P_y$ the equality $\mathrm{Tr}[P_y L(P_x)] = 0$ is satisfied.

Proof. Let $x, y \in \mathbb{C}P_\alpha$ and $P_x \perp P_y$. Then

$$\mathrm{Tr}[P_y L(P_x)] = -\mathrm{i}\,\mathrm{Tr}(P_y[H_\alpha, P_x]) + \sum_k \mathrm{Tr}[P_y(V_k^* P_x V_k)_{\alpha\alpha}]$$
$$-\frac{1}{2}\sum_k \mathrm{Tr}[P_y\{P_x, (V_k V_k^*)_{\alpha\alpha}\}] = \sum_k \mathrm{Tr}[P_y(V_k^* P_x V_k)_{\alpha\alpha}].$$

But

$$(V_k^* P_x V_k)_{\alpha\alpha} = (V_k)^*_{\alpha\alpha} P_x (V_k)_{\alpha\alpha} = 0$$

so the assertion follows. □

We are now in position to show that the diffusion part is necessarily zero.

Lemma 2. $T^{ij}(x) \equiv 0$ for every i, j.

Proof. Because

$$B[\mathrm{Tr}(P_y P)](x) = \mathrm{Tr}[P_y L(P_x)]$$

so, by the above lemma, for every α and every $x, y \in \mathbb{C}P_\alpha$ such that $P_y \perp P_x$ we have that $B[\mathrm{Tr}(P_y P)](x) = 0$. Let us denote the function $z \to \mathrm{Tr}(P_y P_z)$ by $f_y(z)$. Then, becuse f_y is a smooth function,

$$(B_0 f_y)(x) = \int_{\mathbb{C}P_\alpha} \mu_0(x, \mathrm{d}z)\, f_y(z) + \sum_{ij} T^{ij}(x)(\partial_i\partial_j f_y)(x) + \sum_i V^i(x)(\partial_i f_y)(x).$$

Because f_y possesses a minimum at point x, so $\sum_i V^i(x)(\partial_i f_y)(x) = 0$ and we arrive at

$$\int_{\mathbb{C}P_\alpha} \mu_0(x, \mathrm{d}z)\, f_y(z) + \sum_{ij} T^{ij}(x)(\partial_i\partial_j f_y)(x) = 0.$$

But $(\partial_i \partial_j f_y(x))$ and $(T^{ij}(x))$ are positive matrices so, by Schur's lemma, $(T^{ij}(x)\partial_i \partial_j f_y(x))$ is also a positive matrix. It follows that

$$\sum_{ij} T^{ij}(x)\partial_i \partial_j f_y(x) = 0.$$

Now let us introduce a chart at point x, say, $x = [(1, 0, \ldots, 0)]$, (U_0, ϕ_0) such that

$$U_0 = \left\{ [(z_0, z_1, \ldots, z_{n-1})] : z_i \in \mathbb{C}, \sum_i |z_i|^2 = 1, z_0 \neq 0 \right\}$$

$$\phi_0[(z_0, z_1, \ldots, z_{n-1})] = \left(\frac{z_1}{z_0}, \ldots, \frac{z_{n-1}}{z_0} \right) = (x_1, y_1, \ldots, x_{n-1}, y_{n-1})$$

where $x_i = \mathrm{Re}(z_i/z_0)$, $y_i = \mathrm{Im}(z_i/z_0)$. Then $\phi_0(x) = \mathbf{0} \in \mathbb{R}^{2(n-1)}$. Let us choose $y = [(0, 1, 0, \ldots, 0)]$. It is clear that $P_y \perp P_x$ and so

$$\sum_{i,j=1}^{n-1} \left[T^{ij}_{x,x}(x) \frac{\partial^2 (f_y \circ \phi_0^{-1})}{\partial x_i \partial x_j}(\mathbf{0}) + 2T^{ij}_{x,y}(x) \frac{\partial^2 (f_y \circ \phi_0^{-1})}{\partial x_i \partial y_j}(\mathbf{0}) + T^{ij}_{y,y}(x) \frac{\partial^2 (f_y \circ \phi_0^{-1})}{\partial y_i \partial y_j}(\mathbf{0}) \right] = 0.$$

But for every $j \geqslant 2$ we have

$$\frac{\partial^2 (f_y \circ \phi_0^{-1})}{\partial x_j^2}(\mathbf{0}) = \lim_{h \to \infty} \frac{1}{h} \left[\frac{\partial (f_y \circ \phi_0^{-1})}{\partial x_j}(0, \ldots, x_j = h, 0, \ldots, 0) - \frac{\partial (f_y \circ \phi_0^{-1})}{\partial x_j}(\mathbf{0}) \right] = 0.$$

In the same way we prove that for every $j \geqslant 2$

$$\frac{\partial^2 (f_y \circ \phi_0^{-1})}{\partial y_j^2}(\mathbf{0}) = 0.$$

By positivity of the matrix $D^2(f_y \circ \phi_0^{-1})(\mathbf{0})$ we obtain that

$$T^{11}_{x,x}(x) \frac{\partial^2 (f_y \circ \phi_0^{-1})}{\partial x_1^2}(\mathbf{0}) + 2T^{11}_{x,y}(x) \frac{\partial^2 (f_y \circ \phi_0^{-1})}{\partial x_1 \partial y_1}(\mathbf{0}) + T^{11}_{y,y}(x) \frac{\partial^2 (f_y \circ \phi_0^{-1})}{\partial y_1^2}(\mathbf{0}) = 0.$$

Let λ be an embedding $\lambda : \mathbb{C}P^1 \to \mathbb{C}P_\alpha$ given by

$$\lambda[(z_0, z_1)] = [(z_0, z_1, 0, \ldots, 0)].$$

It is clear that $x = \lambda(\boldsymbol{n}_0)$ and $y = \lambda(\boldsymbol{n})$ for some unique $\boldsymbol{n}_0, \boldsymbol{n} \in \mathbb{C}P^1 = S^2$. Let ψ_0 be a chart at $\boldsymbol{n}_0$ given by

$$\psi_0 : \mathbb{C}P^1 - \{\boldsymbol{n}\} \to \mathbb{C} \qquad \psi_0(\boldsymbol{m}) = p \circ \phi_0 \circ \lambda(\boldsymbol{m})$$

where $p = \mathbb{C}^n \to \mathbb{C}$ is the projection onto the first coordinate. So we may write that

$$a^{11}(\boldsymbol{n}_0) \frac{\partial^2 (f_{\boldsymbol{n}} \circ \psi_0^{-1})}{\partial q_1^2}(\mathbf{0}) + 2a^{12}(\boldsymbol{n}_0) \frac{\partial^2 (f_{\boldsymbol{n}} \circ \psi_0^{-1})}{\partial q_1 \partial q_2}(\mathbf{0}) + a^{22}(\boldsymbol{n}_0) \frac{\partial^2 (f_{\boldsymbol{n}} \circ \psi_0^{-1})}{\partial q_2^2}(\mathbf{0}) = 0$$

where $a^{11}(\boldsymbol{n}_0) = T^{11}_{x,x}(x)$, $a^{12}(\boldsymbol{n}_0) = T^{11}_{x,y}(x)$, $a^{22}(\boldsymbol{n}_0) = T^{11}_{y,y}(x)$ and $q_1(\boldsymbol{m}) = x_1(\lambda(\boldsymbol{m}))$, $q_2(\boldsymbol{m}) = y_1(\lambda(\boldsymbol{m}))$. Let us change the chart ψ_0 onto spherical coordinates (θ, φ), $0 \leqslant \theta \leqslant \pi$, $0 \leqslant \varphi \leqslant 2\pi$ in such a way that $\theta(\boldsymbol{n}_0) = \pi/2$, $\varphi(\boldsymbol{n}_0) = 0$, i.e. $\boldsymbol{n}_0 = (1, 0, 0)$ and $\theta(\boldsymbol{n}) = \pi/2$, $\varphi(\boldsymbol{n}) = \pi$, i.e. $\boldsymbol{n} = (-1, 0, 0)$. Because

$$f_{\boldsymbol{n}}(\boldsymbol{m}) = \mathrm{Tr}(P_{\boldsymbol{n}} P_{\boldsymbol{m}}) = \tfrac{1}{2}(1 + \langle \boldsymbol{n}, \boldsymbol{m} \rangle) = \tfrac{1}{2}(1 - \sin\theta \cos\varphi)$$

so

$$\frac{\partial^2 f_{\boldsymbol{n}}}{\partial \theta \partial \varphi}(\boldsymbol{n}_0) = 0 \qquad \frac{\partial^2 f_{\boldsymbol{n}}}{\partial \theta^2}(\boldsymbol{n}_0) = \frac{\partial^2 f_{\boldsymbol{n}}}{\partial \varphi^2}(\boldsymbol{n}_0) = \frac{1}{2}$$

which implies that $\tilde{a}^{11}(\boldsymbol{n}_0) = \tilde{a}^{12}(\boldsymbol{n}_0) = \tilde{a}^{22}(\boldsymbol{n}_0) = 0$, where $\tilde{a}^{ij}$ are the coefficients in the chart (θ, φ). But it is equivalent to

$$T^{11}_{x,x}(x) = T^{11}_{x,y}(x) = T^{11}_{y,y}(x) = 0.$$

Changing $y = [(0, 1, 0, \ldots, 0)]$ into $y = [(0, 0, 1, 0, \ldots, 0)]$ we obtain that

$$T^{22}_{x,x}(x) = T^{22}_{x,y}(x) = T^{22}_{y,y}(x) = 0$$

and so on. Thus, by the positivity, $T^{ij}(x) = 0$ for every i, j. Because x was arbitrary the assertion follows. □

From the above lemma we conclude that the generator B is the closure of

$$B_0 u(x) = V(x)u + \int_E \mu_0(x, \mathrm{d}y)\, u(y) - \mu_0(x, E)u(x).$$

Lemma 3. Let X be a tangent vector to $\mathbb{C}P_\alpha$ at point P_x. Then $P_x + X \geqslant 0 \Leftrightarrow X = 0$.

Proof. Because $X \in T_x\mathbb{C}P_\alpha$ so $P_x X + X P_x = X$. This implies that $P_x X P_x = 0$ and $P_x^\perp X P_x^\perp = 0$, where $P_x^\perp = I - P_x$. Therefore, in a basis $P_x\mathcal{H} \oplus P_x^\perp\mathcal{H}X$ is of the form $\begin{pmatrix} 0 & X^* \\ X & 0 \end{pmatrix}$. So $P_x + X$ is a positive matrix if and only if $X = 0$. □

Lemma 4. $B_0 = A|_{C^\infty}$.

Proof. Because A and B are generators of semigroups which are associated with T_t, for every $x \in E$ we have that $[(B - A)P](x) = 0$. Let $x \in \mathbb{C}P_{\alpha_0}$. Then

$$V(x)P + \sum_{\alpha=1}^{m} \int_{\mathbb{C}P_\alpha} \mu_{0,\alpha}(x, \mathrm{d}y)\, P_y - \mu_0(x, E)P_x - \sum_{\alpha \neq \alpha_0} c_\alpha(x) P_{x_\alpha} + c(x)P_x - v(x)P = 0$$

where $\mu_{0,\alpha}(x, \mathrm{d}y)$ denotes the restriction of $\mu_0(x, \mathrm{d}y)$ onto $\mathbb{C}P_\alpha$. It is an operator valued equation so it has to be satisfied for every α separately. So for any $\alpha \neq \alpha_0$ we get

$$\int_{\mathbb{C}P_\alpha} \mu_{0,\alpha}(x, \mathrm{d}y)\, P_y = c_\alpha(x) P_{x_\alpha}$$

which implies that $\mu_{0,\alpha}(x, \mathrm{d}y) = c_\alpha(x)\delta(x_\alpha)(\mathrm{d}y)$. For α_0 we have

$$\int_{\mathbb{C}P_{\alpha_0}} \mu_{0,\alpha_0}(x, \mathrm{d}y)\, P_y - \mu_0(x, E)P_x + c(x)P_x + V(x) - v(x) = 0.$$

Let us introduce $a(x) = c(x) - \mu_0(x, E)$ and $w(x) = V(x) - v(x)$. Then taking the trace of the above equation we obtain $a(x) \leqslant 0$. Let us assume that $a(x) < 0$. This implies that

$$\frac{1}{|a(x)|} \int_{\mathbb{C}P_{\alpha_0}} \mu_{0,\alpha_0}(x, \mathrm{d}y)\, P_y = P_x - \frac{1}{|a(x)|} w(x).$$

The left-hand side of the above equation gives a positive operator and $w(x) \in T_x\mathbb{C}P_{\alpha_0}$ so, by lemma 3, $w(x) = 0$. Thus we arrive at the contradiction because $\mu_{0,\alpha_0}(x, \{x\}) = 0$. So $a(x) = 0$ and we obtain that

$$\int_{\mathbb{C}P_{\alpha 0}} \mu_{0,\alpha 0}(x, \mathrm{d}y) P_y + w(x) = 0.$$

Evaluating the trace we get that $\mu_{0,\alpha_0}(x, \mathbb{C}P_{\alpha_0}) = 0$. Because it is a positive measure it vanishes on every Borel subset of $\mathbb{C}P_{\alpha_0}$. So $w(x) = 0$ too and hence $A|_{C^\infty} = B_0$. □

Because B is the closure of B_0 and $C^\infty(E)$ is a core for A, $D(A) = D(B)$ and $A = B$. This ends the proof of theorem 4. □

References

[1] Gorini V, Kossakowski A and Sudarshan E C G 1976 Completely positive dynamical semigroups of N-level systems *J. Math. Phys.* **17** 821–5

[2] Lindblad G 1976 On the generators of quantum mechanical semigroups *Comm. Math. Phys.* **48** 119–30

[3] von Neumann J 1955 *Mathematical Foundations of Quantum Mechanics* (Princeton, NJ: Princeton University Press)

[4] Gell-Mann M 1994 *The Quark and the Jaguar* (New York: W H Freeman and Co)

[5] Bell J 1989 Towards an exact quantum mechanics *Themes in Contemporary Physics II Essays in Honor of Julian Schwinger's 70th Birthday* ed S Deser and R J Finkelstein (Singapore: World Scientific)

[6] Bell J 1990 Against measurement, sixty-two years of uncertainty. Historical, philosophical and physical inquiries into the foundations of quantum mechanics *Proc. NATO Advanced Study Institute (August 5–15, Erice) (NATO ASI Series B 226)* ed A I Miller (New York: Plenum)

[7] Paz J P, Habib S and Zurek W 1993 Reduction of the wave packet through decoherence *Phys. Rev.* D **47** 488

[8] Peres A 1995 Relativistic quantum measurements, fundamental problems of quantum theory *Ann. NY. Acad. Sci.* **755**

[9] Ballentine L.E 1990 Limitations of the projection postulate *Found. Phys.* **20** 1329–43

[10] Kärtner F X and Haus H A 1993 Quantum non-demolition measurements and the collapse of the wave function *Phys. Rev.* A **47** 4585–92

[11] Blanchard Ph and Jadczyk A 1997 Time of events in quantum theory *Helv. Phys. Acta* **69** 613–35

[12] Cook R J 1988 What are quantum jumps *Phys. Scr.* T **21** 49–51

[13] Carmichael H 1993 *An Open Systems Approach to Quantum Optics (Lecture Notes in Physics 18*) (Berlin: Springer)

[14] Dalibard J, Castin Y and Mølmer K 1992 Wave-function approach to dissipative processes in quantum optics *Phys. Rev. Lett.* **68** 580–3

[15] Mølmer K, Castin Y and Dalibard J 1993 Monte Carlo wave-function method in quantum optics *J. Opt. Soc. Am.* B **10** 524–38

[16] Dum R, Zoller P and Ritsch H 1992 Monte Carlo simulation of the atomic master equation for spontaneous emission *Phys. Rev.* A **45** 4879–87

[17] Gardiner C W, Parkins A S and Zoller P Wave-function quantum stochastic differential equations and quantum-jump simulation methods *Phys. Rev.* A **46**

[18] Gisin N. 1984 Quantum measurements and stochastic processes *Phys. Rev. Lett.* **52** 1657–60

[19] Gisin N 1989 Stochastic quantum dynamics and relativity *Helv. Phys. Acta* 363–71

[20] Diosi L 1988 Quantum stochastic processes as models for state vector reduction *J. Phys. A: Math. Gen.* **21** 2885–98

[21] Diosi L 1989 Models for universal reduction of macroscopic quantum fluctuations *Phys. Rev.* A **40** 1165–74

[22] Pearle P 1989 Combining stochastic state-vector reduction with spontaneous localization *Phys. Rev.* A **39** 2277–89

[23] Wiseman H M and Milburn G J 1993 Interpretation of quantum jump and diffusion processes illustrated on the Bloch sphere *Phys. Rev.* A **47** 1652–66

[24] Garraway B M and Knight P L 1994 Comparison of quantum-state diffusion and quantum-jump simulations of two-photon processes in a dissipative environment *Phys. Rev.* A **49** 1266–74

[25] Gisin N, Knight P L, Percival I C, Thompson R C and Wilson D C 1993 Quantum state diffusion theory and a quantum jump experiment *J. Mod. Opt.* **40** 1663–7

[26] Diosi L 1986 Stochastic pure state representations for open quantum systems *Phys. Lett.* **114A** 451–4

[27] Ghirardi G, Grassi R and Rimini A 1990 Continuous spontaneous reduction model involving gravity *Phys. Rev.* A **42** 1057–64

[28] Pearle P 1995 True collapse and false collapse *Preprint*

[29] Pearle P and Squires E 1995 Gravity, energy conservation and parameter values in collapse models *Preprint*

[30] Stapp H P The integration of mind into physics. In opus cite under [8]

[31] Hameroff S and Penrose R Orchestrated reduction of quantum coherence in brain microtubules: model for consciousness *Toward a Science of Consciousness—The First Tucson Discussions and Debates* ed S R Hameroff, A Kaszniak and A C Scott (Cambridge, MA: MIT Press) (in press)

[32] Nanopoulos D V 1995 Theory of brain function, quantum mechanics and superstrings *Preprint* CERN-TH/95-128

[33] Blanchard Ph and Jadczyk A 1995 Event-enhanced-quantum theory and piecewise deterministic dynamics *Ann. Phys., Lpz.* **4** 583–99

[34] Partasarathy K R 1992 *An Introduction to Quantum Stochastic Calculus* (Bassel: Birkhäuser)
[35] Gisin N 1989 Stochastic quantum dynamics and relativity *Helv. Phys. Acta* **62** 363–71
[36] Protter P 1990 *Stochastic Integration and Differential Equations. A New Approach* (Berlin: Springer)
[37] Jacod J and Shiryaev A N 1987 *Limit Theorems for Stochastic Processes* (Berlin: Springer)
[38] Barchielli A 1994 Some stochastic differential equations in quantum optics and measurement theory: the case of counting processes *Stochastic Evolution of Quantum States in Open Systems and in Measurement Processes* ed L Diosi and B Lucacs (Singapore: World Scientific)
[39] Barchielli A and Belavkin V P 1991 Measurements continuous in time and a posteriori states in quantum mechanics *J. Phys. A: Math. Gen.* **24** 1495–514
[40] Goldstein J A 1985 *Semigroups of Linear Operators and Applications* (Oxford: Oxford University Press)
[41] Dynkin E 1965 *Markov Processes* (Berlin: Springer)
[42] Ma Z M and Röckner M 1992 *An Introduction to the Theory of (Nonsymmetric) Dirichlet Forms* (New York: Springer)
[43] Mielnik B 1994 The screen problem *Found. Phys.* **24** 1113–29
[44] Muga J G, Brouard S and Macias D 1995 Time of arrival in quantum mechanics *Ann. Phys.* **240** 351–66
[45] Blanchard Ph and Jadczyk A 1996 Relativistic quantum events *Found. Phys.* **26** 1669–81
[46] Amman A 1991 Chirality: A superselection rule generated by the molecular environment *J. Math. Chem.* **6** 1–15
[47] Landsman N P 1997 Observation and superselection in quantum mechanics *Stud. Hist. Phil. Mod. Phys.* to appear
[48] Jibu M and Yasue K 1994 Quantum measurement by quantum brain *Stochasticity and Quantum Chaos, Proc. 3rd Max Born Symp.* ed Z Haba *et al* (Dordrecht: Kluwer)
[49] Zurek W 1991 Decoherence and the transition from quantum to classical *Physics Today* October, 36–45
[50] Zurek W 1993 Preferred states, predictability, classicality and the environment-induced decoherence *Prog. Theor. Phys.* **89** 281–312
[51] See also the review paper of J J Halliwell in the opus cited under [30]

Burgers' flows as Markovian diffusion processes

Piotr Garbaczewski, Grzegorz Kondrat, and Robert Olkiewicz
Institute of Theoretical Physics, University of Wrocław, PL-50 204 Wrocław, Poland
(Received 2 April 1996; revised manuscript received 13 August 1996)

We analyze the unforced and deterministically forced Burgers equation in the framework of the (diffusive) interpolating dynamics that solves the so-called Schrödinger boundary data problem for random matter transport. This entails an exploration of the consistency conditions that allow one to interpret dispersion of passive contaminants in Burgers flow as a Markovian diffusion process. In general, the usage of a continuity equation $\partial_t\rho=-\vec{\nabla}(\vec{v}\rho)$, where $\vec{v}=\vec{v}(\vec{x},t)$ stands for the Burgers field and ρ is the density of transported matter, is at variance with the explicit diffusion scenario. Under these circumstances, we give a complete characterization of the diffusive transport that is governed by Burgers velocity fields. The result extends both to the approximate description of the transport driven by an incompressible fluid and to motions in an infinitely compressible medium. Also, in conjunction with the Born statistical postulate in quantum theory, it pertains to the probabilistic (diffusive) counterpart of the Schrödinger picture quantum dynamics. We give a generalization of this dynamical problem to cases governed by nonconservative force fields when it appears indispensable to relax the gradient velocity field assumption. The Hopf-Cole procedure has been appropriately generalized to yield solutions in that case. [S1063-651X(97)04302-X]

PACS number(s): 02.50.−r, 05.20.−y, 03.65.−w, 47.27.−i

I. BURGERS VELOCITY FIELDS AND THE RELATED STOCHASTIC TRANSPORT PROCESSES

The Burgers equation [1,2] recently has acquired considerable popularity in a variety of physical contexts [3–20]. An exhaustive discussion of its role in acoustic turbulence and gravitational contexts, where the emergence of shock pressure fronts is crucial, can be found in Ref. [17].

As is well known, the logarithmic Hopf-Cole transformation [2] allows one to replace the nonlinear problem (nonlinear diffusion equation [1]) by a linear parabolic equation. Because of this equivalence all gradient-type solutions of the Burgers equation are known exactly.

At the moment we shall preserve the gradient form restriction for Burgers velocity fields, but consider a more general form of the Burgers equation that accounts for an external force field $\vec{F}(\vec{x},t)$:

$$\partial_t\vec{v}+(\vec{v}\cdot\vec{\nabla})\vec{v}=\nu\Delta\vec{v}+\vec{F}(\vec{x},t). \tag{1}$$

Let us mention that many recent investigations were devoted to the analysis of $\mathrm{curl}\vec{v}=\vec{0}$ solutions that are statistically relevant in view of the random initial data choice and/or inclusion of the random forcing term (the random potential in the related Parisi-Kardar equation [11]).

However, irrespective of whether we do or do not need the statistical input, an issue of matter transport driven by those nonlinear velocity fields requires the knowledge of an exact evolution of concentration and/or density fields, much in the spirit of early hydrodynamical studies of advection and diffusion of passive tracers [21,22]; see also [23]. This particular issue is addressed in the present paper, under a simplifying assumption of nonrandom initial data and deterministic force fields.

Following the traditional motivation (applicable both to incompressible and infinitely compressible liquids [1]), we regard the stochastic diffusion process as a primary phenomenon responsible for the emergence of Eq. (1) and thus justifying the ''nonlinear diffusion equation'' phrase in this context.

Knowing the Burgers velocity fields, one is tempted to ask what is the particular dynamics (of matter or probability density fields) that is consistent with the chosen Burgers velocity field evolution. The corresponding passive scalar (tracer or contaminant) advection-in-a-flow problem [14,11,16] is normally introduced through the parabolic dynamics:

$$\partial_t T+(\vec{v}\cdot\vec{\nabla})T=\nu\Delta T; \tag{2}$$

see, e.g., [21–23]. For incompressible fluids, Eq. (2) coincides with the conventional Fokker-Planck equation for the diffusion process. This feature does not persist in the compressible case.

While looking for the stochastic implementation of the microscopic (molecular) dynamics, Eq. (2) [11,16,23,24], it is assumed that the ''diffusing scalar'' (contaminant in the lore of early statistical turbulence models) obeys an Itô equation:

$$d\vec{X}(t)=\vec{v}(\vec{x},t)dt+\sqrt{2\nu}d\vec{W}(t), \tag{3}$$

$$\vec{X}(0)=\vec{x}_0\rightarrow\vec{X}(t)=\vec{x},$$

where the given forced Burgers velocity field is perturbed by the noise term representing a molecular diffusion. In the (by now conventional) Itô representation of diffusion-type random variable $\vec{X}(t)$ one explicitly refers to the standard Brownian motion (e.g., the Wiener process) $\sqrt{2\nu}\vec{W}(t)$, instead of the usually adopted formal white noise integral $\int_0^t\vec{\eta}(s)ds$, coming from the Langevin-type version of Eqs. (3).

Under these premises, while taking for granted that *there is* a diffusion process involved, we cannot view Eqs. (1)–(3) as completely independent (disjoint) problems: the velocity field $\vec{v}$ cannot be quite arbitrarily inferred from Eq. (1) or any other velocity-defining equation without verifying the *consistency* conditions, which would allow one to associate Eqs. (2) and (3) with a well defined random dynamics, and Markovian diffusion in particular [25,26].

In connection with the usage of Burgers velocity fields (with or without external forcing), which in Eqs. (3) clearly are intended to replace the standard *forward drift* of the would-be involved Markov diffusion process, we have not found in the literature any attempt to resolve apparent contradictions arising if Eqs. (2) and/or (3) are defined by means of Eq. (1). In particular, the usage of a continuity equation $\partial_t\rho=-\vec{\nabla}(\vec{v}\rho)$, where $\vec{v}=\vec{v}(\vec{x},t)$ stands for the Burgers field and ρ is the density of transported matter, is at variance with the explicit diffusion scenario. Also, an issue of the necessary *correlation* (cf. [16], Chap. 7.3, devoted to the turbulent transport and the related dispersion of contaminants) between the probabilistic Fokker-Planck dynamics of the diffusing tracer, and this of the passive tracer (contaminant) concentration [Eq. (2)], has been left aside in the literature.

Moreover, rather obvious hesitation could have been observed in attempts to establish the most appropriate matter transport rule, if Eqs. (1)–(3) are adopted. Depending on the particular phenomenological departure point, one either adopts the standard continuity equation [3,4], that is certainly valid to a high degree of accuracy in the low viscosity limit (we refer to the standard terminology that comes from viscous fluid models; here, ν stands for the diffusion constant) $\nu\downarrow 0$ of Eqs. (1)–(3), but incorrect on mathematical grounds *if* there is a diffusion involved *and* simultaneously a solution of Eq. (1) is interpreted as the respective *current* velocity of the flow: $\partial_t\rho(\vec{x},t)=-\vec{\nabla}\cdot[\vec{v}(\vec{x},t)\rho(\vec{x},t)]$. Alternatively, following the white noise calculus tradition telling that the stochastic integral $\vec{X}(t)=\int_0^t\vec{v}(\vec{X}(s),s)ds+\int_0^t\vec{\eta}(s)ds$ implies the Fokker-Planck equation, one adopts [24]: $\partial_t\rho(\vec{x},t)=\nu\Delta\rho(\vec{x},t)-\vec{\nabla}\cdot[\vec{v}(\vec{x},t)\rho(\vec{x},t)]$, which is clearly problematic in view of the classic McKean's discussion of the propagation of chaos for the Burgers equation [27–29] and the derivation of the stochastic ''Burgers process'' in this context: ''the fun begins in trying to describe this Burgers motion as the path of a tagged molecule in an infinite bath of like molecules'' [27].

To put things on solid ground, let us consider a Markovian diffusion process, which is characterized by the transition probability density (generally inhomogeneous in space and time law of random displacements) $p(\vec{y},s,\vec{x},t),0\leqslant s<t\leqslant T$, and the probability density $\rho(\vec{x},t)$ of its random variable $\vec{X}(t),0\leqslant t\leqslant T$. The process is completely determined by these data. For clarity of discussion, we do not impose any spatial boundary restrictions, nor fix any concrete limiting value of T which, in principle, can be moved to infinity.

The conditions valid for any $\epsilon>0$: (a) there holds

$$\lim_{t\downarrow s}\frac{1}{t-s}\int_{|\vec{y}-\vec{x}|>\epsilon}p(\vec{y},s,\vec{x},t)d^3x=0,$$

(b) there exists a (forward) drift

$$\vec{b}(\vec{x},s)=\lim_{t\downarrow s}\frac{1}{t-s}\int_{|\vec{y}-\vec{x}|\leqslant\epsilon}(\vec{y}-\vec{x})p(\vec{x},s,\vec{y},t)d^3y,$$

and (c) there exists a diffusion function (in our case it is simply a diffusion coefficient ν)

$$a(\vec{x},s)=\lim_{t\downarrow s}\frac{1}{t-s}\int_{|\vec{y}-\vec{x}|\leqslant\epsilon}(\vec{y}-\vec{x})^2p(\vec{x},s,\vec{y},t)d^3y,$$

are conventionally interpreted to define a diffusion process [25,26]. Under suitable restrictions the function

$$g(\vec{x},s)=\int p(\vec{x},s,\vec{y},T)g(\vec{y},T)d^3y \tag{4}$$

satisfies the backward diffusion equation [notice that the minus sign appears, in comparison with Eq. (2)]

$$-\partial_s g(\vec{x},s)=\nu\Delta g(\vec{x},s)+[\vec{b}(\vec{x},s)\cdot\vec{\nabla}]g(\vec{x},s). \tag{5}$$

Let us point out that the validity of Eq. (5) is known to be a *necessary* condition for the existence of a Markov diffusion process, whose probability density $\rho(\vec{x},t)$ is to obey the Fokker-Planck equation. Here, the new velocity field, named the forward drift of the process $\vec{b}(\vec{x},t)$, replaces the previously utilized Burgers field $\vec{v}(\vec{x},t)$:

$$\partial_t\rho(\vec{x},t)=\nu\Delta\rho(\vec{x},t)-\vec{\nabla}\cdot[\vec{b}(\vec{x},t)\rho(\vec{x},t)]. \tag{6}$$

The case of particular interest in the nonequilibrium statistical physics literature appears when $p(\vec{y},s,\vec{x},t)$ is a *fundamental solution* of Eq. (5) with respect to variables $\vec{y},s$ [25,26,30]; see, however, [31] for an alternative situation. Then, the transition probability density *also* satisfies the Fokker-Planck equation in the remaining $\vec{x},t$ pair of variables. Let us emphasize that these two equations form an adjoint pair, referring to the slightly counterintuitive for physicists, although transparent for mathematicians [33–37], issue of time reversal of diffusion processes.

After adjusting Eqs. (3) to the present context, $\vec{X}(t)=\int_0^t\vec{b}(\vec{X}(s),s)ds+\sqrt{2\nu}\vec{W}(t)$, we realize [35–38] that for any smooth function $f(\vec{x},t)$ of the random variable $\vec{X}(t)$ the conditional expectation value

$$\lim_{\Delta t\downarrow 0}\frac{1}{\Delta t}\left[\int p(\vec{x},t,\vec{y},t+\Delta t)f(\vec{y},t+\Delta t)d^3y-f(\vec{x},t)\right]$$

$$=(D_+f)(\vec{X}(t),t)=[\partial_t+(\vec{b}\cdot\vec{\nabla})+\nu\Delta]f(\vec{x},t), \tag{7}$$

$$\vec{X}(t)=\vec{x},$$

determines the forward drift $\vec{b}(\vec{x},t)$ (if we set components of $\vec{X}$ instead of f) and allows one to introduce the local field of (forward) accelerations associated with the diffusion process,

which we constrain by demanding (see, e.g., Refs. [35–38] for prototypes of such dynamical constraints):

$$(D_+^2\vec{X})(t)=(D_+\vec{b})(\vec{X}(t),t)$$
$$=[\partial_t\vec{b}+(\vec{b}\cdot\vec{\nabla})\vec{b}+\nu\Delta\vec{b}](\vec{X}(t),t)$$
$$=\vec{F}(\vec{X}(t),t), \tag{8}$$

where, at the moment arbitrary, function $\vec{F}(\vec{x},t)$ may be interpreted as the external deterministic forcing applied to the diffusing system [32]. In particular, if we assume that drifts remain gradient fields, $\mathrm{curl}\vec{b}=\vec{0}$, under the forcing, then those that are allowed by the prescribed choice of $\vec{F}(\vec{x},t)$ *must* fulfill the compatibility condition (notice the conspicuous absence of the standard Newtonian minus sign in this analog of Newton's second law)

$$\vec{F}(\vec{x},t)=\vec{\nabla}\Omega(\vec{x},t), \tag{9}$$

$$\Omega(\vec{x},t)=2\nu\left[\partial_t\Phi+\frac{1}{2}\left(\frac{\vec{b}^2}{2\nu}+\vec{\nabla}\cdot\vec{b}\right)\right].$$

This establishes the connection of the forward drift $\vec{b}(\vec{x},t)=2\nu\nabla\Phi(\vec{x},t)$ with the (Feynman-Kac; cf. [31,32]) potential $\Omega(\vec{x},t)$ of the chosen external force field. The latter connection, without invoking the Feynman-Kac formula, is frequently exploited in the theory of Smoluchowski-type diffusion processes, when the Fokker-Planck equation is transformed into the associated generalized diffusion equation.

One of distinctive features of Markovian diffusion processes with the positive density $\rho(\vec{x},t)$ is that the notion of the *backward* transition probability density $p_*(\vec{y},s,\vec{x},t)$ can be consistently introduced on each finite time interval $0\leqslant s<t\leqslant T$:

$$\rho(\vec{x},t)p_*(\vec{y},s,\vec{x},t)=p(\vec{y},s,\vec{x},t)\rho(\vec{y},s), \tag{10}$$

so that $\int\rho(\vec{y},s)p(\vec{y},s,\vec{x},t)d^3y=\rho(\vec{x},t)$ and $\rho(\vec{y},s)=\int p_*(\vec{y},s,\vec{x},t)\rho(\vec{x},t)d^3x$. This allows one to define (cf. [32,38–40] for a discussion of these concepts in the case of the most traditional Brownian motion and Smoluchowski-type diffusion processes)

$$\lim_{\Delta t\downarrow 0}\frac{1}{\Delta t}\left[\vec{x}-\int p_*(\vec{y},t-\Delta t,\vec{x},t)\vec{y}d^3y\right]$$
$$=(D_-\vec{X})(t)=\vec{b}_*(\vec{X}(t),t), \tag{11}$$

$$(D_-f)(\vec{X}(t),t)=[\partial_t+(\vec{b}_*\cdot\vec{\nabla})-\nu\Delta]f(\vec{X}(t),t).$$

Accordingly, the backward version of the dynamical constraint imposed on the local acceleration field reads

$$(D_-^2\vec{X})(t)=(D_+^2\vec{X})(t)=\vec{F}(\vec{X}(t),t), \tag{12}$$

where under the gradient-drift field assumption, $\mathrm{curl}\vec{b}_*=0$, we have explicitly involved the forced Burgers equation [cf. Eq. (1)]:

$$\partial_t\vec{b}_*+(\vec{b}_*\cdot\vec{\nabla})\vec{b}_*-\nu\Delta\vec{b}_*=\vec{F}. \tag{13}$$

Here [32,35,36], in view of $\vec{b}_*=\vec{b}-2\nu\vec{\nabla}\ln\rho$, we deal with $\vec{F}(\vec{x},t)$ previously introduced in Eqs. (9). A notable consequence is that the Fokker-Planck equation (6) can be transformed to an *equivalent* form of

$$\partial_t\rho(\vec{x},t)=-\nu\Delta\rho(\vec{x},t)-\nabla[\vec{b}_*(\vec{x},t)\rho(\vec{x},t)], \tag{14}$$

which, however, describes a density evolution in the reverse sense of time.

At this point let us recall that Eqs. (5) and (6) form a natural adjoint pair of equations that determine the Markovian diffusion process in the chosen time interval $[0,T]$. Clearly, an adjoint of Eq. (14) reads:

$$\partial_s f(\vec{x},s)=\nu\Delta f(\vec{x},s)-[\vec{b}_*(\vec{x},s)\cdot\vec{\nabla}]f(\vec{x},s), \tag{15}$$

where

$$f(\vec{x},s)=\int p_*(\vec{y},0,\vec{x},s)f(\vec{y},0)d^3y, \tag{16}$$

to be compared with Eqs. (4), (5), and the previously mentioned passive scalar dynamics [Eq. (2)]; see also, e.g., [24]. Here, manifestly, the time evolution of the backward drift is governed by the Burgers equation, and the diffusion equation (15) is correlated [via the definition (10)] with the probability density evolution rule (14).

This pair *only* can be consistently utilized if the diffusion process is to be driven by forced (or unforced) Burgers velocity fields. Certainly, the continuity equation postulated to involve the Burgers field as the current velocity does not hold true in this context.

Let us point out that the study of diffusion in the Burgers flow may begin from first solving the Burgers equation (12) for a chosen external force field, next specifying the probability density evolution (14), and eventually ending with the corresponding ''passive contaminant'' concentration dynamics (15) and (16). All that is in perfect agreement with the heuristic discussion of the concentration dynamics given in Ref. [16], Chap. 7.3, where the ''backward dispersion'' problem with ''time running backwards'' was found necessary to *predict* the concentration.

All that means that Eqs. (1)–(3) can be reconciled in the framework set by Eqs. (4)–(16). Then, the ''nonlinear diffusion equation'' does indeed refer to consistent stochastic diffusion processes.

We are now at the point where the Burgers equation and the related matter transport can be consistently embedded in the general probabilistic framework of the so-called Schrödinger's boundary data (stochastic interpolation) problem [31,32,36,37,40–41], see also [42,43]. In this setting, the familiar Hopf-Cole transformation [2,44] of the Burgers equation into the generalized diffusion equation (yielding explicit solutions in the unforced case) receives a useful generalization.

Indeed, in that framework [31,32], the problem of deducing a suitable Markovian diffusion process was reduced to investigating the adjoint pairs of parabolic partial differential equations, like, e.g., Eqs. (5) and (6) or Eqs. (14) and (15). In

the case of gradient drift fields this amounts to checking [this imposes limitations on the admissible force field potential, cf. also formula (9)] whether the Feynman-Kac kernel

$$k(\vec{y},s,\vec{x},t)=\int \exp\left[-\int_s^t c(\omega(\tau),\tau)d\tau\right]d\mu_{(x,t)}^{(y,s)}(\omega) \qquad (17)$$

is positive and continuous in the open space-time area of interest, and whether it gives rise to positive solutions of the adjoint pair of generalized heat equations:

$$\partial_t u(\vec{x},t)=\nu\Delta u(\vec{x},t)-c(\vec{x},t)u(\vec{x},t), \qquad (18)$$

$$\partial_t v(\vec{x},t)=-\nu\Delta v(\vec{x},t)+c(\vec{x},t)v(\vec{x},t),$$

where $c(\vec{x},t)=(1/2\nu)\Omega(\vec{x},t)$ follows from the previous formulas. In the above, $d\mu_{(\vec{x},t)}^{(\vec{y},s)}(\omega)$ is the conditional Wiener measure over sample paths of the standard Brownian motion.

Solutions of Eqs. (18), upon suitable normalization, give rise to the Markovian diffusion process with the factorized probability density $\rho(\vec{x},t)=u(\vec{x},t)v(\vec{x},t)$, which interpolates between the boundary density data $\rho(\vec{x},0)$ and $\rho(\vec{x},T)$, with the forward and backward drifts of the process defined as follows:

$$\vec{b}(\vec{x},t)=2\nu\frac{\vec{\nabla}v(\vec{x},t)}{v(\vec{x},t)}, \qquad (19)$$

$$\vec{b}_*(\vec{x},t)=-2\nu\frac{\vec{\nabla}u(\vec{x},t)}{u(\vec{x},t)},$$

in the prescribed time interval $[0,T]$. The transition probability density of this process reads:

$$p(\vec{y},s,\vec{x},t)=k(\vec{y},s,\vec{x},t)\frac{v(\vec{x},t)}{v(\vec{y},s)}. \qquad (20)$$

Here, neither k [Eq. (17)] nor p [Eq. (20)] needs to be the fundamental solutions of appropriate parabolic equations; see, e.g., Ref. [31], where an issue of differentiability is analyzed.

The corresponding [since $\rho(\vec{x},t)$ is given] transition probability density (10) of the backward process has the form

$$p_*(\vec{y},s,\vec{x},t)=k(\vec{y},s,\vec{x},t)\frac{u(\vec{y},s)}{u(\vec{x},t)}. \qquad (21)$$

Obviously [31,36], in the time interval $0\leq s<t\leq T$ there holds

$$u(\vec{x},t)=\int u_0(\vec{y})k(\vec{y},s,\vec{x},t)d^3y$$

and

$$v(\vec{y},s)=\int k(\vec{y},s,\vec{x},T)v_T(\vec{x})d^3x.$$

By defining $\Phi_*=\ln u$, we immediately recover the traditional form of the Hopf-Cole transformation for Burgers velocity fields: $\vec{b}_*=-2\nu\nabla\Phi_*$. In the special case of the standard free Brownian motion, there holds $\vec{b}(\vec{x},t)=\vec{0}$ while $\vec{b}_*(\vec{x},t)=-2\nu\vec{\nabla}\ln\rho(\vec{x},t)$.

Our discussion provides a complete identification of the stochastic diffusion process underlying *both* the deterministically forced Burgers velocity dynamics and the related matter transport (14), the latter in terms of suitable density fields. The generalization of the Hopf-Cole procedure to this case involves a powerful methodology of the Feynman-Kac kernel functions and yields exact formulas for solutions for the forced Burgers equation. Let us stress that the connection between the Burgers equation and the generalized (forward) heat equation is not merely a formal trick that generates solutions to the nonlinear problem. The forward equation (18), in fact, carries a complete information about the implicit *backward stochastic evolution*, that is, a Markov diffusion process for which the Burgers-velocity driven transport is appropriate. Notice that the transition probability density (21) obeys the familiar Chapman-Kolmogorov formula. If we wish to analyze a concrete density field governed by this process, any two boundary density data $\rho(\vec{x},0)$ and $\rho(\vec{x},T)$ allow one to deduce the ultimate form of the (more traditional, forward) diffusion process (20), by means of the Schrödinger boundary data problem [31,36]. Then, the adjoint pair of equations (18) gives all details of the dynamics, with (19)–(21) as a necessary consequence. On the other hand, the presented discussion implies a direct import of the shock-type matter density profiles to the general nonequilibrium statistical physics of diffusion-type processes.

II. PROBLEM OF NONCONSERVATIVE FORCING OF BURGERS VELOCITY FIELDS

By embedding the Burgers equation in the Schrödinger interpolation framework, we could consistently handle random transport that is governed by gradient velocity fields and gradient-type external conservative forces. The natural question at this point is how to incorporate the nongradient (rotational, for example) velocity fields and especially the nonconservative forces. This question may be addressed without reservations only in the context of the forced Burgers equation. Recall that the Hopf-Cole transformation is applicable only in the case of gradient velocity fields. Moreover, the involved Schrödinger interpolation framework extends the issue to the domain of nonequilibrium random phenomena, where standard Smoluchowski diffusions [32] are normally discussed in the case of conservative force fields (and drifts in consequence).

Remark: Strikingly, an investigation of typical nonconservative, e.g., electromagnetically, forced diffusions has not been much pursued in the literature, although an issue of deriving the Smoluchowski-Kramers equation (and possibly its large friction limit) from the Langevin-type equation for the charged Brownian particle in the general electromagnetic field has been relegated in Ref. [45], Chap. 6.1, to the status of the innocent-looking exercise. On the other hand, the diffusion of realistic charges in dilute ionic solutions creates a number of additional difficulties due to the apparent Hall

mobility in terms of mean currents induced by the electric field (once assumed to act upon the system); see, e.g., [46–48]. In connection with the electromagnetic forcing of diffusing charges, the gradient field assumption imposes a severe limitation if we account for typical (nonzero circulation) features of the classical motion due to the Lorentz force, with or without the random perturbation component. The purely electric forcing is simpler to handle, since it has a definite gradient field realization; see, e.g., [49] for a recent discussion of related issues. The major obstacle with respect to our previous (Sec. I) discussion is that, if we wish to regard either the force $\vec{F}$ [Eqs. (8) and (12)] or drifts $\vec{b}$, $\vec{b}_*$ to have an electromagnetic origin, then necessarily we need to pass from conservative to nonconservative fields. This subject matter has not been significantly exploited so far in the nonequilibrium statistical physics literature.

With this additional (via the Burgers equation) motivation, let us analyze how the gradient velocity field (and conservative force field) assumption can be relaxed and nonetheless the exact solutions to the Burgers equation can be obtained, *both* in the unforced and forced cases, while involving the primoridal Markovian diffusion process scenario.

It turns out that the crucial point of our previous discussion lies in a *proper* choice of the strictly positive and continuous (in an open space-time area) function $k(\vec{y},s,\vec{x},t)$, which, if we wish to construct a Markov process, has to satisfy the Chapman-Kolmogorov (semigroup composition) equation. It has led us to consider a pair of adjoint partial differential equations, (18), as an alternative to either (5) and (6) or (14) and (15).

The Feynman-Kac integration is predominantly utilized in the quantally oriented literature dealing with Schrödinger operators and their spectral properties [50,51]. We shall exploit some of results of this well developed theory. The pertinent Feynman-Kac potential $c(x,t)$ in Eqs. (17) and (18) is usually assumed to be a continuous and bounded-from-below function, but these restrictions can be substantially relaxed (unbounded functions are allowed in principle) if we wish to consider general Markovian diffusion processes and disregard an issue of the bound state spectrum and this of the ground state of the (self-adjoint) semigroup generator [25,30]. Actually, what we need is merely that the properties of $c(\vec{x},t)$ allow for the kernel k, (17), that is, positive and continuous. This property is crucial for the Schrödinger boundary-data problem analysis.

Taking for granted that suitable conditions are fulfilled [31,50], we can immediately associate with Eqs. (18) an integral kernel of the time-dependent semigroup [the exponential operator should be understood as a time-ordered expression, since in general $H(\tau)$ may not commute with $H(\tau')$ for $\tau \neq \tau'$]:

$$k(\vec{y},s,\vec{x},t)=\left[\exp\left(-\int_s^t H(\tau)d\tau\right)\right](\vec{y},\vec{x}), \tag{22}$$

where $H(\tau)=-\nu\Delta+c(\tau)$ is the pertinent semigroup generator. Then, by the Feynman-Kac formula [43], we get an expression (17) for the kernel, which in turn yields Eqs. (19)–(22); see, e.g., [31]. As mentioned before, Eq. (20) combined with Eq. (17) sets a probabilistic connection between the Wiener measure corresponding to the standard Brownian motion with $\vec{b}(\vec{x},t)=\vec{0}$ and that for the diffusion process with a nonvanishing drift $\vec{b}(\vec{x},t)$, $\mathrm{curl}\vec{b}=\vec{0}$.

Our main purpose is to generalize Eq. (22), so that the positive and continuous (semigroup) kernel function can be associated with stochastic diffusion processes, whose drifts are no longer gradient fields. In particular, the forcing is to be nonconservative.

Since we have no particular hints towards Feynman-Kac-type analysis of rotational motions, it seems instructive to invoke the framework of the Onsager-Machlup approach towards an identification of most probable paths associated with the underlying diffusion process [52–54]. In this context, the nonconservative model system has been investigated in Ref. [55]. Namely, an effectively two-dimensional Brownian motion was analyzed, whose three-dimensional forward drift $\vec{b}(\vec{x}),b_3=0$ in view of $\partial_x b_1 \neq \partial_y b_2$, has $\mathrm{curl}\vec{b} \neq 0$. Then, by the standard variational argument with respect to the Wiener-Onsager-Machlup action [53,55],

$$I\{L(\dot{\vec{x}},\vec{x},t);t_1,t_2\} = \frac{1}{2\nu}\int_{t_1}^{t_2}\left\{\frac{1}{2}[\dot{\vec{x}}-\vec{b}(\vec{x},t)]^2+\nu\vec{\nabla}\cdot\vec{b}(\vec{x},t)\right\}dt, \tag{23}$$

the most probable trajectory, about which major contributions from (weighted) Brownian paths are concentrated, was found to be a solution of the Euler-Lagrange equations, which are formally identical to the equations of motion

$$\ddot{\vec{q}}_{cl}=\vec{E}+\dot{\vec{q}}_{cl}\times\vec{B} \tag{24}$$

of a classical particle of unit mass and unit charge moving in an electric field $\vec{E}$ and the magnetic field $\vec{B}$. The electric field [to be compared with Eq. (9)] is given by

$$\vec{E}=-\vec{\nabla}\Phi, \tag{25}$$

$$\Phi=-\frac{1}{2}(\vec{b}^2+2\nu\vec{\nabla}\cdot\vec{b}),$$

while the magnetic field has the only nonvanishing component in the z direction of R^3:

$$\vec{B}=\mathrm{curl}\vec{b}=\{0,0,\partial_x b_2-\partial_y b_1\}. \tag{26}$$

Clearly, $\vec{B}=\mathrm{curl}\vec{A}$, where $\vec{A}\doteq\vec{b}$ is the electromagnetic vector potential. The simplest example is a notorious constant magnetic field defined by $b_1(\vec{x})=-(B/2)x_2, b_2(\vec{x})=(B/2)x_1$.

One immediately realizes that the Fokker-Planck equation in this case is incompatible with traditional intuitions underlying the Smoluchowski-drift identification: the forward drift is *not* proportional to an external force, but to an electromagnetic potential. Nevertheless, the variational information drawn from the Onsager-Machlup Lagrangian involves the Lorentz force-driven trajectory. Hence, some principal ef-

fects of the electromagnetic forcing are present in the diffusing system, whose drifts display an ''unphysical'' (gauge dependent) form.

On the other hand, if we accept this ''unphysical'' random motion to yield the representation with the nongradient drift $\vec{A}$: $d\vec{X}(t)=\vec{A}(\vec{X}(t),t)dt+\sqrt{2\nu}d\vec{W}(t)$, and consider the corresponding pair (5) and (6) of adjoint diffusion equations with $\vec{A}(\vec{x},t)$ replacing $\vec{b}(\vec{x},t)$, then Eq. (8) tells us that

$$(D_+^2\vec{X})(t)=\partial_t\vec{A}+(\vec{A}\cdot\vec{\nabla})\vec{A}+\nu\Delta\vec{A}$$
$$=-\frac{B^2}{4}\{x_1,x_2,0\}=-\vec{E}(\vec{x}), \tag{27}$$

where $\vec{E}(\vec{x})=(B^2/4)\{x_1,x_2,0\}$, if calculated from Eqs. (25).

We thus arrive at the purely electric forcing with reversed sign [if compared with that coming from the Onsager-Machlup argument (25)] and, somewhat surprisingly, there is no impact of the previously discussed magnetic motion on the level of dynamical constraints [Eqs. (8) and (13)]. The adopted recipe is thus incapable of producing the magnetically forced diffusion process that conforms with arguments of Sec. I. Our toy model is inappropriate and a more sophisticated route must be adopted.

Below, we shall invoke the Feynman-Kac kernel idea (22) [31]. This approach has the clear advantage of elucidating the generic issues that hamper attempts to describe the diffussion processes governed by nonconservative (and electromagnetic in particular) force fields. The Burgers equation and the problem of its nongradient solutions will appear residually as a byproduct of the more general discussion.

Usually, the self-adjoint semigroup generators attract the attention of physicists in connection with the Feynman-Kac formula. Since electromagnetic fields provide the most conventional examples of nonconservative forces, we shall concentrate on their impact on random dynamics.

A typical route towards incorporating electromagnetism comes from quantal motivations via the minimal electromagnetic coupling recipe which preserves the self-adjointness of the generator (Hamiltonian of the system). As such, it constitutes a part of the general theory of Schrödinger operators. A rigorous study of operators of the form $-\triangle+V$ has become a well developed mathematical discipline [50]. The study of Schrödinger operators with magnetic fields, typically of the form $-(\nabla-i\vec{A})^2+V$, is less advanced, although specialized chapters on the magnetic field issue can be found in monographs devoted to functional integration methods [50,56], mostly in reference to seminal papers [57,58].

From the mathematical point of view, it is desirable to deal with magnetic fields that go to zero at infinity, which is certainly acceptable on physical grounds as well. The constant magnetic field (see, e.g., our previous considerations) does not meet this requirement, and its notorious usage in the literature makes us (at the moment) decline the asymptotic assumption and inevitably fall into a number of serious complications.

One obvious obstacle can be seen immediately by taking advantage of the existing results [57]. Namely, an explicit expression for the Feynman-Kac kernel in a constant magnetic field, introduced through the minimal electromagnetic coupling assumption $H(\vec{A})=-\frac{1}{2}(\vec{\nabla}-i\vec{A})^2$, is available (up to irrelevant dimensional constants):

$$\exp[-tH(\vec{A})](\vec{x},\vec{y})=\frac{B}{4\pi\,\sinh(\frac{1}{2}Bt)}\left(\frac{1}{2\pi t}\right)^{1/2}$$
$$\times\exp\left\{-\frac{1}{2t}(x_3-y_3)^2-\frac{B}{4}\coth\left(\frac{B}{2}t\right)\right.$$
$$\times[(x_2-y_2)^2+(x_1-y_1)^2]$$
$$\left.-i\frac{B}{2}(x_1y_2-x_2y_1)\right\}. \tag{28}$$

Clearly, it is *not* real (hence *nonpositive* and directly at variance with the major demand in the Schrödinger interpolation problem, as outlined in Sec. I), except for directions $\vec{y}$ that are parallel to a chosen $\vec{x}$.

Consequently, a bulk of the well developed mathematical theory is of no use for our purposes and new techniques must be developed for a consistent description of the electromagnetically forced diffusion processes along the lines of Sec. I, i.e., within the framework of Schrödinger's interpolation problem. Also, another approach is necessary to generate solutions of the Burgers equation that are not in the gradient form.

III. FORCING VIA FEYNMAN-KAC SEMIGROUPS

The conditional Wiener measure $d\mu_{(\vec{x},t)}^{(\vec{y},s)}(\vec{\omega})$ appearing in the Feynman-Kac kernel definition (17), if unweighted [set $c(\vec{\omega}(\tau),\tau)=0$], gives rise to the familiar heat kernel. This, in turn, induces the Wiener measure P_W of the set of all sample paths, which originate from $\vec{y}$ at time s and terminate (can be located) in the Borel set $A\in R^3$ after time $t-s$: $P_W[A]=\int_A d^3x\int d\mu_{(\vec{x},t)}^{(\vec{y},s)}(\vec{\omega})=\int_A d\mu$, where, for simplicity of notation, the $(\vec{y},t-s)$ labels are omitted and $\mu_{(\vec{x},t)}^{(\vec{y},s)}$ stands for the heat kernel.

Having defined an Itô diffusion $\vec{X}(t)=\int_0^t\vec{b}(\vec{x},u)du+\sqrt{2\nu}\vec{W}(t)$, we are interested in the analogous path measure: $P_{\vec{X}}[A]=\int_A dx\int d\mu_{(\vec{x},t)}^{(\vec{y},s)}(\vec{\omega}_{\vec{X}})=\int_A d\mu(\vec{X})$.

Under suitable (stochastic [32]) integrability conditions imposed on the forward drift, we have granted the absolute continuity $P_X\ll P_W$ of measures, which implies the existence of a strictly positive Radon-Nikodym density. Its canonical Cameron-Martin-Girsanov form [32,50], reads:

$$\frac{d\mu(\vec{X})}{d\mu}(\vec{y},s,\vec{x},t)=\exp\frac{1}{2\nu}\left[\int_s^t\vec{b}(\vec{X}(u),u)d\vec{X}(u)\right.$$
$$\left.-\frac{1}{2}\int_s^t[\vec{b}(\vec{X}(u),u)]^2du\right]. \tag{29}$$

If we assume that drifts are gradient fields, $\mathrm{curl}\vec{b}=0$, then the Ito formula allows one to reduce otherwise troublesome stochastic integration in the exponent of Eq. (29) [50,56] to ordinary Lebesgue integrals:

$$\frac{1}{2\nu}\int_s^t \vec{b}(\vec{X}(u),u)d\vec{X}(u)=\Phi(\vec{X}(t),t)-\Phi(\vec{X}(s),s) - \int_s^t du\left(\partial_t\Phi+\frac{1}{2}\vec{\nabla}\cdot\vec{b}\right)(\vec{X}(u),u). \tag{30}$$

After inserting Eq. (30) into Eq. (29) and next integrating with respect to the conditional Wiener measure, on account of Eq. (9) we arrive at the standard form of the Feynman-Kac kernel (17). Notice that Eq. (30) establishes a probabilistic basis for logarithmic transformations (19) of forward and backward drifts: $b=2\nu\vec{\nabla}\ln v=2\nu\vec{\nabla}\Phi$, $b_*=-2\nu\vec{\nabla}\ln u=-2\nu\vec{\nabla}\Phi_*$. The forward version is commonly used in connection with the transformation of the Fokker-Planck equation into the generalized heat equation, [32,59]. The backward version is the Hopf-Cole transformation, mentioned in Sec. I, used to map the Burgers equation into the very same generalized heat equation as in the previous case [2,42].

However, presently we are interested in nonconservative drift fields, $\mathrm{curl}\vec{b}\neq 0$, and in that case the stochastic integral in Eq. (29) is the major source of computational difficulties [35,50,56], for nontrivial vector potential field configurations. It explains the virtual absence of magnetically forced diffusion problems in the nonequilibrium statistical physics literature.

At this point, some steps of the analysis performed in Ref. [60] in the context of the ''Euclidean quantum mechanics'' (cf. also [37]) are extremely useful. Let us emphasize that the electromagnetic fields we utilize are always meant to be ordinary Maxwell fields with *no* Euclidean connotations (see, e.g., Chap. 9 of Ref. [56] for the Euclidean version of Maxwell theory).

Let us consider a gradient drift-field diffusion problem according to Sec. I, with Eqs. (17) and (30) involved and thus an adjoint pair (18) of parabolic equations completely defining the Markovian diffusion process. Furthermore, let $\vec{A}(\vec{x})$ be the time-independent vector potential for the Maxwellian magnetic field $\vec{B}=\mathrm{curl}\vec{A}$. We pass from the gradient realization of drifts to the new one, generalizing Eq. (19), for which the following decomposition into the gradient and nonconservative part is valid:

$$\vec{b}(\vec{x},t)=2\nu\vec{\nabla}\Phi(\vec{x},t)-\vec{A}(\vec{x}). \tag{31}$$

We denote $\theta(\vec{x},t)\doteq\exp[\Phi(\vec{x},t)]$ and admit that Eq. (31) is a forward drift of an Itô diffusion process with a stochastic differential $d\vec{X}(t)=[2\nu(\nabla\theta/\theta)-\vec{A}]dt+\sqrt{2\nu}d\vec{W}(t)$. On purely formal grounds, we deal here with an example of the Cameron-Martin-Girsanov transformation of the forward drift of a given Markovian diffusion process and we are entitled to ask for a corresponding measure transformation (29).

To this end, let us furthermore *assume* that $\theta(\vec{x},t)=\theta$ solves a partial differential equation

$$\partial_t\theta=-\nu\left(\nabla-\frac{1}{2\nu}\vec{A}(\vec{x})\right)^2\theta+c(\vec{x},t)\theta \tag{32}$$

with the notation $c(\vec{x},t)=(1/2\nu)\Omega(\vec{x},t)$ patterned after Eq. (9). Then, by using the Ito calculus and Eqs. (31) and (32) on the way (see, e.g., Ref. [60]), we can rewrite Eq. (29) as follows:

$$\frac{d\mu(\vec{X})}{d\mu}(\vec{y},s,\vec{x},t)=\exp\frac{1}{2\nu}\left[\int_s^t\left(2\nu\frac{\vec{\nabla}\theta}{\theta}-\vec{A}\right)(\vec{X}(u),u)d\vec{X}(u)-\frac{1}{2}\int_s^t\left(2\nu\frac{\vec{\nabla}\theta}{\theta}-\vec{A}\right)^2(\vec{X}(u),u)du\right] = \frac{\theta(\vec{X}(t),t)}{\theta(\vec{X}(s),s)}\exp\left[-\frac{1}{2\nu}\int_s^t[\vec{A}(u)d\vec{X}(u)+\nu(\vec{\nabla}\cdot\vec{A})(\vec{X}(u))du+\Omega(\vec{X}(u),u)du]\right], \tag{33}$$

where $\vec{X}(s)=\vec{y},\vec{X}(t)=\vec{x}$.

More significant observation is that the Radon-Nikodym density (33), if integrated with respect to the conditional Wiener measure, gives rise to the Feynman-Kac kernel (22) of the *non-self-adjoint* semigroup (suitable integrability conditions need to be respected here as well [60]), with the generator $H_{\vec{A}}=-\nu[\nabla-(1/2\nu)\vec{A}(\vec{x})]^2+c(\vec{x},t)$ defined by the right-hand side of Eq. (32):

$$\partial_t\theta(\vec{x},t)=H_{\vec{A}}\theta(\vec{x},t)=\left[-\nu\Delta+\vec{A}(\vec{x})\cdot\vec{\nabla}+\frac{1}{2}(\vec{\nabla}\cdot\vec{A}(\vec{x}))-\frac{1}{4\nu}[\vec{A}(\vec{x})]^2+c(\vec{x},t)\right]\theta(\vec{x},t) = -\nu\Delta\theta(\vec{x},t)+\vec{A}(\vec{x})\cdot\vec{\nabla}\theta(\vec{x},t)+c_{\vec{A}}(\vec{x},t)\theta(\vec{x},t). \tag{34}$$

Here

$$c_A(\vec{x},t)=c(\vec{x},t)+\frac{1}{2}(\nabla\vec{A})(\vec{x})-\frac{1}{4\nu}[\vec{A}(\vec{x})]^2. \qquad (35)$$

An adjoint parabolic partner of Eq. (34) reads

$$\partial_t\theta_*=-H_{\vec{A}}^{*}\theta_*=\nu\Delta\theta_*+\vec{\nabla}\cdot[\vec{A}(\vec{x})\theta_*]-c_A(\vec{x},t)\theta_*$$
$$=\nu\left[\vec{\nabla}+\frac{1}{2\nu}\vec{A}(\vec{x})\right]^2\theta_*-c(\vec{x},t)\theta_*. \qquad (36)$$

Consequently, our assumptions [Eqs. (31) and (32)] involve a generalization of the adjoint parabolic system (18) to a new adjoint one comprising Eqs. (32) and (36). Obviously, the original form of Eq. (18) is immediately restored by setting $\vec{A}=\vec{0}$, and executing obvious replacements $\theta_*\to u$, $\theta\to v$.

Let us emphasize again that, in contrast to Ref. [62], where the non-Hermitian generator $2\nu H_{\vec{A}}$, Eq. (32), has been introduced as ''the Euclidean version of the Hamiltonian'' $H=-2\nu^2[\nabla-(i/2\nu)\vec{A}]^2+\Omega$, our electromagnetic fields stand for solutions of the usual Maxwell equations and *are not* Euclidean at all.

As long as the coefficient functions (both additive and multiplicative) of the adjoint parabolic system (34) and (36) are not specified, we remain within a general theory of positive solutions for parabolic equations with unbounded coefficients (of particular importance, if we do not impose any asymptotic falloff restrictions) [30,61–63]. The fundamental solutions, if their existence can be granted, usually exist on space-time strips, and generally do not admit unbounded time intervals. We shall disregard these issues at the moment, and assume the existence of fundamental solutions without any reservations.

By exploiting the rules of functional (Malliavin, variational) calculus, under an assumption that we deal with a diffusion (in fact, Bernstein) process associated with an adjoint pair (34) and (35), it has been shown in Ref. [60] that *if* the forward conditonal derivatives of the process exist, then $(D_+\vec{X})(t)=2\nu(\nabla\theta/\theta)-\vec{A}=\vec{b}(\vec{x},t)$, Eq. (32), and

$$(D_+^2\vec{X})(t)=(D_+\vec{X})(t)\times\mathrm{curl}\vec{A}(\vec{x})+\nabla\Omega(\vec{x},t)$$
$$+\nu\ \mathrm{curl}[\mathrm{curl}\vec{A}(\vec{x})], \qquad (37)$$

where $\vec{X}(0)=0$, $\vec{X}(t)=\vec{x}$, $\times$ denotes the vector product in R^3, and $2\nu c=\Omega$.

Since $\vec{B}=\mathrm{curl}\vec{A}=\mu_0\vec{H}$, we identify in the above the standard Maxwell equation for $\mathrm{curl}\vec{H}$ comprising magnetic effects of electric currents in the system: $\mathrm{curl}\vec{B}=\mu_0[\dot{\vec{D}}+\sigma_0\vec{E}+\vec{J}_{ext}]$, where $\vec{D}=\epsilon_0\vec{E}$ while $\vec{J}_{ext}$ represents external electric currents. In case of $\vec{E}=\vec{0}$, the external currents only would be relevant. A demand curl $\mathrm{curl}\vec{A}=\vec{\nabla}(\vec{\nabla}\vec{A})-\Delta\vec{A}=0$ corresponds to a total absence of such currents, and the Coulomb gauge choice $\vec{\nabla}\cdot\vec{A}=0$ would leave us with harmonic functions $\vec{A}(\vec{x})$.

Consequently, a correct expression for the magnetically implemented Lorentz force has appeared on the right-hand side of the forward acceleration formula (37), with the forward drift (31) replacing the classical particle velocity $\dot{\vec{q}}$ of the classical formula (24).

The above discussion implicitly involves quite sophisticated mathematics; hence it is instructive to see that we can bypass the apparent complications by directly invoking the universal definitions (7) and (11) of conditional expectation values, which are based on exploitation of the Itô formula only. Obviously, we assume that the Markovian diffusion process with well defined transition probability densities $p(\vec{y},s,\vec{x},t)$ and $p_*(\vec{y},s,\vec{x},t)$, does exist.

We shall utilize an obvious generalization of canonical definitions (19) of both forward and backward drifts of the diffusion process defined by the adjoint parabolic pair (18), as suggested by Eq. (31) with $\vec{A}=\vec{A}(\vec{x})$:

$$\vec{b}=2\nu\frac{\vec{\nabla}\theta}{\theta}-\vec{A},\quad \vec{b}_*=-2\nu\frac{\vec{\nabla}\theta_*}{\theta_*}-\vec{A}. \qquad (38)$$

We also demand that the corresponding adjoint equations (34) and (36) *are* solved by θ and θ_*, respectively.

Taking for granted that identities $(D_+\vec{X})(t)=\vec{b}(\vec{x},t),\vec{X}(t)=\vec{x}$, and $(D_-\vec{X})(t)=\vec{b}_*(\vec{x},t)$ hold true, we can easily evaluate the forward and backward accelerations [substitute Eq. (38), and exploit Eqs. (34) and (36)]:

$$(D_+\vec{b})(\vec{X}(t),t)=\partial_t\vec{b}+(\vec{b}\cdot\vec{\nabla})\vec{b}+\nu\Delta\vec{b}$$
$$=\vec{b}\times\vec{B}+\nu\ \mathrm{curl}\vec{B}+\vec{\nabla}\Omega \qquad (39)$$

and

$$(D_-\vec{b}_*)(\vec{X}(t),t)=\partial_t\vec{b}_*+(\vec{b}_*\cdot\vec{\nabla})\vec{b}_*-\nu\Delta\vec{b}_*$$
$$=\vec{b}_*\times\vec{B}-\nu\mathrm{curl}\vec{B}+\vec{\nabla}\Omega. \qquad (40)$$

Let us notice that the forward and backward acceleration formulas *do not* coincide as was the case before [cf. Eqs. (8) and (12)]. There is a definite time asymmetry in the local description of the diffusion process in the presence of general magnetic fields, unless $\mathrm{curl}\vec{B}=0$. The quantity which is explicitly time-reversal invariant can be easily introduced:

$$\vec{v}(\vec{x},t)=\tfrac{1}{2}(\vec{b}+\vec{b}_*)(\vec{x},t) \qquad (41)$$

$$\Rightarrow\tfrac{1}{2}(D_+^2+D_-^2)(\vec{X}(t))=\vec{v}\times\vec{B}+\vec{\nabla}\Omega.$$

As yet there is no trace of Lorentzian electric forces, unless extracted from the term $\vec{\nabla}\Omega(\vec{x},t)$. We shall accomplish this step in Sec. IV.

For a probability density $\theta_*\theta=\rho$ of the related Markovian diffusion process [31,36], we would have fulfilled both the Fokker-Planck and the continuity equations: $\partial_t\rho=\nu\Delta\rho-\vec{\nabla}(\vec{b}\rho)=-\vec{\nabla}(\vec{v}\rho)=-\nu\Delta\rho-\vec{\nabla}(\vec{b}_*\rho)$, as before (cf. Sec. I).

In the above, Eq. (40) can be regarded as the Burgers equation with a general external magnetic (plus other external force contributions if necessary) forcing, and its definition is an outcome of the underlying mathematical structure related to the adjoint pair (32) and (36) of parabolic equations.

Our construction shows that solutions of the magnetically forced Burgers equation (40) are given in the form (38). In reverse, the mere assumption about the decomposition of drifts (38) into the gradient and nongradient part implies that the corresponding evolution equation (40) is the Burgers equation with the nonconservative forcing. The force term has a specific Lorentz form. Although we invoke electromagnetism, the decomposition (38) can be regarded to refer to an abstract nongradient component. In analogy to the previous Onsager-Machlup example, Eqs. (24)–(28), the fictituous Lorentz force term would arise anyway.

IV. SCHRÖDINGER'S INTERPOLATION IN A CONSTANT MAGNETIC FIELD AND QUANTALLY INSPIRED GENERALIZATIONS

Presently, we shall confine our attention to the simplest case of a constant magnetic field, defined by the vector potential $\vec{A}=\{-(B/2)x_2,+(B/2)x_1,0\}$. Here, $\vec{B}=\{0,0,B\}$, $\vec{\nabla}\cdot\vec{A}=0$, and $\mathrm{curl}\vec{B}=\vec{0}$, which significantly simplifies formulas (31)–(41).

As emphasized before, most of our discussion was based on the existence assumption for fundamental solutions of the (adjoint) parabolic equations (32) and (36). For magnetic fields, which do not vanish at spatial infinities (hence for our ''simplest'' choice), the situation becomes rather complicated. Namely, an expression for

$$c_{\vec{A}}(\vec{x},t)=c(\vec{x},t)-\frac{B^2}{16\nu}(x_1^2+x_2^2) \tag{42}$$

includes a *repulsive* harmonic oscillator contribution.

For the existence of a well defined Markovian diffusion process it appears necessary that a nonvanishing contribution from an unbounded from above $c(\vec{x},t)$ would counterbalance the harmonic repulsion. To see that this *must be* the case, let us formally constrain $\theta(\vec{x},t)=\exp[\Phi(\vec{x},t)]$ to yield [in accordance with Eq. (9)] the identity:

$$c(\vec{x},t)=\partial_t\Phi+\nu[\vec{\nabla}\Phi]^2+\nu\triangle\Phi=0. \tag{43}$$

Then, we deal with the simplest version of the adjoint system (34) and (36) where, in view of $\vec{\nabla}\cdot\vec{A}=0=c$, there holds:

$$\partial_t\theta=-\nu\left[\vec{\nabla}-\frac{1}{2\nu}\vec{A}\right]^2\theta=-\nu\Delta\theta+\vec{A}\cdot\vec{\nabla}\theta-\frac{1}{4\nu}[\vec{A}]^2\theta, \tag{44}$$

$$\partial_t\theta_*=\nu\left[\vec{\nabla}+\frac{1}{2\nu}\vec{A}\right]^2\theta_*=\nu\Delta\theta_*+\vec{A}\cdot\vec{\nabla}\theta_*+\frac{1}{4\nu}[\vec{A}]^2\theta_*.$$

With our choice, $\mathrm{curl}\vec{A}=\{0,0,B\}$, Eqs. (44) *do not* possess a fundamental solution, which would be well defined for *all* $(\vec{x},t)\in R^3\times R^+$: everything because of the harmonic repulsion term in the forward parabolic equation. We can prove (this purely mathematical argument is not reproduced in the present paper) that the function

$$k(\vec{y},s,\vec{x},t)=\frac{B}{4\pi\,\sin[\frac{1}{2}B(t-s)]}\left(\frac{1}{2\pi(t-s)}\right)^{1/2}$$
$$\times\exp\left\{-\frac{1}{2(t-s)}(x_3-y_3)^2-\frac{B}{4}\cot\left(\frac{B}{2}(t-s)\right)[(x_2-y_2)^2+(x_1-y_1)^2]-\frac{B}{2}(x_1y_2-x_2y_1)\right\} \tag{45}$$

only when restricted to times $t-s\leqslant\pi/B$ is an acceptable example of a *unique* positive (actually, positivity extends to times $t-s\leqslant 2\pi/B$) fundamental solution of the system (43), (rescaled to yield $\nu\to\frac{1}{2}$). Here, formally, Eq. (45) can be obtained from the expression (28) by the replacement $\vec{A}\to-i\vec{A}$.

An immediate insight into a harmonic repulsion obstacle can be achieved after an x-y plane rotation of Cartesian coordinates: $x_1'=x_1\cos(\omega t)-x_2\sin(\omega t)$, $x_2'=x_1\sin(\omega t)+x_2\cos(\omega t)$, $x_3'=x_3$, $t'=t$, with $\omega=B/4\sqrt{\nu}$. Then, Eqs. (44) get transformed into an adjoint pair:

$$\partial_{t'}\theta=-\nu\Delta'\theta-\omega^2(x_1'^2+x_2'^2)\theta, \tag{46}$$

$$\partial_{t'}\theta_*=\nu\Delta'\theta_*+\omega^2(x_1'^2+x_2'^2)\theta_*.$$

Notice that the transformation $\omega\to i\omega$ would replace repulsion in Eqs. (46) by harmonic attraction. On the other hand, we can get rid of the repulsive term by assuming that $c(\vec{x},t)$ [Eq. (42)] does not identically vanish. For example, we can formally demand that, instead of Eq. (43), $c(\vec{x},t)=+(B^2/8\nu)(x_1^2+x_2^2)$ plays the role of an electric potential. Then, harmonic attraction replaces repulsion in the final form of Eqs. (34) and (36).

As a byproduct, we are given a transition probability density of the diffusion process governed by the adjoint system [cf. Eq. (27)]:

$$\partial_t\theta=-\nu\Delta\theta+\vec{A}\cdot\vec{\nabla}\theta, \tag{47}$$

$$\partial_t\theta_*=\nu\Delta\theta_*+\vec{A}\cdot\vec{\nabla}\theta_*.$$

with $\vec{A}=(B/2)\{-x_2,x_1,0\}$. Namely, by means of the previous x-y plane rotation, Eqs. (47) are transformed into a pair of time adjoint heat equations:

$$\partial_{t'}\theta=-\nu\Delta'\theta,\quad \partial_{t'}\theta_*=\nu\triangle'\theta_*, \tag{48}$$

whose fundamental solution is the standard heat kernel.

Finding explicit analytic solutions of rather involved equations (34) and (36) is a formidable task on its own, in contrast to much simpler unforced or conservatively forced dynamics issue.

Interestingly, we can produce a number of examples by invoking the quantum Schrödinger dynamics. This quantum inspiration has been proved to be very useful in the past [36,37]. At this point, we shall follow the idea of Ref. [31], where the strategy developed for solving the Schrödinger boundary data problem has been applied to quantally induced stochastic processes (e.g., Nelson's diffusions [35,38]). They were considered as a particular case of the general theory appropriate for nonequilibrium statistical physics processes as governed by the adjoint pair (18), and exclusively in conjunction with Born's statistical postulate in quantum theory.

The Schrödinger picture quantum evolution is then consistently representable as a Markovian diffusion process. All that follows from the previously outlined Feynman-Kac kernel route [31,32,35,36,38,40,41], based on exploiting the adjoint pairs of parabolic equations. However, the respective semigroup theory has been developed for pure gradient drift fields, hence without reference to any impact of electromagnetism on the pertinent diffusion process, and electromagnetism is definitely ubiquitous in the world of quantum phenomena.

Let us start from an ordinary Schrödinger equation for a charged particle in an arbitrary external electromagnetic field, in its standard dimensional form. To conform with the previous notation let us absorb the charge e and mass m parameters in the definition of $\vec{A}(\vec{x})$ and the potential $\phi(\vec{x})$, e.g., we consider B instead of $(e/m)B$ and ϕ instead ϕ/m. Additionally, we set ν instead of $(\hbar/2m)$. Then, we have

$$i\partial_t\psi(\vec{x},t)=-\nu\left(\vec{\nabla}-\frac{i}{2\nu}\vec{A}\right)^2\psi(\vec{x},t)+\frac{1}{2\nu}\phi(\vec{x})\psi(\vec{x},t). \tag{49}$$

The standard Madelung substitution $\psi=\exp(R+iS)$ allows one to introduce the real functions $\theta=\exp(R+S)$ and $\theta_*=\exp(R-S)$ instead of complex ones $\psi,\overline{\psi}$. They are solutions of an adjoint parabolic system (34) and (36), where the impact of Eq. (49) is encoded in a specific functional form of the otherwise arbitrary potential $c(\vec{x},t)$:

$$c(\vec{x},t)=\frac{1}{2\nu}\Omega(\vec{x},t)=\frac{1}{2\nu}[2Q(\vec{x},t)-\phi(\vec{x})], \tag{50}$$

$$Q(\vec{x},t)=2\nu^2\frac{\Delta\rho^{1/2}(\vec{x},t)}{\rho^{1/2}(\vec{x},t)}=2\nu^2\{\Delta R(\vec{x},t)+[\vec{\nabla}R(\vec{x},t)]^2\}.$$

The quantum probability density $\rho(\vec{x},t)=\psi(\vec{x},t)\overline{\psi}(\vec{x},t)=\theta(\vec{x},t)\theta_*(\vec{x},t)$ displays a factorization $\rho=\theta\theta_*$ in terms of solutions of adjoint parabolic equations, which we recognize to be characteristic for probabilistic solutions (Markov diffusion processes) of the Schrödinger boundary data problem (cf. Sec. I) [31,32,36,40]. It is easy to verify the validity of the Fokker-Planck equation whose forward drift has the form (38). Also, Eqs. (39) and (40) do follow with $\Omega=2Q-\phi$.

By defining $\vec{E}=-\vec{\nabla}\phi$ [with ϕ utilized instead of $(e/m)\phi$], we immediately arrive at the complete Lorentz force contribution in all acceleration formulas (before, we have used $\mathrm{curl}\vec{B}=0$):

$$\partial_t\vec{b}+(\vec{b}\cdot\vec{\nabla})\vec{b}+\nu\Delta\vec{b}=\vec{b}\times\vec{B}+\vec{E}+\nu\ \mathrm{curl}\vec{B}+2\vec{\nabla}Q, \tag{51}$$

$$\partial_t\vec{b}_*+(\vec{b}_*\cdot\vec{\nabla})\vec{b}_*-\nu\Delta\vec{b}_*=\vec{b}_*\times\vec{B}+\vec{E}-\nu\ \mathrm{curl}\vec{B}+2\vec{\nabla}Q.$$

Moreover, the velocity field named the current velocity of the flow, $\vec{v}=\frac{1}{2}(\vec{b}+\vec{b}_*)$, enters the familiar local conservation laws (see also [32] for a discussion of how the ''quantum potential'' Q affects such laws in case of the standard Brownian motion and Smoluchowski-type diffusion processes)

$$\partial\rho=-\vec{\nabla}(\vec{v}\rho), \tag{52}$$

$$\partial_t\vec{v}+(\vec{v}\cdot\vec{\nabla})\vec{v}=\vec{v}\times\vec{B}+\vec{E}+\vec{\nabla}Q.$$

A comparison with Eqs. (33)–(43) shows that Eqs. (50)–(53) can be regarded as the specialized version of the general external forcing problem with an explicit electromagnetic (Lorentz force-inducing) contribution and an arbitrary term of nonelectromagnetic origin, which we denote by $c(\vec{x},t)$ again. Obviously, c is represented in Eq. (50), by $(1/\nu)Q(\vec{x},t)$.

We have therefore arrived at the following ultimate generalization of the adjoint parabolic system (18), that encompasses the nonequilibrium statistical physics and essentially quantum evolutions on an equal footing (with no clear-cut discrimination between these options, as in Ref. [31]) and gives rise to an external (Lorentz) electromagnetic forcing:

$$\partial_t\theta(\vec{x},t)=\left[-\nu\left(\vec{\nabla}-\frac{1}{2\nu}\vec{A}\right)^2-\frac{1}{2\nu}\phi(\vec{x})+c(\vec{x},t)\right]\theta(\vec{x},t), \tag{53}$$

$$\partial_t\theta_*(\vec{x},t)=\left[\nu\left(\vec{\nabla}+\frac{1}{2\nu}\vec{A}\right)^2+\frac{1}{2\nu}\phi(\vec{x})-c(\vec{x},t)\right]\theta_*(\vec{x},t).$$

A subsequent generalization encompassing time-dependent electromagnetic fields is immediate.

The adjoint parabolic pair of equations (53) can thus be regarded to determine a Markovian diffusion process in exactly the same way as Eq. (18) did. If only a suitable choice of vector and scalar potentials in Eqs. (53) guarrantees a continuity and positivity of the involved semigroup kernel [take the Radon-Nikodym density of the form (33), with $\Omega\to-\phi+\Omega$, and integrate with respect to the conditional Wiener measure], then the mere knowledge of such integral kernel suffices for the implementation of steps (18)–(22), with $u\to\theta_*$, $v\to\theta$. To this end it is not at all necessary that

$k(\vec{x},s,\vec{y},t)$ be a fundamental solution of Eqs. (53). A sufficient condition is that the semigroup kernel is a continuous (and positive) function. The kernel may not even be differentiable; see, e.g., Ref. [31] for a discussion of that issue which is typical for quantal situations.

After adopting Eqs. (53) as the principal dynamical ingredient of the electromagnetically forced Schrödinger interpolation, we must slightly adjust the emerging acceleration formulas. Namely, they have the form (51), but we need to replace $2Q(\vec{x},t)$ by, from now an arbitrary, potential $\Omega(\vec{x},t)=2\nu c(\vec{x},t)$. The second equation in Eqs. (53) also takes a new form:

$$\partial_t\vec{v}+(\vec{v}\cdot\vec{\nabla})\vec{v}=\vec{v}\times\vec{B}+\vec{E}+\vec{\nabla}(\Omega-Q); \tag{54}$$

see, e.g., Ref. [32] for more detailed explanation of this step. The presence in Eqs. (53) of the density-dependent $-\vec{\nabla}Q$ term finds its origin in the identity $\vec{b}-\vec{b}_*=2\nu\nabla\rho(\vec{x},t)$ and is a necessary consequence of the involved (forced in the present case) Brownian motion; see, e.g., [39,64,65].

Finally, the second of equations (51) with Ω replacing $2Q$ is the most general form of the Burgers equation with an external forcing, where the electromagnetic (Lorentz force) contribution has been extracted for convenience. Solutions of this equation must be sought for in the form (38), which generalizes the logarithmic Hopf-Cole transformation to nongradient drift fields. Equations (53) are the associated parabolic partial differential (generalized heat) equations, which completely determine probabilistic solutions (Markovian diffusion processes) of the Schrödinger boundary data (interpolation) problem. In turn, for this particular random transport, the forced Burgers velocity fields play the role of backward drifts of the process.

V. OUTLOOK

Our discussion, albeit motivated by the issue of diffusive matter transport that is consistently driven by Burgers velocity fields (this extends both to the compressible and incompressible cases), has little to do with classical fluids. The emergence of shock pressure fronts is more natural in the compressible situation. This shock profile possibility (inherent to the Burgers equation) has been imported to the nonequilibrium statistical physics of random phenomena by exploring the idea of Schrödinger's interpolation problem and revealing its connection with the Burgers dynamics. That has been the subject of Sec. I.

The next important result (a preliminary discussion of rotational Burgers fields can be found in Ref. [23]) amounts to relaxing the gradient-field assumption (that is crucial for the validity of the Hopf-Cole transformation). In Secs. II and III we have analyzed the ways to generalize the Feynman-Kac kernel strategy so that the involved (drifts) velocity fields admit the nongradient form. Our analysis was perfomed with rather explicit electromagnetic connotations. Equations (34) and (36) generalize the adjoint pair (18) to diffusion processes with nongradient drifts (38).

As follows from Eq. (40), the very presence of the nongradient term in the decomposition (38) implies that the corresponding evolution equation for the velocity field (backward drift of the process) is the Burgers equation with the specific Lorentz-type forcing.

Section IV extends the discussion to quantally implemented diffusion processes, where the minimal electromagnetic coupling is a celebrated recipe. This quantal motivation allows to arrive at the adjoint system (53), that incorporates an electric contribution and allows one to define and solve the Burgers equation with the combined conservative and nonconservative (electromagnetic, in particular) forcing. Let us emphasize again that a transformation of the Burgers equation (whatever the force term is) into a generalized diffusion equation is not merely a formal linearization trick. This [1] ''nonlinear diffusion equation'' does indeed refer to a well defined stochastic diffusion process, but a complete information about its features is encoded in the involved parabolic equations.

ACKNOWLEDGMENTS

Two of the authors (P.G. and R.O.) received financial support from the KBN through research Grant No. 2 P302 057 07. P.G. would like to express his gratitude to Professor Ana Bela Cruzeiro and Professor Jean-Claude Zambrini for enlightening discussions.

[1] J. M. Burgers, *The Nonlinear Diffusion Equation* (Reidel, Dordrecht, 1974).
[2] E. Hopf, Commun. Pure Appl. Math. **3**, 201 (1950).
[3] S. F. Shandarin and B. Z. Zeldovich, Rev. Mod. Phys. **61**, 185 (1989).
[4] S. Albeverio, A. A. Molchanov and D. Surgailis, Prob. Theory Relat. Fields **100**, 457 (1994).
[5] Y. Hu and W. A. Woyczynski, in *Chaos—The Interplay Between Stochastic and Deterministic Behaviour*, edited by P. Garbaczewski, M. Wolf, and A. Weron, Lecture Notes in Physics Vol. 457 (Springer-Verlag, Berlin, 1995), p. 135.
[6] S. N. Gurbatov and A. I. Saichev, Zh. Éksp. Teor. Fiz . **80**, 689 (1981).
[7] Z. She, E. Aurell, and U. Frisch, Commun. Math. Phys. **148**, 623 (1992).
[8] Ya. G. Sinai, Commun. Math. Phys. **148**, 601 (1992).
[9] J.D. Fournier and U. Frisch, J. Mech. Theor. Appl. **2**, 699 (1983).
[10] W. A. Woyczynski, in *Nonlinear Waves and Weak Turbulence*, edited by N. Fitzmaurice *et al.* (Birkaäuser, Boston, 1993), p. 279.
[11] J. P. Bouchaud, M. Mézard, and G. Parisi, Phys. Rev. E **52**, 3656 (1995).
[12] A. M. Polyakov, Phys. Rev. E **52**, 6183 (1995).
[13] M. Kardar, G. Parisi, and Y. C. Zhang, Phys. Rev. Lett. **56**, 889 (1986).

[14] B. I. Shraiman and E. D. Siggia, Phys. Rev. E **49**, 2912 (1994).
[15] A. Chekhlov and V. Yakhot, Phys. Rev. E **51**, 2739 (1995).
[16] A. S. Monin and A. M. Yaglom, *Statistical Fluid Mechanics* (MIT Press, Cambridge, MA, 1973).
[17] S. N. Gurbatov, A. N. Malakhov, and A. I. Saichev, *Nonlinear Random Waves and Turbulence in Nondispersive Media: Waves, Rays, Particles* (Manchester University Press, Manchester, 1991).
[18] A. Truman and H. Z. Zhao, J. Math. Phys. **37**, 283 (1996).
[19] H. Holden, T. Lindstrøm, B. Øksendal, J. Ubøe, and T. S. Zhang, Commun. Part. Diff. Eq. **19**, 119 (1994).
[20] J. B. Walsh, in *École d'Été de Probabilités de Saint-Flour XIV*, edited by R. Carmona, H. Kesten, and J. B. Walsh, Lecture Notes in Mathematics Vol. 1180 (Springer-Verlag, Berlin, 1986), p. 265.
[21] P. G. Saffman, J. Fluid Mech. **8**, 273 (1960).
[22] A. A. Townsend, Proc. R. Soc. A **209**, 418 (1951).
[23] A. I. Saichev and W. A. Woyczynski, Physica D (to be published).
[24] A. I. Saichev and W. A. Woyczynski, SIAM J. Appl. Math. (to be published).
[25] A. Friedman, *Partial Differential Equations of Parabolic Type* (Prentice-Hall, Englewood Cliffs, NJ, 1964).
[26] W. Horsthemke and R. Lefever, *Noise-Induced Transitions* (Springer-Verlag, Berlin, 1984).
[27] H. P. McKean, in *Lecture Series in Differential Equations*, edited by A. K. Aziz (Van Nostrand, Amsterdam, 1969), Vol. II, p. 177.
[28] P. Calderoni and M. Pulvirenti, Ann. Inst. Henri Poincaré **39**, 85 (1983).
[29] H. Osada and S. Kotani, J. Math. Soc. Jpn. **37**, 275 (1985).
[30] M. Krzyżański and A. Szybiak, Lincei-Rend. Sc. Fis. Mat. Nat. **28**, 26 (1959).
[31] P. Garbaczewski and R. Olkiewicz, J. Math. Phys. **37**, 730 (1996).
[32] Ph. Blanchard and P. Garbaczewski, Phys. Rev. E **49**, 3815 (1994).
[33] U. G. Haussmann and E. Pardoux, Ann. Prob. **14**, 1188 (1986).
[34] H. Föllmer, in *Stochastic Processes—Mathematics and Physics*, edited by S. Albeverio, Ph. Blanchard, and L. Streit, Lecture Notes in Physics Vol. 1158 (Springer-Verlag, Berlin, 1985), p. 119.
[35] E. Nelson, *Quantum Fluctuations* (Princeton University Press, Princeton, 1985).
[36] J. C. Zambrini, J. Math. Phys. **27**, 2307 (1986).
[37] J. C. Zambrini, in *Chaos—The Interplay Between Stochastic and Deterministic Behaviour* (Ref. [5]), p. 393.
[38] E. Nelson, *Dynamical Theories of the Brownian Motion* (Princeton University Press, Princeton, 1967).
[39] P. Garbaczewski and J. P. Vigier, Phys. Rev. A **46**, 4634 (1992).
[40] P. Garbaczewski and R. Olkiewicz, Phys. Rev. A **51**, 3445 (1995).
[41] P. Garbaczewski, J. R. Klauder, and R. Olkiewicz, Phys. Rev. E **51**, 4114 (1995).
[42] S. Albeverio, Ph. Blanchard, and R. Høegh-Krohn, in *Stochastic Aspects of Classical and Quantum Systems*, edited by S. Albeverio *et al.*, Lecture Notes in Mathematics Vol. 1109 (Springer-Verlag, Berlin, 1985), p. 189.
[43] M. Freidlin, *Functional Integration and Partial Differential Equations* (Princeton University Press, Princeton, 1985).
[44] W. H. Fleming and H. M. Soner, *Controlled Markov Processes and Viscosity Solutions* (Springer-Verlag, Berlin, 1993).
[45] Z. Schuss, *Theory and Applications of Stochastic Differential Equations* (Wiley, New York, 1980).
[46] J. B. Hubbard and P. G. Wolynes, J. Chem. Phys. **75**, 3051 (1981).
[47] W. Sung and H. L. Friedman, J. Chem. Phys. **87**, 649 (1987).
[48] H. Mori, Prog. Theor. Phys. **33**, 243 (1965).
[49] A. F. Izmailov, S. Arnold, S. Holler, and A. S. Myerson, Phys. Rev. E **52**, 1325 (1995).
[50] B. Simon, *Functional Integration and Quantum Physics* (Academic Press, New York, 1979).
[51] J. Glimm and A. Jaffe, *Quantum Physics—A Functional Integral Point of View* (Springer-Verlag, Berlin, 1981).
[52] H. Hasegawa, Prog. Theor. Phys. **56**, 44 (1976).
[53] K. L. C. Hunt, J. Chem. Phys. **75**, 976 (1981),
[54] M. Roncadelli, Phys. Rev. E **52**, 4661 (1995).
[55] F. W. Wiegel, J. Ross, Phys. Lett. **84A**, 465 (1981).
[56] G. Roepstorff, *Path Integral Approach to Quantum Physics* (Springer-Verlag, Berlin, 1994).
[57] J. Avron, I. Herbst, and B. Simon, Duke Math. J. **45**, 847 (1978).
[58] J. Avron, I. Herbst, and B. Simon, Commun. Math. Phys. **79**, 529 (1981).
[59] P. Garbaczewski, Phys. Lett. A **175**, 7 (1993).
[60] A. B. Cruzeiro and J. C. Zambrini, J. Funct. Anal. **96**, 62 (1991).
[61] A. M. Ilin, A. S. Kalashnikov, and O. A. Oleinik, Usp. Mat. Nauk **27**, 65 (1962).
[62] P. Besala, Ann. Pol. Math. **29**, 403 (1975).
[63] D. G. Aronson and P. Besala, Colloq. Math. **18**, 125 (1967).
[64] B. T. Geilikman, Zh. Éksp. Teor. Fiz. **17**, 830 (1947).
[65] P. Garbaczewski, Phys. Lett. A **162**, 129 (1992).

BURGERS VELOCITY FIELDS AND ELECTROMAGNETIC FORCING IN DIFFUSIVE (MARKOVIAN) MATTER TRANSPORT*

P. GARBACZEWSKI, G. KONDRAT, AND R. OLKIEWICZ

Institute of Theoretical Physics, University of Wrocław
M. Borna 9, 50-204 Wrocław, Poland

(Received October 4, 1996)

We explore a connection of the unforced and deterministically forced Burgers equation for local velocity fields with probabilistic solutions (here, Markovian diffusion processes) of the so-called Schrödinger boundary data problem. An issue of deducing the most likely interpolating dynamics from the given initial and terminal probability density data is investigated to give account of the perturbation by external electromagnetic fields. A suitable modification of the Hopf–Cole logarithmic transformation extends the standard framework, both in the Burgers and Schrödinger's interpolation cases, to non-gradient drift fields and forces.

PACS numbers: 02.50. -r, 05.20. +j, 03.65. -w, 47.27. -i

1. The Burgers equation in Schrödinger's interpolation problem

The Schrödinger problem of deducing the detailed microscopic dynamics from the given input-output statistics data is known to admit a particular class of solutions in terms of Markov diffusion processes, [1–8]. That especially pertains to an explicit modelling of any unknown in detail physical process solely on the basis of the available statistics (conditional probabilities and averages, invariant measures, time-dependent probability densities, density boundary-data) presumed to refer to random motions with a given finite time of duration.

At this point, let us invoke a probabilistic problem, originally due to Schrödinger: given two strictly positive (usually on an open space-interval) boundary probability densities $\rho_0(x), \rho_T(x)$ for a process with the time of duration $T \geq 0$. Can we uniquely identify the stochastic process interpolating between them?

* Presented by P. Garbaczewski at the IX Symposium on Statistical Physics, Zakopane, Poland, September 23–28, 1996.

The answer is known to be affirmative, if we assume the interpolating process to be Markovian. In particular, we can get here a unique Markovian diffusion process which is specified by the joint probability distribution

$$m_T(A,B) = \int\limits_A d^3x \int\limits_B d^3y\, m_T(\vec{x},\vec{y})\,, \tag{1}$$

$$\int d^3y\, m_T(\vec{x},\vec{y}) = \rho_0(\vec{x})\,,$$

$$\int d^3x\, m_T(\vec{x},\vec{y}) = \rho_T(y)\,,$$

where

$$m_T(\vec{x},\vec{y}) = u_0(\vec{x})\, k(x,0,y,T)\, v_T(\vec{y}) \tag{2}$$

and the two unknown functions $u_0(\vec{x})$, $v_T(\vec{y})$ come out as solutions of *the same sign* of the integral identities (1). Provided, we have at our disposal a continuous bounded strictly positive (ways to relax this assumption were discussed in Ref. [4]) integral kernel $k(\vec{x},s,\vec{y},t), 0 \leq s < t \leq T$.

We shall confine further attention to cases governed by the familiar Feynman–Kac kernels. Then, the solution of the Schrödinger boundary-data problem in terms of the interpolating Markovian diffusion process is found to rely on the adjoint pairs of parabolic equations. In case of gradient forward drift fields, the process can be determined by checking (this imposes limitations on the admissible potential) whether the Feynman–Kac kernel

$$k(\vec{y},s,\vec{x},t) = \int \exp\left[-\int\limits_s^t c(\vec{\omega}(\tau),\tau)d\tau\right] d\mu_{(\vec{x},t)}^{(\vec{y},s)}(\omega) \tag{3}$$

is positive and continuous in the open space-time area of interest (then, additional limitations on the path measure need to be introduced, [3]), and whether it gives rise to positive solutions of the adjoint pair of generalized heat equations:

$$\begin{aligned} \partial_t u(\vec{x},t) &= \nu\triangle u(\vec{x},t) - c(\vec{x},t)u(\vec{x},t)\,, \\ \partial_t v(\vec{x},t) &= -\nu\triangle v(\vec{x},t) + c(\vec{x},t)v(\vec{x},t)\,. \end{aligned} \tag{4}$$

Here, a function $c(\vec{x},t)$ is restricted only by the positivity and continuity demand for the kernel (3), see *e.g.* [2]. In the above, $d\mu_{(\vec{x},t)}^{(\vec{y},s)}(\omega)$ is the conditional Wiener measure over sample paths of the standard Brownian motion.

Solutions of (4), upon suitable normalization give rise to the Markovian diffusion process with the *factorized* probability density $\rho(\vec{x},t) = u(\vec{x},t)v(\vec{x},t)$

which, while evolving in time, interpolates between the boundary density data $\rho(\vec{x},0)$ and $\rho(\vec{x},T)$. The interpolation admits a realization in terms of Markovian diffusion processes with the respective forward and backward drifts defined as follows:

$$\vec{b}(\vec{x},t) = 2\nu\frac{\nabla v(\vec{x},t)}{v(\vec{x},t)}\,,$$
$$\vec{b}_*(\vec{x},t) = -2\nu\frac{\nabla u(\vec{x},t)}{u(\vec{x},t)} \tag{5}$$

in the prescribed time interval $[0,T]$.

The related transport equations for the densities easily follow. For the forward interpolation, the familiar Fokker–Planck equation holds true:

$$\partial_t\rho(\vec{x},t) = \nu\triangle\rho(\vec{x},t) - \nabla[\vec{b}(\vec{x},t)\rho(\vec{x},t)]\,, \tag{6}$$

while for the backward interpolation we have:

$$\partial_t\rho(\vec{x},t) = -\nu\triangle\rho(\vec{x},t) - \nabla[\vec{b}_*(\vec{x},t)\rho(\vec{x},t)]\,. \tag{7}$$

We have assumed that drifts are gradient fields, $\operatorname{curl}\vec{b} = 0$. As a consequence, those that are allowed by the prescribed choice of $c(\vec{x},t)$ *must* fulfill the compatibility condition

$$c(\vec{x},t) = \partial_t\Phi + \tfrac{1}{2}\left(\frac{b^2}{2\nu} + \nabla b\right) \tag{8}$$

which establishes the Girsanov-type connection of the forward drift $\vec{b}(\vec{x},t) = 2\nu\nabla\Phi(\vec{x},t)$ with the Feynman–Kac, *c.f.* [2, 3], potential $c(\vec{x},t)$. In the considered Schrödinger's interpolation framework, the forward and backward drift fields are connected by the identity $\vec{b}_* = \vec{b} - 2\nu\nabla\ln\rho$.

One of the distinctive features of Markovian diffusion processes with the positive density $\rho(\vec{x},t)$ is that, given the transition probability density of the (forward) process, the notion of the *backward* transition probability density $p_*(\vec{y},s,\vec{x},t)$ can be consistently introduced on each finite time interval, say $0 \le s < t \le T$:

$$\rho(\vec{x},t)p_*(\vec{y},s,\vec{x},t) = p(\vec{y},s,\vec{x},t)\rho(\vec{y},s)\,, \tag{9}$$

so that

$$\int \rho(\vec{y},s)p(\vec{y},s,\vec{x},t)d^3y = \rho(\vec{x},t)$$

and

$$\rho(\vec{y},s) = \int p_*(\vec{y},s,\vec{x},t)\rho(\vec{x},t)d^3x\,.$$

The transport (density evolution) equations (6) and (7) refer to processes running in opposite directions in a fixed, common for both, time-duration period. The forward one, (6), executes an interpolation from the Borel set A to B, while the backward one, (7), executes an interpolation from B to A, compare *e.g.* the defining identities (1).

The knowledge of the Feynman–Kac kernel (3) implies that the transition probability density of the forward process reads:

$$p(\vec{y},s,\vec{x},t) = k(\vec{y},s,\vec{x},t)\frac{v(\vec{x},t)}{v(\vec{y},s)}\,. \tag{10}$$

while the corresponding (derivable from (10), since $\rho(\vec{x},t)$ is given) transition probability density of the backward process has the form:

$$p_*(\vec{y},s,\vec{x},t) = k(\vec{y},s,\vec{x},t)\frac{u(\vec{y},s)}{u(\vec{x},t)}\,. \tag{11}$$

Obviously, [2,6], in the time interval $0 \le s < t \le T$ there holds:

$$\begin{aligned} u(\vec{x},t) &= \int u_0(\vec{y})k(\vec{y},s,\vec{x},t)d^3y\,,\\ v(\vec{y},s) &= \int k(\vec{y},s,\vec{x},T)v_T(\vec{x})d^3x\,. \end{aligned} \tag{12}$$

Now, we are at the point, where a connection of the previous probabilistic formalism with an issue of the Burgers velocity-driven matter transport, [5], can be disclosed.

The prototype nonlinear field equation named the Burgers or "nonlinear diffusion" equation (typically without, [9,10], the forcing term $\vec{F}(\vec{x},t)$):

$$\partial_t\vec{v}_B + (\vec{v}_B\nabla)\vec{v}_B = \nu\triangle\vec{v}_B + \vec{F}(\vec{x},t) \tag{13}$$

recently has acquired a considerable popularity in the variety of physical contexts, [5].

Burgers velocity fields can be analysed on their own with different (including random) choices of the initial data and/or force fields. However, we are interested in the possible diffusive matter transport that is locally governed by Burgers flows, *c.f.* [5]. In this particular connection, let us point out a conspicuous hesitation that could have been observed in attempts to establish the most appropriate matter transport rule, if any diffusion-type microscopic dynamics assumption is adopted to underlie the "nonlinear diffusion" (13).

Depending on the particular phenomenological departure point, one either adopts the standard continuity equation, [11,12], that is certainly valid

to a high degree of accuracy in the so-called low viscosity limit $\nu \downarrow 0$, but incorrect on mathematical grounds *if* there is a genuine Markovian diffusion process involved *and* simultaneously a solution of (13) stands for the respective *current* velocity of the flow: $\partial_t \rho(\vec{x}, t) = -\nabla[\vec{v}(\vec{x}, t)\rho(\vec{x}, t)]$.

Alternatively, following the white noise calculus tradition telling that the stochastic integral

$$\vec{X}(t) = \int_0^t \vec{v}_B(\vec{X}(s), s)ds + \int_0^t \vec{\eta}(s)ds$$

necessarily implies the Fokker–Planck equation, one is tempted to adopt: $\partial_t \rho(\vec{x}, t) = \nu \triangle \rho(\vec{x}, t) - \nabla[\vec{v}_B(\vec{x}, t)\rho(\vec{x}, t)]$ which is clearly problematic in view of the classic Mc Kean's discussion of the propagation of chaos for the Burgers equation, [13–15] and the derivation of the stochastic "Burgers process" in this context: "the fun begins in trying to describe this Burgers motion as the path of a tagged molecule in an infinite bath of like molecules", [13].

To put things on the solid ground, let us consider a Markovian diffusion process, which is characterized by the transition probability density (generally inhomogeneous in space and time law of random displacements) $p(\vec{y}, s, \vec{x}, t)$, $0 \leq s < t \leq T$, and the probability density $\rho(\vec{x}, t)$ of its random variable $\vec{X}(t)$, $0 \leq t \leq T$. The process is completely determined by these data. For clarity of discussion, we do not impose any spatial boundary restrictions, nor fix any concrete limiting value of T which, in principle, can be moved to infinity.

Let us confine attention to processes defined by the standard backward diffusion equation. Under suitable restrictions (boundedness of involved functions, their continuous differentiability) the function:

$$g(\vec{x}, s) = E\{g(\vec{X}(T))|\vec{X}(s) = \vec{x}; s \leq T\} = \int p(\vec{x}, s, \vec{y}, T)g(\vec{y}, T)d^3y\,, \quad (14)$$

satisfies the equation

$$-\partial_s g(\vec{x}, s) = \nu \triangle g(\vec{x}, s) + [\vec{b}(\vec{x}, s)\nabla]g(\vec{x}, s)\,. \quad (15)$$

Let us point out that the validity of (14) is known to be a *necessary* condition for the existence of a Markov diffusion process, whose probability density $\rho(\vec{x}, t)$ is to obey the Fokker–Planck equation (the forward drift $\vec{b}(\vec{x}, t)$ replaces the previously utilized Burgers velocity $\vec{v}_B(\vec{x}, t)$).

The case of particular interest, in the traditional nonequilibrium statistical physics literature, appears when $p(\vec{y}, s, \vec{x}, t)$ is a *fundamental solution* of (15) with respect to variables $\vec{y}, s$, [16–18], see however [2] for an analysis of alternative situations. Then, the transition probability density satisfies *also*

the second Kolmogorov (*e.g.* the Fokker–Planck) equation in the remaining $\vec{x}, t$ pair of variables. Let us emphasize that these two equations form an adjoint pair of partial differential equations, referring to the slightly counter-intuitive for physicists, though transparent for mathematicians, [6,7,19–22], issue of time reversal of diffusions.

We can consistently introduce the random variable of the process in the form

$$\vec{X}(t) = \int_0^t \vec{b}(\vec{X}(s), s)\, ds + \sqrt{2\nu}\vec{W}(t)\,.$$

Then, in view of the standard rules of the Itô stochastic calculus, [6,7,22,23], we realize that for any smooth function $f(\vec{x}, t)$ of the random variable $\vec{X}(t)$ the conditional expectation value:

$$\lim_{\Delta t \downarrow 0} \frac{1}{\Delta t} \left[\int p(\vec{x}, t, \vec{y}, t + \Delta t) f(\vec{y}, t + \Delta t) d^3y - f(\vec{x}, t)\right]$$
$$= (D_+ f)(\vec{X}(t), t) = (\partial_t + \vec{b}\nabla + \nu\Delta) f(\vec{x}, t)\,, \qquad (16)$$

where $\vec{X}(t) = \vec{x}$, determines the forward drift $\vec{b}(\vec{x}, t)$ of the process (if we set components of $\vec{X}$ instead of f) and, moreover, allows to introduce the local field of (forward) accelerations associated with the diffusion process, which we *constrain* by demanding (see *e.g.* Refs [6,7,22,23] for prototypes of such dynamical constraints):

$$(D_+^2 \vec{X})(t) = (D_+ \vec{b})(\vec{X}(t), t) = (\partial_t \vec{b} + (\vec{b}\nabla)\vec{b} + \nu\Delta\vec{b})(\vec{x}, t) = \vec{F}(\vec{x}, t)\,, \quad (17)$$

where $\vec{X}(t) = \vec{x}$ and, at the moment arbitrary, function $\vec{F}(\vec{x}, t)$ may be interpreted as an external forcing applied to the diffusing system, [3].

By invoking (9), we can also define the backward derivative of the process in the conditional mean (*c.f.* [3,24,25] for a discussion of these concepts in case of the most traditional Brownian motion and Smoluchowski-type diffusion processes)

$$\lim_{\Delta t \downarrow 0} \frac{1}{\Delta t} \left[\vec{x} - \int p_*(\vec{y}, t - \Delta t, \vec{x}, t)\vec{y} d^3y\right] = (D_- \vec{X})(t) = \vec{b}_*(\vec{X}(t), t) \quad (18)$$

$$(D_- f)(\vec{X}(t), t) = (\partial_t + \vec{b}_*\nabla - \nu\Delta) f(\vec{X}(t), t)\,.$$

Accordingly, the backward version of the acceleration field reads

$$(D_-^2 \vec{X})(t) = (D_+^2 \vec{X})(t) = \vec{F}(\vec{X}(t), t)\,, \qquad (19)$$

where in view of $\vec{b}_* = \vec{b} - 2\nu\nabla \ln \rho$ we have explicitly fulfilled the *forced Burgers equation*:

$$\partial_t \vec{b}_* + (\vec{b}_*\nabla)\vec{b}_* - \nu\triangle\vec{b}_* = \vec{F} \tag{20}$$

and, [3,6,22], under the gradient-drift field assumption, curl $\vec{b}_* = 0$, we deal with $\vec{F}(\vec{x},t) = 2\nu\nabla c(\vec{x},t)$ where the Feynman–Kac potential (3) is explicitly involved.

Let us notice that the familiar (linearization of the nonlinear problem) Hopf–Cole transformation, [10,26], of the Burgers equation into the generalized diffusion equation (yielding explicit solutions in the unforced case) has been explicitly used before (the second formula (4)) in the framework of the Schrödinger interpolation problem. In fact, by defining $\Phi_* = \log u$, we immediately recover the traditional form of the Hopf–Cole transformation for Burgers velocity fields: $\vec{b}_* = -2\nu\nabla\Phi_*$. In the standard considerations that allows to map a nonlinear (unforced Burgers) equation into a linear, heat, equation. In the special case of the standard free Brownian motion, there holds $\vec{b}(\vec{x},t) = 0$ while $\vec{b}_*(\vec{x},t) = -2\nu\nabla \log \rho(\vec{x},t)$.

2. The problem of electromagnetic forcing in the Schrödinger interpolating dynamics

It turns out the crucial point of our previous discussion lies in a *proper* choice of the strictly positive and continuous, in an open space-time area, function $k(\vec{y},s,\vec{x},t)$ which, if we wish to construct a Markov process, has to satisfy the Chapman–Kolmogorov (semigroup composition) equation. It has led us to consider a pair of adjoint parabolic differential equations, as an alternative to more familiar Fookker–Planck and backward diffusion equations.

In the quantally oriented literature dealing with Schrödinger operators and their spectral properties, [27–29], the potential $c(x,t)$ is usually assumed to be a continuous and bounded from below function, but these restrictions can be substantially relaxed (unbounded functions are allowed in principle) if we wish to consider general Markovian diffusion processes and disregard an issue of the bound state spectrum and this of the ground state of the (self-adjoint) semigroup generator, [16,17]. Actually, what we need is merely that properties of $c(\vec{x},t)$ allow for the kernel k which is positive and continuous function. By taking for granted that suitable conditions are fulfilled, [2,27], we can immediately associate with equations (4) an integral kernel of the time-dependent semigroup (the exponential operator should be understood as time-ordered expression, since in general $H(\tau)$ may not commute with

$H(\tau')$ for $\tau \neq \tau'$):

$$k(\vec{y}, s, \vec{x}, t) = \left[\exp(-\int_s^t H(\tau)d\tau)\right](\vec{y}, \vec{x}), \tag{21}$$

where $H(\tau) = -\nu\triangle + c(\tau)$ is the pertinent semigroup generator. Then, by the Feynman–Kac formula, [30], we get a standard path integral expression (3) for the kernel, which in turn yields (5)–(8), see *e.g.* [2]. The above formalism is known, [3], to encompass the standard Smoluchowski-type diffusions in conservative force fields.

Strikingly, an investigation of electromagnetically forced diffusions has not been much pursued in the literature, although an issue of deriving the Smoluchowski–Kramers equation (and possibly its large friction limit) from the Langevin-type equation for the charged Brownian particle in the general electromagnetic field has been relegated in Ref. [31], Chap. 6.1 to the status of the innocent-looking exercise. On the other hand, the diffusion of realistic charges in dilute ionic solutions creates a number of additional difficulties due to the apparent Hall mobility in terms of mean currents induced by the electric field (once assumed to act upon the system), see *e.g.* [32,33] and [34].

In connection with the electromagnetic forcing of diffusing charges, the gradient field assumption imposes a severe limitation if we account for typical (nonzero circulation) features of the classical motion due to the Lorentz force, with or without the random perturbation component. The purely electric forcing is simpler to handle, since it has a definite gradient field realization, see *e.g.* [35] for a recent discussion of related issues. The major obstacle with respect to our previous (Section 1) discussion is that, if we wish to regard either the force $\vec{F}$, or drifts $\vec{b}$, $\vec{b}_*$ to have an electromagnetic provenience, then necessarily we need to pass from conservative to nonconservative fields. This subject matter has not been significantly exploited so far in the nonequilibrium statistical physics literature.

Usually, the selfadjoint semigroup generators attract the attention of physicists in connection with the Feynman–Kac formula. A typical route towards incorporating electromagnetism comes from quantal motivations via the minimal electromagnetic coupling recipe which preserves the selfadjointness of the generator (Hamiltonian of the system). As such, it constitutes a part of the general theory of Schrödinger operators. A rigorous study of operators of the form $-\triangle + V$ has become a well developed mathematical discipline, [27]. The study of Schrödinger operators with magnetic fields, typically of the form $-(\nabla - i\vec{A})^2 + V$, is less advanced, although specialized chapters on the magnetic field issue can be found in monographs devoted

to functional integration methods, [27, 36], mostly in reference to seminal papers [37, 38].

From the mathematical point of view, it is desirable to deal with magnetic fields that go to zero at infinity, which is certainly acceptable on physical grounds as well. The constant magnetic field does not meet this requirement, and its notorious usage in the literature makes us (at the moment) to decline the asymptotic assumption and inevitably fall into a number of serious complications.

One obvious obstacle can be seen immediately by taking advantage of the existing results, [37]. Namely, an explicit expression for the Feynman–Kac kernel in a constant magnetic field, introduced through the minimal electromagnetic coupling recipe $H(\vec{A}) = -\frac{1}{2}(\nabla - i\vec{A})^2$, is available (up to irrelevant dimensional constants):

$$\exp\left[-tH(\vec{A})\right](\vec{x},\vec{y}) = \left[\frac{B}{4\pi\sinh(\frac{1}{2}Bt)}\right]\left(\frac{1}{2\pi t}\right)^{1/2}$$
$$\times\exp\left\{-\frac{1}{2t}(x_3-y_3)^2-\frac{B}{4}\coth\left(\frac{B}{2}t\right)[(x_2-y_2)^2+(x_1-y_1)^2]-i\frac{B}{2}(x_1y_2-x_2y_1)\right\}. \tag{22}$$

Clearly, it is *not* real (hence *non-positive* and directly at variance with the major demand in the Schrödinger interpolation problem, as outlined in Section 1), except for directions $\vec{y}$ that are parallel to a chosen $\vec{x}$.

Consequently, a bulk of the well developed mathematical theory is *of no use* for our purposes and new techniques must be developed for a consistent description of the electromagnetically forced diffusion processes along the lines of Section 1, *i.e.* within the framework of Schrödinger's interpolation problem.

3. Forcing via Feynman–Kac semigroups

The conditional Wiener measure $d\mu^{(\vec{y},s)}_{(\vec{x},t)}(\vec{\omega})$, appearing in the Feynman–Kac kernel definition (3), if unweighed (set $c(\vec{\omega}(\tau),\tau)=0$) gives rise to the familiar heat kernel. This, in turn, induces the Wiener measure P_{W} of the set of all sample paths,which originate from $\vec{y}$ at time s and terminate (can be located) in the Borel set $A\in R^3$ after time $t-s$:

$$P_{\mathrm{W}}[A] = \int_A d^3x \int d\mu^{(\vec{y},s)}_{(\vec{x},t)}(\vec{\omega}) = \int_A d\mu\,,$$

where, for simplicity of notation, the $(\vec{y},t-s)$ labels are omitted and $\mu^{(\vec{y},s)}_{(\vec{x},t)}$ stands for the heat kernel.

Having defined an Itô diffusion

$$\vec{X}(t) = \int_0^t \vec{b}(\vec{x}, u)du + \sqrt{2\nu}\vec{W}(t)\,,$$

we are interested in the analogous path measure:

$$P_{\vec{X}}[A] = \int_A dx \int d\mu_{(\vec{x},t)}^{(\vec{y},s)}(\vec{\omega}_{\vec{X}}) = \int_A d\mu(\vec{X})\,.$$

Under suitable (stochastic, [3]) integrability conditions imposed on the forward drift, we have granted the absolute continuity $P_X \ll P_W$ of measures, which implies the existence of a strictly positive Radon–Nikodym density. Its canonical Cameron–Martin–Girsanov form, [3,27], reads:

$$\frac{d\mu(\vec{X})}{d\mu}(\vec{y}, s, \vec{x}, t) = \exp\frac{1}{2\nu}\left[\int_s^t \vec{b}(\vec{X}(u), u)d\vec{X}(u) - \frac{1}{2}\int_s^t [\vec{b}(\vec{X}(u), u)]^2 du\right]. \tag{23}$$

If we assume that drifts are gradient fields, $\operatorname{curl}\vec{b} = 0$, then the Itô formula allows to reduce, otherwise troublesome, stochastic integration in the exponent of (23), [27,36], to ordinary Lebesgue integrals:

$$\frac{1}{2\nu}\int_s^t \vec{b}(\vec{X}(u), u)d\vec{X}(u) = \Phi(\vec{X}(t), t) - \Phi(\vec{X}(s), s) - \int_s^t du\,[\partial_t\Phi + \frac{1}{2}\nabla\vec{b}](\vec{X}(u), u)\,. \tag{24}$$

After inserting (24) to (23) and next integrating with respect to the conditional Wiener measure, on account of (10) we arrive at the standard form of the Feynman–Kac kernel (3). Notice that (24) establishes a probabilistic basis for logarithmic transformations (5) of forward and backward drifts: $b = 2\nu\nabla \ln v = 2\nu\nabla\Phi$, $b_* = -2\nu\nabla \ln u = -2\nu\nabla\Phi_*$. The forward version is commonly used in connection with the transformation of the Fokker–Planck equation into the generalized heat equation, [3,39,40]. The backward version is just the Hopf–Cole transformation, mentioned in Section 1, used to map the Burgers equation into the very same generalized heat equation, [10].

However, presently we are interested in non-conservative drift fields, $\operatorname{curl}\vec{b} \neq 0$, and in that case the stochastic integral in (23) is the major source of computational difficulties, [22,27,36], for nontrivial vector potential field

configurations. It explains the virtual absence of magnetically forced diffusion problems in the nonequilibrium statistical physics literature.

At this point, some steps of the analysis performed in Ref. [41] in the context of the "Euclidean quantum mechanics", *c.f.* also [7], are extremely useful. Let us emphasize that electromagnetic fields we utilize, are always meant to be ordinary Maxwell fields with *no* Euclidean connotations (see *e.g.* Chap. 9 of Ref. [36] for the Euclidean version of Maxwell theory).

Let us consider a gradient drift-field diffusion problem according to Section 1, with (2), (24) involved and thus an adjoint pair (4) of parabolic equations completely defining the Markovian diffusion process. Furthermore, let $\vec{A}(\vec{x})$ be the time-independent vector potential for the Maxwellian magnetic field $\vec{B} = \operatorname{curl} \vec{A}$. We pass from the gradient realization of drifts to the new one, generalizing (5), for which the following decomposition into the gradient and nonconservative part is valid:

$$\vec{b}(\vec{x}, t) = 2\nu \nabla \Phi(\vec{x}, t) - \vec{A}(\vec{x}) , \tag{25}$$

We denote $\theta(\vec{x}, t) \doteq \exp[\Phi(\vec{x}, t)]$ and admit that (25) is a forward drift of an Itô diffusion process with a stochastic differential

$$d\vec{X}(t) = \left[2\nu \frac{\nabla \theta}{\theta} - \vec{A}\right] dt + \sqrt{2\nu} d\vec{W}(t) .$$

On purely formal grounds, we deal here with an example of the Cameron–Martin–Girsanov transformation of the forward drift of a given Markovian diffusion process and we are entitled to ask for a corresponding measure transformation, (23).

To this end, let us furthermore *assume* that $\theta(\vec{x}, t) = \theta$ solves a partial differential equation

$$\partial_t \theta = -\nu \left[\nabla - \frac{1}{2\nu} \vec{A}(\vec{x})\right]^2 \theta + c(\vec{x}, t)\theta \tag{26}$$

with the notation $c(\vec{x}, t)$ patterned after (8). Then, by using the Itô calculus and (25), (26) on the way, see *e.g.* Ref. [41], we can rewrite (23) as follows:

$$\begin{aligned} &\frac{d\mu(\vec{X})}{d\mu}(\vec{y}, s, \vec{x}, t) \\ &= \exp \frac{1}{2\nu} \left[\int_s^t (2\nu \frac{\nabla \theta}{\theta} - \vec{A})(\vec{X}(u), u) d\vec{X}(u) - \frac{1}{2} \int_s^t (2\nu \frac{\nabla \theta}{\theta} - \vec{A})^2 (\vec{X}(u), u)\, du\right] \\ &= \frac{\theta(\vec{X}(t), t)}{\theta(\vec{X}(s), s)} \exp \left[-\frac{1}{2\nu} \int_s^t [\vec{A}(u) d\vec{X}(u) + \nu(\nabla \vec{A})(\vec{X}(u)) du + \Omega(\vec{X}(u), u) du]\right] , \end{aligned} \tag{27}$$

where $\vec{X}(s) = \vec{y}$, $\vec{X}(t) = \vec{x}$ and $\Omega(\vec{x}, t) = 2\nu c(\vec{x}, t)$.

More significant observation is that the Radon–Nikodym density (27), if integrated with respect to the conditional Wiener measure, gives rise to the Feynman–Kac kernel (21) of the *non-selfadjoint* semigroup (suitable integrability conditions need to be respected here as well, [41]), with the generator $H_{\vec{A}} = -\nu[\nabla - \frac{1}{2\nu}\vec{A}(\vec{x})]^2 + c(\vec{x}, t)$ defined by the right-hand-side of (26):

$$\begin{aligned} \partial_t \theta(\vec{x}, t) &= H_{\vec{A}}\theta(\vec{x}, t) \\ &= \left[-\nu\triangle + \vec{A}(\vec{x})\nabla + \frac{1}{2}(\nabla\vec{A}(\vec{x})) - \frac{1}{4\nu}[\vec{A}(\vec{x})]^2 + c(\vec{x}, t)\right]\theta(\vec{x}, t) \\ &= -\nu\triangle\theta(\vec{x}, t) + \vec{A}(\vec{x})\nabla\theta(\vec{x}, t) + c_{\vec{A}}(\vec{x}, t)\theta(\vec{x}, t)\,. \end{aligned} \tag{28}$$

Here:

$$c_A(\vec{x}, t) = c(\vec{x}, t) + \frac{1}{2}(\nabla\vec{A})(\vec{x}) - \frac{1}{4\nu}[\vec{A}(\vec{x})]^2\,. \tag{29}$$

An adjoint parabolic partner of (28) reads:

$$\begin{aligned} \partial_t\theta_* &= -H^*_{\vec{A}}\theta_* = \nu\triangle\theta_* + \nabla[\vec{A}(\vec{x})\theta_*] - c_A(\vec{x}, t)\theta_* \\ &= \nu\left[\nabla + \frac{1}{2\nu}\vec{A}(\vec{x})\right]^2\theta_* - c(\vec{x}, t)\theta_*\,. \end{aligned} \tag{30}$$

Consequently, our assumptions (25), (26) involve a generalization of the adjoint parabolic system (14) to a new adjoint one comprising (26), (30). Obviously, the original form of (14) is immediately restored by setting $\vec{A} = \vec{0}$, and executing obvious replacements $\theta_* \to u$, $\theta \to v$.

Let us emphasize again, that in contrast to Ref. [41], where the non-Hermitean generator $2\nu H_{\vec{A}}$, (26), has been introduced as "the Euclidean version of the Hamiltonian" $H = -2\nu^2(\nabla - \frac{i}{2\nu}\vec{A})^2 + \Omega$, our electromagnetic fields stand for solutions of the usual Maxwell equations and *are not* Euclidean at all.

As long as the coefficient functions (both additive and multiplicative) of the adjoint parabolic system (28), (30) are not specified, we remain within a general theory of positive solutions for parabolic equations with unbounded coefficients (of particular importance, if we do not impose any asymptotic fall off restrictions), [16,43–45]. The fundamental solutions, if their existence can be granted, usually live on space-time strips, and generally do not admit unbounded time intervals. We shall disregard these issues at the moment, and assume the existence of fundamental solutions without any reservations.

By exploiting the rules of functional (Malliavin, variational) calculus, under an assumption that we deal with a diffusion (in fact, Bernstein) process associated with an adjoint pair (28), (30), it has been shown in Ref. [41]

that *if* the forward conditional derivatives of the process exist, then $(D_+\vec{X})(t) = 2\nu\frac{\nabla\theta}{\theta} - \vec{A} = \vec{b}(\vec{x},t)$, (32) and:

$$(D_+^2\vec{X})(t) = (D_+\vec{X})(t) \times \text{curl}\,\vec{A}(\vec{x}) + \nabla\Omega(\vec{x},t) + \nu\text{curl}\,(\text{curl}\,\vec{A}(\vec{x}))\,, \quad (31)$$

where $\vec{X}(0) = 0$, $\vec{X}(t) = \vec{x}$, $\times$ denotes the vector product in R^3 and $2\nu c = \Omega$.

Since $\vec{B} = \text{curl}\,\vec{A} = \mu_0\vec{H}$, we identify in the above the standard Maxwell equation for curl $\vec{H}$ comprising magnetic effects of electric currents in the system: $\text{curl}\,\vec{B} = \mu_0[\dot{\vec{D}} + \sigma_0\vec{E} + \vec{J}_{\text{ext}}]$ where $\vec{D} = \epsilon_0\vec{E}$ while $\vec{J}_{\text{ext}}$ represents external electric currents. In case of $\vec{E} = \vec{0}$, the external currents only would be relevant. A demand $\text{curl}\,\text{curl}\,\vec{A} = \nabla(\nabla\vec{A}) - \triangle\vec{A} = 0$ corresponds to a total absence of such currents, and the Coulomb gauge choice $\nabla\vec{A} = 0$ would leave us with harmonic functions $\vec{A}(\vec{x})$.

Consequently, a correct expression for the magnetically implemented Lorentz force has appeared on the right-hand-side of the forward acceleration formula (31), with the forward drift (25) replacing the classical particle velocity $\vec{q}$ of the normal classical formula.

The above discussion implicitly involves quite sophisticated mathematics, hence it is instructive to see that we can bypass the apparent complications by directly invoking the universal definitions (16) and (18) of conditional expectation values, that are based on exploitation of the Itô formula only. Obviously, under an assumption that the Markovian diffusion process with well defined transition probability densities $p(\vec{y},s,\vec{x},t)$ and $p_*(\vec{y},s,\vec{x},t)$, does exist.

We shall utilize an obvious generalization of canonical definitions (5) of both forward and backward drifts of the diffusion process defined by the adjoint parabolic pair (4), as suggested by (25) with $\vec{A} = \vec{A}(\vec{x})$:

$$\vec{b} = 2\nu\frac{\nabla\theta}{\theta} - \vec{A}\,, \quad \vec{b}_* = -2\nu\frac{\nabla\theta_*}{\theta_*} - \vec{A}\,. \quad (32)$$

We also demand that the corresponding adjoint equations (28), (30) *are* solved by θ and θ_* respectively.

Taking for granted that identities $(D_+\vec{X})(t) = \vec{b}(\vec{x},t)$, $\vec{X}(t) = \vec{x}$ and $(D_-\vec{X})(t) = \vec{b}_*(\vec{x},t)$ hold true, we can easily evaluate the forward and backward accelerations (substitute (32), and exploit the equations (28), (30)):

$$(D_+\vec{b})(\vec{X}(t),t) = \partial_t\vec{b} + (\vec{b}\nabla)\vec{b} + \nu\triangle\vec{b}$$
$$= \vec{b}\times\vec{B} + \nu\,\mathrm{curl}\,\vec{B} + \nabla\,\Omega \qquad (33)$$

and

$$(D_-\vec{b}_*)(\vec{X}(t),t) = \partial_t\vec{b}_* + (\vec{b}_*\nabla)\vec{b}_* - \nu\triangle\vec{b}_*$$
$$= \vec{b}_*\times\vec{B} - \nu\,\mathrm{curl}\,\vec{B} + \nabla\,\Omega\,. \qquad (34)$$

Let us notice that the forward and backward acceleration formulas *do not* coincide as was the case before (*c.f.* Eq. (17)). There is a definite time-asymmetry in the local description of the diffusion process in the presence of general magnetic fields, unless $\mathrm{curl}\,\vec{B} = 0$. The quantity which is explicitly time-reversal invariant can be easily introduced:

$$\vec{v}(\vec{x},t) = \tfrac{1}{2}(\vec{b}+\vec{b}_*)(\vec{x},t) \Rightarrow \tfrac{1}{2}(D_+^2 + D_-^2)(\vec{X}(t)) = \vec{v}\times\vec{B} + \nabla\,\Omega\,. \qquad (35)$$

As yet there is no trace of Lorentzian electric forces, unless extracted from the term $\nabla\,\Omega(\vec{x},t)$.

For a probability density $\theta_*\theta = \rho$ of the related Markovian diffusion process, [2,6], we would have fulfilled both the Fokker–Planck and the continuity equations: $\partial_t\rho = \nu\triangle\rho - \nabla(\vec{b}\rho) = -\nabla(\vec{v}\rho) = -\nu\triangle\rho - \nabla(\vec{b}_*\rho)$, as before (*c.f.* Section 1).

In the above, the equation (34) can be regarded as the Burgers equation with a general external magnetic (plus other external force contributions if necessary) forcing, and its definition is an outcome of the underlying mathematical structure related to the adjoint pair (26), (30) of parabolic equations. Our construction shows that the solution of the magnetically forced Burgers equation needs to be sought in the form (32).

Two of the authors (P. G. and R. O.) received a financial support from the KBN research grant No 2 P302 057 07. P. G. would like to express his gratitude to Professors Ana Bela Cruzeiro and Jean-Claude Zambrini for enlightening discussions.

REFERENCES

[1] P. Garbaczewski, J.R. Klauder, R. Olkiewicz, *Phys. Rev.* **E51**, 4114 (1995).
[2] P. Garbaczewski, R. Olkiewicz, *J. Math. Phys.* **37**, 732 (1996).
[3] Ph. Blanchard, P.Garbaczewski, *Phys. Rev.* **E49**, 3815 (1994).
[4] P. Garbaczewski, *Acta Phys. Pol.* **B27**, 617 (1996).

[5] P. Garbaczewski, G. Kondrat, *Phys. Rev. Lett.* **77**, 2608 (1996).

[6] J.C. Zambrini, *J. Math. Phys.* **27**, 3207 (1986).

[7] J.C. Zambrini, pp. 393, in: *Chaos-The Interplay Between Stochastic and Deterministic Behaviour*, eds P. Garbaczewski, M. Wolf, A. Weron, LNP vol 457, Springer-Verlag, Berlin 1995.

[8] T. Mikami, *Commun. Math. Phys.* **135**, 19 (1990).

[9] J.M. Burgers, *The Nonlinear Diffusion Equation*, Reidel, Dordrecht 1974.

[10] E. Hopf, *Commun. Pure Appl. Math.* **3**, 201 (1950).

[11] S.F. Shandarin, B.Z. Zeldovich, *Rev. Mod. Phys.* **61**, 185 (1989).

[12] S. Albeverio, A.A. Molchanov, D. Surgailis, *Prob. Theory Relat. Fields* **100**, 457 (1994).

[13] H.P. Mc Kean, pp. 177, in: *Lecture Series in Differential Equations*, vol. II, ed. A.K. Aziz, Van Nostrand, Amsterdam 1969.

[14] P. Calderoni, M. Pulvirenti, *Ann. Inst. Henri Poincaré*, **39**, 85 (1983).

[15] H. Osada, S. Kotani, *J. Math. Soc. Japan*, **37**, 275 (1985).

[16] M. Krzyżański, A. Szybiak, *Lincei-Rend. Sc. Fis. Mat. e Nat.* **28**, 26 (1959).

[17] A. Friedman, *Partial Differential Equations of Parabolic type*, Prentice-Hall, Englewood, NJ 1964.

[18] W. Horsthemke, R. Lefever, *Noise-Induced Transitions*, Springer-Verlag, Berlin 1984.

[19] U.G. Haussmann, E. Pardoux, *Ann. Prob.* **14**, 1188 (1986).

[20] H. Föllmer,, in: *Stochastic Processes-Mathematics and Physics*, eds S. Albeverio, Ph. Blanchard, L. Streit, LNP vol. 1158, Springer-Verlag, Berlin 1985, p. 119.

[21] H. Hasegawa, *Progr.Theor. Phys.* **55**, 90 (1976).

[22] E. Nelson, *Quantum Fluctuations*, Princeton University Press, Princeton 1985.

[23] E. Nelson, *Dynamical Theories of the Brownian Motion*, Princeton University Press, Princeton 1967.

[24] P. Garbaczewski, J.P. Vigier, *Phys. Rev.* **A46**, 4634 (1992).

[25] P. Garbaczewski, R. Olkiewicz, *Phys. Rev.* **A51**, 3445 (1995).

[26] W.H. Fleming, H.M. Soner, *Controlled Markov Processes and Viscosity Solutions*, Springer-Verlag, Berlin 1993.

[27] B. Simon, *Functional Integration and Quantum Physics*, Academic Press, New York 1979.

[28] J. Glimm, A. Jaffe, *Quantum Physics-A Functional Integral Point of View*, Springer-Verlag, Berlin 1981.

[29] K.L. Chung, Z. Zhao, *From Brownian Motion to Schrödinger Equation*, Springer-Verlag, Berlin 1995.

[30] M. Freidlin, *Functional Integration and Partial Differential Equations*, Princeton University Press, Princeton 1985.

[31] Z. Schuss, *Theory and Applications of Stochastic Differential Equations*, Wiley, NY 1980.

[32] J.B. Hubbard, P.G. Wolynes, *J. Chem. Phys.* **75**, 3051 (1981).

[33] W. Sung, H.L. Friedman, *J. Chem. Phys.* **87**, 649 (1987).
[34] H. Mori, *Progr. Theor. Phys.* **33**, 243 (1965).
[35] A.F. Izmailov, S. Arnold, S. Holler, A.S. Myerson, *Phys. Rev.* **E52**, 1325 (1995).
[36] G. Roepstorff, *Path Integral Approach to Quantum Physics*, Springer-Verlag, Berlin 1994.
[37] J. Avron, I. Herbst, B. Simon, *Duke Math. Journ.* **45**, 847 (1978).
[38] J. Avron, I. Herbst, B. Simon, *Commun. Math. Phys.* **79**, 529 (1981).
[39] H. Risken, *The Fokker-Planck Equation*, Springer-Verlag, Berlin 1989.
[40] P. Garbaczewski, *Phys. Lett.* **A175**, 7 (1993).
[41] A.B. Cruzeiro, J.C. Zambrini, *J. Funct. Anal.* **96**, 62 (1991), see also [42].
[42] H. Hasegawa, *Phys. Rev.* **D33**, 2508 (1986).
[43] A.M. Ilin, A.S. Kalashnikov, O.A. Oleinik, *Usp. Mat. Nauk* (in Russian), **27**, 65 (1962).
[44] P. Besala, *Ann. Polon. Math.* **29**, 403 (1975).
[45] D.G. Aronson, P. Besala, *Colloq. Math.* **18**, 125 (1967).

Pergamon

Chaos, Solitons & Fractals, Vol. 9, No. 1/2, pp. 29–41, 1998

Printed in Great Britain
0960-0779/98 $19.00 + 0.00

PII: S0960-0779(97)00046-5

Schrödinger's Interpolating Dynamics and Burgers' Flows†

PIOTR GARBACZEWSKI, GRZEGORZ KONDRAT and ROBERT OLKIEWICZ

Institute of Theoretical Physics, University of Wrocław, Pl. M. Borna 9, PL-50 204 Wrocław, Poland

Abstract—We discuss a connection (and a proper place in this framework) of the unforced and deterministically forced Burgers equation for local velocity fields of certain flows, with probabilistic solutions of the so-called Schrödinger interpolation problem. The latter allows us to reconstruct the microscopic dynamics of the system from the available probability density data, or the input–output statistics in the phenomenological situations. An issue of deducing the most likely dynamics (and matter transport) scenario from the given initial and terminal probability density data, appropriate e.g. for studying chaos in terms of density, is here exemplified in conjunction with Born's statistical interpretation postulate in quantum theory, that yields stochastic processes which are compatible with the Schrödinger picture of free quantum evolution. © 1998 Elsevier Science Ltd. All rights reserved

1. THE SCHRÖDINGER RECONSTRUCTION PROBLEM: MOST LIKELY MICROSCOPIC DYNAMICS FROM THE INPUT–OUTPUT STATISTICS DATA

Probability measures, both invariant and non-trivially time-dependent, often on different levels of abstraction, are ubiquitous in diverse areas of physics. According to pedestrian intuition [1], one normally expects that any kind of time development (dynamics, be they deterministic or random) analysable in terms of probability under suitable mathematical restrictions may give rise to a well-defined stochastic process. Non-Markovian implementations are regarded as close to reality, but the corresponding Markovian approximations (when appropriate) are easier to handle analytically.

Given a dynamical law of motion (for a particle as an example), in many cases one can associate with it (compute or approximate the observed frequency data) a probability distribution and various mean values. In fact, it is well known that inequivalent finite difference random motion problems may give rise to the same continuous approximant (like, for example, in the case of the diffusion equation representation of discrete processes). Also, in the study of nonlinear dynamical systems, specifically those exhibiting the so-called deterministic chaos [2–4], given almost any (basically one-dimensional in the cited references) probability density, it is possible to construct an infinite number of deterministic finite difference equations, whose iterates are chaotic and which give rise to this *a priori* prescribed density.

Studying dynamics in terms of densities of probability measures instead of individual paths (trajectories) of a physical system is a respectable tool [3], even if we know exactly the pertinent microscopic dynamics.

Under general circumstances, the main task of a physicist is to fit a concrete dynamical model (through a clever guess or otherwise) to available phenomenological data. Then, the

†Presented by P. Garbaczewski at the *International Conference on Applied Chaotic Systems*, Inowłodz, Poland, September 26–30, 1996.

distinction between the chaotic (nonlinear, deterministic) and purely stochastic implementations may not be sharp enough to allow for a clean discrimination between those options: the intrinsic interplay between the stochastic and deterministic modelling of physical phenomena [4] blurs access to reality and certainly precludes a definitive choice of one type of modelling against another.

An *inverse* operation of deducing the detailed (possibly individual, microscopic) dynamics, which are either compatible with a given probability measure (we shall mostly be interested in those admitting densities) or induce their own time evolution, cannot have a unique solution. However, the level of ambiguity can be substantially reduced, if we invoke the so-called Schrödinger problem of reconstructing the microscopic dynamics from the given input–output statistics data and/or from the *a priori* known time development of a given probability density. The problem is known to give rise to a particular class of solution (*most likely* interpolations), in terms of Markov diffusion processes [5–8].

In its original formulation, due to Schrödinger [5–9], one seeks the answer to the following question: given two strictly positive (usually on an open space-interval) boundary probability densities $\rho_0(\vec{x})$, $\rho_T(\vec{x})$ for a process with duration $T > 0$, can we *uniquely* identify the stochastic process interpolating between them?

Another version of the same problem [5] departs from a given (Fokker–Planck-type) probability density evolution and investigates the circumstances allowing us to deduce a unique random process from these dynamics. We shall pay some attention to this issue in Section 3.

The answer to the above Schrödinger's question is known to be affirmative, if we assume the interpolating process to be Markovian. In particular, we can get here a unique Markovian diffusion process which is specified by the joint probability distribution

$$m_T(A,B) = \int_A \mathrm{d}^3x \int_B \mathrm{d}^3y m_T(\vec{x},\vec{y})$$

$$\int \mathrm{d}^3y m_T(\vec{x},\vec{y}) = \rho_0(\vec{x}) \tag{1}$$

$$\int \mathrm{d}^3x m_T(\vec{x},\vec{y}) = \rho_T(\vec{y})$$

where

$$m_T(\vec{x},\vec{y}) = u_0(\vec{x})k(\vec{x},0,\vec{y},T)v_T(\vec{y}) \tag{2}$$

and the two unknown functions $u_0(\vec{x})$, $v_T(\vec{y})$ come out as solutions of *the same sign* of the integral identities (1). Provided we have at our disposal a continuous bounded strictly positive (ways to relax this assumption were discussed in Ref. [10]) integral kernel $k(\vec{x},s,\vec{y},t)$, $0 \le s \le T$.

We shall confine further attention to cases governed by the familiar Feynman–Kac kernels. Then, the solution of the Schrödinger boundary-data problem in terms of the interpolating Markovian diffusion process is found to be completely specified by the adjoint pair of parabolic equations. In case of gradient forward drift fields, the pertinent process can be determined by checking (this imposes limitations on the admissible potential) whether the Feynman–Kac kernel

$$k(\vec{y},s,\vec{x},t) = \int \exp\left[-\int_s^t c(\vec{\omega}(\tau),\tau)\,\mathrm{d}\tau\right] \mathrm{d}\mu_{(\vec{x},t)}^{(\vec{y},s)}(\vec{\omega}) \tag{3}$$

is positive and continuous in the open space–time area of interest (then, additional

limitations on the path measure need to be introduced [11]), and whether it gives rise to positive solutions of the adjoint pair of generalised heat equations:

$$\begin{aligned} \partial_t u(\vec{x},t) &= \nu\Delta u(\vec{x},t) - c(\vec{x},t)u(\vec{x},t) \\ \partial_t v(\vec{x},t) &= -\nu\Delta v(\vec{x},t) + c(\vec{x},t)v(\vec{x},t). \end{aligned} \tag{4}$$

Here, a function $c(\vec{x},t)$ is restricted only by the positivity and continuity demand for the kernel (3), see e.g. Ref. [12]. In the above, $d\mu_{(\vec{x},t)}^{(\vec{y},s)}$ is the conditional Wiener measure over sample paths of the standard Brownian motion.

Solutions of (4), upon suitable normalisation, give rise to the Markovian diffusion process with the *factorised* probability density $\rho(\vec{x},t) = u(\vec{x},t)v(\vec{x},t)$ which, while evolving in time, interpolates between the boundary density data $\rho(\vec{x},0)$ and $\rho(\vec{x},T)$. The interpolation admits a realisation in terms of Markovian diffusion processes with the respective forward and backward drifts defined as follows:

$$\begin{aligned} \vec{b}(\vec{x},t) &= 2\nu\frac{\nabla v(\vec{x},t)}{v(\vec{x},t)} \\ \vec{b}_*(\vec{x},t) &= -2\nu\frac{\nabla u(\vec{x},t)}{u(\vec{x},t)} \end{aligned} \tag{5}$$

in the prescribed time interval $[0,T]$.

The related transport equations for the densities follow easily. For the forward interpolation, the familiar Fokker–Planck equation holds true:

$$\partial_t\rho(\vec{x},t) = \nu\Delta\rho(\vec{x},t) - \nabla[\vec{b}(\vec{x},t)\rho(\vec{x},t)] \tag{6}$$

while for the backward interpolation we have:

$$\partial_t\rho(\vec{x},t) = -\nu\Delta\rho(\vec{x},t) - \nabla[\vec{b}_*(\vec{x},t)\rho(\vec{x},t)]. \tag{7}$$

We have assumed that drifts are gradient fields, $\operatorname{curl}\vec{b} = 0$. As a consequence, those that are allowed by the prescribed choice of $c(\vec{x},t)$ *must* fulfil the compatibility condition:

$$c(\vec{x},t) = \partial_t\Phi + \frac{1}{2}\left(\frac{\vec{b}^2}{2\nu} + \nabla\vec{b}\right) \tag{8}$$

which establishes the Girsanov-type connection of the forward drift $\vec{b}(\vec{x},t) = 2\nu\nabla\Phi(\vec{x},t)$ with the Feynman–Kac, cf. Refs [11, 12], potential $c(\vec{x},t)$. In the considered Schrödinger's interpolation framework, the forward and backward drift fields are connected by the identity $\vec{b}_* = \vec{b} - 2\nu\nabla\ln\rho$.

One of the distinctive features of Markovian diffusion processes with positive density $\rho(\vec{x},t)$ is that, given the transition probability density of the (forward) process, the notion of the *backward* transition probability density $p_*(\vec{y},s,\vec{x},t)$ can be consistently introduced on each finite time interval, say $0 \le s < t \le T$:

$$\rho(\vec{x},t)p_*(\vec{y},s,\vec{x},t) = p(\vec{y},s,\vec{x},t)\rho(\vec{y},s) \tag{9}$$

so that

$$\int \rho(\vec{y},s)p(\vec{y},s,\vec{x},t)\,d^3y = \rho(\vec{x},t)$$

and

$$\rho(\vec{y},s) = \int p_*(\vec{y},s,\vec{x},t)\rho(\vec{x},t)\,\mathrm{d}^3x.$$

The transport (density evolution) eqns (6) and (7) refer to processes running in opposite directions in a fixed, common to both, time duration. The forward one (eqn (6)) executes an interpolation from the Borel set A to B, while the backward one (eqn (7)) executes an interpolation from B to A, compare e.g. the defining identities (1).

The knowledge of the Feynman-Kac kernel (3) implies that the transition probability density of the forward process reads:

$$p(\vec{y},s,\vec{x},t) = k(\vec{y},s,\vec{x},t)\,\frac{v(\vec{x},t)}{v(\vec{y},s)} \tag{10}$$

while the corresponding (derivable from eqn (10) since $\rho(\vec{x},t)$ is given) transition probability density of the backward process has the form:

$$p_*(\vec{y},s,\vec{x},t) = k(\vec{y},s,\vec{x},t)\,\frac{u(\vec{y},s)}{u(\vec{x},t)}. \tag{11}$$

Obviously [7, 12], in the time interval $0 \le s < t \le T$ there holds:

$$\begin{aligned} u(\vec{x},t) &= \int u_0(\vec{y})k(\vec{y},s,\vec{x},t)\,\mathrm{d}^3y \\ v(\vec{y},s) &= \int k(\vec{y},s,\vec{x},T)v_T(\vec{x})\,\mathrm{d}^3x. \end{aligned} \tag{12}$$

Consequently, the system (4) fully determines the underlying random motions, forward and backward, respectively.

2. THE BURGERS EQUATION IN SCHRÖDINGER'S INTERPOLATION

The prototype nonlinear field equation named the Burgers or 'nonlinear diffusion' equation (typically without [13, 14] the forcing term $\vec{F}(\vec{x},t)$):

$$\partial_t\vec{v}_B + (\vec{v}_B\nabla)\vec{v}_B = \nu\Delta\vec{v}_B + \vec{F}(\vec{x},t) \tag{13}$$

has recently acquired considerable popularity in a variety of physical contexts [15].

By dropping the force term in eqn (13), we are left with a commonly used form of the 'nonlinear diffusion equation' whose solutions are known exactly, in view of the Hopf–Cole linearising transformation mapping (13) into the heat equation. Here, $\partial_t\vec{v}_B + (\vec{v}_B\nabla)\vec{v}_B = \nu\Delta\vec{v}_B$ is mapped into $\partial_t\theta = \nu\Delta\theta$ by means of the substitution $\vec{v}_B = -2\nu\nabla\ln\theta$. This linearisation of the Burgers equation is normally regarded as devoid of any deeper physical meaning, and specifically the link with stochastic processes determined by the heat equation has not received proper attention. Our previous analysis shows that the

intrinsic interplay between the deterministic and random evolution, appropriate for a large class of classically chaotic systems, extends to a much wider framework.

Burgers velocity fields can be analysed on their own with different (including random) choices of the initial data and/or force fields. However, we are interested in the possible diffusive matter transport that is locally governed by Burgers flows, cf. Ref. [15]. In this particular connection, let us point out a conspicuous hesitation that could have been observed in attempts to establish the most appropriate matter transport rule, if any diffusion-type microscopic dynamics assumption is adopted to underlie the 'nonlinear diffusion' eqn (13).

Depending on the particular phenomenological departure point, one either adopts the standard continuity equation [16, 17], that is certainly valid to a high degree of accuracy in the so-called low viscosity limit $\nu \downarrow 0$, but incorrect on mathematical grounds *if* there is a genuine Markovian diffusion process involved *and* simultaneously a solution of eqn (13) stands for the respective *current* velocity of the flow: $\partial_t \rho(\vec{x},t) = -\nabla[\vec{v}(\vec{x},t)\rho(\vec{x},t)]$.

Alternatively, following the white noise calculus tradition telling us that the stochastic integral $\vec{X}(t) = \int_0^t \vec{v}_B(\vec{X}(s),s)\,\mathrm{d}s + \int_0^t \vec{\eta}(s)\,\mathrm{d}s$ necessarily implies the Fokker–Planck equation, one is tempted to adopt $\partial_t \rho(\vec{x},t) = \nu\Delta\rho(\vec{x},t) - \nabla[\vec{v}_B(\vec{x},t)\rho(\vec{x},t)]$, which is clearly problematic in view of the classic McKean's discussion of the propagation of chaos for the Burgers equation [18–20], and the derivation of the stochastic 'Burgers process' in this context: "the fun begins in trying to describe this Burgers motion as the path of a tagged molecule in an infinite bath of like molecules" [18].

To put things on solid ground, let us consider a Markovian diffusion process, which is characterised by the transition probability density (generally inhomogeneous in space and time law of random displacements) $p(\vec{y},s,\vec{x},t)$, $0 \le s \le t \le T$, and the probability density $\rho(\vec{x},t)$ of its random variable $\vec{X}(t)$, $0 \le t \le T$. The process is completely determined by these data. For clarity of discussion, we do not impose any spatial boundary restrictions, nor fix any concrete limiting value of T, which, in principle, can be moved to infinity.

Let us confine our attention to processes defined by the standard backward diffusion equation. Under suitable restrictions (boundedness of involved functions, their continuous differentiability) the function:

$$g(\vec{x},s) = \int p(\vec{x},s,\vec{y},T)g(\vec{y},T)\,\mathrm{d}^3y \tag{14}$$

satisfies the equation

$$-\partial_s g(\vec{x},s) = \nu\Delta g(\vec{x},s) + [\vec{b}(\vec{x},s)\nabla]g(\vec{x},s). \tag{15}$$

Let us point out that the validity of eqn (14) is known to be a *necessary* condition for the existence of a Markov diffusion process, whose probability density $\rho(\vec{x},t)$ is to obey the Fokker–Planck equation (the forward drift $\vec{b}(\vec{x},t)$ replaces the previously utilized Burgers velocity $\vec{v}_B(\vec{x},t)$.

The case of particular interest, in the traditional non-equilibrium statistical physics literature, appears when $p(\vec{y},s,\vec{x},t)$ is a *fundamental solution* of eqn (15) with respect to variables $\vec{y}$, s [21–23], see, however, Ref. [12] for an analysis of alternative situations. Then, the transition probability density satisfies *also* the second Kolmogorov (e.g. the Fokker–Planck) equation in the remaining $\vec{x}$, t pair of variables. Let us emphasize that these two equations form an adjoint pair of partial differential equations, referring to the

slightly counter-intuitive for physicists, though transparent for mathematicians [7, 24–27], issue of time reversal of diffusions.

We can consistently introduce the random variable of the process in the form $\vec{X}(t) = \int_0^t \vec{b}(\vec{X}(s),s)\,\mathrm{d}s + \sqrt{2\nu}\vec{W}(t)$. Then, in view of the standard rules of the Itô stochastic calculus [7, 27, 28], we realise that for any smooth function $f(\vec{x},t)$ of the random variable $\vec{X}(t)$ the conditional expectation value:

$$\lim_{\Delta t \downarrow 0} \frac{1}{\Delta t}\left[\int p(\vec{x},t,\vec{y},t+\Delta t) f(\vec{y},t+\Delta t)\,\mathrm{d}^3 y - f(\vec{x},t)\right] = (D_+ f)(\vec{X}(t),t) - (\partial_t + \vec{b}\nabla + \nu\Delta) f(\vec{x},t) \quad (16)$$

where $\vec{X}(t) = \vec{x}$ determines the forward drift $\vec{b}(\vec{x},t)$ of the process (if we set components of $\vec{X}$ instead of f) and, moreover, allows us to introduce the local field of (forward) accelerations associated with the diffusion process, which we *constrain* by demanding (see e.g. Refs [7], [27] and [28] for prototypes of such dynamical constraints):

$$\begin{aligned}(D_+^2 \vec{X})(t) &= (D_+ \vec{b})(\vec{X}(t),t) = (\partial_t \vec{b} + (\vec{b}\nabla)\vec{b} + \nu\Delta\vec{b})(\vec{x},t) \\ &= \vec{F}(\vec{x},t)\end{aligned} \quad (17)$$

where $\vec{X}(t) = \vec{x}$ and the, at the moment arbitrary, function $\vec{F}(\vec{x},t)$ may be interpreted as an external force applied to the diffusing system [11].

By invoking eqn (9), we can also define the backward derivative of the process in the conditional mean (cf. Refs [11], [29] and [30] for a discussion of these concepts in the case of the most traditional Brownian motion and Smoluchowski-type diffusion processes):

$$\begin{aligned}&\lim_{\Delta t \downarrow 0} \frac{1}{\Delta t}\left[\vec{x} - \int p_*(\vec{y},t-\Delta t,\vec{x},t)\vec{y}\,\mathrm{d}^3 y\right] = (D_- \vec{X})(t) - \vec{b}_*(\vec{X}(t),t). \\ &(D_- f)(\vec{X}(t),t) = (\partial_t + \vec{b}_*\nabla - \nu\Delta) f(\vec{X}(t),t)\end{aligned} \quad (18)$$

Accordingly, the backward version of the acceleration field reads

$$(D_-^2 \vec{X})(t) = (D_+^2 \vec{X})(t) = \vec{F}(\vec{X}(t),t) \quad (19)$$

where, in view of $\vec{b}_* = \vec{b} - 2\nu\nabla \ln \rho$, we have explicitly fulfilled the *forced Burgers equation*:

$$\partial_t \vec{b}_* + (\vec{b}_*\nabla)\vec{b}_* - \nu\Delta\vec{b}_* = \vec{F} \quad (20)$$

and [7, 11, 27] under the gradient-drift field assumption $\operatorname{curl} \vec{b}_* = 0$, we deal with $\vec{F}(\vec{x},t) = 2\nu\nabla c(\vec{x},t)$ where the Feynman–Kac potential (3) is explicitly involved.

Let us notice that the familiar (linearisation of the nonlinear problem) Hopf–Cole transformation [14, 31] of the Burgers equation into the generalised diffusion equation (yielding explicit solutions in the unforced case) has been explicitly used before (the second formula in eqn (4)) in the framework of the Schrödinger interpolation problem. In fact, by defining $\Phi_* = \log u$, we immediately recover the traditional form of the Hopf–Cole transformation for Burgers velocity fields $\vec{b}_* = -2\nu\nabla\Phi_*$. With the standard considerations that allow us to map a nonlinear (unforced Burgers) equation into a linear, heat equation.

In the special case of the standard free Brownian motion, there holds $\vec{b}(\vec{x},t) = 0$ while $\vec{b}_*(\vec{x},t) = -2\nu\nabla \log \rho(\vec{x},t)$.

Let us point out that eqn (7) is, in fact, the only transport equation where the Burgers velocity field is allowed to be indisputably present, under the diffusive scenario assumption [15]. The standard continuity equation is certainly inappropriate for non-zero values of the diffusion constant ν.

3. RECONSTRUCTION OF THE MICROSCOPIC DYNAMICS FROM THE PROBABILITY DENSITY DATA: OBSTACLES EXEMPLIFIED

We have mentioned before that another version of the Schrödinger boundary data problem [5] departs directly from a given (Fokker–Planck-type) probability density evolution and investigates the circumstances allowing us to deduce a unique random process from these dynamics. Surely solutions of the Fokker–Planck equation itself do not yet determine the underlying stochastic process. Additional assumptions are always necessary and a number of traps must be avoided.

As a particular guide to these obstacles, we shall refer to the familiar free quantum evolution that is regarded as the time adjoint parabolic problem, exactly in the spirit of our previous discussion.

In our previous paper [30], the major conclusion was that in order to give a definitive probabilistic description of the quantum dynamics as a *unique* diffusion process solving Schrödinger's interpolation problem, a suitable Feynman–Kac semigroup must be singled out. Let us point out that the measure preserving dynamics, permitted in the presence of conservative force fields, was investigated in Ref. [11].

The present analysis was performed quite generally and extends to the dynamics affected by time dependent external potentials, with no clear-cut discrimination between the non-equilibrium statistical physics and essentially quantum evolutions. The formalism of Section 1 encompasses both groups of problems. Nevertheless, it is quite illuminating to see directly how sensitive, even in the simplest cases, the formalism is with respect to any attempt to relax our previous assumptions and the Schrödinger interpolation problem rules-of-the-game. Specifically in the quantum domain, where the seemingly trivial case of the free evolution, which is non-stationary, needs the general parabolic system (4) to be considered. Even worse, then the system (4) displays a non-trivial nonlinearity: the parabolic equations are coupled by the effective, solution dependent potential. At first glance, this feature might seem to exclude the existence of any conceivable Feynman–Kac (dynamical semigroup) kernel, and in consequence any common-sense law of random displacements (i.e. the transition probability density) governing the pertinent stochastic evolution. Certainly, the existence of fundamental solutions in this case is far from obvious.

At this point, let us emphasize that our principal goal is to take seriously the Schrödinger picture of quantum dynamics under the premises of the Born statistical postulate. Hence, once we select *as appropriate* a concrete quantal interpolation between the prescribed (phenomenologically supported in particular) input–output statistics data $\rho_0(x)$ and $\rho_T(x)$ in terms of $\rho(x,t) = \bar{\phi}(x,t)\psi(x,t)$, $t \in [0,T]$, where $\psi(x,t)$ solves the Schrödinger equation then, on exactly the same footing, we are entitled to look for an alternative probabilistic explanation (or *appropriate* description) of the very same interpolation, in terms of a well-defined Markov stochastic (eventually diffusion) process.

We shall proceed in the spirit of Section 1, while restricting our discussion to the free Schrödinger dynamics. Following Ref. [30] we shall discuss the rescaled problem so as to eliminate all dimensional constants.

The free Schrödinger evolution $i\partial_t\psi = -\Delta\psi$ implies the following propagation of a specific Gaussian wave packet:

$$\psi(x,0) = (2\pi)^{-1/4}\exp\left(-\frac{x^2}{4}\right) \to \psi(x,t) = \left(\frac{2}{\pi}\right)^{1/4}(2+2it)^{-1/2}\exp\left[-\frac{x^2}{4(1+it)}\right]. \tag{21}$$

So that

$$\rho_0(x) = |\psi(x,0)|^2 = (2\pi)^{-1/2}\exp\left[-\frac{x^2}{2}\right] \to \rho(x,t) = |\psi(x,t)|^2$$

$$= [2\pi(1+t^2)]^{-1/2}\exp\left[-\frac{x^2}{2(1+t^2)}\right] \tag{22}$$

and the Fokker–Planck equation (easily derivable from the standard continuity equation $\partial_t\rho = -\nabla(v\rho)$, $v(x,t) = xt/(1+t^2)$) holds true:

$$\partial_t\rho = \Delta\rho - \nabla(b\rho), \quad b(x,t) = -\frac{1-t}{1+t^2}x. \tag{23}$$

The Madelung factorization $\psi = \exp(R + iS)$ implies (notice that $v = 2\nabla S$ and $b = 2\nabla(R + S)$) that the related real functions $\theta(x,t) = \exp(R+S)$ and $\theta_*(x,t) = \exp(R-S)$ read:

$$\theta(x,t) = [2\pi(1+t^2)]^{-1/4}\exp\left(-\frac{x^2}{4}\frac{1-t}{1+t^2} - \frac{1}{2}\arctan t\right)$$

$$\theta_*(x,t) = [2\pi(1+t^2)]^{-1/4}\exp\left(-\frac{x^2}{4}\frac{1+t}{1+t^2} + \frac{1}{2}\arctan t\right). \tag{24}$$

They solve a suitable version of the general parabolic eqn (4), namely:

$$\partial_t\theta = -\Delta\theta + \frac{1}{2}\Omega\theta$$

$$\partial_t\theta_* = \Delta\theta_* - \frac{1}{2}\Omega\theta_* \tag{25}$$

with

$$\frac{1}{2}\Omega(x,t) = \frac{x^2}{2(1+t^2)^2} - \frac{1}{1+t^2} = 2\frac{\Delta\rho^{1/2}}{\rho^{1/2}} - Q(x,t). \tag{26}$$

By setting $t = T$ we associate with the above dynamics the terminal density $\rho_T(x)$, and then the concrete Schrödinger boundary data problem for the stochastic interpolation $\rho_0(x) \to \rho_T(x)$, eqn (1).

To capture the spirit of our previous discussion, we shall replace eqn (25) by the more general eqn (4), where only the potential $c(x,t)$ will be identified with the above $\frac{1}{2}\Omega(x,t)$. Then, we shall look for solutions $u(x,t)$, $v(x,t)$ of these parabolic equations, and in particular we shall identify the quantally implemented functions $\theta_*(x,t)$, $\theta(x,t)$, eqn (24), *among* them. Effectively, this amounts to the previously mentioned linearisation of the nonlinear parabolic system.

In view of the relatively simple form of the probability density $\rho(x,t)$, eqn (22), one might be tempted to guess (more or less fortunately) the transition probability density, consistent with the propagation eqn (22). However, it is well known that there are many stochastic

processes implying eqn (22) for all $t \in [0,T]$, which will not necessarily have much in common with the original wavefunction dynamics, eqn (21). In general they are incompatible with the corresponding parabolic system (cf. eqns (4) and (25)). If it happens otherwise, the reason for this proliferation of would-be consistent stochastic processes is rooted in exploiting the particular functional form of solutions, instead of relying on the form-independent arguments, e.g. eqn (4).

Let us consider some simple examples which, albeit coming under very special circumstances (free dynamics with a specific initial wave packet choice, and no zeros admitted in the course of the propagation), clearly indicate how important is the *proper choice* of the Feynman–Kac kernel. The virtue of a parabolic system (4) is that its form is universal for the Schrödinger dynamics, and thus does not depend on a particular functional form of solutions nor of external potentials. It appears that the system (4) sets a very rigid framework for the probabilistic manifestations (e.g. stochastic processes) of the quantum Schrödinger dynamics.

Example 1. We shall demonstrate that an improper (*not* through eqn (4) or eqn (25)), but fortunate, choice of the kernel might lead to an alternative stochastic representation of the quantum dynamics of eqn (22).

Let us begin by directly introducing the transition probability density:

$$p(y,s,x,t) = [2\pi(t^2 - s^2)]^{-1/2} \exp\left[-\frac{(x-y)^2}{2(t^2 - s^2)} \right] \tag{27}$$

which for all intermediate times $0 \le s < t \le T$ executes a desired propagation $\rho(x,t) = \int p(y,s,x,t)\rho(y,s)\,dy$, eqn (22). Clearly, the Chapman–Kolmogorov identity $\int p(y,s,z,\tau)p(z,\tau,x,t)\,dz = p(y,s,x,t)$ holds true, and the properties (the first one for all $\epsilon > 0$):

$$\begin{aligned} &\lim_{\Delta t \downarrow 0} \frac{1}{\Delta t} \int_{|x-y|>\epsilon} p(y,t,x,t+\Delta t)\,dx = 0 \\ &\lim_{\Delta t \downarrow 0} \frac{1}{\Delta t} \int_{-\infty}^{+\infty} (x-y)p(y,t,x,t+\Delta t)\,dx = 0 \\ &\lim_{\Delta t \downarrow 0} \frac{1}{\Delta t} \int_{-\infty}^{+\infty} (x-y)^2 p(y,t,x,t+\Delta t)\,dx = 2t \end{aligned} \tag{28}$$

tell us that the law of random displacements $p(y,s,x,t)$, eqn (27), can be attributed to a Markov diffusion process associated with the parabolic (Fokker–Planck) equation:

$$\partial_t \rho = t\Delta_x \rho. \tag{29}$$

In fact, our $p(y,s,x,t)$ is a fundamental solution of this equation with respect to x, t variables, while obeying the time adjoint parabolic equation in the remaining (e.g. y, s) pair of variables:

$$\partial_s p(y,s,x,t) = -s\Delta_y p(y,s,x,t). \tag{30}$$

This diffusion has a vanishing forward drift and the quadratic in time variance (the diffusion coefficient equals t), hence its local characteristics are completely divorced from those of the Nelson process [30] derivable from the solution eqn (21) of the Schrödinger equation.

Interestingly, since $p(y,s,x,t)$ itself is a perfect, strictly positive and continuous in all variables (Markov) semigroup kernel, nothing prevents us from performing the Schrödinger problem analysis eqn (1) with the boundary densities $\rho_0(x)$ and $\rho_T(x)$ defined by the above free evolution problem. However, we shall proceed otherwise and, having given explicit

solutions of the parabolic system (25), introduce another strictly positive and continuous in all variables function:

$$k_1(y,s,x,t) = p(y,s,x,t)\frac{\theta(y,s)}{\theta(x,t)} = [2\pi(t^2-s^2)]^{-1/2}\left(\frac{1+t^2}{1+s^2}\right)^{1/4}\exp\left[-\frac{(x-y)^2}{2(t^2-s^2)}\right]$$
$$\times\exp\left[-\frac{y^2}{4}\frac{1-s}{1+s^2}+\frac{x^2}{4}\frac{1-t}{1+t^2}\right]\exp\left[\frac{1}{2}(\arctan t-\arctan s)\right] \tag{31}$$

and observe that the Schrödinger system (1) in the present situation is involved as well, since trivially there holds:

$$\rho_0(x) = \theta_*(x,0)\int k_1(x,0,y,T)\theta(y,T)\,dy$$
$$\rho_T(x) = \theta(x,T)\int k_1(y,0,x,T)\theta_*(y,0)\,dy. \tag{32}$$

Disregarding the derivation which has led us to eqn (22), we can simply consider eqn (22) as the Schrödinger system of equations with a fixed kernel and boundary density data. Then, we immediately infer that by Jamison's theorem [6], its unique (up to a coefficient) solution is constituted by the pair $\theta_*(x,0)$, $\theta(x,t)$ of functions, already determined by eqn (24). Moreover, $k_1(y,s,x,t)$ obeys the Chapman–Kolmogorov composition rule:

$$\int k_1(y,s,z,\tau)k_1(z,\tau,x,t)\,dz = \int p(y,s,z,\tau)\frac{\theta(y,s)}{\theta(z,\tau)}p(z,\tau,x,t)\frac{\theta(z,\tau)}{\theta(x,t)}dz$$
$$= p(y,s,x,t)\frac{\theta(y,s,)}{\theta(x,t)} = k_1(y,s,x,t). \tag{33}$$

In view of $\int p(y,s,x,t)\,dx = 1$ for all $s<t$, we have:

$$\int k_1(x,s,y,t)\theta(y,t)\,dy = \theta(x,s) \tag{34}$$

and, since $\theta\theta_* = \rho$, we get:

$$\int k_1(y,s,x,t)\theta_*(y,s)\,dy = \int \theta_*(y,s,)p(y,s,x,t)\frac{\theta(y,s)}{\theta(x,t)}dy = \frac{1}{\theta(x,t)}\int \rho(y,s)p(y,s,x,t)\,dy$$
$$= \frac{\rho(x,t)}{\theta(x,t)} = \theta_*(x,t). \tag{35}$$

Thus, undoubtedly, we have in hand a complete solution of the Schrödinger boundary data problem (1): for the once-chosen kernel k_1, this solution is unique, and compatible with the dynamics of the corresponding Schrödinger wavefunction. But, the constructed stochastic process is completely incongruent with the standard wisdom about Nelson's diffusion processes [7, 27, 28, 30]. The reason is clear: our analysis was performed for a particular solution, whose functional form allows for an alternative stochastic representation. But, let us stress the point, if we look for the functional-form-independent construction, it is the parabolic system (4) from which one should depart.

Anyway, even the inappropriate choice of the integral kernel k_1 does allow us to derive

the quantum mechanically implemented dynamics of eqn (22) from, respectively, $\theta(x,T)$ and $\theta_*(x,0)$ by means of the propagation formulas (4). The probability density evolves in time correctly, but the vanishing drift and the linear-in-time diffusion coefficient situate this stochastic process outside the scope set by eqns (25) and (4).

Example 2. We shall demonstrate that another choice of the kernel, still with no reference to the system (4), will allow us to reproduce the stochastic propagation with the probability density, drifts and diffusion coefficient of Nelson's stochastic mechanics, which however is *not* Nelson's process for the quantum evolution (22). We are inspired by our previous paper [30], where an interesting stochastic propagation, compatible with eqn (22), was introduced by means of the transition probability density:

$$p_{y,s}(x,t) = [4\pi(t-s)]^{-1/2} \exp\left[-\frac{(x-c_{t,s}y)^2}{4(t-s)}\right]$$

$$p_{y,s}(x,s) = \delta(x-y), \quad 0 \le s < t \le T \tag{36}$$

$$c_{t,s} = \left[\frac{(1-t)^2+2s}{1+s^2}\right]^{1/2}.$$

Here, the density $\rho(y,s)$, eqn (22), is propagated into the corresponding $\rho(x,t)$ according to the rule $\rho(x,t) = \int p_{y,s}(x,t)\rho(y,s)\,dy$, for all intermediate times $0 \le s < t \le T$. As noticed in Ref. [30], this propagation is somewhat pathological since it *does not* obey the Chapman–Kolmogorov composition rule: $\int p_{y,s}(z,\tau)p_{z,\tau}(x,t)\,dz \neq p_{y,s}(x,t)$ and thus p cannot be interpreted as a transition density of the Markov process.

However, if we were to naively proceed like in Example 1 and define the strictly positive continuous function:

$$k_2(y,s,x,t) = p_{y,s}(x,t)\frac{\theta(y,s)}{\theta(x,t)} \tag{37}$$

where $0 \le s < t \le T$ and $\theta(x,t)$ is given by eqn (24), then the Schrödinger system (32), with k_2 replacing k_1, trivially appears. Indeed, because $\int p_{y,s}(x,t)\,dx = 1$ for $s < t$, there holds:

$$\theta_*(x,0)\int k_2(x,0,y,T)\theta(y,T)\,dy = \theta_*(x,0)\int p_{x,0}(y,T)\theta(x,0)\,dy = \theta_*(x,0)\theta(x,0) = \rho_0(x)$$

$$\theta(x,T)\int k_2(y,0,x,T)\theta_*(y,0)\,dy = \int p_{y,0}(x,T)\theta(y,0)\theta_*(y,0)\,dy \tag{38}$$

$$= \int p_{y,0}(x,T)\rho(y,0)\,dy = \rho_T(x).$$

As a consequence, if we analyse the above Schrödinger system with the boundary data $\rho_0(x)$ and $\rho_T(x)$ fixed by eqn (22) (as before) but with the new kernel k_2, then somewhat unexpectedly the same pair as before, $\theta(x,0)$, $\theta_*(x,T)$, necessarily comes out as a solution. Let us emphasize that the solution is unique for the chosen kernel k_2, albeit it coincides with the unique (as well) solution previously associated with the kernel k_1 (cf. Example 1).

The meaning of the uniqueness of solution of the Schrödinger system [6] becomes clear: if we have prescribed the boundary density data the solution is unique for a chosen kernel, but there are many kernels which may give rise to the very same solution.

The pathology (non-Markovian density) of $p_{y,s}(x,t)$ extends to $k_2(y,s,x,t)$ and the semigroup composition rule is invalid in this case. Nevertheless, we can blindly repeat the step (32), with k_2 instead of k_1, so reproducing the evolution (22). Moreover, in the present

case [30], we can exploit the standard recipe to evaluate the forward drift of a conventional diffusion:

$$\lim_{\Delta t \downarrow 0} \frac{1}{\Delta t}\left[\int y p_{x,t}(y,t+\Delta t)\,dy - x\right] = b(x,t) = -\frac{1-t}{1+t^2}x. \tag{39}$$

Clearly, it is the forward drift of the Nelson diffusion [27, 30] associated with eqn (24), and it consistently appears in the corresponding Fokker–Planck eqn (6).

Let us observe that $p_{y,s}(x,t)$ solves the first Kolmogorov equation with respect to x,t:

$$\begin{aligned} \partial_t p_{y,s}(x,t) &= \Delta_x p_{y,s}(x,t) - b_{y,s}(t)\nabla_x p_{y,s}(x,t) \\ b_{y,s}(t) &= y\frac{\partial c_{t,s}}{\partial t}. \end{aligned} \tag{40}$$

As such, it can be exploited to construct a genuine Markov process, albeit disconnected from the quantal dynamics (22). Namely, we can define another solution of eqn (40), in variables x_1,t_1:

$$\begin{aligned} p_{y,s}(x_1,t_1,x_2,t_2) &= [4\pi(t_2-t_1)]^{-1/2}\exp\left[-\frac{(x_2-x_1-cy)^2}{4(t_2-t_1)}\right] \\ c &= c_{t_2,s} - c_{t_1,s}, \quad 0 \le s < t_1 < t_2 \le T \end{aligned} \tag{41}$$

with $c_{t,s}$ given by eqn (36). It is easy to verify that the transition density (41) actually *is* a fundamental solution, and as such satisfies the second Kolmogorov equation with respect to x_2, t_2 for each fixed y, s label, $0 \le s < t_1 < t_2 \le T$. Consequently, we have in hand the (y,s) family of well-defined Markovian transition probability densities $p_{y,s}$ for random propagation scenarios. Indeed, to this end one needs to check the (apparent) compatibility conditions: (a) $p_{y,s}(x_1,t,x_2,t) = \delta(x_2-x_1)$; (b) $\int p_{y,s}(x_1,t_1,x_2,t_2)p_{y,s}(x_1,t_1)\,dx_1 = p_{y,s}(x_2,t_2)$: and in addition (c) $\int p_{y,s}(x_1,t_1,x_2,t_2)p_{y,s}(x_2,t_2,x_3,t_3)\,dx_2 = p_{y,s}(x_1,t_1,x_3,t_3)$, where $0 \le s < t_1 < t_2 < t_3 \le T$ and $p_{y,s}(x,t)$ plays the role of the density of the Markov process. The identity (c) in the above is the Chapman–Kolmogorov formula.

To avoid the above obstacles, the only how-to-proceed procedure is provided by the route outlined before, e.g. that leading from the Feynman–Kac kernel to the associated Markov diffusion process via Schrödinger's boundary-data problem. A complete solution to this particular issue, in the quantum dynamics context, has been given elsewhere [8, 12, 29, 30].

Acknowledgement—P. G. and R. O. received financial support from KBN Research Grant No. 2 P302 057 07.

REFERENCES

1. Kac, M. and Logan, J., In *Fluctuation Phenomena*, eds E. W. Montroll and J. L. Lebowitz, North-Holland, Amsterdam, 1976.
2. Mackey, M. C. and Glass, L., *From Clocks to Chaos: Rhythms of Life*, Princeton University Press, Princeton, 1988.
3. Lasota, A. and Mackey, M. C., *Chaos, Fractals, and Noise*, Springer-Verlag, Berlin, 1994.
4. Beck, C., In *Chaos—The Interplay Between Stochastic and Deterministic Behaviour*, LNP Vol. 457, eds P. Garbaczewski, M. Wolf and A. Weron, Springer-Verlag, Berlin, 1995, p. 3.
5. Mikami, T., *Commun. Math. Phys.*, 1990, **135**, 19.
6. Jamison, B. and Wahrsch, Z., *Verw. Geb.*, 1974, **30**, 65.
7. Zambrini, J. C., *J. Math. Phys.*, 1986, **27**, 3207.
8. Garbaczewski, P., Klauder, J. R. and Olkiewicz, R., *Phys. Rev. E*, 1995, **51**, 4114.
9. Schrödinger, E., *Ann. Inst. Henri Poincare*, 1932, **2**, 269.
10. Garbaczewski, P., *Acta Phys. Polon. B*, 1996, **27**, 617.

11. Blanchard, Ph. and Garbaczewski, P., *Phys. Rev. E*, 1994, **49,** 3815.
12. Garbaczewski, P. and Olkiewicz, R., *J. Math. Phys.*, 1996, **37,** 732.
13. Burgers, J. M., *The Nonlinear Diffusion Equation*. Reidel, Dordrecht, 1974.
14. Hopf, E., *Commun. Pure Appl. Math.*, 1950, **3,** 201.
15. Garbaczewski, P. and Kondrat, G., *Phys. Rev. Lett.*, 1996, **77,** 2608.
16. Shandarin, S. F. and Zeldovich, B. Z., *Rev. Mod. Phys.*, 1989, **61,** 185.
17. Albeverio, S., Molchanov, A. A. and Surgailis, D., *Prob. Theory Relat. Fields*, 1994, **100,** 457.
18. McKean, H. P, In *Lecture Series in Differential Equations*, Vol. II, ed. A. K. Aziz. Van Nostrand, Amsterdam, 1969, p. 177.
19. Calderoni, P. and Pulvirenti, M., *Ann. Inst. Henri Poincaré*, 1983, **39,** 85.
20. Osada, H. and Kotani, S., *J. Math. Soc. Jpn.*, 1985, **37,** 275.
21. Krzyzański, M. and Szybiak, A., *Lincei-Rend. Sc. fis. mat. e nat.*, 1959, **28,** 26.
22. Friedman, A., *Partial Differential Equations of Parabolic Type*. Prentice-Hall, Englewood Cliffs, NJ, 1964.
23. Horsthemke, W. and Lefever, R., *Noise-Induced Transitions*. Springer-Verlag, Berlin, 1984.
24. Haussmann, U. G. and Pardoux, E., *Ann. Prob.*, 1986, **14,** 1188.
25. Föllmer, H., In *Stochastic Processes—Mathematics and Physics*, LNP Vol. 1158, eds S. Albeverio, Ph. Blanchard and L. Streit. Springer-Verlag, Berlin, 1985, p. 119.
26. Hasegawa, H., *Progr. Theor. Phys.*, 1976, **55,** 90.
27. Nelson, E., *Quantum Fluctuations*. Princeton University Press. Princeton, NJ, 1985.
28. Nelson, E., *Dynamical Theories of the Brownian Motion*. Princeton University Press, Princeton, NJ, 1967.
29. Garbaczewski, P. and Vigier, J. P., *Phys. Rev. A*, 1992, **46,** 4634.
30. Garbaczewski, P. and Olkiewicz, R., *Phys. Rev. A*, 1995, **52,** 3445.
31. Fleming, W. H. and Soner, H. M., *Controlled Markov Processes and Viscosity Solutions*. Springer-Verlag, Berlin, 1993.

J. Phys. A: Math. Gen. **33** (2000) 5901–5912. Printed in the UK PII: S0305-4470(00)07137-7

Ergodicity for generalized Kawasaki dynamics

G Kondrat†, S Peszat‡ and B Zegarlinski
Department of Mathematics, Imperial College, London SW7 2BZ, UK
E-mail: gkon@ift.uni.wroc.pl, napeszat@cyf-kr.edu.pl and b.zegarlinski@ic.ac.uk

Received 23 August 1999, in final form 20 April 2000

Abstract. We give a necessary and sufficient condition for a Gibbs measure μ on the product space $\Omega = (S^1)^{\mathbb{Z}^d}$ to satisfy the spectral gap or the logarithmic Sobolev inequality with the following quadratic form:

$$\mu\mathcal{K}(f) \equiv \int \sum_{k\in\mathbb{Z}^d} \left(\sum_{j\in k+Y} a_{j-k} \nabla_j f \right)^2 \mathrm{d}\mu \qquad f \in C_0^\infty(\Omega)$$

where Y is a finite set and a_l are integers. As a consequence we prove that the generalized Kawasaki dynamics decays exponentially to equilibrium in the supremum norm in a strong mixing region.

1. Introduction

It is well known that the Kawasaki dynamics for discrete spin systems exhibits a different behaviour from the Glauber dynamics and even at high temperatures the decay to equilibrium is very slow (cf [De, BZ1, BZ2, JLQY, LY, CM]). Naturally one can ask what happens in the case of generalized Kawasaki dynamics [ZZ] with a continuous single spin space, where the generator $\mathcal{L}$ is formally given as follows:

$$\mu(f(-\mathcal{L}f)) = \sum_{|i-j|=1} \mu|\nabla_i f - \nabla_j f|^2 \tag{1.1}$$

with μ being an equilibrium measure and the summation on the right-hand side is extending over the nearest-neighbour sites of an integer lattice. As indicated in [ZZ] such a model is of interest for describing a ferroelectric gas.

We show that, in contrast to the discrete case, if the single spin space is given by a unit circle, due to an additional 'gauge' symmetry, at high temperatures the generalized Kawasaki dynamics is hypercontractive. We also show that such a dynamics has the property of a finite speed of propagation of information, that is it can be strongly approximated by finite-dimensional dynamics. This together with the hypercontractivity property implies a strong exponential decay to equilibrium in the supremum norm.

It is now well known that the above-mentioned features are present in the models of dynamics with a generator defined by the following standard Dirichlet form:

$$\mu\mathcal{D}(f) \equiv \int \sum_{k\in\mathbb{Z}^d} |\nabla_k f|^2 \,\mathrm{d}\mu \qquad f \in C_0^\infty(\Omega) \tag{1.2}$$

† On leave from: Institute of Theoretical Physics, University of Wroclaw, Pl. Maxa Borna 9, 50-204 Wroclaw, Poland.
‡ On leave from: Institute of Mathematics, Polish Academy of Sciences, Św. Tomasza 30/7, 31-027 Kraków, Poland.

0305-4470/00/335901+12$30.00

in the mixing region (see, e.g., [HS2, GZ1, GZ2]) for some earlier study of the models with continuous symmetry see [F, HS1] (for existence, uniqueness and some regularity properties of the corresponding processes) and [W] (including ergodicity in the uniform norm but at very high temperatures). Despite this similarity, even in our simple setting with a single spin space given by a circle, these two dynamics can by no means be considered to be equivalent. To indicate an example we mention that (by a simple choice of trial functions), one can easily see that the corresponding quadratic forms (1.1) and (1.2) are not equivalent. (Although naturally the latter one multiplied by a positive constant dominates the former.) One could also have a different critical behaviour of both dynamics.

In the special case of a rotator system with spins taking values in a circle, we show that there is a transformation of a potential which allows one to transform some 'gauge'-invariant dynamics corresponding to a non-diagonal quadratic form (such as the generalized Kawasaki dynamics) to one given in (1.2), but with a properly transformed measure. In this restricted sense one can talk about a correspondence between two dynamics related to quadratic forms having an *a priori* different form.

The organization of the paper is as follows. After a preliminary section 2, we consider in section 3 the spin systems with a single spin space given by the unit circle and a smooth finite-range potential. For such systems we formulate a necessary and sufficient condition for a spectral gap and logarithmic Sobolev inequality to be true with some general class of Dirichlet forms, which we will call 'the square of the field forms'. The proof of this result based on an appropriate change of integration variables and a mixing property for a transformed potential is given in section 4. Section 5 contains a general example of a system with a small potential for which the required conditions are satisfied. In section 6 we discuss the construction of a Markov semigroup with generator corresponding to a general square of the field form. Finally, in section 7 we explain how to apply our general results to prove the exponential decay to equilibrium in the uniform norm for the generalized Kawasaki dynamics.

2. Preliminaries

Let $\mathbb{Z}^d$ be the d-dimensional integer lattice with the norm $|k| = \max_{1\leqslant i\leqslant d} |k^i|$. We write $k \sim j$ iff $|k-j| = 1$. We use $\mathcal{F}$ to denote the set of all non-empty $\Lambda \subset \mathbb{Z}^d$ with the cardinality $|\Lambda| < \infty$.

As a single spin space we consider the unit circle S^1, and our configuration space is the space $\Omega = (S^1)^{\mathbb{Z}^d}$ endowed with the product topology.

Given a non-empty $\Lambda \subseteq \mathbb{Z}^d$ we denote by $B_\Lambda(\Omega)$, $C_\Lambda(\Omega)$ and $C^\infty_\Lambda(\Omega)$ the spaces of bounded measurable, continuous and infinitely differentiable real-valued functions on Ω depending only on the variables ω_k, $k \in \Lambda$. We say that a function is *local* iff it belongs to $B_\Lambda(\Omega)$ for some $\Lambda \in \mathcal{F}$. We use $B_0(\Omega)$, $C_0(\Omega)$ and $C^\infty_0(\Omega)$ to denote the classes of bounded measurable, continuous and infinitely differentiable local functions on Ω. For a bounded function f on Ω, we denote by $\|f\|_{\mathrm{u}}$ the supremum norm of f. Let $\Lambda \subseteq \mathbb{Z}^d$, and let $\eta, \omega \in \Omega$. We denote by $\eta \bullet_\Lambda \omega$ the element of Ω determined by $(\eta \bullet_\Lambda \omega)_k = \eta_k$, $k \in \Lambda$ and $(\eta \bullet_\Lambda \omega)_k = \omega_k$, $k \notin \Lambda$. Given $\Lambda \subseteq \mathbb{Z}^d$, $f : \Omega \to \mathbb{R}$, and $\omega \in \Omega$ we denote by $f_\Lambda(\cdot|\omega)$ the function $f_\Lambda(\eta|\omega) = f(\eta \bullet_\Lambda \omega)$, $\eta \in \Omega$. For a (Borel) probability measure μ on Ω we use the following notation for the corresponding expectation:

$$\mu f = \int_\Omega f(\omega)\mu(\mathrm{d}\omega).$$

Let $C^\infty_0(\Omega)^2 \ni (f, g) \mapsto \mathcal{K}(f, g) \in C^\infty_0(\Omega)$ be a non-negative definite quadratic form which vanishes if f or g is a constant function. We set $\mathcal{K}(f) \equiv \mathcal{K}(f, f)$.

Definition 2.1. A probability measure μ on Ω satisfies the *spectral gap inequality with respect to* $\mathcal{K}$, in short $\mu \in \mathbf{SG}(\mathcal{K})$, if there is a constant $C < \infty$ such that

$$\mu(f - \mu f)^2 \leqslant C\mu\mathcal{K}(f) \qquad \text{for every } f \in C_0^\infty(\Omega).$$

We say that μ satisfies the *logarithmic Sobolev inequality with respect to* $\mathcal{K}$, in short $\mu \in \mathbf{LS}(\mathcal{K})$, if there is a constant $C < \infty$ such that

$$\mu f^2 \log \frac{f^2}{\mu f^2} \leqslant C\mu\mathcal{K}(f) \qquad \text{for every } f \in C_0^\infty(\Omega).$$

Remark 2.1. It is well known (see, e.g., [S]) that if $\mu \in \mathbf{LS}(\mathcal{K})$, then $\mu \in \mathbf{SG}(\mathcal{K})$.

In the present paper we denote by ν the normalized Lebesgue measure on S^1, and by μ_0 the corresponding product measure on Ω. For $\Lambda \subseteq \mathbb{Z}^d$, $\omega \in \Omega$ and $f \in B(\Omega)$ we set

$$\langle f \rangle_\Lambda(\omega) = \mu_0 f_\Lambda(\cdot|\omega) \qquad \text{and} \qquad \partial_\Lambda f(\omega) = \langle f \rangle_\Lambda(\omega) - f(\omega).$$

If $\Lambda = \{k\}$, then we will write ∂_k instead of $\partial_{\{k\}}$. Finally, by ∇_k we denote the gradient operator with respect to the kth variable.

A *potential* is by definition a family $\Phi \equiv \{\Phi_X : X \in \mathcal{F}\}$ of functions $\Phi_X \in C_X(\Omega)$ such that

$$\|\Phi\| \equiv \sup_{i \in \mathbb{Z}^d} \sum_{X \in \mathcal{F}:\ X \ni i} \|\Phi_X\|_{\mathrm{u}} < \infty.$$

The corresponding local energy functional is defined by

$$U_\Lambda = - \sum_{X \in \mathcal{F}:\ X \cap \Lambda \neq \emptyset} \Phi_X \qquad \Lambda \in \mathcal{F}.$$

By $\mathcal{E}(\Phi)$ we denote the *local specification* corresponding to Φ, that is the following family of operators

$$\mathbb{E}_\Lambda f = \frac{\langle f \exp\{-U_\Lambda\}\rangle_\Lambda}{\langle \exp\{-U_\Lambda\}\rangle_\Lambda} \qquad f \in B(\Omega) \quad \Lambda \in \mathcal{F}.$$

If $\Lambda = \{k\}$ for some point $k \in \mathbb{Z}^d$, we simplify the notation writing $U_k \equiv U_{\{k\}}$ and $\mathbb{E}_k \equiv \mathbb{E}_{\{k\}}$. We say that a probability measure μ on Ω is a *Gibbs measure for* $\mathcal{E}(\Phi)$ iff

$$\mu \mathbb{E}_\Lambda f = \mu f \qquad \text{for all } \Lambda \in \mathcal{F} \quad \text{and} \quad f \in \mathcal{C}_0(\Omega).$$

We denote by $\mathcal{G}(\Phi)$ the set of all Gibbs measures for $\mathcal{E}(\Phi)$.

Remark 2.2. Note that as Ω is a compact Polish space and the local specification maps the set of continuous functions into itself, $\mathcal{G}(\Phi) \neq \emptyset$ for any potential on Ω.

We say that a potential Φ has *finite range* if there is an $R \in \mathbb{Z}_+$ such that $\Phi_X \equiv 0$ for all X with $\operatorname{diam} X \geqslant R$.

Let us denote by Λ_n the cube $[-n, n]^d \cap \mathbb{Z}^d$. For a potential Φ and a set $\Gamma \in \mathcal{F}$ such that $0 \in \Gamma$, we introduce a potential $\Phi^{(n)}$ with a cut-off as follows:

$$\Phi_X^{(n)} = \begin{cases} \Phi_X & \text{if} \quad X + \Gamma \subseteq \Lambda_n \\ 0 & \text{otherwise.} \end{cases}$$

Let

$$U^{(n)} = - \sum_{X \in \mathcal{F}} \Phi_X^{(n)}.$$

Then, as $\Phi_X^{(n)} \equiv 0$ if $X \not\subseteq \Lambda_n$,

$$\mu^{(n)}(\mathrm{d}\omega) = \frac{\exp\{-U^{(n)}(\omega)\}}{\langle \exp\{-U^{(n)}\}\rangle_{\Lambda_n}}\mu_0(\mathrm{d}\omega)$$

is the unique Gibbs measure for $\mathcal{E}(\Phi^{(n)})$. The following lemma will be useful in the next section.

Lemma 2.1. *Let Φ be a finite-range potential, let $\Gamma \in \mathcal{F}$, $0 \in \Gamma$. Then there is a subsequence $\{n_j\}$ and a Gibbs measure $\mu \in \mathcal{G}(\Phi)$ such that*

$$\lim_{j\to\infty} \mu^{(n_j)} f = \mu f \qquad \text{for every } f \in C(\Omega). \tag{2.1}$$

Under our assumptions, the proof follows from the fact that for any given finite set $X \in \mathcal{F}$ there is an N such that for all $n > N$ one has

$$\mu^{(n)}\mathbb{E}_X f = \mu^{(n)} f$$

and one can choose a convergent subsequence to a Gibbs measure.

We use $\mathcal{G}_\Gamma(\Phi)$ to denote the class of all Gibbs measures $\mu \in \mathcal{G}(\Phi)$ such that (2.1) holds true for some sequence $\{n_j\}$. Lemma 2.1 ensures that $\mathcal{G}_\Gamma(\Phi) \neq \emptyset$.

3. Spectral gap and logarithmic Sobolev inequality for non-diagonal forms

Let $Y \in \mathcal{F}$, $Y \neq \emptyset$ and $\boldsymbol{a} = (a_i)_{i\in Y} \in (\mathbb{Z}\setminus\{0\})^Y$ be such that

$$0 \in Y \qquad 0 \notin \text{convex hull of } (Y\setminus\{0\}) \qquad \text{and} \qquad a_0 \in \{-1, 1\}. \tag{3.1}$$

Later on we will use θ to denote a pair $(Y, \boldsymbol{a})$ satisfying (3.1). Let

$$\mathcal{K}_\theta(f)(\omega) = \sum_{k\in\mathbb{Z}^d}\Bigg(\sum_{j\in k+Y} a_{j-k}\nabla_j f(\omega)\Bigg)^2 \qquad f \in C_0^\infty(\Omega). \tag{3.2}$$

In our considerations an important role is played by the following transformation of variables $\xi_\theta : \Omega \to \Omega$:

$$\big(\xi_\theta(\omega)\big)_j = \sum_{k\in j-Y} a_{j-k}\omega_k \qquad j \in \mathbb{Z}^d \quad \omega \in \Omega.$$

For $X \in \mathcal{F}$ we set

$$\mathcal{A}(X) = \{\tilde{X} \in \mathcal{F} :\ \tilde{X} - Y = X\}.$$

Given a potential Φ we introduce a transformed potential $\Phi^\theta \equiv \{\Phi_X^\theta :\ X \in \mathcal{F}\}$ as follows:

$$\Phi_X^\theta = \begin{cases} 0 & \text{if} \quad \mathcal{A}(X) = \emptyset \\ \displaystyle\sum_{\tilde{X}\in\mathcal{A}(X)} \Phi_{\tilde{X}} \circ \xi_\theta & \text{if} \quad \mathcal{A}(X) \neq \emptyset. \end{cases} \tag{3.3}$$

Let us denote by $\mathcal{D}$ the following (diagonal) square of the field

$$\mathcal{D}(f)(\omega) = \sum_{k\in\mathbb{Z}^d} |\nabla_k f(\omega)|^2 \qquad f \in C_0^\infty(\Omega).$$

We will prove the following equivalence theorem

Theorem 3.1. *Suppose that Φ is a finite-range potential such that there is a unique Gibbs measure $\mu \in \mathcal{G}(\Phi)$. Let Φ^θ be the corresponding transformed potential given by* (3.3). *Then:*

(a) $\mu \in \mathbf{SG}(\mathcal{K}_\theta)$ if and only if for any $\tilde{\mu} \in \mathcal{G}_{-Y}(\Phi^\theta)$ one has $\tilde{\mu} \in \mathbf{SG}(\mathcal{D})$.
(b) $\mu \in \mathbf{LS}(\mathcal{K}_\theta)$ if and only if for any $\tilde{\mu} \in \mathcal{G}_{-Y}(\Phi^\theta)$ one has $\tilde{\mu} \in \mathbf{LS}(\mathcal{D})$.

4. Proof of theorem 3.1

Let $\mathcal{E}(\Phi^\theta) = \{\mathbb{E}^\theta_\Lambda : \Lambda \in \mathcal{F}\}$ be the local specification corresponding to Φ^θ, that is

$$\mathbb{E}^\theta_\Lambda f = \frac{\langle f \exp\{-U^\theta_\Lambda\}\rangle_\Lambda}{\langle \exp\{-U^\theta_\Lambda\}\rangle_\Lambda} \qquad \text{where} \quad U^\theta_\Lambda = -\sum_{X\in\mathcal{F}:X\cap\Lambda\neq\emptyset} \Phi^\theta_X.$$

Since

$$\sum_{X\in\mathcal{F}:X\cap\Lambda\neq\emptyset} \Phi^\theta_X = \sum_{\tilde{X}\in\mathcal{F}:(\tilde{X}-Y)\cap\Lambda\neq\emptyset} \Phi_{\tilde{X}}\circ\xi_\theta = \sum_{\tilde{X}\in\mathcal{F}:\tilde{X}\cap(\Lambda+Y)\neq\emptyset} \Phi_{\tilde{X}}\circ\xi_\theta$$

we have

$$U^\theta_\Lambda = U_{\Lambda+Y}\circ\xi_\theta \qquad \Lambda\in\mathcal{F} \tag{4.1}$$

and consequently

$$\mathbb{E}^\theta_\Lambda f = \frac{\langle f \exp\{-U_{\Lambda+Y}\circ\xi_\theta\rangle_\Lambda}{\langle \exp\{-U_{\Lambda+Y}\circ\xi_\theta\rangle_\Lambda} \qquad f\in C^\infty_0(\Omega) \quad \Lambda\in\mathcal{F}.$$

Note that if Φ has a finite range, the same is true for Φ^θ.

Lemma 4.1. *Assume (3.1). Then for all cubes $\Lambda_n = [-n,n]^d\cap\mathbb{Z}^d$ and $\Lambda_l = [-l,l]^d\cap\mathbb{Z}^d$ satisfying $\Lambda_l - Y\subseteq\Lambda_n$, and for every $f\in C_{\Lambda_l}(\Omega)$ one has*

$$\langle f\circ\xi_\theta\rangle_{\Lambda_n} = \langle f\rangle_{\Lambda_n} = \langle f\rangle_{\Lambda_l}.$$

Proof. Let Λ_n, Λ_l be such that $\Lambda_l - Y\subseteq\Lambda_n$. The proof will be completed as soon as we can show that the following transformation of variables:

$$\eta_k = \begin{cases} \omega_k & \text{if} \quad k\in\Lambda_n\setminus(\Lambda_l - Y) \\ \big(\xi_\theta(\omega)\big)_k & \text{if} \quad k\in\Lambda_l - Y \end{cases}$$

preserves the measure μ_0 on $\Omega_n = (S^1)^{\Lambda_n}$. To this end we introduce a lexicographic order $\{k_i\}$, $i = 1,\dots,|\Lambda_n|$ in Λ_n satisfying

$$\{k_i : i = 1,\dots,|\Lambda_n\setminus(\Lambda_l - Y)|\} = \Lambda_n\setminus(\Lambda_l - Y)$$

and for $i > |\Lambda_n\setminus(\Lambda_l - Y)|$,

$$(k_i - Y)\cap(\Lambda_l - Y) = \{k_r : |\Lambda_n\setminus(\Lambda_l - Y)| < r\leqslant i\}.$$

The existence of such an order is guaranteed by (3.1). Now consider the Jacobian matrix

$$A = \left\{\frac{\partial\eta_{k_i}}{\partial\omega_{k_j}}\right\} \qquad i,j = 1,\dots,|\Lambda_n|.$$

Clearly, A is an upper-triangular matrix. Since $a_0\in\{-1,1\}$, the elements on its diagonal are from $\{-1,1\}$. Thus $|\det A| = 1$, which completes the proof. □

Lemma 4.2. *Assume that the hypothesis of theorem 3.1 is fulfilled. Let $\tilde{\mu}\in\mathcal{G}_{-Y}(\Phi^\theta)$. Then $\tilde{\mu} f\circ\xi_\theta = \mu f$ for every $f\in C_0(\Omega)$.*

Proof. Let $\tilde{\mu} \in \mathcal{G}_{-Y}(\Phi^{\theta})$. Then there is a sequence $\{n_j\}$ such that

$$\tilde{\mu} f = \lim_{j\to\infty} \frac{\left\langle f \exp\{-\tilde{U}^{(n_j)}\}\right\rangle_{\Lambda_{n_j}}}{\left\langle \exp\{-\tilde{U}^{(n_j)}\}\right\rangle_{\Lambda_{n_j}}} \qquad f \in C_0(\Omega)$$

where

$$\tilde{U}^{(n)} = -\sum_{X\in\mathcal{F}:\ X-Y\subseteq\Lambda_n} \Phi^{\theta}_X.$$

Since μ is a unique Gibbs measure for $\mathcal{E}(\Phi)$, lemma 2.1 yields that there is a subsequence $\{m_j\}$ of $\{n_j\}$ such that

$$\mu f = \lim_{j\to\infty} \frac{\left\langle f \exp\{-U^{(m_j)}\}\right\rangle_{\Lambda_{m_j}}}{\left\langle \exp\{-U^{(m_j)}\}\right\rangle_{\Lambda_{m_j}}} \qquad f \in C_0(\Omega)$$

where

$$U^{(n)} = -\sum_{X\in\mathcal{F}:\ X-Y-Y\subseteq\Lambda_n} \Phi_X.$$

Now note that

$$\tilde{U}^{(n)} = -\sum_{X\in\mathcal{F}:\ X-Y\subseteq\Lambda_n} \Phi^{\theta}_X = -\sum_{\tilde{X}\in\mathcal{F}:\ \tilde{X}-Y-Y\subseteq\Lambda_n} \Phi_{\tilde{X}} \circ \xi_{\theta} = U^{(n)} \circ \xi_{\theta}.$$

Thus, for any $f \in C_0(\Omega)$, we have

$$\tilde{\mu} f \circ \xi_{\theta} = \lim_{j\to\infty} \frac{\left\langle (f \exp\{-U^{(m_j)}\}) \circ \xi_{\theta}\right\rangle_{\Lambda_{m_j}}}{\left\langle \exp\{-U^{(m_j)}\} \circ \xi_{\theta}\right\rangle_{\Lambda_{m_j}}} \qquad f \in C_0(\Omega).$$

Combining this with (4.1) and lemma 4.1 we obtain the desired conclusion. □

Proof of theorem 3.1. Let us observe that

$$\nabla_k (f \circ \xi_{\theta}) = \left(\sum_{j\in k+Y} a_{j-k} \nabla_j f \right) \circ \xi_{\theta} \qquad \text{for} \quad f \in C_0^{\infty}(\Omega) \quad k \in \mathbb{Z}^d.$$

Thus

$$\mathcal{D}(f \circ \xi_{\theta}) = \mathcal{K}_{\theta}(f) \circ \xi_{\theta} \qquad \text{for} \quad f \in C_0^{\infty}(\Omega) \quad k \in \mathbb{Z}^d.$$

Now assume that $\mu \in \mathcal{G}(\Phi)$ satisfies $\mathbf{SG}(\mathcal{K}_{\theta})$. Let $\tilde{\mu} \in \mathcal{G}_{-Y}(\Phi^{\theta})$. Then, by lemma 4.2 for any $f \in C_0^{\infty}(\Omega)$ we have

$$\begin{aligned}\tilde{\mu}\big(f \circ \xi_{\theta} - \tilde{\mu} f \circ \xi_{\theta}\big)^2 = \mu\big(f - \mu f\big)^2 &\leqslant C\mu\mathcal{K}_{\theta}(f) = C\tilde{\mu}\mathcal{K}_{\theta}(f) \circ \xi_{\theta} \\ &\leqslant C\tilde{\mu}\mathcal{D}(f \circ \xi_{\theta}).\end{aligned}$$

Since $f \mapsto f \circ \xi_{\theta}$ is a bijection on $C_0^{\infty}(\Omega)$, $\tilde{\mu}$ satisfies $\mathbf{SG}(\mathcal{D})$. Assume now that $\tilde{\mu} \in \mathcal{G}_{-Y}(\Phi^{\theta})$ satisfies $\mathbf{SG}(\mathcal{D})$. Then for all f we have

$$\mu\big(f - \mu f\big)^2 = \tilde{\mu}\big(f \circ \xi_{\theta} - \tilde{\mu} f \circ \xi_{\theta}\big)^2 \leqslant C\tilde{\mu}\mathcal{D}(f \circ \xi_{\theta}) \leqslant C\mu\mathcal{K}_{\theta}(f).$$

Thus μ satisfies $\mathbf{SG}(\mathcal{K}_{\theta})$, and the proof of the first part of the theorem is completed. The same arguments can be applied in a proof of the second part concerning logarithmic Sobolev inequalities. □

5. Dobrushin–Shlosman mixing and logarithmic Sobolev inequalities

Definition 5.1. We say that the local specification $\mathcal{E}(\Phi)$ satisfies the *Dobrushin–Shlosman mixing condition* iff there is an $X \in \mathcal{F}$ with $0 \in X$, and a family of non-negative numbers $\alpha_{l,j}$ for $l \notin X$ and $j \in X$ such that

$$\beta = 1 - \frac{1}{|X|} \sum_{l \notin X,\, j \in X} \alpha_{l,j} > 0 \tag{5.1}$$

and for all $l \notin X$, $k \in \mathbb{Z}^d$, $f \in C_0^\infty(\Omega)$ and $Z \subseteq X$ one has

$$\|\partial_{l+k} \mathbb{E}_{k+Z} f - \mathbb{E}_{k+Z} \partial_{l+k} f\|_{\mathrm{u}} \leqslant \sum_{j \in X} \alpha_{l,j} \|\partial_{j+k} f\|_{\mathrm{u}}. \tag{5.2}$$

Remark 5.1. Note that if the potential family is shift-invariant, then it satisfies the Dobrushin–Shlosman condition iff (5.1) holds and if (5.2) is satisfied for $k = 0$.

Remark 5.2. The Dobrushin–Shlosman condition ensures the uniqueness of the Gibbs measure μ for $\mathcal{E}(\Phi)$ (see, e.g., [S]).

For further references we recall the following result of Stroock and Zegarlinski (see, e.g., [S, SZ1], or [SZ2]).

Theorem 5.1. *Assume that Φ is a C^2 potential of finite range, and that the local specification $\mathcal{E}(\Phi)$ satisfies the Dobrushin–Shlosman mixing condition. Then the unique Gibbs measure μ satisfies* $\mathbf{LS}(\mathcal{D})$.

As a direct consequence of theorems 3.1 and 5.1 we have;

Corollary 5.1. *Let Φ be a C^2 potential of finite range. If $\mathcal{E}(\Phi)$ and $\mathcal{E}(\Phi^\theta)$ satisfy the Dobrushin–Shlosman mixing condition, then the unique Gibbs measure $\mu \in \mathcal{G}(\Phi)$ satisfies* $\mathbf{LS}(\mathcal{K}_\theta)$.

In the next result we show that there always exists a high-temperature region where our conditions are satisfied.

Proposition 5.1 (Small potential case). *Let Φ be a C^2 potential of a finite range R. Assume that*

$$\begin{aligned} &\sup_{k \in \mathbb{Z}^d} \|U_{\{k+Y\}}\|_{\mathrm{u}} < \tfrac{1}{4} \log\left(1 + (R + \operatorname{diam} Y)^{-1}\right) \\ &\sup_{k \in \mathbb{Z}^d} \|U_k\|_{\mathrm{u}} < \tfrac{1}{4} \log\left(1 + R^{-1}\right). \end{aligned} \tag{5.3}$$

Then there is a unique Gibbs measure μ for $\mathcal{E}(\Phi)$, and μ satisfies $\mathbf{LS}(\mathcal{K}_\theta)$.

Proof. Note that the range of Φ^θ is less than or equal to $R + \operatorname{diam} Y$. According to corollary 5.1 it is enough to show that (5.3) implies that $\mathcal{E}(\Phi^\theta)$ and $\mathcal{E}(\Phi)$ satisfy the Dobrushin–Shlosman mixing condition with $X = \{0\}$. To do this we have to prove that there are positive constants α and $\tilde{\alpha}$ satisfying $(R + \operatorname{diam} Y)\alpha < 1$ and $R\tilde{\alpha} < 1$ such that

$$\|\partial_l \mathbb{E}_k^\theta f - \mathbb{E}_k^\theta \partial_l f\|_{\mathrm{u}} \leqslant \alpha \|\partial_k f\|_{\mathrm{u}} \qquad \text{for all } k \neq l \quad \text{and} \quad f \in C_0^\infty(\Omega) \tag{5.4}$$

and

$$\|\partial_l \mathbb{E}_k f - \mathbb{E}_k \partial_l f\|_{\mathrm{u}} \leqslant \tilde{\alpha} \|\partial_k f\|_{\mathrm{u}} \qquad \text{for all } k \neq l \quad \text{and} \quad f \in C_0^\infty(\Omega). \tag{5.5}$$

Let $k, l \in \mathbb{Z}^d$, $k \neq l$. Note that for all f and ω we have

$$\begin{aligned}\left[\partial_l, \mathbb{E}_k^\theta\right] f(\omega) &= \left(\partial_l \mathbb{E}_k^\theta f - \mathbb{E}_k^\theta \partial_l f\right)(\omega) \\ &= \int_\Omega \int_\Omega \left(\rho_k(x \bullet_l (y \bullet_k \omega)) - \rho_k(y \bullet_k \omega)\right) f(x \bullet_l (y \bullet_k \omega)) \mu(\mathrm{d}x) \mu(\mathrm{d}y)\end{aligned}$$

where the density ρ_k of $\mathbb{E}_k^\theta$ is given by

$$\rho_k(\omega) = \frac{\exp\{-U_k^\theta(\omega)\}}{\left\langle \exp\{-U_k^\theta\}\right\rangle(\omega)} \qquad \omega \in \Omega.$$

Using (4.1) we obtain

$$\rho_k(\omega) = \frac{\exp\{-U_{k+Y} \circ \xi_\theta(\omega)\}}{\left\langle \exp\{-U_{k+Y} \circ \xi_\theta\}\right\rangle(\omega)} \qquad \omega \in \Omega.$$

Since

$$\int_\Omega \rho_k(x \bullet_l (y \bullet_k \omega)) \mu_0(\mathrm{d}y) = 1 = \int_\Omega \rho_k(y \bullet_k \omega) \mu_0(\mathrm{d}y)$$

we have

$$\left[\partial_l, \mathbb{E}_k^\theta\right] f(\omega) = -\int_\Omega \int_\Omega (\rho_k(x \bullet_l (y \bullet_k \omega)) - \rho_k(y \bullet_k \omega))(\partial_k f)(x \bullet_l (y \bullet_k \omega)) \mu_0(\mathrm{d}x) \mu_0(\mathrm{d}y).$$

Thus (5.4) holds true with

$$\begin{aligned}\alpha &= \sup_k \sup_{x,y,\omega \in \Omega} \left(\frac{\rho_k(x \bullet_l (y \bullet_k \omega))}{\rho_k(y \bullet_k \omega)} - 1 \right) \leqslant \sup_k \sup_{\omega, v \in \Omega} \frac{\rho_k(\omega)}{\rho_k(v)} - 1 \\ &\leqslant \sup_k \exp\{4 \|U_{k+Y}\|_{\mathrm{u}}\} - 1\end{aligned}$$

having the desired property. In the same way one can show that (5.3) yields (5.5) with $R\tilde{\alpha} < 1$. □

6. A class of infinite-volume stochastic dynamics

In this section we briefly describe the construction of an infinite-volume Markov semigroup corresponding to a general square of the field form $\mathcal{K}$. We consider a configuration space given by a product space $\Omega \equiv \boldsymbol{M}^{\mathbb{Z}^d}$, where $\boldsymbol{M}$ is a smooth compact and connected Riemannian manifold. Let $\mathcal{W} \equiv \{W_i\}_{i \in \mathbb{Z}^d}$ be a collection of C^∞ vector fields defined as a following lift of the given smooth vector fields w_i on $\boldsymbol{M}$:

$$W_i f(\omega) \equiv w_i f(\omega_i | \omega).$$

Given a finite set Y we define the following vector fields on Ω:

$$W_Y \equiv \sum_{j \in Y} W_j.$$

With this notation we introduce the following square of the field forms:

$$\mathcal{K}(f) \equiv \sum_{k \in \mathbb{Z}^d} (W_{k+Y} f)^2$$

with a domain including smooth cylinder functions $f \in C_0^\infty(\Omega)$. Given a local specification $\mathcal{E}(\Phi)$ corresponding to a smooth potential of finite range, we can now introduce the following elementary Markov operators on $C^2(\Omega)$:

$$\mathcal{L}_Y f \equiv W_Y^2 f + \beta_Y \cdot W_Y f$$

where we have set

$$\beta_Y \equiv \operatorname{div} W_Y + W_Y U_Y$$

with

$$\operatorname{div} W_Y \equiv \sum_{j \in Y} \operatorname{div}_j W_j$$

and $\operatorname{div}_j W_j$ is defined by the corresponding lift of $\operatorname{div} w_j$ on the manifold $\boldsymbol{M}$. With this notation one can see that

$$\mathbb{E}_Y (W_Y f)^2 = \mathbb{E}_Y (f(-\mathcal{L}_Y f)).$$

For later purposes we introduce the following free Markov generator:

$$\mathcal{L}^0 \equiv \sum_{k \in \mathbb{Z}^d} W_{k+Y}^2 f.$$

We note that $\mathcal{L}^0$ is local, that is for any $f \in C^2$ dependent only on ω_j, $j \in \Lambda_f$, one has

$$\mathcal{L}^0 f = \sum_{k \in \mathbb{Z}^d} W_{(k+Y) \cap \Lambda_f}^2 f$$

and therefore $\Lambda_{\mathcal{L}^0 f} \subset \Lambda_f$. This property allows us to easily define a Markov semigroup $P_t^0 \equiv \mathrm{e}^{t\mathcal{L}^0}$ on $C_0(\Omega)$. For any finite set $\Lambda \in \mathcal{F}$ we introduce a finite-volume generator

$$\mathcal{L}_\Lambda f \equiv \mathcal{L}^0 f + \sum_k \beta_{(k+Y) \cap \Lambda} \cdot W_{(k+Y) \cap \Lambda} f$$

with a convention that $\beta_\emptyset \equiv 0$. We note that $\mathcal{L}_\Lambda$ is again local and therefore it is easy to construct the corresponding Markov semigroup $P_t^{(\Lambda)} \equiv \mathrm{e}^{t\mathcal{L}_\Lambda}$ on $C_0(\Omega)$.

With the above assumptions and notation the following result is true.

Theorem 6.1. *Suppose that*

$$\sup_{k \in \mathbb{Z}^d, X \subset Y} \|\beta_{k+X}\|_{\mathrm{u}} < \infty$$

and

$$D \equiv \sup_{k \in \mathbb{Z}^d, Z, \Lambda \in \mathcal{F} : |Z| \leqslant |Y|} \|W_Z(\beta_{(k+Y) \cap \Lambda})\|_{\mathrm{u}} < \infty.$$

Then for any $f \in C_0^1(\Omega)$ the following limit exists:

$$P_t f \equiv \lim_{\Lambda \to \infty} P_t^{(\Lambda)} f$$

with the generator $\mathcal{L}$ satisfying

$$\mu(f(-\mathcal{L} f)) = \mathcal{K}(f).$$

Moreover, the following exponential approximation property is true: for any $A \in (0, \infty)$ there is $B \in (0, \infty)$ such that

$$\|P_t f - P_t^{(\Lambda)} f\|_{\mathrm{u}} \leqslant \mathrm{e}^{-At} C(f)$$

with some constant $C(f) \in (0, \infty)$ dependent only on f and the field $\mathcal{W}$, provided that

$$\operatorname{dist}(\Lambda_f, \mathbb{Z}^d \setminus \Lambda) \geqslant Bt.$$

Proof. For $\Lambda_1 \in \mathcal{F}$ and $\Lambda_2 \equiv \Lambda_1 \cup \{i\}$, we have

$$P_t^{(\Lambda_2)} f - P_t^{(\Lambda_1)} f = \int_0^t \mathrm{d}s \, \frac{\mathrm{d}}{\mathrm{d}s} P_{t-s}^{(\Lambda_1)} P_s^{(\Lambda_2)} f = \int_0^t \mathrm{d}s \, P_{t-s}^{(\Lambda_1)} (\mathcal{L}_{\Lambda_2} - \mathcal{L}_{\Lambda_1}) P_s^{(\Lambda_2)} f. \tag{6.1}$$

Next we note that

$$(\mathcal{L}_{\Lambda_2} - \mathcal{L}_{\Lambda_1}) F = \sum_{k:\mathrm{dist}(k+Y,i)\leqslant R} \left[\beta_{(k+Y)\cap\Lambda_2} W_{(k+Y)\cap\Lambda_2} - \beta_{(k+Y)\cap\Lambda_1} W_{(k+Y)\cap\Lambda_1} \right] \tag{6.2}$$

where R is the range of the interaction. Hence taking into the account that we consider Markov semigroups here, we obtain

$$\| P_t^{(\Lambda_2)} f - P_t^{(\Lambda_1)} f \|_{\mathrm{u}} \leqslant \sup_{k\in\mathbb{Z}^d, X\subset Y} \| \beta_{k+X} \|_{\mathrm{u}} \sum_{Z:\ \exists k\ \mathrm{dist}(k+Y,i)\leqslant R, Z\subset k+Y} \int_0^t \mathrm{d}s \, \| W_Z P_s^{(\Lambda_2)} f \|_{\mathrm{u}}. \tag{6.3}$$

Thus to complete the proof it is sufficient to obtain a bound for $\| W_Z P_s^{(\Lambda_2)} f \|_{\mathrm{u}}$ for $Z \subset k + Y$, $k \in \mathbb{Z}^d$. To this end we note that

$$W_Z P_s^{(\Lambda_2)} f = P_s^{(\Lambda_2)} W_Z f + \int_0^s \mathrm{d}\tau \, P_{s-\tau}^{(\Lambda_2)} [W_Z, \mathcal{L}_{\Lambda_2}] P_\tau^{(\Lambda_2)} f. \tag{6.4}$$

Noting that $[W_Z, \mathcal{L}^0] = 0$ we have

$$\begin{aligned} [W_Z, \mathcal{L}_{\Lambda_2}] &= \left[W_Z, \sum_k \beta_{(k+Y)\cap\Lambda_2} W_{(k+Y)\cap\Lambda_2} \right] \\ &= \sum_{k:\mathrm{dist}(Z,(k+Y)\cap\Lambda_2)\leqslant R} W_Z (\beta_{(k+Y)\cap\Lambda_2}) W_{(k+Y)\cap\Lambda_2}. \end{aligned} \tag{6.5}$$

From (6.4) and (6.5) we conclude that

$$\| W_Z P_s^{(\Lambda_2)} f \|_{\mathrm{u}} \leqslant \| W_Z f \|_{\mathrm{u}} + D \sum_{k:\mathrm{dist}(Z,(k+Y)\cap\Lambda_2)\leqslant R} \int_0^s \mathrm{d}\tau \, \| W_{(k+Y)\cap\Lambda_2} P_s^{(\Lambda_2)} f \|_{\mathrm{u}} \tag{6.6}$$

with

$$D \equiv \sup_{k\in\mathbb{Z}^d, Z, \Lambda\in\mathcal{F}:|Z|\leqslant|Y|} \| W_Z (\beta_{(k+Y)\cap\Lambda}) \|_{\mathrm{u}}.$$

Given the inequality (6.6) the rest of the proof goes in a standard way (see, e.g., [GZ1]). □

7. Exponential decay to equilibrium for Kawasaki dynamics

Let the single spin space be given by S^1. We choose Y to be a set consisting of the origin and one of its nearest neighbours i_1 and $\boldsymbol{a} = \{-1, +1\}$. Then by theorem 3.1 a unique Gibbs measure μ_Φ related to a finite-range potential Φ satisfies **SG** or **LS** with the corresponding form

$$\bar{\mathcal{K}}(f) \equiv \sum_k |(\nabla_{k+i_1} - \nabla_k) f|^2$$

provided these inequalities remain true for a unique Gibbs measure μ_{Φ^θ} with the diagonal form. This naturally implies that **SG**, respectively, **LS**, is true for the form

$$\mathcal{K}(f) \equiv \sum_{j,k:|j-k|=1} |(\nabla_k - \nabla_j) f|^2$$

which is not smaller than $\bar{\mathcal{K}}$. As we have indicated in section 5 such a situation is true for any potential of finite range, provided the temperature of the system is sufficiently high (cf proposition 5.1). In particular, if $\mathbf{LS}(\mathcal{K})$ is satisfied, then the corresponding semigroup is hypercontractive. This together with the strong approximation property (theorem 6.1) allows one to apply the general strategy of Holley and Stroock (see, e.g., [SZ1]) to prove the uniform exponential decay to equilibrium. Thus we conclude with the following result.

Theorem 7.1. *Suppose for a finite-range potential Φ, the local specification $\mathcal{E}(\Phi^\theta)$ satisfies the mixing condition. Then the Kawasaki dynamics $P_t \equiv \mathrm{e}^{t\mathcal{L}}$ is strongly exponentially ergodic, that is for any function $f \in C_0^1(\Omega)$ we have*

$$\| P_t f - \mu_\Phi f \|_{\mathrm{u}} \leqslant C_\alpha \mathrm{e}^{-\alpha m t} \sum_k \| \nabla_k f \|_{\mathrm{u}}$$

with $m \equiv \mathrm{gap}_{\mathbb{L}_2(\mu)}(-\mathcal{L})$ and any $\alpha \in (0, 1)$ with a constant $C_\alpha \equiv C_\alpha(\Lambda_f)$ dependent only on Λ_f and the choice of α.

We stress that our mixing requirement involves the transformed potential. We note that the conditions are always satisfied in one dimension (as our transformation ξ^θ transforms finite-range potentials into finite-range potentials). Clearly, in higher dimensions the domain of strong mixing may depend on the potential (but in any case there always exists a non-trivial high-temperature region where the required mixing is true).

Acknowledgments

This work was supported by EPSRC grants GR/K 76801 and GR/L48867 and 2266/W/ift/98.

References

[BZ1] Bertini L and Zegarlinski B 1999 Coercive inequalities for Kawasaki dynamics: the product case *Markov Process. Rel. Fields* **5** 125–62

[BZ2] Bertini L and Zegarlinski B 1999 Coercive inequalities for Gibbs measures *J. Funct. Anal.* **162** 257–86

[CM] Cancrini and Martinelli F On the spectral gap of Kawasaki dynamics under a mixing condition revisited mp_arc 5 *Preprint* 99-27

[De] Deuschel J D 1991 Algebraic $\mathbb{L}^2$ decay of attractive critical processes on the lattice *Ann. Probab.* **22** 264–83

[DS] Dobrushin R L and Shlosman S B 1985 Constructive criterion for the uniqueness of Gibbs field, completely analytical Gibbs fields, statistical physics and dynamical systems. Rigorous results *2nd Colloq. Workshop on Random Fields: Rigorous Results in Statistical Mechanics (Koszeg) (Progress in Physics vol 10)* ed J Fritz, A Jaffe and D Szasz (Boston, MA: Birkhäuser) pp 347–70, 371–403

[F] Faris W G 1979 The stochastic Heisenberg model *J. Funct. Anal.* **32** 342–52

[GZ1] Guionnet A and Zegarlinski B 1996 Decay to equilibrium in random spin systems on a lattice *Commun. Math. Phys.* **181** 703–32

[GZ2] Guionnet A and Zegarlinski B 1997 Decay to equilibrium in random spin systems on a lattice, II *J. Stat. Phys.* **86** 899–904

[HS1] Holley R and Stroock D W 1981 Diffusions on an infinite-dimensional torus *J. Funct. Anal.* **42** 29–63

[HS2] Holley R and Stroock D 1987 Logarithmic Sobolev inequalities and stochastic Ising models *J. Stat. Phys.* **46** 1159–94

[JLQY] Janvresse E, Landim C, Quastel J and Yau H T Relaxation to equilibrium of conservative dynamics I: zero range processes *Preprint*

[LY] Lu S L and Yau H T 1993 Spectral gap and logarithmic Sobolev inequality for Kawasaki dynamics and Glauber dynamics *Commun. Math. Phys.* **156** 399–433

[S] Stroock D W 1993 Logarithmic Sobolev inequalities for Gibbs states Dirichlet forms *Lectures Given at the 1st Session of the Centro Internazionale Matematico Estivo (CIME) (Varenna, 1992) (Lecture Notes in Mathematics vol 1563)* ed G Dell'Antonio and U Moscom (Berlin: Springer) pp 194–230

[SZ1] Stroock D W and Zegarlinski B 1992 Logarithmic Sobolev inequality for continuous spin system *J. Funct. Anal.* **104** 299–326

[SZ2] Stroock D W and Zegarlinski B 1992 The equivalence of the logarithmic Sobolev inequality and the Dobrushin–Shlosman mixing condition *Commun. Math. Phys.* **149** 175–93

[W] Wick W D 1981 Convergence to equilibrium of the stochastic Heisenberg model *Commun. Math. Phys.* **81** 361–77

[ZZ] Zhengping Zhang 1995 Generalized Kawasaki dynamics of the Heisenberg model *Phys. Rev.* E **51** 4155–8

Three types of outflow dynamics on square and triangular lattices and universal scaling

Grzegorz Kondrat and Katarzyna Sznajd-Weron*
Institute of Theoretical Physics, University of Wrocław, pl. Maxa Borna 9, 50-204 Wrocław, Poland
(Received 3 June 2007; revised manuscript received 11 November 2007; published 27 February 2008)

In this paper we propose a generalization of the one-dimensional outflow dynamics (KD). The rule is introduced as a simplification of Galam dynamics (GD) proposed in an earlier paper. We simulate three types of outflow dynamics, GD, Stauffer *et al.* dynamics, and KD, both on the square and triangular lattices and show whether the outflow dynamics is sensitive to the lattice structure. Moreover, we took into account several types of initial configuration—random, "stripes," and "circle." We investigate the dependence between the mean relaxation time and the initial density p of up-spins for each type of initial conditions, as well as dependence between the mean relaxation time and the size of the system. As a result, we show differences and similarities between three types of the outflow dynamics.

DOI: 10.1103/PhysRevE.77.021127 PACS number(s): 05.50.+q

I. INTRODUCTION

The outflow dynamics was introduced to describe the opinion change in society. The idea was based on the fundamental social phenomenon called "social validation."

Under the outflow dynamics a system eventually always reaches consensus, like in the famous voter model [1–3]. Several other models describing opinion dynamics were introduced by Deffuant [4], Hegselmann and Krause [5], Krapivsky and Redner [6], and Galam [7].

In this paper, however, we do not focus on social applications of our model (for those interested, reviews can be found in Refs. [8–11]). On the contrary, we investigate here the dynamics from the theoretical point of view.

In this paper we pay particular attention to a generalization of the one-dimensional outflow dynamics to higher dimensions. Several possibilities of such a generalization to the square lattice were proposed by Stauffer *et al.* [12] (see Sec. II) but only some of them were used in the later literature [8–11]. In Ref. [13] we presented comparative studies of the two most interesting generalizations out of all proposed in Ref. [12]. Only slight quantitative differences have been found between these two generalizations.

The outflow dynamics on the triangular lattice were considered only in one paper [14]. In this paper the author studied the generalization of the Sznajd model to the triangular lattice with spreading of mixed opinion and with the pure antiferromagnetic opinion—a pair of two neighboring spins on a triangular lattice influenced its eight neighbors.

Up till now no studies on the influence of the lattice geometry, in the case of regular lattices, for spins endowed with the outflow dynamics were provided. However, the influence of the topology for the relaxation under the outflow dynamics in a case of complex networks has been investigated in Refs. [15–18]. In Ref. [15] the time evolution of the system was studied using different network topologies, starting from different initial opinion densities. A transition from consensus in one opinion to the other was found at the same percentage of initial distribution no matter which type of complex network was used. On the other hand, results presented in Ref. [19] suggest that lattice geometry may influence the network dynamics.

In a broad sense the notion of consensus in a network is a particular case of what can be called coherence or full synchronization between sets of coupled elements, subject to some sort of local dynamics or updating rule [19,20]. In the paper [19] the influence of lattice geometry in network dynamics, using a binary cellular automaton with nearest-neighbor interactions, has been studied. It was shown that geometric structures are more cohesive than others, tending to keep a given initial configuration.

The first general question we pose in this paper is the following: Is the outflow dynamics sensitive to the lattice topology (like in the case of binary cellular automaton on regular networks [19]) or not (as suggested in the case of complex networks [15])? To answer this question we present results for several types of the outflow dynamics on the square and triangular lattices coming from regular studies on the mean relaxation time.

The second question we pose in this paper is connected to the differences between particular forms of the outflow dynamics. As mentioned above, several generalizations [12,14–18] from one to higher dimensions were proposed, but no regular comparative studies were provided. In Ref. [13] we presented comparative studies of two types of the outflow dynamics on the square lattice and we found no qualitative differences. However, we did not check how the results would change with a lattice topology or with the type of initial conditions. To complete this approach we decided here to treat the matter systematically. Moreover, we introduce in this paper one more type of generalization of one-dimensional outflow dynamics into two dimensions, which is a simplification of one of the dynamics studied in Ref. [13]. All three dynamics are simulated both on square and triangular lattices. We start from different initial densities of up-spins in several types of initial conditions. We measure the mean relaxation time as a function of initial densities of up-spins as well as the dependence between the mean relaxation time and the lattice size. We show that in some cases universal scaling laws exist, while in others they do not.

*kweron@ift.uni.wroc.pl; URL: http://www.ift.uni.wroc.pl/~kweron

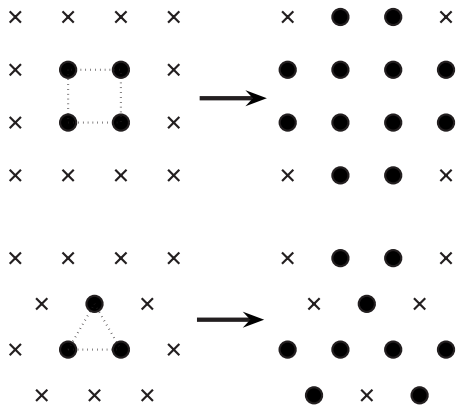

FIG. 1. Stauffer *et al.* dynamical rules of SM on the square (upper panel) and triangular (bottom) lattice. On the square lattice a 2×2 panel of four neighbors (elementary cell) leaves its eight neighbors unchanged, if all four center spins are not parallel. On the triangular lattice a panel of three spins (elementary cell) influences six neighbors along three chains of four spins each, centered about the panel.

II. MODEL

In this paper we consider the generalizations of the one-dimensional outflow dynamics to higher dimensions. Let us begin with recalling the one-dimensional outflow dynamics, described in detail in Ref. [21]. In the original model [22] the pair of neighboring spins S_i and S_{i+1} have been chosen and if $S_iS_{i+1}=1$ the two neighbors of the pair followed its direction, i.e., $S_{i-1}\rightarrow S_i(=S_{i+1})$ and $S_{i+2}\rightarrow S_{i+1}(=S_i)$. Such a rule has been used also in all later papers dealing with the one-dimensional case of the model. However, the case in which $S_iS_{i+1}=-1$ was noted as far less obvious. Several possibilities has been proposed up till now and in general one-dimensional outflow dynamics can be written as [21]:

$$S_i(\tau+1) = \begin{cases} 1 & \text{if } S_{i+1}(\tau)+S_{i+2}(\tau)>0, \\ -S_i(\tau) \text{ with prob } W_0 & \text{if } S_{i+1}(\tau)+S_{i+2}(\tau)=0, \\ -1 & \text{if } S_{i+1}(\tau)+S_{i+2}(\tau)<0. \end{cases} \tag{1}$$

The most known case is for $W_0=0$ and also this case has been generalized into two dimensions. Several possibilities of such a generalization to the square lattice were proposed by Stauffer *et al.* [12]. Six different rules were introduced, but only the following two have been used in later publications: A 2×2 panel of four neighbors leaves its eight neighbors unchanged, if all four center spins are not parallel (see Fig. 1); a neighboring pair persuades its six neighbors to follow the pair orientation if and only if the two pair spins are parallel.

With both these rules complete consensus is always reached as a steady state. Moreover, a phase transition is observed—initial densities below 1/2 of up-spins lead to all spins down and densities above 1/2 to all spins up for large enough systems [12].

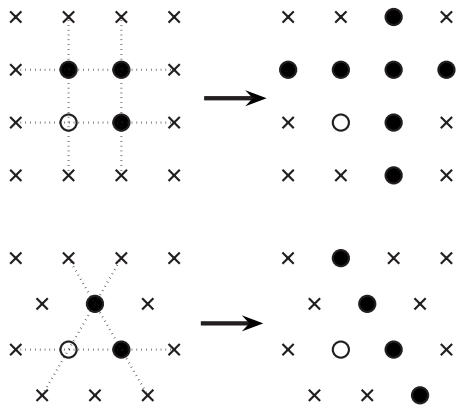

FIG. 2. Galam's dynamical rules of SM on the square (upper panel) and triangular (bottom) lattice. The one-dimensional rule is applied to each of the four (on the square lattice) or three (on the triangular lattice) chains of four spins each, centered about the elementary cell.

Galam (see Stauffer [12]) showed that the updating rule of the one-dimensional SM can be transformed exactly into two dimensions in the following way (see Fig. 2): The one-dimensional rule is applied to each of the four chains of four spins each, centered about two horizontal and two vertical pairs.

In Ref. [13] we compared two rules in which a panel of four spins influenced eight nearest neighbors, i.e., Galam [Galam dynamics (GD)] and the first of Stauffer *et al.* rules [Stauffer *et al.* dynamics (SD)] on the square lattice. This comparison seems to be quite important, since Stauffer *et al.* generalization is more attractive from a social point of view, while the Galam rule is much easier for generalization to other systems (in particular, it was used in the so-called TC model [23,24]). No qualitative difference has been found between these two dynamics.

Here we propose further simplification of the GD—the one-dimensional rule is applied not to each but only one randomly selected chain of four spins (see Fig. 3). The one invented by one of us (G.K.) and introduced here is the dynamics we call KD.

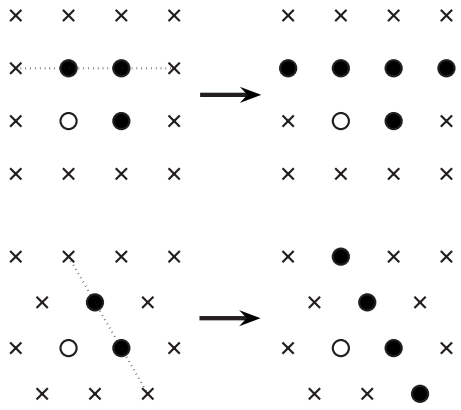

FIG. 3. *K* dynamics of SM on the square and triangular lattice. The one-dimensional rule is applied to only one, randomly selected chain of four spins, centered about elementary cell.

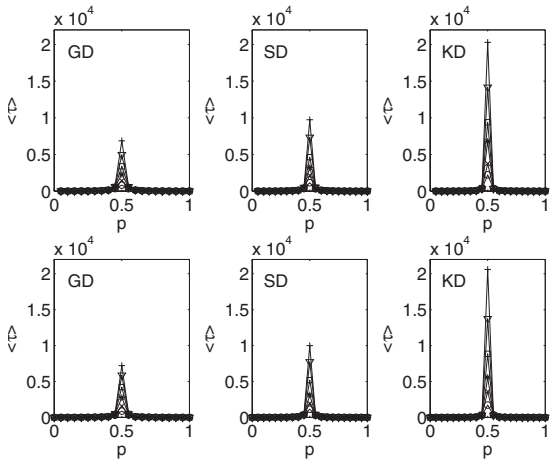

FIG. 4. Comparison of mean relaxation times under three rules (SD, GD, and KD) from a random initial state consisting of p up-spins for two types of two-dimensional lattices—square (upper panel) and triangular (bottom). In each plot results for several lattice sizes, from $L=50$ (◯) to $L=100$ (+), are presented. It is clearly seen that KD for $p=0.5$ is the slowest dynamics on both lattices. Results are averaged over 10^3 samples.

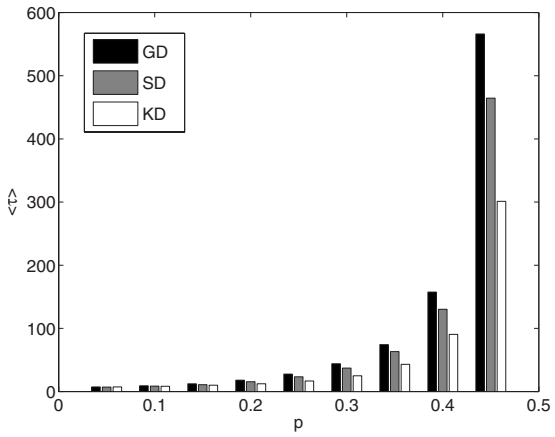

FIG. 5. Comparison of mean relaxation times under three rules (SD, GD, and KD) from a random initial state consisting of $p<0.5$ up-spins for a two-dimensional triangular lattice of 10^4 nodes. It can be seen that KD for $p<0.5$ is the fastest dynamics among all three dynamics. The same result was obtained also for the square lattice. All results are averaged over 10^3 samples.

We compare all three dynamics (SD, GD, and KD) on the square and triangular lattices. As in the previous paper [13] we measure the mean relaxation time from an initial state consisting of p up-spins. However, in this paper we consider not only random initial configuration but also two types of ordered initial conditions.

III. RELAXATION TIME FROM RANDOM INITIAL CONDITIONS

We have measured the mean relaxation time from a random initial state consisting of p up-spins for all three types of the outflow dynamics on the square and triangular lattices $L\times L$ using Monte Carlo simulations (we adopted here periodic boundary conditions). We have averaged the relaxation time over 10^3 samples. It should be noticed that in SD (Fig. 1) and GD (Fig. 2) $f_{\max}=8$ spins (on the square lattice) and $f_{\max}=6$ spins (on the triangular lattice) can be changed at maximum in elementary time step, while only two spins can be changed within KD (on both lattices), i.e., $f_{\max}=2$ (see Fig. 3). To compare relaxation times properly we have divided them by $f_{\max}$.

We have found the phase transition for all dynamics—for $p<0.5$ the "all spins up" state is never reached, while for $p>0.5$ this state is obtained with probability 1 (the same result was obtained previously in Ref. [12,13] on the square lattice). Moreover, critical slowing down is observed at $p=0.5$ (see Fig. 4). For $L\to\infty$ we expect the $\delta(0.5)$ function.

It is seen (Fig. 4) that for $p=0.5$, i.e., in the critical point, GD is the fastest dynamics on both lattices, while KD is definitely the slowest one:

$$\tau_{\mathrm{GD}}(0.5) < \tau_{\mathrm{SD}}(0.5) < \tau_{\mathrm{KD}}(0.5). \tag{2}$$

However from Fig. 4 this is not visible if the relation (4) is valid also outside the critical point. If we look at Fig. 5 we see that for $p<0.5$ the situation is completely reversed and, in general,

$$\tau_{\mathrm{GD}}(p\neq 0.5) > \tau_{\mathrm{SD}}(p\neq 0.5) > \tau_{\mathrm{KD}}(p\neq 0.5). \tag{3}$$

We should now address a very intriguing question—why is the dynamics which is the slowest in the critical point the fastest outside this point and vice versa? Is it connected somehow to a spatial structure which is created for a different initial concentration p of up-spins? It can be observed that for $p<0.5$ a concentration $c(t)$ of up-spins decreases very fast and after a short time (50–200 MCS) small compact clusters of up-spins are created (Fig. 6). On the contrary, for $p=0.5$ initially concentration of up-spins does not change significantly and only fluctuates around $c(0)=p$ but the system orders and after a short time (50–200 MCS) a large cluster of up-spins is created (Fig. 6)

To check this hypothesis, in the next two sections (i.e., in Secs. IV and V) we investigate the evolution of the system under three outflow dynamics from the following two types of ordered initial conditions. (1) "Stripes:" Initially, the system is divided by the straight border into two horizontal

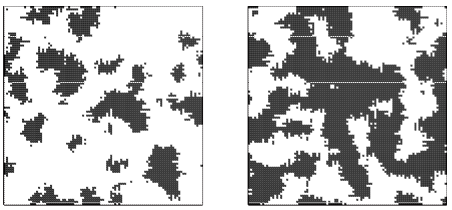

FIG. 6. Configurations of the system under outflow dynamics (type KD) after 200 MCS from a random initial state consisting of $p=0.45$ (left panel, present density of up-spins is 0.2513) and $p=0.5$ (right panel, present density of up-spins is 0.5225) up-spins for a two-dimensional square lattice of 10^4 nodes. The same results are observed for all three dynamics.

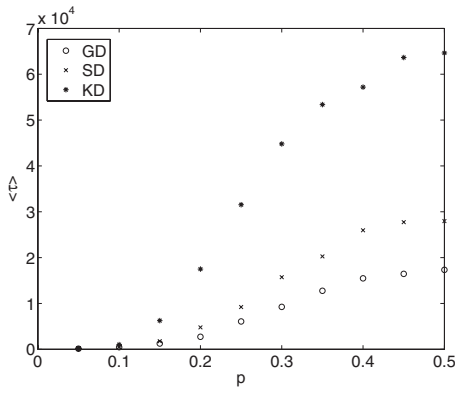

FIG. 7. Mean relaxation times under three rules (SD, GD, and KD) for a two-dimensional $L\times L$ square lattice ($L=100$, i.e., 10^4 nodes). Initially the system is divided by the straight border into two horizontal stripes: pL-width stripe of up-spins and $(1-p)L$-width stripe of down-spins. Results are averaged over 10^3 samples.

stripes—pL-width stripe of up-spins and $(1-p)L$-width stripe of down-spins, i.e., p is again the initial density of up-spins. (2) "Circle:" Initially, a single compact round cluster of up-spins in the middle of the lattice consists of down-spins; p is again the initial density of up-spins.

IV. RELAXATION TIME FROM "STRIPES"

In this section we investigate the relaxation of the system under three types of outflow dynamics from the ordered initial conditions which we call "stripes"—initially the system is divided by the straight border into two horizontal stripes: pL-width stripe of up-spins and $(1-p)L$-width stripe of down-spins, i.e., p is again the initial density of up-spins. For "stripes" no phase transition is observed. Moreover, relaxation under GD is the fastest, while under KD it is the slowest among all three dynamics for all values of initial density of up-spins p (Fig. 7). The same result was obtained for random initial conditions with $p=0.5$, i.e., in the critical point (Fig. 4):

$$\tau_{\mathrm{GD}} < \tau_{\mathrm{SD}} < \tau_{\mathrm{KD}}. \tag{4}$$

As we have seen in the previous section for random initial conditions and $p=0.5$ after a short time a large cluster of up-spins is created (Fig. 6) for all three dynamics. Here we can see that large clusters (stripes) are most unstable under GD and most stable under KD. These results may explain why relaxation from random initial conditions for $p=0.5$ is fastest under GD and slowest under KD.

The second interesting result connected with the relaxation from "stripes" is the lack of the phase transition. However, this could be understood looking at the evolution of the system's configuration. In Fig. 8 snapshots of the sample relaxation under SD on a two-dimensional square lattice is presented. It is seen that relaxation from "stripes" is quasi-one-dimensional in a sense that the structure of the stripes is conserved, although the border between them is no longer straight but rough. Evolution consists of movement of the

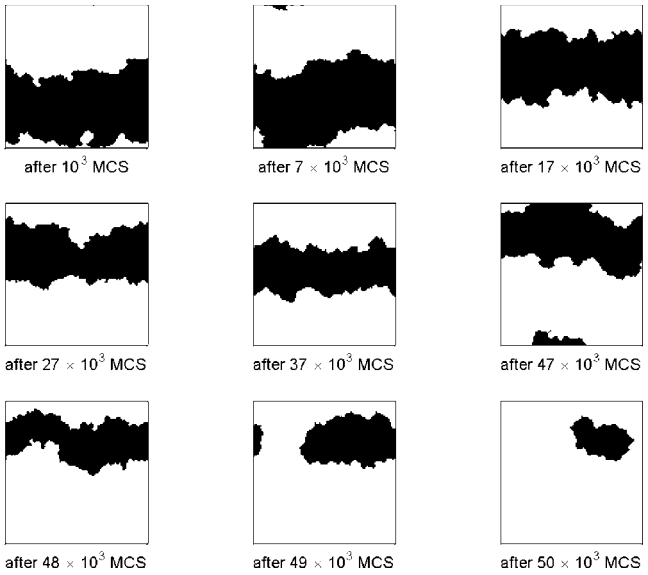

FIG. 8. Snapshots of the sample relaxation under SD on a two-dimensional $L\times L$ square lattice ($L=100$, i.e., 10^4 nodes). Initially the system is divided by the straight border into two equal horizontal stripes. Here $p=0.5$.

stripes, roughening the border between them and changing the width of the stripes. Eventually, one of the stripes breaks at one point to form a simply connected cluster and from this moment the evolution leads the system very fast to the final state with all spins in the same state. The same scenario was observed for all three dynamics and for all values of p. It should be mentioned here that "stripes" configuration is the steady state of zero-temperature Glauber dynamics. Several years ago the following question was raised by Spirin *et al.* [28,29]: "*What happens when an Ising ferromagnet, with spins endowed with Glauber dynamics, is suddenly cooled from a high temperature to zero temperature?*" The first expectation was that the system should eventually reach the ground state. However, this is true only for a one-dimensional system. On the square lattice there exist many metastable states that consist of alternating vertical (or horizontal) stripes of widths ≥ 2. These arise because a straight boundary between up and down phases is stable in zero-temperature Glauber dynamics. As we see this is not the case of the outflow dynamics under which the system eventually always reaches the ground state. This result is certainly also a contribution to the discussion about differences between inflow (zero-temperature Glauber) and outflow dynamics (see [21] and references therein).

Thus the lack of the phase transition from "stripes" can probably be explained by the absence of the phase transition in one-dimensional outflow dynamics described by the formula (1) (see also [21]). In Fig. 9 the mean relaxation times from a random initial state consisting of p up-spins for outflow dynamics in one dimension with $W_0=0$ is presented for several lattice sizes. The case of W_0 is consistent with definitions of our two-dimensional dynamics, i.e., under one-dimensional outflow dynamics the pair of neighboring spins S_i and S_{i+1} is chosen and if $S_iS_{i+1}=1$ then the two nearest neighbors of the pair follow its direction. It is seen that no

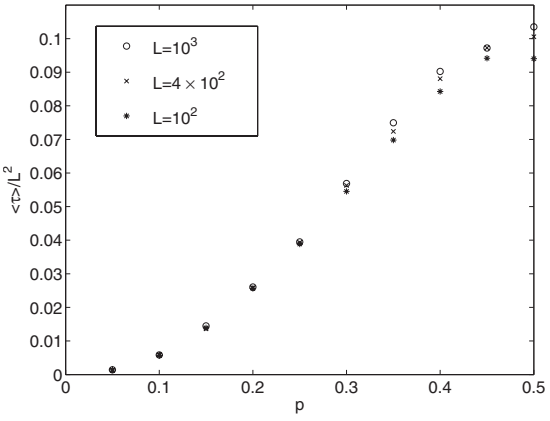

FIG. 9. Mean relaxation times from a random initial state consisting of p up-spins for outflow dynamics in one dimension are presented for several lattice sizes. Under one-dimensional outflow dynamics the pair of neighboring spins S_i and S_{i+1} is chosen and if $S_iS_{i+1}=1$, then the two nearest neighbors of the pair follow its direction. It is clearly visible that in this case the mean relaxation time scales with the lattice size as $\sim L^2$ analogous to the voter model [1–3]. The results presented on the plot are averaged over 10^4 samples.

phase transition is observed. Moreover, the mean relaxation time τ perfectly scales with the size of the system L as $\tau \sim L^2$ for all p. The same scaling law has been obtained already for other one-dimensional consensus dynamics like zero-temperature Glauber dynamics or voter model and can be calculated analytically [1–3].

The similarity between relaxation under one-dimensional dynamics and relaxation under outflow dynamics from "stripes" in two dimensions suggests the existence of a similar scaling law between the mean relaxation time $\langle\tau\rangle$ and the size $N=L\times L$ of the system also in two dimensions. The mean relaxation times from "stripes" consisting of p up-spins for several lattice sizes are presented in Fig. 10. It was obtained that the relaxation time can be scaled with the system's size for all three dynamics with the same scaling exponent $\tau\sim L^a$, $a\approx 3.5$ (see Fig. 10).

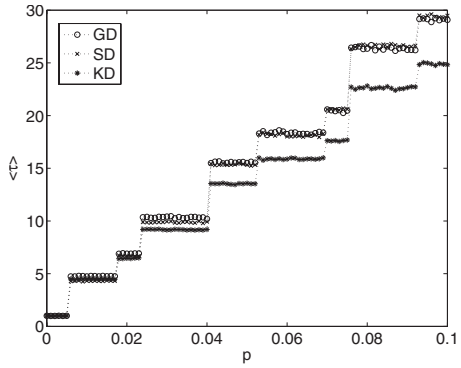

FIG. 11. Mean relaxation times under three rules (SD, GD, and KD) for a small two-dimensional $L\times L$ triangular lattice ($L=25$, i.e., 625 nodes). Initially there is a single compact round cluster of up-spins of radius $R\approx L\sqrt{p/\pi}$ (the value of $p=0.1$ corresponds here to the radius $R=\sqrt{19}\approx 4.36$). The results are averaged over 10^3 samples.

V. RELAXATION TIME FROM "CIRCLE"

In this section we briefly present the results for the relaxation of the system under three types of outflow dynamics from the ordered initial conditions which we call "circle"—initially there is a single compact round cluster of up-spins in the middle of the lattice consisting of down-spins. As we have seen in Fig. 6 starting from random initial conditions the evolution after short times creates small compact isolated clusters. On the other hand, it was observed that for random initial conditions and $p\neq 0.5$ relaxation under KD is fastest, while under GD it is slowest among all three dynamics. Simulations from the "circle" type of initial conditions can help in understanding this relation [see Eq. (3)].

In Fig. 11 we present the mean relaxation times under three rules (SD, GD, and KD) for small two-dimensional $L\times L$ triangular lattice ($L=25$, i.e., 625 nodes) in the case of "circle" initial conditions consisting of pL^2 up-spins (i.e., p is again density of up-spins). It can be seen that in this case we have

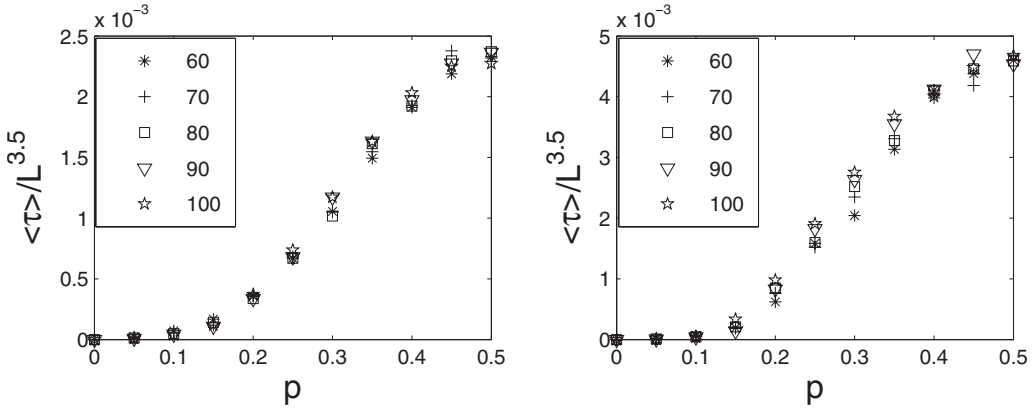

FIG. 10. Mean relaxation times for a two-dimensional $L\times L$ triangular lattice under SD (left panel) and KD (right panel). Initially the system is divided by the straight border into two horizontal stripes: pL-width stripe of up-spins and $(1-p)L$-width stripe of down-spins. In this case the relaxation time scales as $\sim L^{3.5}$ for all three dynamics. The results are averaged over 10^3 samples.

$$\tau_{KD} < \tau_{SD} \approx \tau_{GD}. \quad (5)$$

This behavior is similar to the case of random initial conditions with $p \neq 0.5$, where KD was also the fastest one.

This result shows that small round clusters are more stable under GD, contrary to infinite clusters (like stripes) which are most stable for KD. Summarizing results for random, "stripes," and "circle" initial conditions, we obtain the following:

$$\tau_{KD} > \tau_{SD} > \tau_{GD}$$

"stripes" for all p and random initial conditions for $p=0.5$,

$$\tau_{KD} < \tau_{SD} < \tau_{GD}$$

random initial conditions for $p=0.5$, and

$$\tau_{KD} < \tau_{SD} \approx \tau_{GD}$$

"circle" for p investigated.

VI. IS THE SCALING UNIVERSAL?

It has been found both analytically and numerically that dependence between the mean relaxation time τ and the size of the system L can be expressed by a simple scaling law $\tau \sim L^2$ in the case of a one-dimensional voter model [1–3]. The same scaling is valid also for relaxation in one dimension under zero-temperature Glauber (inflow) dynamics as well as outflow dynamics (see Fig. 9).

In two dimensions a situation is much more complicated. It was found that for a two-dimensional voter model from random initial conditions and $p=0.5$ the following scaling law is valid: $\tau \sim N \log N$ [1–3]. However, this scaling law is valid neither for two-dimensional inflow nor outflow dynamics. It was observed [27–31] that for the Ising ferromagnet with spins endowed with zero-temperature Glauber dynamics there exist many metastable states that consist of alternating vertical (or horizontal) stripes of widths ≥ 2. If we start from random initial conditions and let the system evolve under inflow dynamics, we eventually reach the final "stripes" configuration in 1/3 of the simulations [28]. Because a straight boundary between up and down phases is stable in zero-temperature Glauber dynamics we will never leave such a "stripe" state—for this reason the mean relaxation time is infinite. As we have seen in previous sections (Secs. III and IV), this is not the case for outflow dynamics under which the system eventually always reaches the ground state.

The question is whether the scaling law obtained for the two-dimensional voter model is valid in the case of outflow dynamics. Up till now we have found the scaling law for systems endowed with outflow dynamics initially ordered in "stripes" configuration (see Fig. 7). In this case the mean relaxation time τ scales with the system size $N=L\times L$ as $\tau \sim L^{3.5}$ for all three outflow dynamics both on the square and triangular lattice. However, this scaling is not valid in a case of random initial conditions. It occurs that for random initial conditions with the density p of up-spins we can find p-dependent scaling laws: $\tau \sim L^{a(p)}$ (see Fig. 12).

As we see for consensus dynamics with binary variables, scaling laws are universal in one dimension. It should be mentioned here that all these results have been obtained in the case of random sequential updating. It would be interesting for future work to check whether the same scaling is obtained for other types of updating such as, e.g., synchronous or c-synchronous updating [21].

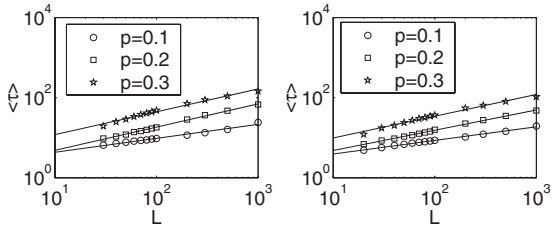

FIG. 12. Scaling of the mean relaxation time with the system size for the Stauffer *et al.* rule. Initial state consists of p randomly distributed up-spins for two types of two-dimensional $L\times L$ lattices—square (left panel) and triangular (right panel). Similar scaling is observed also for GD and KD. It is visible that the scaling exponent for random initial conditions is p-dependent. Results are averaged over 10^3 samples and the largest simulated lattice consists of $N=10^3\times 10^3=10^6$ nodes.

Contrary to one dimension, even within the outflow dynamics no single scaling law can be found in two dimensions—it depends strongly on the initial configuration of the system. However, a very intriguing result connected with scaling can be obtained if we look at the distribution of relaxation times instead of mean relaxation time alone.

VII. DISTRIBUTION OF RELAXATION TIMES

In the mean field approach [25] and in a one-dimensional system it has been found that the distribution of waiting times has an exponential tail with a p-independent exponent. Results for the square lattice for SD and GD were presented in Ref. [13]. Under both dynamics the distribution of relaxation times has an exponential tail, but the exponent is p-dependent. Interestingly, the dependence between the exponent and the initial number of up-spins is identical for both dynamics. It should be mentioned here that in Ref. [12] it was shown that for $p=0.5$ the distribution of relaxation times deviates from the log-normal distribution for SD. However, they plotted a histogram (i.e., an estimate of the probability distribution function) instead of the cumulative distribution function (CDF) and presented it in the log-log scale. In Ref. [13] to compare our results with the results obtained in Ref. [12] we calculated both the cumulative distribution function (in fact, the tail $1-\mathrm{CDF}$) and the histogram of relaxation times. It occurs that our results agree with those presented in Ref. [12]. Already in Ref. [13] the deviation from single exponential decay has been visible. However, for large relaxation times exponential decay for both the histogram and the cumulative distribution function tail was observed in agreement with the results obtained by Slanina and Lavicka for the complete graph [25] and with Schulze [26] who got an exponential decay on the square lattice by introducing both local and global interactions.

In this paper we will not present the histogram of the relaxation times. Instead we focus only on the tail of the

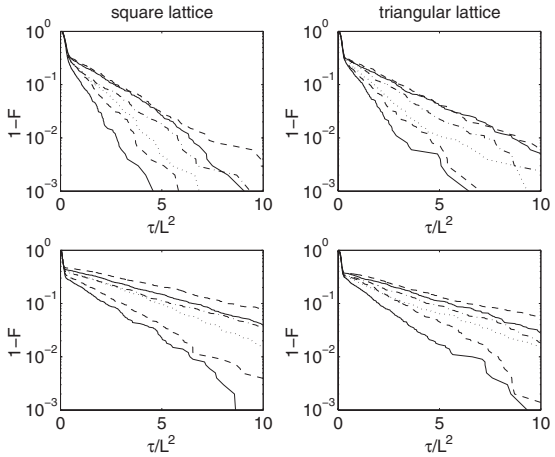

FIG. 13. Tail of the cumulative distribution function of the relaxation time $1-F$ (where F denotes CDF) vs τ/L^2 from a random initial state consisting of $p=0.5$ up-spins for SD (top panels) and KD (bottom panels) in a semilog scale are presented. The lattice size runs from $L=50$ (lowest curve) to $L=100$ (uppermost curve). Two regimes—short and long time—are visible for both dynamics in the case of square and triangular lattices. For the short time regime all curves collapse to a single line if we divide the relaxation time τ by the lattice size $N=L^2$. Analogous results are obtained for GD.

cumulative distribution function $1-\mathrm{CDF}$. We would like to explain here our choice and persuade that such a choice gives much more reliable results in estimating distributions. Usually, a histogram is used, because such a representation is much more intuitive. However, such a representation, contrary to CDF, is not one-valued because we are free to choose the number of intervals to which we divide all results. It can be seen very often that the same results look different just because of this not one-valued choice. Moreover, a statistics (i.e., number of results that are represented by one point) in a case of histogram is worse than in a case of CDF, which is clearly visible on plots—in a case of CDF the plot is much smoother. The last reason for which we choose CDF is the following: The histogram is only an estimation of the probability distribution function. For all these reasons we decided to focus on CDF.

In all three dynamics short and long time regimes are observed. These two time regimes are much more visible if we divide relaxation times by the lattice size (see Fig. 13), i.e., we plot the tail the cumulative distribution function of relaxation time $1-\mathrm{CDF}$ versus τ/L^2 instead of τ. Interestingly, results for the short time regime scale with the lattice size with a simple exponent 2. The same exponent is valid for all three dynamics on both square and triangular lattices. It should be mentioned here that for one-dimensional outflow (as well as inflow) dynamics curves for all lattice sizes collapse to a single line if we divide the relaxation time by L^2; this result agrees with the scaling of the mean relaxation time with lattice size $\tau \sim L^2$.

The result obtained from the distribution for the relaxation time is very intriguing and certainly needs deeper investigation which we leave for a future work.

VIII. CONCLUSIONS

In this paper we proposed a generalization of the one-dimensional outflow dynamics (KD). The rule was introduced as a simplification of Galam dynamics (GD) proposed in Ref. [12]. In a previous paper [13] we compared the relaxation from a random initial state consisting of p up-spins under two outflow dynamics on the square lattice [Stauffer *et al.* (SD) [12] and GD]. Here, similar to the previous paper, we have investigated the mean relaxation time from an initial state consisting of p up-spins. However, in this paper we simulated all three types of outflow dynamics, GD, SD, and KD, both on the square and triangular lattices. Moreover, we took into account several types of initial configuration—random, "stripes," and "circle."

Simulation results showed that the relaxations on both lattices (square and triangular) are identical for all three outflow dynamics contrary to results obtained for two-states cellular automaton [19] but in agreement with the results for outflow dynamics on various complex networks [15].

We have found the phase transition for all dynamics—for $p<0.5$ the "all spins up" state is never reached, while for $p>0.5$ this state is obtained with probability 1 (the same result was obtained previously in Refs. [12,13] on the square lattice). Interestingly, in the critical point, GD is the fastest dynamics and KD is definitely the slowest, while outside of the critical point the situation is reversed. We have addressed a very intriguing question—why is the dynamics which is the slowest one in the critical point the fastest one outside this point and vice versa? We connected this behavior with a spatial structure which is created for different initial concentrations p of up-spins—for $p<0.5$ small compact isolated clusters are created, while for $p=0.5$ an infinite cluster is occurring. Starting from two types of ordered states, we have shown that small round clusters are most stable under GD contrary to infinite clusters (like stripes) which are most stable for KD. Summarizing results for random, "stripes," and "circle" initial conditions, we have obtained the following:

$$\tau_{\mathrm{KD}} > \tau_{\mathrm{SD}} > \tau_{\mathrm{GD}}$$

"stripes" for all p and random initial conditions for $p=0.5$,

$$\tau_{\mathrm{KD}} < \tau_{\mathrm{SD}} < \tau_{\mathrm{GD}}$$

random initial conditions for $p=0.5$, and

$$\tau_{\mathrm{KD}} < \tau_{\mathrm{SD}} \approx \tau_{\mathrm{GD}}$$

"circle" for p investigated.

Another interesting result has been obtained while looking at the scaling laws. Both the analytic and numerical approaches in the case of the one-dimensional voter model [1–3] lead to the conclusion that dependence between the mean relaxation time τ and the size of the system Ł can be expressed by a simple scaling law $\tau \sim L^2$. The same scaling is also valid for relaxation in one dimension under zero-temperature Glauber (inflow) dynamics as well as outflow dynamics. On the contrary, for two dimensions even within the outflow dynamics no single scaling law can be found—it depends strongly on the initial configuration of the system.

Probably the most intriguing, yet still preliminary, result presented in this paper is connected with the distribution of relaxation times. For one-dimensional outflow (as well as inflow) dynamics curves for all lattice sizes collapse to a single line if we divide the relaxation time by L^2; this result agrees with the scaling of the mean relaxation time with lattice size $\tau \sim L^2$. In the case of a two-dimensional system in all three dynamics a short and a long time regime in the distribution of relaxation times are observed. These two time regimes are much more visible if we divide relaxation times by the lattice size, i.e., we plot the tail of the cumulative distribution function of relaxation time $1-\mathrm{CDF}$ versus τ/L^2 instead of τ. Interestingly, the results for the short time regime scale with the lattice size with the same simple exponent 2 as obtained for one-dimensional systems. These interesting results certainly require further investigation.

ACKNOWLEDGMENTS

K.S.-W. gratefully acknowledges the financial support of the Polish Ministry of Science and Higher Education through the scientific Grant No. N N202 0194 33.

[1] T. M. Liggett, *Stochastic Interacting Systems: Contact, Voter, and Exclusion Processes* (Springer-Verlag, New York, 1999).
[2] P. L. Krapivsky, Phys. Rev. A **45**, 1067 (1992).
[3] M. Mobilia, A. Petersen, and S. Redner, J. Stat. Mech.: Theory Exp. 2007, P08029.
[4] G. Deffuant, D. Neau, F. Amblard, and G. Weisbuch, Adv. Complex Syst. **3**, 87 (2000).
[5] R. Hegselmann and U. Krause, J. Artif. Soc. Soc. Simul. **5**(3), 2 (2002).
[6] P. L. Krapivsky and S. Redner, Phys. Rev. Lett. **90**, 238701 (2003).
[7] S. Galam, Physica A **336**, 56 (2004).
[8] D. Stauffer, Comput. Phys. Commun. **146**, 93 (2002).
[9] B. Schechter, New Sci. **175**, 42 (2002).
[10] S. Fortunato and D. Stauffer, in *Extreme Events in Nature and Society*, edited by S. Albeverio, V. Jentsch, and H. Kantz (Springer, Berlin, Heidelberg, 2005).
[11] K. Sznajd-Weron, Acta Phys. Pol. B **36**, 2537 (2005).
[12] D. Stauffer, A. O. Sousa, and M. De Oliveira, Int. J. Mod. Phys. C **11**, 1239 (2000).
[13] S. Krupa and K. Sznajd-Weron, Int. J. Mod. Phys. C **16**, 1771 (2005).
[14] I. Chang, Int. J. Mod. Phys. C **12**, 1509 (2001).
[15] A. O. Sousa and J. R. Sanchez, Physica A **361**, 319 (2006).
[16] M. C. Gonzalez, A. O. Sousa, and H. J. Herrmann, Int. J. Mod. Phys. C **15**, 45 (2004).
[17] A. O. Sousa, Physica A **348**, 701 (2005).
[18] Y. S. Tu, A. O. Sousa, L. J. Kong, and M. R. Liu, Int. J. Mod. Phys. C **16**, 1149 (2005).
[19] A. S. Ribeiro and P. G. Lind, Phys. Scr. **T118**, 165 (2005).
[20] P. G. Lind, J. A. C. Gallas, and H. J. Herrmann, Phys. Rev. E **70**, 056207 (2004).
[21] K. Sznajd-Weron and S. Krupa, Phys. Rev. E **74**, 031109 (2006).
[22] K. Sznajd-Weron and J. Sznajd, Int. J. Mod. Phys. C **11**, 1157 (2000).
[23] K. Sznajd-Weron, Phys. Rev. E **70**, 037104 (2004).
[24] R. J. Glauber, J. Math. Phys. **4**, 294 (1963).
[25] F. Slanina and H. Lavicka, Eur. Phys. J. B **35**, 279 (2003).
[26] C. Schulze, Int. J. Mod. Phys. C **15**, 867 (2004).
[27] S. Redner and P. L. Krapivsky, J. Phys. A **31**, 9229 (1998).
[28] V. Spirin, P. L. Krapivsky, and S. Redner, Phys. Rev. E **63**, 036118 (2001).
[29] V. Spirin, P. L. Krapivsky, and S. Redner, Phys. Rev. E **65**, 016119 (2001).
[30] A. Lipowski, Physica A **268**, 6 (1999).
[31] D. Stauffer and P.M.C. de Oliveira, Eur. Phys. J. B **30**, 587 (2002).

Percolation framework in Ising-spin relaxation

Grzegorz Kondrat and Katarzyna Sznajd-Weron*
Institute of Theoretical Physics, University of Wrocław, Maxa Borna 9, 50-204 Wrocław, Poland
(Received 13 July 2008; published 21 January 2009)

We introduce a framework based on the percolation idea to investigate the relaxation under zero-temperature Glauber and outflow dynamics on $L\times L$ square and triangular lattices. This helps us to understand the appearance of a double time regime in the survival probability. We show that the first, short-time, regime corresponds to relaxation through droplets and the second, long-time, regime corresponds to relaxation through stripes. For both dynamics the probability that the system becomes ordered through droplets (which indicates fast relaxation) is about 2/3.

DOI: 10.1103/PhysRevE.79.011119 PACS number(s): 05.50.+q

Systems quenched from a disordered into an ordered phase (such as the Ising model quenched from initial temperature $T_0=\infty$ to final $T_F=0$) in the thermodynamic limit never reach the final ferromagnetic steady state. This is one of the reasons why the theory of phase ordering kinetics has remained a challenge for more than four decades (for a review, read [1]). Moreover, Spirin *et al.* [2] showed that even a simple two-dimensional Ising ferromagnet has a large number of metastable states with respect to zero-temperature Glauber dynamics [3] and, therefore, at zero temperature the system could get stuck forever in one of the metastable states that consists of alternating vertical or horizontal stripes—from now on we call it the stripe configuration (S). This is understood on the basis of the definition of zero-temperature Glauber dynamics, which involves picking a spin at random and flipping it according to the direction of a majority of its nearest neighbors. If there is no majority, the spin is flipped with probability 1/2. Thus a straight interface does not evolve. A slight difference between square and triangular lattices in the probability $P_{\mathrm{str}}(\infty)$ that the system eventually reaches a stripe state was found in [4]: $P_{\mathrm{str}}(\infty)=0.315$ and 0.344 on the square and triangular lattices, respectively. Moreover, in the case of the square lattice in about 0.04 of all simulations a diagonal stripe (DS) configuration appears [2].

Very interesting behavior is exhibited by the survival probability $S(t)$ that the system has not yet reached its final state by time t. On a semilogarithmic plot $S(t)$ lies on a straight line with a large negative slope and then crosses over to another line with smaller negative slope [2]. Recently, similar behavior of $S(t)$ was observed for Ising spins under outflow dynamics [5], which originally was introduced to describe opinion change in a society [6].

A number of social experiments have shown that, when faced with a strong group consensus, people often conform even if they believe that the group may be in error. However, even a single visible dissenter from the group's position emboldens others to resist conformity [7]. This observation was recently expressed in a simple one-dimensional "united we stand, divided we fall" model of opinion formation [6]. The model was later renamed the Sznajd model by Stauffer *et al.* [8] and generalized to a two-dimensional square lattice. In its two-dimensional version the model has found a number of social applications (for reviews, see [9–13]), but in this paper we investigate it from the theoretical point of view. The crucial difference between the Sznajd model and zero-temperature Glauber dynamics [3] is that information flows outward from the center nodes to the surrounding neighborhood and not the other way around—hence the name outflow dynamics. It should be mentioned that, although one-dimensional outflow dynamics obeys detailed balance, no finite-temperature version of the outflow rule has been proposed up till now. It seems that the temperature cannot be introduced into our dynamics without breaking the detailed balance condition, but further studies concerning this issue are definitely needed. Moreover, in contrast to Glauber dynamics, generalization of the one-dimensional rule to higher dimensions is neither straightforward nor unambiguous. Several types of two-dimensional outflow dynamics have been already introduced [5,8,9], and recently three of them have been investigated from the theoretical point of view [5]. For all three investigated outflow dynamics, a short- and a long-time regime have been observed. The short-time regime (fast relaxation) was observed for about 2/3 of all trials [5].

In this paper, we introduce a framework based on the percolation idea to investigate the evolution of the configuration under zero-temperature Glauber and outflow dynamics on two-dimensional square and triangular lattices (suggestions that percolation phenomena can influence zero-temperature dynamics have appeared already in [14]). This helps us to understand the appearance of two time regimes in the survival probability $S(t)$. We focus here only on one type of outflow dynamics defined below, but the same results could be obtained for other types of two-dimensional outflow dynamics investigated in [5]. Let us begin with the definition of the dynamics. The system consists of $L\times L$ Ising spins $S_i=\pm 1$ $(i=1,\ldots,L^2)$ placed on a two-dimensional lattice with periodic boundary conditions. In the case of the square lattice, in each update a 2×2 panel of four neighbors is selected randomly. If all four spins in a panel are parallel then the panel flips its eight nearest neighbors to the unanimous direction of the four spins in the panel. In other cases, these eight neighbors are left unchanged. Similarly we define the dynamics on a triangular lattice (for details see [5]). Under outflow dynamics the system eventually always reaches a ferromagnetic steady state, in contrast to zero-temperature Glauber dynamics. For this reason outflow dynamics is sim-

*kweron@ift.uni.wroc.pl; http://www.ift.uni.wroc.pl/~kweron

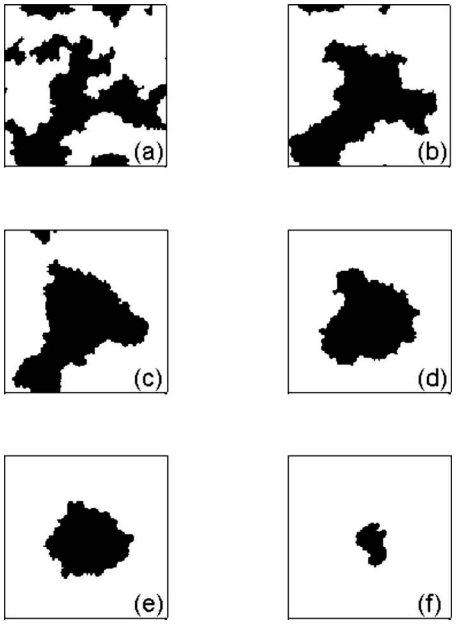

FIG. 1. Snapshots of the sample relaxation under outflow dynamics on a two-dimensional 100×100 square lattice from a random initial state consisting of 50% up spins after (a) 100, (b) 300, (c) 400, (d) 1000, (e) 1500, and (f) 2300 Monte Carlo steps (MCS). In this trial, after a relatively short time (about 300 MCS) a simply connected cluster (droplet) is formed.

pler to analyze and the percolation framework is easier to understand.

Let us begin with presenting two sample relaxations under our outflow dynamics on a 100×100 square lattice (see Figs. 1 and 2). Initially, the system consists of randomly distributed equal numbers of up (50%) and down (50%) spins. After a relatively short time in each relaxation only one of two types of configurations is created—droplets (Fig. 1) or stripes (Fig. 2). In the stripe configuration one of the stripes eventually breaks at one point to form a droplet and from this moment the evolution of the system leads very quickly to the ferromagnetic steady state. This observation led us to the following postulate: A system quenched from a disordered to an ordered phase evolves through droplets (fast relaxation) or stripes (slow relaxation). The first, short-time, regime in the survival probability $S(t)$ corresponds to relaxation through droplets, and the second, long-time, regime to relaxation through stripes. We expect that the above postulate is valid not only in the case of outflow but also zero-temperature Glauber dynamics. To confirm this postulate we introduce now a framework based on the percolation idea.

In the following the quantity of central interest will be the connectivity of clusters of given spins (up or down) in a specified direction (top to bottom or left to right). We say that the connectivity is nonzero (1) in a given direction (e.g., left-right) if two opposite edges of the system (left and right) can be connected via a continuous path composed of the given spins [e.g., for spins up we denote the left-right connectivity as $P_{\mathrm{LR}}(\uparrow)=1$ and so on]. For one type of spins there are four distinct possibilities of overall connectivity: zero in both directions (00), nonzero in one direction (01 or 10), and nonzero in both (11). As we deal with two types of spins,

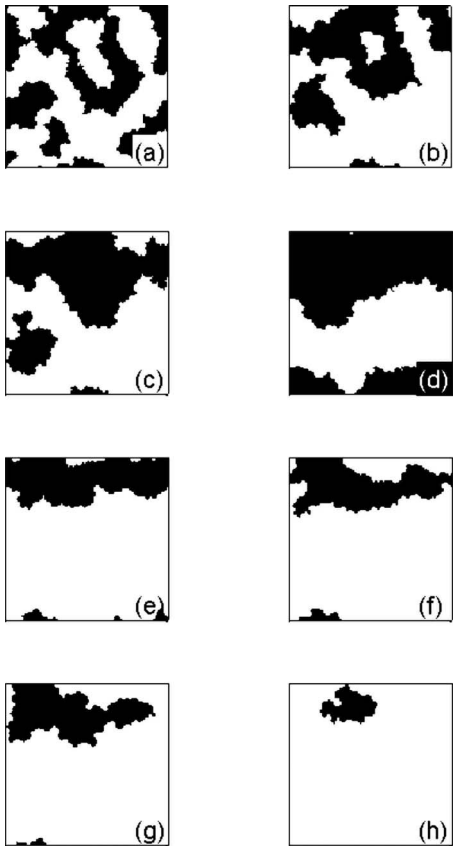

FIG. 2. Snapshots of the sample relaxation under outflow dynamics on a two-dimensional 100×100 square lattice from a random initial state consisting of 50% up spins after (a) 100, (b) 300, (c) 500, (d) 5000, (e) 14 000, (f) 15 000, (g) 15 100, and (h) 16 000 Monte Carlo steps (MCS). In this trial after a relatively short time (about 1000 MCS) the stripe configuration is formed. Eventually, one of the stripes breaks at one point to form a simply connected cluster, and from this moment the evolution of the system leads very quickly to the final state with all spins in the same state.

there are (at least in principle) 16 various combinations of connectivity possible. In the hard wall boundary conditions some configurations are forbidden, e.g., up spins connected vertically while down spins are connected horizontally. With periodic boundary conditions, however, all possibilities are valid; see Fig. 3 for a short review. Some configurations [the first four—the chessboard, stripes (horizontal or vertical) on chessboard, and odd configurations] are so exceptional that we have never observed them in real simulations. The main idea of the percolation framework analysis of system dynamics consists in counting how much time the system spends in each configuration in its history from the random initial state toward the steady final state. In order to obtain information in as clear and compact way as possible, for each simulation sample, we provide four cumulative times spent by the system in the following configurations: droplet (D), stripes (S), diagonal stripes (DS), and transient (T). The diagonal stripes configuration is generally defined as having full connectivity in both directions (horizontal and vertical) for both spin orientations (up and down): [11-11]—see Fig. 3. Its name comes from the simplest example of this configuration in the

TYPE	$[P_{TB}(\uparrow)\ P_{LR}(\uparrow) - P_{TB}(\downarrow)\ P_{LR}(\downarrow)]$	SAMPLE
chessboard	[0 0 – 0 0]	
stripes on chessboard (horizontal)	[0 1 – 0 0] [0 0 – 0 1]	
stripes on chessboard (vertical)	[1 0 – 0 0] [0 0 – 1 0]	
odd	[0 1 – 1 0] [1 0 – 0 1]	
(a)		
droplet (D)	[1 1 – 0 0] [0 0 – 1 1]	
stripes (S) (horizontal)	[0 1 – 0 1]	
stripes (S) (vertical)	[1 0 – 1 0]	
transient state (T)	[0 1 – 1 1] [1 1 – 0 1]	
transient state (T)	[1 0 – 1 1] [1 1 – 1 0]	
diagonal stripes (DS)	[1 1 – 1 1]	
(b)		

FIG. 3. All possible configurations with respect to connectivity of up and down spins on a lattice with periodic boundary conditions. In the middle column a digit 1 appearing at a given position indicates the connectivity of spins up or down in the vertical (TB) or horizontal (LR) direction. The first four types, although theoretically possible, do not appear in real simulations.

shape of alternating stripes angled at 45° to the horizontal. Here the periodicity of the boundary conditions is crucial, otherwise there is no possibility of connectivity in both directions for both spin components. The last configuration's name (T) comes from the fact that these states do not last long and are possibly a by-product of a transition between more stable configurations. In order to speed up the simulations, we decided to make a check of the configuration type not continuously, but at certain times. We verified that our choice of checking time interval (=1 MCS) did not affect the quality of the results.

Application of the percolation framework analysis to our outflow dynamics helps in understanding the shape of the survival probability obtained in previous work [5]. The data confirm our postulate of either fast evolution through droplets or slow evolution through stripes. The times spent by the system in various configurations are presented in Fig. 4 for our outflow dynamics on a periodic square lattice of size $L=100$. There are shown data collected from $N=1000$ simulations. For each simulation the relaxation time is the abscissa of the symbols. For each configuration type appearing (D, S, DS, T) its cumulative time is the ordinate. Thus for each simulation there are four points at the same abscissa value,

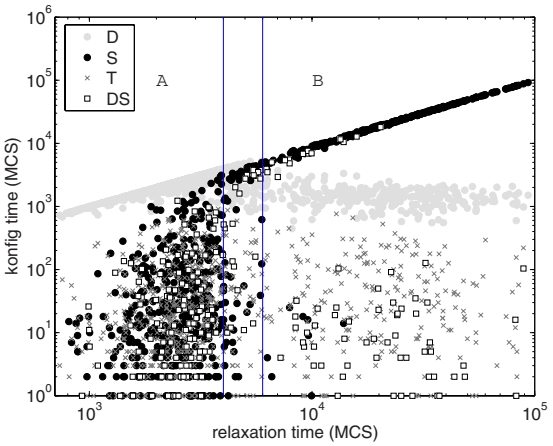

FIG. 4. (Color online) Relaxation under outflow dynamics on two-dimensional 100×100 square lattice from random initial state consisting of 50% up spins; the data from $N=10^3$ simulation are presented. Symbols show how much time the system spends in given configuration type before reaching the final state. For short relaxation times ($\tau<4\times10^3$ MCS) the evolution goes mostly through the droplet state (D), while for longer relaxation times nearly 100% of the time is spent in the stripe configuration (S) [occasionally in the diagonal stripe (DS) configuration]. The crossover time (here approximately 4×10^3 MCS) coincides with the time where the change of slope appears in the survival probability [5].

representing the contributions of particular configuration types to the total relaxation time. For example, let us consider a simulation having relaxation time 10 000 MCS. Let us assume that during the evolution toward its final state the system spent 2000 MCS in D configurations, 7950 MCS in S configurations, 45 MCS in T configurations, and 5 MCS in DS configurations. Thus resulting from this particular simulation there appear four points on the plot having the following coordinates: (10 000, 2000), (10 000, 7950), (10 000, 45), and (10 000, 5). The proximity of a symbol to the line $y=x$ indicates that the system dwells in the corresponding configuration most of the time until relaxation. The log-log setting of the plot makes it possible to bring out more details interesting for further analysis. Let us assume that a particular configuration type (say X) dominated the system history until the final state in all simulations with relaxation times from some interval. Thus one would see that symbols corresponding to this configuration type X would group high in the plot along the line $y=x$ (or very close to this line) on the mentioned interval. The other, much rarer configuration types would be found as symbols at the bottom of the same plot. On the other hand if there was a case of equally long-lasting configuration types (say, each types D, S, T, and DS took 25% of the relaxation time), the points would all lie well below the line $y=x$ (this is not the case in the considered set of data, however). There is yet another possibility—in different simulations of given relaxation times various configuration types dominate. In such a case it could be seen on the plot that the different symbols approach the line $y=x$ (in our case we have there a transition region; see further in the text).

All simulations considered in Fig. 4 naturally split into

two sets—one ($\mathcal{A}$), for which the droplet configuration dominates (this is the case for all simulations with relaxation time smaller than 4×10^3 MCS) and the second ($\mathcal{B}$), where the system spends most of the time in the stripe configuration (here belong all simulations with relaxation times greater than 6×10^3 MCS). To the latter also belong the rare simulations for which long-lived diagonal stripes are observed. There is also a third, transition region (relaxation times between 4×10^3 and 6×10^3 MCS) consisting of simulations for which the dominant configuration type is not unique. Then there is a considerable probability of finding simulations with various dominant configuration types.

In the set $\mathcal{A}$ (short relaxation times) we attribute different values of the droplet dwelling time to different sizes of the droplet arising from the random initial state (for bigger droplets the relaxation time is longer [5]). The dynamics of the samples from the set $\mathcal{B}$ is different: most of the time the system spends in the stripe configuration, after which the stripe breaks and the resulting droplet evolves according to the previous scenario (pertaining to the set $\mathcal{A}$). In this case the droplet part of the total time remains at the same level (about 1.5×10^3 MCS on Fig. 4); this is because the droplet arising from breaking the stripe has more or less the same size (of order of half the size of the system). In the case of the stripes their dwelling time has a much broader distribution, resulting not only from the differences in width of the stripes that arise from the random initial state, but mainly from behavior similar to a Brownian random walk. For the stripe configuration the rather straight interface between clusters of spins with different orientations has equal chance to move in either direction (for the droplet the direction of the interface movement is always toward its center). The characteristic time limiting from above the set $\mathcal{A}$ (here about 4×10^3 MCS) coincides exactly with the time of change in the slope of the survival probability [5]. These two regimes of exponential dependence correspond to evolution through either the droplet or stripe configuration (the former are interestingly always about 2/3 of all cases).

From the above analysis there appears the following scenario for the dynamics of the system. At the first stage, when the system starts its evolution from a totally random state with 50% spins up and 50% spins down (i.e., quenched from infinite temperature) small clusters tend to either grow or disappear and the characteristic length in the system (the mean width of the clusters) approaches the system size. The interface between clusters of opposite spins gets smoother and smoother. At a certain (rather short) time the state of the system belongs to either the droplet, stripe, or diagonal stripe configuration. In the first case (D) it is known [5] that the droplet relaxes to the final steady state relatively fast via shrinking (it has been proved already that every smooth closed curve in the plane asymptotically approaches a shrinking circular shape [15,16]). In the case when the system in the first stage is in the stripe configuration, the evolution is much slower (stripes at some points get thicker, at others get thinner). One of the stripes eventually narrows to make a break, the cluster becomes simply connected, and the configuration switches to a droplet. The only configuration not discussed yet—the transient one (T)—appears for short periods and only either at the beginning of the simulations

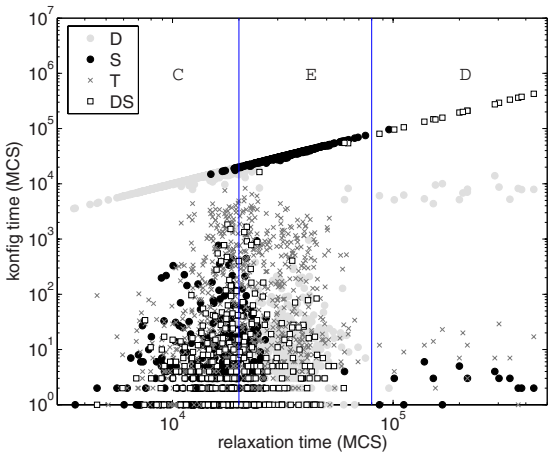

FIG. 5. (Color online) Relaxation under Glauber (inflow) dynamics on two-dimensional 100×100 square lattice from a random initial state consisting of 50% up spins; the data from $N=10^3$ simulation are presented. Symbols show how much time the system spends in a given configuration type before reaching the final state. For short relaxation times ($\tau<2\times10^4$ MCS) the evolution goes mostly through the droplet state (D). For much longer relaxation times ($>8\times10^4$ MCS) nearly 100% of the time is spent in the diagonal stripe configuration (DS). For intermediate relaxation times the stripe configuration (S) dominates. The crossover time (here approximately 2×10^4 MCS) coincides with the time where the change of slope appears in the survival probability [5].

(when the system "decides" whether to go through the stripe configuration or directly through the droplet configuration) or at switching times, when the system changes its configuration (e.g., DS$\rightarrow D$). Our extensive simulations proved that all above statements remain valid for outflow dynamics on a triangular lattice as well.

In the case of Glauber dynamics the overall dynamics characteristic is somewhat similar, but a bit more complicated. This is because in this dynamics the regular stripe configuration (with straight line interfaces) is the final one (in contrast to the outflow dynamics, where it always decays to the ferromagnetic state with all spins parallel). In Fig. 5 there are presented data for Glauber dynamics simulations, but here the relaxation time is measured until the system reaches any of its final states (including regular stripes). There is a natural partition into three sets of simulations: set $\mathcal{C}$ with evolution mostly through droplets (it corresponds to the set $\mathcal{A}$ of the previous dynamics), set $\mathcal{D}$ with the evolution leading mostly through diagonal stripes (somewhat similar to the set $\mathcal{B}$), and set $\mathcal{E}$ of samples leading to the final regular stripe configuration, characterized by the absolute majority of stripe configurations.

Cases from the set $\mathcal{C}$ correspond exactly to the previously described set $\mathcal{A}$ of outflow dynamics. The only difference between the set $\mathcal{D}$ and the previously considered set $\mathcal{B}$ is that in the set for Glauber dynamics there is evolution only through diagonal stripes, since the horizontal and vertical stripes no longer decay to the ferromagnetic state and they form the new set $\mathcal{E}$. Depending whether the system decides at an early stage to evolve through the droplet configuration, stripes, or diagonal stripes, we got the shortest, moderate,

and longest relaxation times, respectively. In the plot of survival probability of Ref. [2] the change of the slope coincides with the largest time in the set $\mathcal{C}$ (here 2×10^4 MCS). The relative size of the set $\mathcal{C}$ (the probability that the system chooses the droplet configuration) is here also $2/3$, as it was in the case of outflow dynamics. This universal constant for outflow dynamics [5] and for Glauber dynamics on a square lattice as well as on a triangular one (we checked that Glauber dynamics on a triangular lattice also conforms with the previous conclusions for a square lattice) must have some simple explanation, but unfortunately it needs further investigations. One can suppose that this property is of a fundamental nature for the broader class of zero-temperature dynamics considered in the literature [17,18].

We believe that the percolation framework we proposed in this paper could be used to study relaxation not only in the case of zero-temperature Ising-spin dynamics, but also in a much broader class of coarsening systems. Our method gives deeper insight into the relaxing system than the survival probability. It cannot describe configurations in detail, as was done, for example, in [19]. On the other hand, it gives general information on the system structure during relaxation, which may help to find some universal features of the dynamics investigated.

K.S.-W. gratefully acknowledges the financial support of the Polish Ministery of Science and Higher Education through the Scientific Grant No. N N202 0194 33.

[1] A. J. Bray, Adv. Phys. **43**, 357 (1994).
[2] V. Spirin, P. L. Krapivsky, and S. Redner, Phys. Rev. E **63**, 036118 (2001).
[3] R. J. Glauber, J. Math. Phys. **4**, 294 (1963).
[4] V. Spirin, P. L. Krapivsky, and S. Redner, Phys. Rev. E **65**, 016119 (2001).
[5] G. Kondrat and K. Sznajd-Weron, Phys. Rev. E **77**, 021127 (2008).
[6] K. Sznajd-Weron and J. Sznajd, Int. J. Mod. Phys. C **11**, 1157 (2000).
[7] D. G. Myers, *Social Psychology*, 9th ed. (McGraw-Hill, New York, 2006).
[8] D. Stauffer, A. O. Sousa, and S. M. De Oliveira, Int. J. Mod. Phys. C **11**, 1239 (2000).
[9] D. Stauffer, Comput. Phys. Commun. **146**, 93 (2002).
[10] B. Schechter, New Sci. **175**, 42 (2002).
[11] S. Fortunato and D. Stauffer, in *Extreme Events in Nature and Society*, edited by S. Albeverio, V. Jentsch, and H. Kantz (Springer, Berlin, 2005).
[12] K. Sznajd-Weron, Acta Phys. Pol. B **36**, 2537 (2005).
[13] C. Castellano, S. Fortunato, and V. Loreto, e-print arXiv:0710.3256v1, Rev. Mod. Phys. (to be published).
[14] A. Lipowski, Physica A **268**, 6 (1999).
[15] M. E. Gage and R. S. Hamilton, J. Diff. Geom. **23**, 69 (1986).
[16] M. A. Grayson, J. Diff. Geom. **26**, 285 (1987).
[17] C. M. Newman and D. L. Stein, Phys. Rev. Lett. **82**, 3944 (1999).
[18] C. Godreche and J. M. Luck, J. Phys.: Condens. Matter **17**, S2573 (2005).
[19] P. L. Krapivsky, S. Redner, and J. Tailleur, Phys. Rev. E **69**, 026125 (2004).

On phase transitions in quantum continuous gases in the Maxwell–Boltzmann statistics

J. Stat. Mech. (2010) P01022

(http://iopscience.iop.org/1742-5468/2010/01/P01022)

Journal of Statistical Mechanics: Theory and Experiment
An IOP and SISSA journal

On phase transitions in quantum continuous gases in the Maxwell–Boltzmann statistics

Marek Gorzelańczyk and Grzegorz Kondrat[1]

Institute of Theoretical Physics, University of Wrocław, plac Maxa Borna 9, 50-204 Wrocław, Poland
E-mail: magor@ift.uni.wroc.pl and gkon@ift.uni.wroc.pl

Received 14 October 2009
Accepted 24 December 2009
Published 29 January 2010

Online at stacks.iop.org/JSTAT/2010/P01022
doi:10.1088/1742-5468/2010/01/P01022

Abstract. In our work we investigate properties of the equilibrium Gibbs state in the thermodynamical limit. Using Ginibre's approach we reduce the problem to the analysis of integral equations on Wiener measures. We show a new method for studying these equations via positive operators on cones. By examining the spectrum of shifted Kirkwood–Salsburg operators we obtain new domains where phase transitions do not occur.

Keywords: rigorous results in statistical mechanics, quantum phase transitions (theory)

J. Stat. Mech. (2010) P01022

[1] Author to whom any correspondence should be addressed.

1742-5468/10/P01022+7$30.00

Contents

J. Stat. Mech. (2010) P01022

1. Introduction

In quantum statistical mechanics there are very few rigorous results. Bose and Fermi ideal gases are the only models for which there exists a full theory. These models are far from being realistic however. For more physical potentials the only strict results come from Ginibre [1]. In his paper it is shown that there is no phase transition in very low density gases. In our work we prove that the domain free from phase transitions for a wide class of physical potentials is much broader and the possibility of phase transitions is limited to much higher gas densities.

Equilibrium statistical mechanics is usually [2] described via the equilibrium Gibbs state in the grand canonical ensemble:

$$\omega^{\beta,\mu}(A) = \frac{\mathrm{Tr}[\mathrm{e}^{-\beta K}A]}{\mathrm{Tr}[\mathrm{e}^{-\beta K}]}, \tag{1}$$

where $K = H - \mu N$, $\beta, \mu \in \mathbf{R}$, and $\mathrm{e}^{-\beta K}$ is a trace class operator. Researching phase transitions requires introduction of the finite volume Gibbs state:

$$\omega^{\beta,\mu}_{\sigma,\Lambda}(A) = \frac{\mathrm{Tr}[\mathrm{e}^{-\beta(H_{\sigma,\Lambda}-\mu N_\Lambda)}A]}{\mathrm{Tr}[\mathrm{e}^{-\beta(H_{\sigma,\Lambda}-\mu N_\Lambda)}]} \tag{2}$$

and the analysis of properties of the thermodynamic limit of the Gibbs state:

$$\omega^{\beta,\mu}_{\sigma}(A) = \lim_{\Lambda\to\infty} \omega^{\beta,\mu}_{\sigma,\Lambda}(A). \tag{3}$$

The latter consists of detailed investigation of its existence, uniqueness, temperature ($\beta = 1/kT$) and activity ($z = \exp(\beta\mu)$) dependence, and self-adjoint extensions of the Hamiltonian with boundary conditions σ.

In our work we follow methods developed by Ginibre [1]. Having used the Feynman–Kac formula we see a resemblance between the Gibbs state's integral representation on Wiener measures and correlation functions of quantum mechanics. Analogously we construct Kirkwood–Salsburg type integral equations (KS), that are very convenient in investigating the Gibbs state's thermodynamical limit. Here we write the integral equations in operator form and analyze their spectral properties.

In the second section we use positive operators on cones in real Banach space, as in [3], where classical KS operators were successfully investigated. This approach allows us to conclude that the activity $z = -r(\mathbf{K}_\Lambda)$ belongs to the spectrum of the KS integral

operator. Since only positive values of the activity z have definite physical meaning, we have to deal with spectral properties of the KS operator also for $z > r(\mathbf{K}_\Lambda)$.

In the third section we analyze the spectrum of the shifted KS operator $(\mathbf{K}_\Lambda + C\mathbb{1})$. By the use of positive operators we improve on known estimates of the spectral radius of the KS operator. One of the more important points relies on getting rid of the unphysical weight ξ that appears in norm estimates. As a result of our investigations of the shifted operator $\mathbf{K}_\Lambda + C\mathbb{1}$, we find a new domain free from phase transitions in the Maxwell–Boltzmann statistics.

2. Basic notions

Let Λ be a bounded, connected open set in $\mathbf{R}^\nu$ with piecewise C^1 boundary $\partial\Lambda$. Let $\Omega(\Lambda, \beta, n)$ be the set of families of n continuous functions $\omega^n = (\omega_1, \ldots, \omega_n)$, each from the interval $[0, \beta]$ to Λ, such that for all $i < j$ and all $t \in [0, \beta]$ we have $\omega_i(t) - \omega_j(t) \neq 0$. The set Ω_0 of single, continuous functions (trajectories) $\omega(t)$: $[0, \beta] \to \mathbf{R}^\nu$ is a Banach space with the norm $\|\omega\| = \sup_t |\omega(t)|$.

Let $B_\xi(\Lambda)$ be the set of real, continuous functions $\mathbf{\Phi}$ on $\bigcup_{n=0}^\infty \Omega(\Lambda, \beta, n)$ such that $\mathbf{\Phi} = \{\varphi(\omega^n)\}_{n=0}^\infty$ is bounded for each n and on each sector $\Omega(\Lambda, \beta, n)$ the function is symmetric with respect to permutations of their arguments. The space $B_\xi(\Lambda)$ with the norm

$$\|\mathbf{\Phi}\| = \sup_n \left[\xi^{-n} \sup_{\omega^n \in \Omega(\Lambda,\beta,n)} |\varphi(\omega^n)| \right] \tag{4}$$

is the Banach space for $\xi > 0$.

According to the theorem 6.3.9 of [2]:

$$\int_B \chi_\Lambda(\omega)\, \mathrm{d}\mu_{x,y}^{\sigma,\Lambda,\beta}(\omega) = \int_B \chi_\Lambda(\omega)\, \mathrm{d}\mu_{x,y}^{\beta}(\omega), \tag{5}$$

where the characteristic function

$$\chi_\Lambda(\omega) = \begin{cases} 1 & \text{if } \omega(t) \in \Lambda \quad \text{for all } t \in [0, \beta] \\ 0 & \text{otherwise,} \end{cases} \tag{6}$$

and $B \subset \Omega(\Lambda, \beta, 1)$, the trajectories that do not hit the boundary $\partial\Lambda$ will not feel the effect of the boundary condition σ.

In our discussion we restrict ourselves to continuous functions, since all non-continuous functions form a set of Wiener measure $\mathrm{d}\mu$ zero [1].

In the space $B_\xi \equiv B_\xi(\mathbf{R}^\nu)$ we introduce an integral operator:

$$(\mathbf{k\Phi})(\omega^m) = \sum_{n=0}^\infty \frac{1}{n!} \int \mathrm{d}\tilde{\omega}^n\, k(\omega_1, \tilde{\omega}^n)\, \varphi(\omega'^m, \tilde{\omega}^n) \tag{7}$$

for $m > 1$, and

$$(\mathbf{k\Phi})(\omega^1) = \sum_{n=1}^\infty \frac{1}{n!} \int \mathrm{d}\tilde{\omega}^n\, k(\omega_1, \tilde{\omega}^n)\, \varphi(\tilde{\omega}^n), \tag{8}$$

J. Stat. Mech. (2010) P01022

where $\omega'^m = (\omega_2, \omega_3, \ldots, \omega_m)$ and

$$k(\omega_1, \tilde{\omega}^n) = \prod_{j=1}^{n} \left\{ \exp\left[-\int_0^\beta V(\omega_1(t) - \tilde{\omega}_j(t))\, \mathrm{d}t \right] - 1 \right\}. \tag{9}$$

In the above equations we integrate over the Wiener measure:

$$\mathrm{d}\tilde{\omega}^k = \mathrm{d}\tilde{\omega}_1 \cdots \mathrm{d}\tilde{\omega}_k, \tag{10}$$

where

$$\mathrm{d}\tilde{\omega}_k = \int_\Lambda \mathrm{d}\mu_{u,u}^{\sigma,\Lambda,\beta}(\tilde{\omega}_k)\, \mathrm{d}u, \tag{11}$$

and the variable u denotes starting and ending points of a trajectory $\tilde{\omega}_k$ [2].

Here we assume that the potential V is non-negative, bounded and regular, so

$$k(\omega, \tilde{\omega}) \leq 0, \tag{12}$$

and

$$C = \sup_\omega \int |k(\omega, \tilde{\omega})|\, \mathrm{d}\tilde{\omega} < \infty. \tag{13}$$

The KS operator $\mathbf{K} = E\mathbf{k}$, where

$$(E\mathbf{\Phi})(\omega^n) = \exp[-\beta W(\omega_1, \omega'^n)]\, \varphi(\omega^n), \tag{14}$$

and $W(\omega_1, \omega'^n) = \sum_{j=2}^n V(\omega_1 - \omega_j)$ for $n > 1$ and $W(\omega_1, \omega'^1) = 0$.

Now we introduce the projector Π_Λ:

$$(\Pi_\Lambda \mathbf{\Phi})(\omega^n) = \prod_{j=1}^{n} \chi_\Lambda(\omega_j)\, \varphi(\omega^n), \tag{15}$$

where the characteristic function $\chi_\Lambda(\omega_j) = 1$ if $\omega_j(t) \in \Lambda$ for all $t \in [0, \beta]$ and 0 otherwise.

The KS operator in finite volume reads

$$\mathbf{K}_\Lambda = \Pi_\Lambda E\mathbf{k}\Pi_\Lambda. \tag{16}$$

Let us here recall some definitions from the theory of cones [4].

Definition 1. A cone in a linear space F is a convex subset $K \subset F$ such that $x \in F \Rightarrow tx \in K$ for all $t \geq 0$, and $-x \notin K$.

Definition 2. A cone is generating if $\forall_{x \in F} \exists_{x_1, x_2 \in K}\ x = x_1 - x_2$.

Definition 3. Let K be a cone in the Banach space F. We say that two elements $x_1, x_2 \in F$ are in the relation $x_1 \preceq x_2$ if $x_2 - x_1 \in K$.

Definition 4. A cone K in a Banach space F is normal if from the inequality $0 \preceq x \preceq y$ there follows the condition $\|x\| \leq M\|y\|$ for some constant M.

Definition 5. Let us consider the Banach space F with the cone $K \subset F$. A linear operator $A : F \to F$ is positive if $AK \subset K$.

Let $D_\xi(\Lambda)$ denote the following cone contained in the space $B_\xi(\Lambda)$:

$$(-1)^m \varphi(\omega^m) \geq 0. \tag{17}$$

Analogously $D_\xi = D_\xi(\mathbf{R}^\nu)$ is a cone contained in the space B_ξ.

Proposition 1. *Operators $-\mathbf{k}$ and $-\mathbf{K}_\Lambda$ are positive with respect to cones D_ξ and $D_\xi(\Lambda)$, respectively.*

Proof. The positivity results from the following inequality for kernels:

$$(-1)^n k(\omega_1, \tilde{\omega}^n) \geq 0. \tag{18}$$

□

Proposition 2. *The cones D_ξ and $D_\xi(\Lambda)$ are normal and generating.*

Proof. The thesis follows directly from the definitions of the cones; the arguments are similar to those for the simple case of the cone made up from non-negative functions. □

Let us consider the spectral radius $r(-\mathbf{K}_\Lambda)$.

Proposition 3. *The point $r(-\mathbf{K}_\Lambda)$ belongs to the spectrum of the operator $-\mathbf{K}_\Lambda$.*

Proof. First let us note that $r(-\mathbf{K}_\Lambda) > 0$. Then the assumptions of theorem 8.1 from chapter 2 of [4] are satisfied owing to the propositions 1 and 2, and the thesis of the proposition 3 results from the cited theorem. □

As we are interested in finding an upper bound on the positive part of the spectrum of the operator $\mathbf{K}_\Lambda$, we have to consider the shifted operator $\mathbf{K}_\Lambda + C\mathbb{1}$.

3. Main results

For λ in the resolvent set of the operator $\mathbf{K}_\Lambda$ we have

$$\rho_\Lambda = (\lambda \mathbb{1} - \mathbf{K}_\Lambda)^{-1} \hat{\alpha}. \tag{19}$$

Here $\hat{\alpha}(\omega^n) = 0$ for $n > 1$ and $\hat{\alpha}(\omega^1) \equiv 1$.

Expanding the above around C we can write

$$\rho_\Lambda = \frac{1}{\lambda + C} \sum_{n=0}^{\infty} \left(\frac{\mathbf{K}_\Lambda + C\mathbb{1}}{\lambda + C} \right)^n \hat{\alpha}. \tag{20}$$

We get the following:

Proposition 4.

$$\|(\mathbf{K}_\Lambda + C\mathbb{1})^n \hat{\alpha}\| \leq \|\mathbf{D}^n\| \cdot \|\hat{\alpha}\|, \tag{21}$$

where we introduce an auxiliary operator $\mathbf{D}$ on the Banach space B_ξ with matrix elements

$$D_{ij} = \frac{C^{j-i+1}}{(j-i+1)!} \qquad \text{for } j - i + 1 \geq 0 \quad \text{and} \quad 0 \text{ otherwise.} \tag{22}$$

J. Stat. Mech. (2010) P01022

Proof. Let us write the operator $\mathbf{K}_\Lambda$ as a sum of separate terms acting on different sectors of the Fock space each:

$$(\mathbf{K}_\Lambda \mathbf{\Phi})(\omega^k) = \sum_l \mathbf{J}_{k\,l}\,\varphi(\omega^l). \tag{23}$$

Let us introduce one more symbol:

$$\underline{\mathbf{J}_{k\,l}} = \mathbf{J}_{k\,l} + \delta_{k\,l}\,C\,\mathbb{1}. \tag{24}$$

In the above the symbol $\delta_{k\,l}$ stands for the standard Kronecker delta. Now we go to the LHS of proposition 4:

$$\|(\mathbf{K}_\Lambda + C\mathbb{1})^n \hat{\alpha}\| \leq \sup_k \left[\xi^{-k} \sum \sup_{\omega^k \in \Omega(\Lambda,\beta,k)} |(\underline{\mathbf{J}_{k\,l_1}}\,\underline{\mathbf{J}_{l_1\,l_2}} \cdots \underline{\mathbf{J}_{l_{n-1}1}}\,\hat{\alpha})(\omega^k)|\right], \tag{25}$$

where the sum is taken over all sequences $(l_1, l_2, \ldots, l_{n-1})$ such that $l_{i+1} - l_i + 1 \geq 0$ for each $i = 0, 1, \ldots, n-1$ (we assume that $l_0 = k$ and $l_n = 1$).

Now let us notice that for any i and j we have the estimate

$$\sup_{\omega^i \in \Omega(\Lambda,\beta,i)} |(\underline{\mathbf{J}_{i\,j}}\,\varphi)(\omega^i)| \leq \frac{C^{j-i+1}}{(j-i+1)!} \cdot \sup_{\omega^j \in \Omega(\Lambda,\beta,j)} |\varphi(\omega^j)|, \tag{26}$$

which is valid for all $\varphi(\omega^i)$ either non-negative or non-positive in each sector of the Fock space independently (that is $\varphi(\omega^i) \cdot c_i \geq 0$ for each ω^i; here c_i is a function $\mathbf{N} \to \{-1, +1\}$).

For $i \neq j$ the estimate (26) comes directly from the definition of the operator $\mathbf{K}_\Lambda$ and the formula (7). In the case of $i = j$ the above estimate reduces to

$$\sup_{\omega^i \in \Omega(\Lambda,\beta,i)} |\mathbf{J}_{i\,i}\,\varphi(\omega^i) + C\varphi(\omega^i)| \leq C \cdot \sup_{\omega^i \in \Omega(\Lambda,\beta,i)} |\varphi(\omega^i)|. \tag{27}$$

Let us see that two terms in the absolute value have different signs. This derives from the fact that in $\mathbf{J}_{j\,j}$ there appears to be only one term of the sum (7) for $n = 1$, and from the inequality (12). Since

$$\sup_{\omega^i \in \Omega(\Lambda,\beta,i)} |\mathbf{J}_{i\,i}\,\varphi(\omega^i)| \leq \sup_{\omega^i \in \Omega(\Lambda,\beta,i)} |C\varphi(\omega^i)|, \tag{28}$$

the formula (27) is straightforward.

Having proven the estimate (26) we now continue with the formula (25). First let us note that in subsequent applications of the operator $\underline{\mathbf{J}_{l_i\,l_{i+1}}}$ on the vector $\hat{\alpha}$ for varying i we stay within the domain of the functionals of definite sign.

Applying the estimate (26) recursively to the RHS of (25) we arrive at

$$\begin{aligned}\|\,(\mathbf{K}_\Lambda + C\mathbb{1})^n\,\hat{\alpha}\| &\leq \sup_k \left[\xi^{-k} \sum D_{k\,l_1}\,D_{l_1\,l_2}\,\ldots\,D_{l_{n-1}1} \sup_{\omega \in \Omega(\Lambda,\beta,1)} |\hat{\alpha}(\omega)|\right] \\ &\leq \|\mathbf{D}^{n+1}\| \cdot \|\hat{\alpha}\|\end{aligned}$$

and the proposition 4 is proved. □

Taking the nth root of the equation (21), going to the limit $n \to \infty$ and applying the Cauchy criterion for the convergence to the series (20) we obtain its convergence for

$$|\lambda + C| > r(\mathbf{D}), \tag{29}$$

J. Stat. Mech. (2010) P01022

where the spectral radius $r(\mathbf{D}) \leq \mathrm{e}^{C}$. Thus the series (20) is certainly convergent on the set

$$D = \{\lambda : |\lambda + C| > \exp(C)\}. \tag{30}$$

Let us define

$$\rho = \frac{1}{\lambda + C} \sum_{n=0}^{\infty} \left(\frac{\mathbf{K} + C\mathbb{1}}{\lambda + C} \right)^{n} \hat{\alpha}. \tag{31}$$

Let us fix the trajectories set ω^n. Then we have the following:

Proposition 5. *The functions from the family* $\{\rho_\Lambda(\omega^n)(\lambda)\}$ *are analytic and are jointly bounded on the set* D.

Proof. Analyticity of the functions is clear; joint boundedness comes from the expansion (20) and the definition of the set D. □

Then we have:

Proposition 6. *The family* $\{\rho_\Lambda(\omega^n)(\lambda)\}$ *is convergent to* $\{\rho(\omega^n)(\lambda)\}$ *almost uniformly on the set* D.

Proof. In view of proposition 5 and the fact that the family considered, $\rho_\Lambda(\lambda)$, is convergent to $\rho(\lambda)$ for big λ (the case treated by Ginibre in [1]), use of Vitali's theorem gives the result. □

The existence and analyticity of all correlation functions $\rho(\lambda)$ implies the existence of the unique Gibbs measure in the thermodynamic limit.

Thus we obtain the following:

Theorem. *There exists a unique limit of the equilibrium Gibbs state that is analytical with respect to the thermodynamic parameter* z, *which physically means no phase transitions for*

$$z < \frac{1}{\exp(C) - C}. \tag{32}$$

References

[1] Ginibre J, 1970 *Statistical Mechanics and Quantum Field Theory* ed C DeWitt and R Stora (New York: Gordon and Breach) p 327
Ginibre J, 1965 *J. Math. Phys.* **6** 238

[2] Bratelli O and Robinson D W, 1981 *Operator Algebras and Quantum Statistical Mechanics II* (New York: Springer)

[3] Gorzelańczyk M, 2006 *J. Funct. Anal.* **239** 683

[4] Krasnoselskij M A, Lifshits E A and Sobolev A V, *Positive linear systems*, 1989 *The Method of Positive Operators* (*Sigma Series in Applied Mathematics* vol 5) (Berlin: Heldermann)

J. Stat. Mech. (2010) P01022

International Journal of Modern Physics C
Vol. 21, No. 4 (2010) 559–566

DOI: 10.1142/S0129183110015312

World Scientific
www.worldscientific.com

SPONTANEOUS REORIENTATIONS IN A MODEL OF OPINION DYNAMICS WITH ANTICONFORMISTS

GRZEGORZ KONDRAT and KATARZYNA SZNAJD-WERON*

Institute of Theoretical Physics
University of Wroclaw, Pl. Maxa Borna 9
50-204 Wroclaw, Poland
**kweron@ift.uni.wroc.pl*

Received 8 March 2010
Accepted 11 March 2010

In this paper we investigate a model (based on the idea of the outflow dynamics), in which only conformity and anticonformity can lead to the opinion change. We show that for low level of anticonformity the consensus is still reachable but spontaneous reorientations between two types of consensus ("all say yes" or "all say no") appear.

Keywords: Opinion dynamics; Sznajd model; agent-based models; finite-size systems.

PACS Nos.: 89.65.-s, 64.60.De, 64.60.an.

1. Introduction

In the past decade many models of opinion dynamics has been studied by physicists (for the recent review see Ref. 1). Among them several simple discrete models based on the famous Ising model, such as Voter model,[2] majority models[3,4] or Sznajd model,[5] have been proposed to describe consensus formation. The force which leads to consensus is conformity — one of the most observed response to the social influence. In all three models mentioned above a kind of conformity has been introduced. In the Voter model a single person is able to convince others, within the majority rule, individuals follow majority opinion and in the Sznajd model unanimity is needed to convince others. Although the conformity is the major paradigm of the social influence, it is known that other types of social response are also possible.

People feel uncomfortable when they appear too different from others, but they also feel uncomfortable when they appear like everyone else.[6] There is an experimental evidence for asserting uniqueness — sometimes people to assert their uniqueness can change their own opinion, when they realize that this opinion is shared by others.[6] Therefore asserting uniqueness can lead to so-called anticonformity. In 1963 Willis (reviewed recently in Ref. 7) has proposed a two-dimensional model of possible responses to social influence, in which both conformers and anticonformers are

similar in the sense that both acknowledge the group norm (the conformers agree with the norm, the anticonformers disagree).

Obviously the anticonformity is quite rare in comparison to the conformity. The natural question is whether the existence of the very small probability of anticonformity can influence the opinion dynamics. Will the consensus be still possible in the society with anticonformists? In this paper we decided to introduce the probability of anticonformal behavior to one of the consensus models. Recently a generalized one-dimensional model based on the original Sznajd model has been proposed to incorporate some diversity or randomness in human activity.[9] In this paper we investigate a special case of this extended model, in which both conformity and anticonformity are possible. We check how the small probability of anticonformal behavior in the presence of the strong conformity can influence the opinion dynamics. It has been known for long that conformity/anticonformity is to some extent a product of cultural conditions.[8] There are some experimental motivations for such statement. For example, Frager in 1970 conducted experiments among Japanese students and found a lower level of conformity compared with the US results and some evidence for anticonformity.[10] From this point of view a ratio between the probability of conformity and anticonformity could be related to the cultural or political conditions.

It should be mentioned here that for the first time, the effects of contrarian choices on the opinion dynamics has been investigated by Galam.[11] In his paper he has defined a contrarian as an agent who adopts the choice opposite to the prevailing choice of others whatever this choice is. Contrarians in the Galam's majority model play the similar role as anticonformists in our model. However, contrarians adopt the choice opposite to the majority instead of unanimous majority, which is the case of anticonformity.

2. The Model

We consider a chain of L Ising spins $S_i = \pm 1$, $i = 1, \ldots, L$ with periodic boundary conditions. At each step two consecutive spins are chosen at random, and they influence their outer neighbors. In the most popular version of the Sznajd model, inspired by the observation that an individual who breaks the unanimity principle reduces the social pressure of the group dramatically,[6] only the unanimous majority influences the neighborhood. In the paper,[9] all possible configurations of four consecutive spins has been considered. Two randomly selected middle spins decide the outcome of the update step (following in Ref. 9, we write them in brackets). The action of a selected pair has been considered independently on each direction. Thus all different possible elementary cases make up a following list: ($[AA]A$, $[AA]B$, $[AB]A$, and $[AB]B$), where the symbols A and B stand for different opinions, i.e. $A = -B = \pm 1$. To determine the dynamics, the vector of probabilities $\mathbf{p} = (p_1, p_2, p_3, p_4)$ of change for the third spin (one that is outside brackets) has been introduced[9]:

$$p_1 : [AA]A \to [AA]B\,, \tag{1}$$

$$p_2 : [AA]B \to [AA]A\,, \tag{2}$$

$$p_3 : [AB]A \to [AB]B\,, \tag{3}$$

$$p_4 : [AB]B \to [AB]A\,. \tag{4}$$

The first parameter, p_1, describes the chance of spontaneous appearame of an anticonformist opinion and the complementary probability $p_1' = 1 - p_1$ describes the situation, where in the same conditions the opinion is not changed. Second parameter, p_2, is a chance of convincing an individual to the other opinion, shared by his two consecutive neighbors — i.e. conformity. Again $p_2' = 1 - p_2$ is a probability of one's opinion remaining unaltered with the presence of conformity among his two consecutive neighbors. In this paper we investigate the special case, in which only conformity and anticonformity can lead to the opinion change, thus $p_3 = p_4 = 0$. The case in which $p_2 = 1$ and $p_1 = p_3 = p_4 = 0$ corresponds to the Sznajd model. In this paper we have decided to investigate the case in which $p_2 = 1$ and $p_1 \in (0, 1)$ is the only parameter of the model. To investigate the model, we provide Monte Carlo simulations with the random sequential updating mode and thus the time t is measured in the Monte Carlo Sweeps (MCS) which consists of L elementary updatings.

3. Results

The quantity, which is usually measured in such models, is the public opinion m as a function of time t. In this kind of models the public opinion is equivalent to the magnetization:

$$m = \frac{1}{L} \sum_{i=1}^{N} S_i\,. \tag{5}$$

In the case of $p_1 = 0$, which corresponds to the deterministic rule of the Sznajd model, the system reaches the ferromagnetic steady state (consensus from the social point of view). Once $p_1 > 0$ the system never reaches any absorbing state and the opinion dynamics depends on anticonformity probability p_1. The time evolution of public opinion $m(t)$ is presented in Figs. 1–3. It can be seen that consensus ($m = \pm 1$) is reached only for small values of p_1 (Fig. 1), while for larger values of anticonformity consensus is not reached and public opinion fluctuates around its mean value $m = 0$ (Figs. 2–3). One can also notice that the amplitude of the fluctuations decrease with p_1, on the other hand the frequency of fluctuations increase with p_1. This tendency is valid for all values of p_1 and thus the time of consensus state ("all up" or "all down") decreases with p_1. For very small values of p_1 the system spends most of the time in one of the extreme consensus state and in the limiting case $p_1 = 0$ the consensus becomes the absorbing steady state.

To analyze more precisely the dependence between the consensus time and the level of anticonformity p_1 let us introduce the mean relative time of consensus

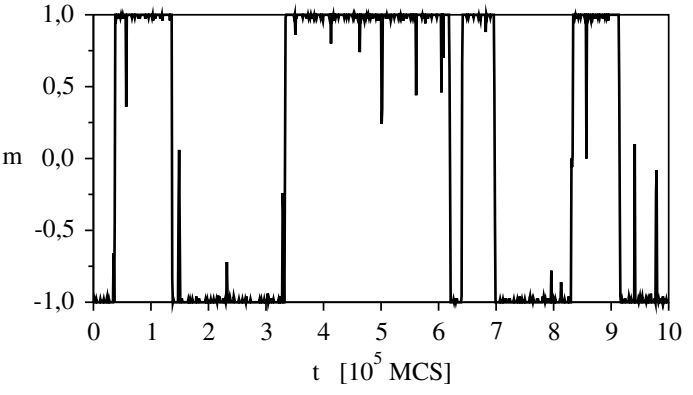

Fig. 1. The time evolution of the public opinion m in the system of $L = 100$ individuals as a function of time for the probability of anticonformity $p_1 = 0.003$. It can be seen that society for most of the time is in a consensus state ($m = \pm 1$), but from time to time spontaneous reorientations occur. From the social point of view this means that, on the one hand society polarizes to given opinion due to the conformity, but on the other hand spontaneous (and rather rapid) changes of polarization are possible, due to the weak anticonformity.

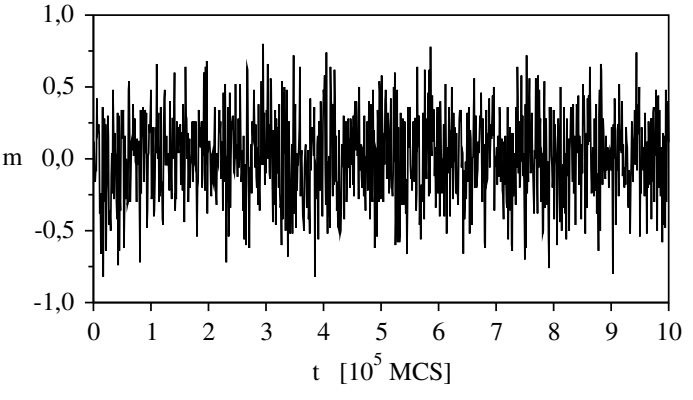

Fig. 2. The time evolution of the public opinion m in the system of $L = 100$ individuals as a function of time for the probability of anticonformity $p_1 = 0.1$. It can be seen that already for this level of anticonformity, consensus is not reached and the public opinion oscillates around its mean value $m = 0$.

$\langle \tau_c \rangle$ as a mean number of MCS for which $|m| = 1$ divided by the total number of sweeps in the simulation. The dependence between the mean relative time of consensus $\langle \tau_c \rangle$ and p_1 is presented in Fig. 4. For small values of p_1 this dependence is exponential, i.e. $\langle \tau_c \rangle \sim \exp(-\alpha p_1)$, with $\alpha = \alpha(L) \sim (3/2)L$. This means that although the relative time of consensus decrease with p_1, consensus is still possible for larger values of p_1. No qualitative change of behavior is seen while looking at $\langle \tau_c \rangle$ as a function of anticonformity. On the other hand, if we look at Figs. 1–3 it seems that there is some qualitative difference between opinion dynamics presented

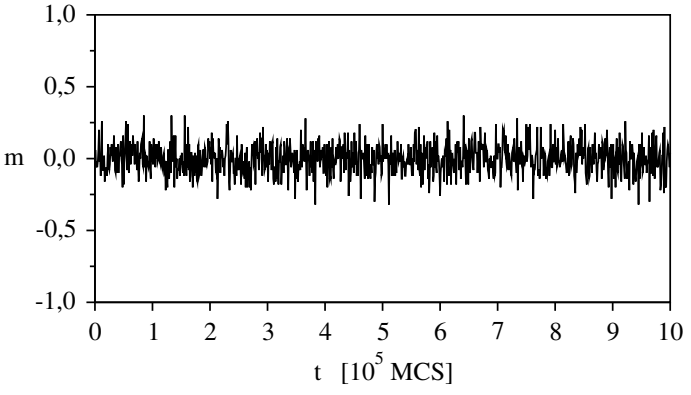

Fig. 3. The time evolution of the public opinion m in the system of $L = 100$ individuals as a function of time for the probability of anticonformity $p_1 = 0.9$. It can be seen that for this level of anticonformity consensus is not reached, similarly to the Fig. 2. The difference between the case $p_1 = 0.1$ and $p = 0.9$ is visible in the fluctuations around the mean value $m = 0$ — the amplitude of the fluctuations decreases with p_1, on the other hand the frequency of fluctuations increases with p_1.

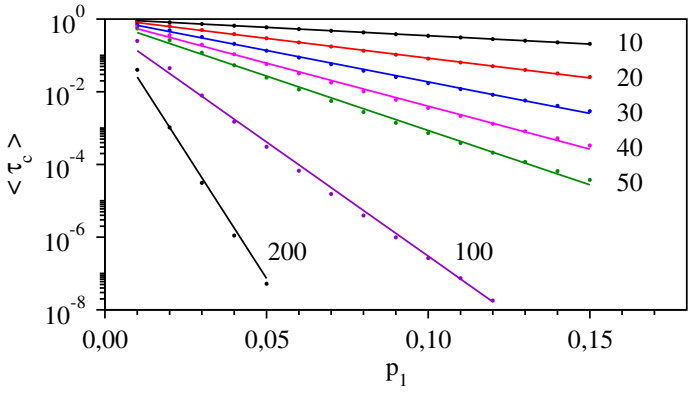

Fig. 4. (Color online) The dependence between the mean relative time of consensus $\langle \tau_c \rangle$ and the level of anticonformity p_1 for several lattice sizes (from $L = 10$ to $L = 200$). For small values of p_1 this dependence is exponential, i.e. $\langle \tau_c \rangle \sim \exp(-\alpha p_1)$, with $\alpha = \alpha(L) \sim (3/2)L$.

in Figs. 1–3. In Fig. 1 the system is ferromagnetically ordered for most of the time and spontaneous transitions between two opposite ferromagnetic states are observed.

Therefore, let us now check the dependence between control parameter p_1 and the mean reorganization time $\langle t_r \rangle$, defined as a mean time between arriving at two consecutive opposite consensus states. More precisely we monitor the events of time, at which the system attains the given consensus ($m = \pm 1$) for the first time since it was in the last opposite state $m = \mp 1$. It occurs that there is an optimal value of p_1 for which the mean reorganization time $\langle t_r \rangle$ is the shortest (see Fig. 5). From the social point of view this means that there is a special level of anticonformity for

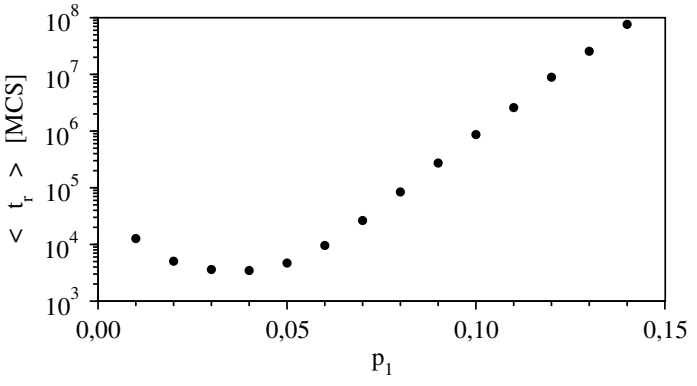

Fig. 5. The dependence between the mean reorganization time $\langle t_r \rangle$ and the level of anticonformity p_1 for the lattice size $L = 100$.

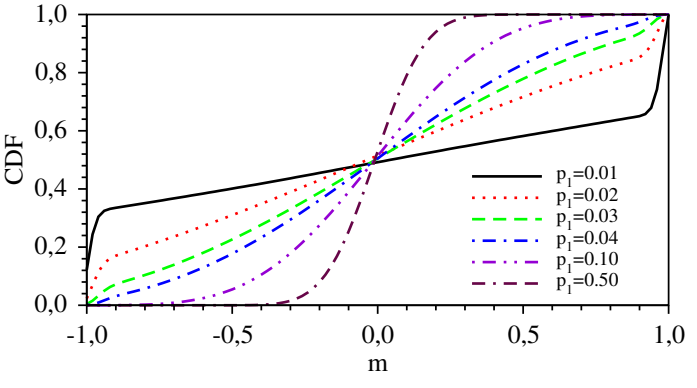

Fig. 6. (Color online) The cumulative distribution function CDF of the public opinion m for several values of anticonformity level p_1 and the lattice size $L = 100$. It can be seen that for $p_1 \leq 0.04$ the curve is $\sim$-shaped and for certain value $p = p^* \in (0.03, 0.04)$ there is the qualitative change in convexity to the $\sim$-shape.

which reorganizations ("revolutions") are the most frequent. The optimal value of p_1 is roughly inversely proportional to the system size L. Thus their product $p_1 L$, describing the mean number of acts of anticonformity per one Monte Carlo sweep, remains constant independently on the system size.

Now we can show that, indeed, there is a qualitative change in the opinion dynamics for a certain value of p_1 and this value corresponds to the optimal value of p_1, i.e. value for which the mean reorganization time $\langle t_r \rangle$ is the shortest. To do this let us present the cumulative distribution function CDF of the public opinion m. In Fig. 6 it can be seen that for $p_1 \leq 0.04$, the curve is $\sim$-shaped and for certain value $p_1 = p^* \in (0.03, 0.04)$, the shape of CDF changes qualitatively to the $\simeq$-shape (the change in convexity). While for $p_1 \leq 0.03$ the system for most of the time is in the consensus state, for $p_1 \geq 0.04$ the consensus state is probably extremely low.

One should notice (see Fig. 5) that the optimal value of p_1 also lies in the interval (0.03, 0.04) and thus corresponds to p^*.

4. Summary

We have proposed a new model of opinion dynamics with anticonformists based on the general model proposed by Kondrat.[9] In our model only conformity (with probability 1) and anticonformity (with probability p_1) can lead to the opinion change. According to Willis, both conformers and anticonformers are similar in the sense that both acknowledge the group norm (the conformers agree with the norm, the anticonformers disagree). In our model a pair of neighboring individuals sharing the same opinion will influence its neighborhood (so-called outflow dynamics — the idea taken from the Sznajd model). To investigate the model, we have provided Monte Carlo simulations with the random sequential updating mode. It occurs that for small values of anticonformity level consensus is still reached, but it is not the absorbing steady state as in the case of $p_1 = 0$. For small values of p_1 spontaneous reorientations occur, which can be understood from the social point of view, as complete repolarizations (e.g. spontaneous transition from dictatorship to democracy). We have shown that there is a special value of anticonformity level $p_1 = p^*$ below which the system stays for most of the time in the consensus state and spontaneous reorientations occur. Above this value the consensus is almost impossible and qualitative change is visible in the cumulative distribution function of the public opinion m.

Spontaneous reorientations in an Ising spin system has already been observed more than 25 years ago by Binder and Landau.[12] They have shown that in the Glauber kinetic Ising model transitions from $+m$ to $-m$ are quite often on small lattices below critical temperature. Indeed in our model, p_1 plays the role of the temperature.[9] Such spontaneous transitions are usually reported as finite size effects,[12,13] which is also the case in this paper. However, it should be stressed that social systems have always finite size and thus such finite size phenomena are important. Review on finite size effects in several models of the opinion dynamics can be found in Ref. 13.

The main criticism connected with such simple social models concerns usually oversimplifications of the assumptions. We do not want to convince anybody that there is no free will or no external factors influencing individual choices. We have only shown that even in the conformistic societies with very low (but nonzero) level of anticonformity, spontaneous reorientations of the public opinion are possible. There is no need to introduce any external field nor strong leader to explain these social repolarizations. This seems to be quite an important result in the social perspective.

References

1. C. Castellano, S. Fortunato and V. Loreto, *Rev. Mod. Phys.* **81**, 591 (2009).

2. T. Liggett, *Stochastic Interacting Systems: Contact Voter, and Exclusion Processes* (Springer-Verlag, New York, 1999).
3. S. Galam, *Eur. Phys. J. B* **25**, 403 (2002).
4. P. L. Krapivsky and S. Redner, *Phys. Rev. Lett.* **90**, 238701 (2003).
5. K. Sznajd-Weron and J. Sznajd, *Int. J. Mod. Phys. C* **11**, 1157 (2000).
6. D. Myers, *Social Psychology* (The McGraw-Hill Companies, Inc., 1996).
7. P. Nail, G. MacDonald and D. Levy, *Psychological Bulletin* **126**, 454 (2000).
8. R. Bond and P. Smith, *Psychological Bulletin* **119**, 111 (1996).
9. G. Kondrat, arXiv:0912.1466v2.
10. R. Frager, *J. Personality Soc. Psychology* **15**, 203 (1970).
11. S. Galam, *Physica A* **333**, 453 (2004).
12. K. Binder and D. P. Landau, *Phys. Rev. B* **30**, 1477 (1984).
13. R. Toral and C. Tessone, *J. Commun. Comput. Phys.* **2**, 177 (2007).

Percolation and jamming in random sequential adsorption of linear segments on a square lattice

Grzegorz Kondrat* and Andrzej Pękalski†
Institute of Theoretical Physics, University of Wrocław, pl. M. Borna 9, 50-204 Wrocław, Poland
(Received 5 September 2000; published 20 April 2001)

We present the results of a study of random sequential adsorption of linear segments (needles) on sites of a square lattice. We show that the percolation threshold is a nonmonotonic function of the length of the adsorbed needle, showing a minimum for a certain length of the needles, while the jamming threshold decreases to a constant with a power law. The ratio of the two thresholds is also nonmonotonic and it remains constant only in a restricted range of the needles length. We determine the values of the correlation length exponent for percolation, jamming, and their ratio.

DOI: 10.1103/PhysRevE.63.051108 PACS number(s): 05.40.−a, 64.60.Ak

I. INTRODUCTION

The problem of percolation is an old one [1] but still new results appear and some unsolved questions remain [2]. In general site percolation is defined on a *d*-dimensional lattice where each site can be either occupied with the probability c or empty with the probability $1-c$. Neighboring occupied sites form a cluster. If it is so large that it reaches the two opposite edges of the lattice, e.g., top and bottom, the cluster is said to be percolating. The lowest concentration of occupied sites for which there is a percolating (or spanning) cluster for an infinite lattice is called the percolation threshold c_p [2].

Another realization of the percolation problem is random sequential adsorption (RSA), in which objects (point particles, segments, rectangles, etc.) are put on randomly chosen sites and the objects do not move [3]. It is also possible to consider RSA in a continuum [4].

Jamming is a problem related to RSA percolation [3]. Again objects are placed randomly on the lattice sites until a concentration c_j is reached, where there is no room on the lattice for the next object. For pointlike particles $c_j=1$, but for spatially extended entities $c_j<1$. Continuum models of jamming also exist [3].

The RSA models irreversible dissociation [5] and binding of large ligands to polymer chains [6]. Another area of applicability is the deposition of large molecules on solid surfaces, like proteins [7] or macromolecules on biological membranes [8]. The isotropic-nematic transition in the hard rods such as polymers, has been studied first by Flory [9] and later, e.g., in Ref. [10]. Spatial organization of needles into a well-organized nematic phase is however a different problem, not considered here. General forms of percolation models have a wide range of applications—from chemisorption, spatially disordered systems, porous materials, car parking, and ecology [3], to separating the good and bad people at the entrance to Hades [11]. For overview of percolation, jamming, and related problems see Ref. [3].

In a recently published paper [12] Vanderwalle *et al.* studied the relation between the two transitions—percolation and jamming. They used two kinds of objects—linear segments of length 2 to 10 and square blocks. They have found that the ratio of the two threshold concentrations c_p and c_j is constant $c_p/c_j \approx 0.62$, regardless of the length of the needle.

In the present paper we extend the study of Vanderwalle *et al.* to larger lattices and longer objects (we consider only linear segments). In particular we shall check the claim that the c_p/c_j ratio does not depend on the length of the needles.

II. MODEL

We consider a square lattice of size $L\times L$. On the sites of the lattice we put randomly linear segments (needles) of a given length a, with the constraint that the needles cannot cross each other, although they may touch themselves. We used hard boundary conditions, i.e., the needles may touch the edge of the lattice but they cannot stick out of it—each needle must lay totally inside the lattice. Adopting open boundary conditions does not affect the results.

To achieve simulation efficiency, our algorithm of deposition needles consists of two parts designed for two different regimes. First when the current concentration of the needles is small, we chose randomly, from a uniform distribution, the orientation (vertical or horizontal) and position of the upper left end of the needle to be inserted. If there is enough space on the lattice, the needle is deposited, if not, we pass to the next try. After a certain number of adsorption trials we switch to the other regime where the dense routine is applied. A list of all empty sites and orientations still available is made. From that list a site is randomly chosen. We determine the direction of the needle and check whether the needle can be put there. In any case the site is removed from the list. The process is continued untill the last item on the list. Such organization saves time, since we avoid inserting needles into densely packed regions.

A cluster is defined as a group of sites linked by the needles. If there is an uninterrupted path between the top and the bottom of the lattice, the cluster is said to be percolating or spanning, and the concentration of occupied sites defines the percolation threshold c_p. The concentration at which no more needles could be put on the lattice without violating the constraint determines the jamming threshold c_j.

We have considered lattices of sizes $L=30$, 100, 300, 1000, 2500 and needles of length $a=1,\ldots,2000$. On the

*Email address : gkon@ift.uni.wroc.pl
†Email address: apekal@ift.uni.wroc.pl

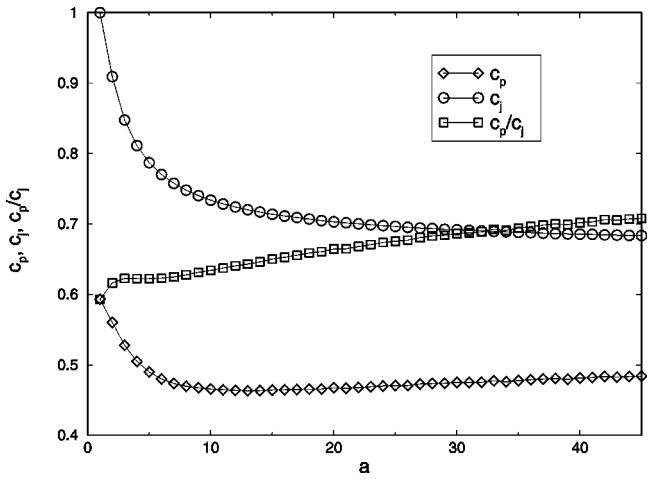

FIG. 1. Thresholds for percolation c_p, jamming c_j, and their ratio c_p/c_j vs needles' length a. Lattice size $L=2500$. Averaged over 100 samples. The x axis is in arb. units in all figures.

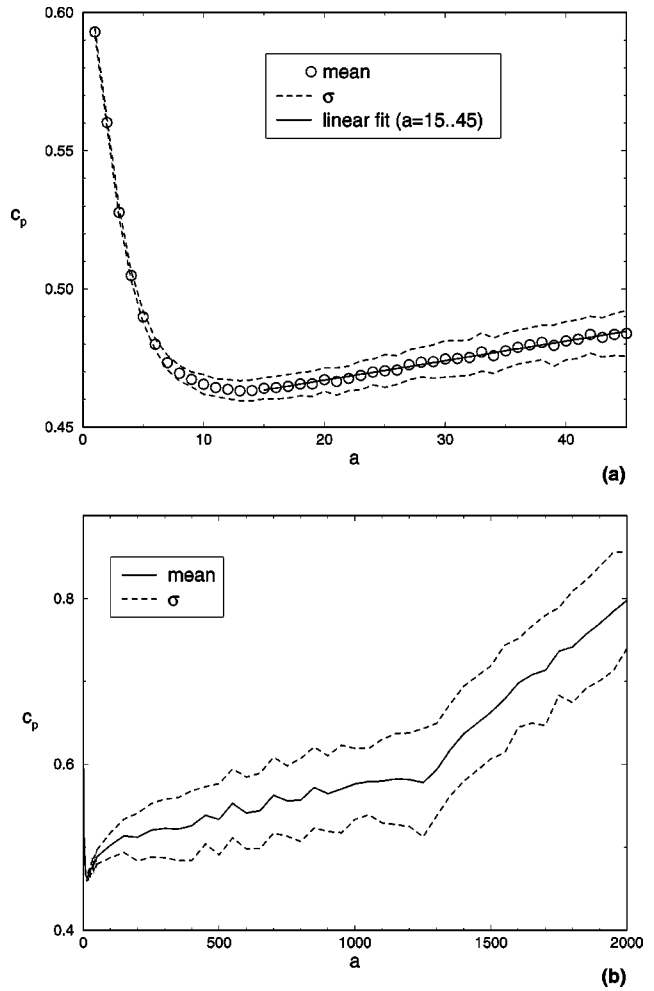

FIG. 2. Percolation threshold c_p vs needles' length a. $L=2500$, 100 runs. (a) Short needles $a=1,\ldots,45$; (b) long needles $a=1,\ldots,2000$.

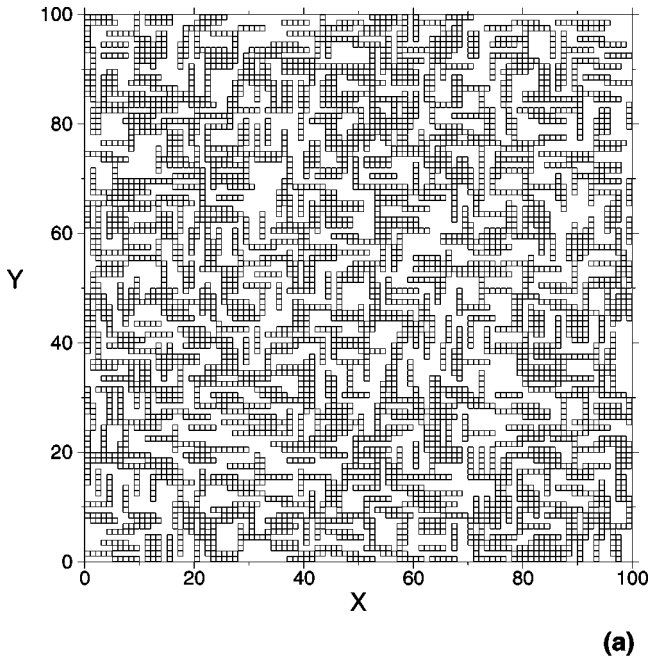

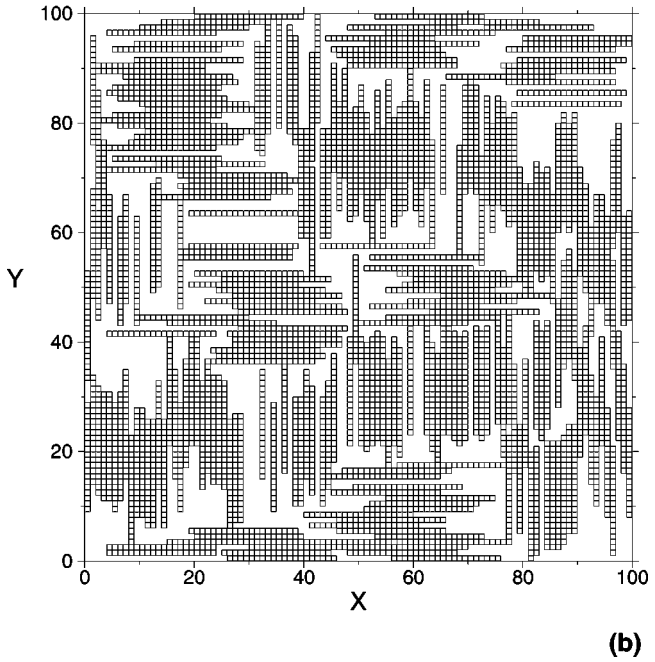

FIG. 3. Snapshot of a spatial distribution of needles at the percolation threshold for $L=100$. (a) $a=5$, (b) $a=20$. The y axes are in arb. units.

smallest lattices only smaller needles were located. Averaging was done over 100 independent runs. We have checked that averaging over 1000 runs did not reduce the error (mean standard deviation - σ) in a marked way.

III. RESULTS

Our main results of the simulations are presented in Fig. 1, where the percolation and jamming thresholds, as well as their ratio, are plotted against the length of the needles (a

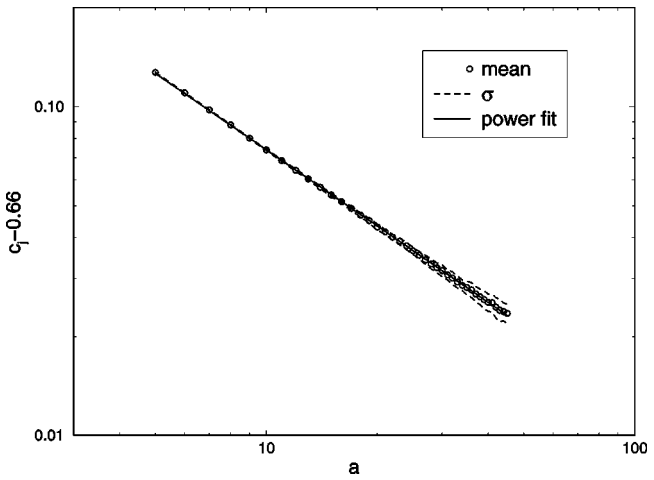

FIG. 4. Jamming threshold c_j vs needles' length a on a log–log plot. $L=2500$, 100 runs. $a=5,\ldots,45$.

$=1,\ldots,45$). These data are obtained for lattice size $L=2500$. As convergence and error analysis shows (see below) we can safely accept them as the asymptotic ($L\to\infty$) values.

The percolation threshold for $a=1,\ldots,13$ diminishes, then it begins to grow linearly with the slope 0.000 71. The minimum value $c_{p\min}=0.463$ is reached for $a=13$. As seen in Fig. 2, the σ increases with the size of the needles starting from $0.001(a=1)$ up to $0.008(a=45)$. The increase of the percolation threshold for longer a is however quite clear. The appearance of this unexpected feature is connected with the condition that the needles may touch themselves but they cannot cross. In the simulations where the restriction has been lifted we observed no minimum but a monotonic decrease. In the model considered here the needles have the tendency to align in parallel not only with respect to the edges of the lattice but also to themselves (see Fig. 3); hence the needles form compact clusters. In the case of horizontally oriented needles, in order to move, e.g., two steps down, two

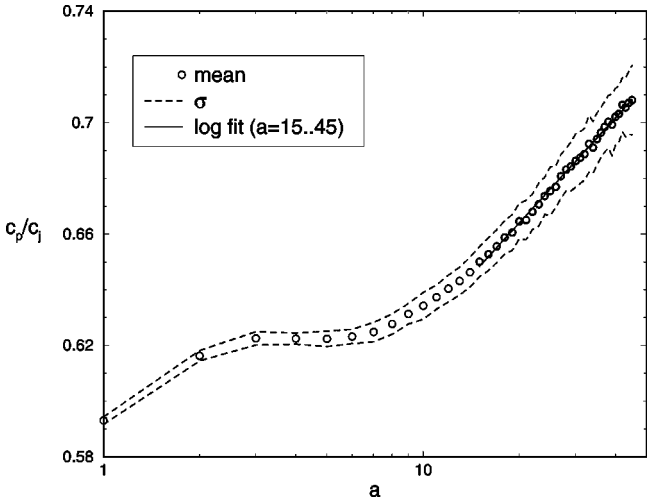

FIG. 5. Percolation to jamming thresholds ratio c_p/c_j vs needles' length a. $L=2500$, 100 runs. Logaritmic fit for $a=15,\ldots,45$.

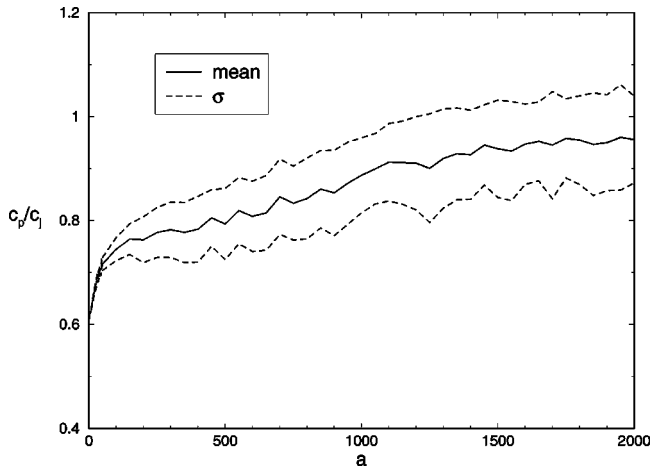

FIG. 6. Percolation to jamming thresholds ratio c_p/c_j vs needles' length a. $L=2500$, 100 runs. $a=1,\ldots,2000$.

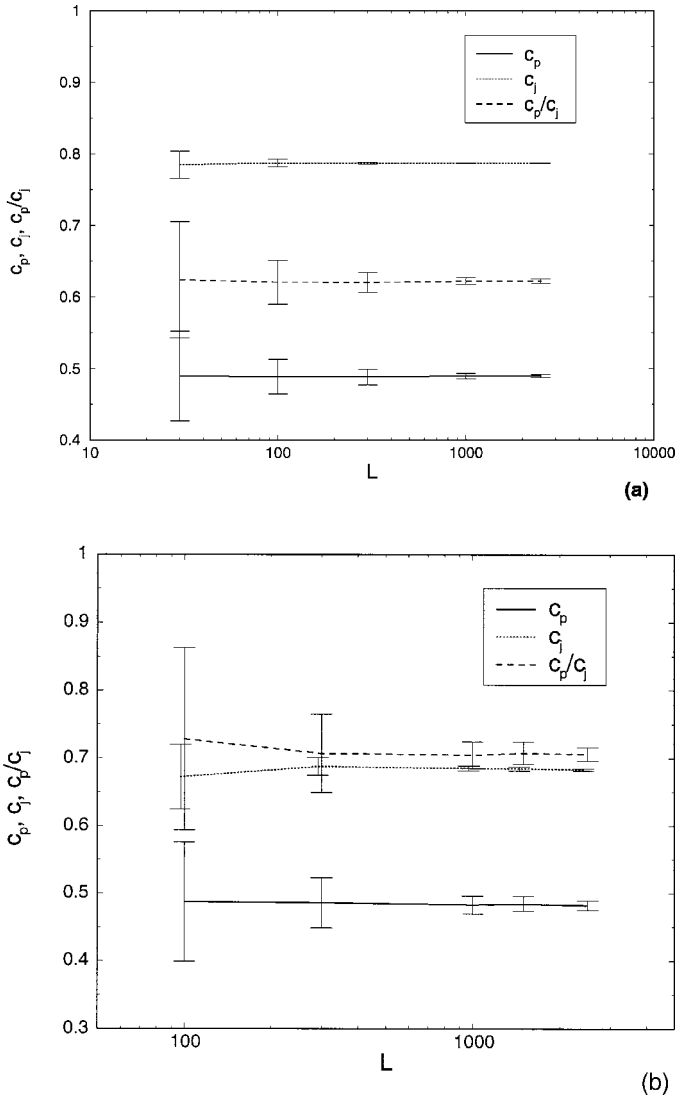

FIG. 7. Convergence analysis of percolation c_p, jamming thresholds c_j, and their ratio c_p/c_j, vs lattice size L. 100 runs. (a) $a=5$, (b) $a=45$.

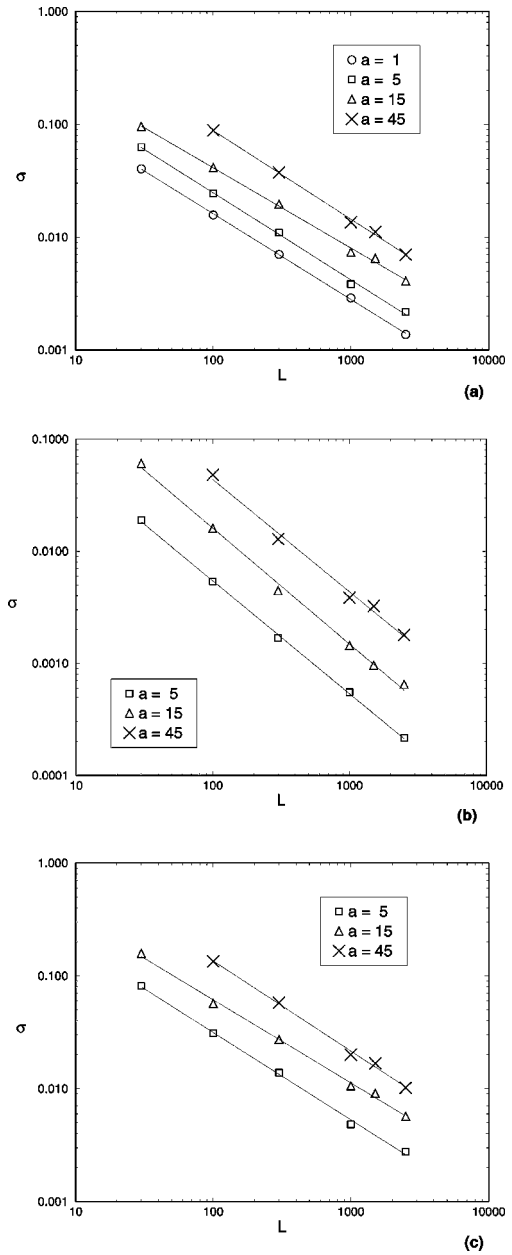

FIG. 8. Deviation analysis. σ vs lattice size L for several values of the needles' length. (a) Percolation, (b) jamming, and (c) percolation to jamming ratio.

needles of length a are needed. The longer are the needles the higher is the percentage of occupied sites necessary for passing these two steps. The increase of $c_p(a)$ is to a certain degree compensated by vertically oriented needles, which however also form clusters, thus offering many equivalent ways for percolation. Further simulations for much longer needles indicate continuous increase in c_p, although at a slower rate—see Fig. 2(b). The jamming thresholds obtained from the simulations have much smaller error than that for percolation and even for $a=45$ it is below 0.002. Values of c_j, as a function of a, decrease according to a power law (very good fit for all $a \geqslant 5$) approaching the asymptotic value $c_j^* = 0.66 \pm 0.01$ (see Fig. 4):

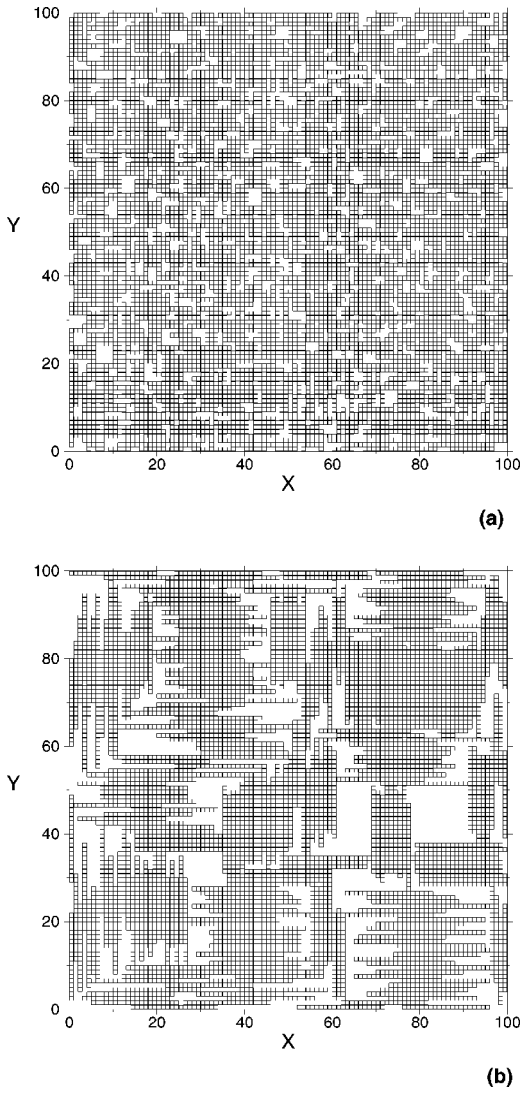

FIG. 9. Snapshot of a spatial distribution of needles at the jamming threshold for $L=100$. (a) $a=5$, (b) $a=20$. The y axes are in arb. units.

$$c_j = c_j^* + 0.44 a^{-0.77}. \tag{1}$$

The uncertainty of the exponent derived from the graph analysis equals 0.02. Clearly this behavior differs essentially from bare power law postulated in Ref. [4]:

$$c_j \sim a^{-0.2}, \tag{2}$$

for the continuum (off-lattice) case of RSA of randomly oriented and highly anisotropic (length to wide) rectangles. Their a coincides with our length of needles a. In the discrete case we did not observe the maximum of c_j at $a=2$ reported in Ref. [4]. The reason is that on the lattice the number of possible orientations of the needles is restricted to $z/2$ (where z is the coordination number of the lattice) in contrast to the continuum case. It is interesting that the asymptotic concentration for jamming (for $a \to \infty$) is 0 off lattice and it remains finite in the discrete case.

Another interesting quantity in our model is the ratio c_p/c_j as a function of a (see Fig. 5). It grows for $a=1,\ldots,3$, then it stabilizes untill $a=7$ and then it grows again. The plateau value of $c_p/c_j \approx 0.62$, the constant found in Ref. [12]. The growth for longer needles ($15 \leqslant a \leqslant 45$) could be fitted by a logarithmic dependence

$$c_p/c_j \sim 0.50 + 0.13 \log a. \tag{3}$$

Further simulations for longer needles (see Fig. 6) support our claim of monotonic increase in c_p/c_j over a wide range of a (even up to $a=2000$). We may conclude therefore that the universality claimed in Ref. [12] holds only in a rather restricted range of $a \in [3,7]$. As a matter of fact, the value of c_p/c_j for $a>7$ shown in Table I of Ref. [12] is greater than those for $a \leqslant 7$ but the authors attribute it to the finite-size effects. This is however most probably just the beginning of the growth of c_p/c_j.

We analyzed the dependence of the obtained thresholds on the lattice size L and needles' length a focusing on convergence. It appeared that for the ratio $a/L<1/3$ the values of c_p and c_j do not vary much with increasing L (keeping a constant)—see Figs. 7(a) and 7(b). The error bars (here σ) however decrease rapidly with L, while the difference of the thresholds for different lattice sizes is much smaller than the appropriate error. Thus it is safe to take the values of the thresholds from the simulations with $L=2500$ as the asymptotic (exact) ones.

The finite-size effects can clearly be seen in Fig. 2(b), where c_p is drawn against $a=1,\ldots,2000$ for $L=2500$. At $a=L/2$ we can notice a sharp change in the slope of the function $c_p(a)$.

Consider now the dependence of σ of $c_p, c_j, c_p/c_j$ on the lattice size. σ is analogous to the quantity Δ defined in Ref. [12] as the sharpness of the transition (nonpercolating to percolating or nonjammed to jammed). Here however the power-law approach to the asymptotic value $p(\infty)-p(L) \sim L^{-1/\nu}$ [cf. formula (3) in Ref. [12]] does not hold. We have found (see Fig. 8) that the σ for percolation (Δ_p), jamming (Δ_j), and the c_p/c_j ratio (Δ_r) decrease with the lattice size according to the power laws

$$\Delta_p \sim L^{-1/\nu_p}, \quad 1/\nu_p = 0.75 \pm 0.05,$$

$$\Delta_j \sim L^{-1/\nu_j}, \quad 1/\nu_j = 1.00 \pm 0.05,$$

$$\Delta_r \sim L^{-1/\nu_r}, \quad 1/\nu_r = 0.77 \pm 0.05. \tag{4}$$

Here ν corresponds to the correlation length exponent [2]

$$\xi \sim |c - c_p|^{-\nu}. \tag{5}$$

These values are, within the error bars, the same for all $a=1,\ldots,45$ and agree with those found by Vanderwalle *et al.* [12] Also Nakamura [13] found $\nu_j = 1.0 \pm 0.1$ for RSA of square blocks. It seems therefore that the exponents ν are good candidates for universal quantities.

Examples of spatial arrangements of shorter ($a=5$) and longer ($a=20$) needles on a lattice 100×100 are shown in Figs. 3 (percolation) and 9 (jamming). Analysis based on examination of different runs shows some regularity in the needles distribution—we have found that the needles near the edges have the tendency to stick along the borders. Longer needles, for obvious reasons, form clusters of parallel alignment, as was already observed in Ref. [12].

IV. CONCLUSIONS

We have performed extensive simulations of RSA using linear segments of size $a=1,\ldots,45$ on square lattice sites. We have found that the percolation threshold is a nonmonotonic function of a, having a minimum due to parallel orientation of the needles, at $a=13$, while the jamming threshold decreases to a nonzero constant with a as a power law. The ratio of the two thresholds is nonmonotonic too—after initial growth it stabilizes for some values of a, and then it grows logarithmically. Whether the asymptotic value is equal to one or less is an interesting question. To answer it unequivocally is unfortunately beyond our computing power. The values of the correlation length exponent ν, for percolation, jamming thresholds, and the ratio of the two, do not depend on the length of the needles and they are, within the error bars, equal to those found elsewhere [12,13] for deposition of needles, rectangles, or squares.

ACKNOWLEDGMENTS

The authors are grateful to M. Droz, J. O. Indekeu, Z. Koza, and N. Vandewalle for helpful comments.

[1] S.R. Broadbent and J.M. Hammersley, Cambridge Philos. Soc. **53**, 629 (1957).
[2] D. Stauffer, Physica A **242**, 1 (1997); D. Stauffer and A. Aharony, *Introduction to Percolation Theory* (Taylor and Francis, London, 1994).
[3] J.W. Evans, Rev. Mod. Phys. **65**, 1281 (1993).
[4] R.D. Vigil and R.M. Ziff, J. Chem. Phys. **91**, 2599 (1989).
[5] A.C. Balazs and I.R. Epstein, Biopolymers **23**, 1249 (1984).
[6] E.A. Boucher, Trans. Faraday Soc. **69**, 1839 (1973).
[7] J.J. Ramsden, Phys. Rev. Lett. **71**, 295 (1993).
[8] L. Finegold and J.T. Donnell, Nature (London) **278**, 443 (1979)
[9] P.J. Flory, Proc. R. Soc. London, Ser. A **234**, 73 (1956).
[10] H. Weber, W. Paul, and K. Binder, Phys. Rev. E **59**, 2168 (1999).
[11] C. Domb, E. Stoll, and T. Schneider, Contemp. Phys. **21**, 577 (1980).
[12] N. Vanderwalle, S. Galam, and M. Kramer, Eur. Phys. J. B **14**, 407 (2000).
[13] M. Nakamura, J. Phys. A **19**, 2345 (1986).

Percolation and jamming in random bond deposition

Grzegorz Kondrat and Andrzej Pękalski
Institute of Theoretical Physics, University of Wrocław, pl. M. Borna 9, 50-204 Wrocław, Poland
(Received 15 June 2001; published 24 October 2001)

A model is presented in which on the bonds of a square lattice linear segments (''needles'') of a constant length a are randomly placed. We investigate the dependence of the percolation and jamming thresholds on the length of the needles. The difference from the standard site deposition problem is demonstrated. We show that the system undergoes a transition at $a=6$. When shorter needles are used, the system first becomes percolating before becoming jammed. For longer needles the lattice becomes jammed but there is no percolation. We present evidence that the transition is due to different clustering of the short and long needles. We also determine the Fisher exponent, obtaining the same value as for standard two-dimensional percolation .

DOI: 10.1103/PhysRevE.64.056118 PACS number(s): 64.60.Ak, 05.40.−a

I. INTRODUCTION

Recently there has been much theoretical and experimental interest in random sequential adsorption (RSA) models. In this approach finite objects are randomly deposited, one by one, onto an initially empty substrate (e.g., a lattice or a continuous surface), and are adsorbed if there is no overlapping with previously adsorbed objects. These kinds of models have a wide range of applications in physics, chemistry, biology, etc. for describing processes in which microscopical steps are irreversible.

A large group of RSA problems was motivated by the study of kinetics of some chemical reactions, e.g., simple cyclization reactions (see Ref. [1], in which the RSA approach itself originates), irreversible dissociation from polymer chains [2], and the binding of large ligands to polymer chains [3]. Another area of applicability is the desorption of large molecules like proteins on solid surfaces [4] or macromolecules on biological membranes [5]. Many properties of growth processes in three-dimensional solid state physics [6] are well described by the RSA approach as well. Also some ecological [7] and sociological problems [8] were successfully solved using RSA. For an extensive overview of the field, see Ref. [9].

In the context of RSA the notion of jamming is very important. A system reaches a jamming point if no more objects can be adsorbed due to the lack of available space. The jamming threshold c_j is then defined as a fraction of occupied surface at that moment.

The problem of percolation is an old one [10], but there are still new results and new questions being posed [11,12]. In a standard formulaton on a d-dimensional lattice each site can be occupied with a probability c (or empty with a probability $1-c$). Neighboring occupied sites form a cluster. The cluster is said to be percolating if it reaches two opposite edges of the lattice (e.g., the top and bottom). The lowest concentration of occupied sites for which there is a percolating cluster for an infinite lattice limit is called the percolation threshold c_p [11].

There are many applications of percolation theory, especially in spatially disordered systems, porous media and critical phenomena. For an overview see, e.g., Ref [13].

Apart from the relatively well known case of the RSA of spheres (modelling, e.g., adsorption of spherical molecules [4]) there is an interesting domain of the study of RSA of rectangles or line segments. These models can be used in describing the characteristics of composites or materials made in the process of adsorption of rodlike polymers or conducting needles [14]. In these models (both continuous and discrete) the central point of interest is often the kinetics of the process. However, here we concentrate on the dependence of thresholds on the length ratio a of adsorbed objects (rectangles). As the continuous approach differs in some predictions from the lattice site one [e.g., the jamming threshold $c_j(a)\to 0$ as $a\to\infty$ for the continuous case [15] and $c_j(a)\to c_j^*\neq 0$ for the discrete case [16]], there are also features that distinguish between the site and bond formulation of the discrete (lattice) problem. To the best of our knowledge a needles' adsorption on bonds has never been considered in the literature.

II. MODEL

Here we investigate a system in which linear segments (''needles'') of length a are randomly placed on the bonds of the square lattice. The needles may touch but they cannot cross each other or have a common bond. At each step of the simulation we randomly generate (from uniform distribution) the position and orientation of the needle to be inserted. If there is no possibility of depositing the needle, we discard it and go on to the next step. The essential difference between the site deposition investigated, e.g., in Refs. [16,17] and the present study is that now the two closest parallel needles themselves do not touch— a connecting path is realized only by vertical and horizontal needles touching somewhere on their length. As before [16], we use hard boundary conditions, meaning that no part of any needle may stick out from the lattice. We have verified that allowing for open boundary conditions does not alter the results.

We investigate two phenomena, percolation and jamming. The percolation threshold is defined as a concentration c_p of needles at which there is an uninterrupted path, following the bonds occupied by the needles, from the top to the bottom of the lattice [11]. The smallest possible length of the needles, $a=1$, corresponds to the standard bond percolation, for which we recover the well-known result $c_p=0.5$ [11]. The

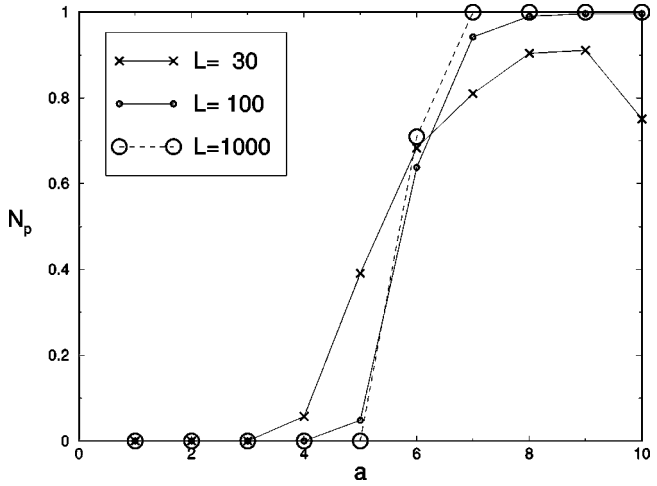

FIG. 1. Probability N_p for the absence of percolation in the system vs needle length $a=1\ldots6$ for lattice sizes $L=30$, 100, and 1000, averaged over 1000 samples.

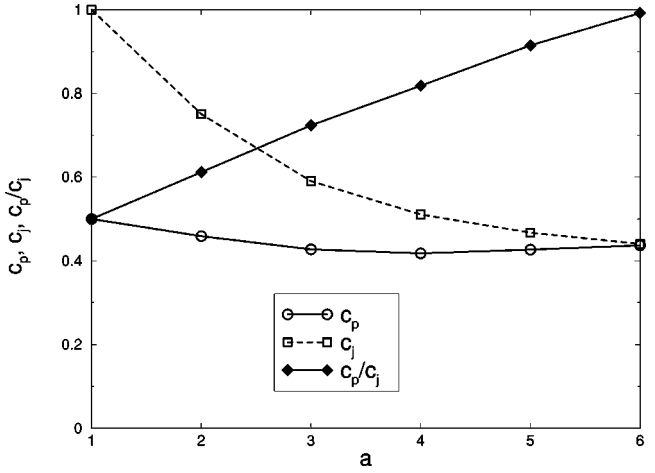

FIG. 2. Thresholds for percolation c_p, jamming c_j, and their ratio c_p/c_j for $a=1\ldots6$. The lattice size is $L=1000$, averaged over 100 samples.

jamming threshold is defined as a concentration c_j of needles, above which it is impossible to add another needle of a given length to the lattice [9].

We shall study, using Monte Carlo simulations, the dependence of the two thresholds and their ratio on the length a of the needles. We shall also compare the results with those obtained for site percolation and jamming [16]. Most of the results were found for a $L=1000$ square lattice (although smaller and larger lattices, $L=30$, 100, 300, and 3000, were also considered) and averaged over 100 independent runs. We have checked that the statistics is not much improved by averaging over 1000 runs.

III. RESULTS

We have found that percolation in the system sets in only for short needles with $a\leqslant a^*=6$. In the case of longer needles no percolating cluster exists for large enough lattices (e.g., out of 1000 samples for $a=7$, only two percolate on a 300×300 lattice, but none on a 1000×1000 lattice). The longer the needles, the higher the chance of absence of percolation (jamming sets in in the system first). This probability is drawn in Fig. 1 against the needle length. The transition from a percolating to a nonpercolating system occurs at a rather narrow range of the needle length. Asymptotically ($L\rightarrow\infty$) we expect a step function. A possible explanation for the existence of a nonpercolating regime is discussed further. This behavior distinguishes between the bond problem and the site one, since in the latter we can always reach percolation threshold for all needle lengths [16]. The absence of percolation was reported earlier in a different context and for the site problem; see, e.g., Ref. [18] in the case of the RSA of squares, or a more general model [19] of RSA of rectangles, both on site square lattices.

The variation of the percolation threshold c_p with increasing needle length a is shown in Fig. 2 (we consider only $a\leqslant6$, since above this point there is no percolation). The uncertainties of the c_p are below 0.004; therefore, we are convinced that there is a minimum for $a=a_{min}=4$. As there was a similar minimum for the site problem (see Ref. [15]), for longer needles ($a_{min}=13$), we expect the same mechanism to be responsible for both phenomena. For longer needles there is a competition between enlarging the range of connection and the increasing difficulty in restoring connection (for details, see Ref. [16]). For $a\geqslant6$, however, it is so difficult for one needle to become connected to others that percolation does not appear. The difference between sites and bonds here is crucial. In the site problem two close parallel needles can be connected via other parallel needles lying in between them. In a bond problem, however, even the two closest parallel needles remain disconnected unless they both touch the same perpendicular needle. Thus we suppose that for long needles small clusters work as shields, preventing the formation of a connected network of bonds in the system. Another argument supporting our conjecture is found by a direct inspection of snapshots of the needle arrangement, an example of which can be seen in Fig. 3. The state of a system of needles with $a=8$ at the jamming point is shown there.

In order to obtain some more insight into the problem, we have also examined the cluster structure of the system at jamming, when no more needles can be added. As we can see in Fig. 4, there is a clear change in the shape for $a=6$. For small a most of the mass carried by the needles constitutes a large percolating cluster. For long needles more and more mass is accumulated in very small clusters, especially in single isolated needles. That is, 2.5% of the total mass is concentrated in such needles for $a=4$, and 16.5% for $a=7$.

To establish a connection between our model and other percolation critical phenomena we have verified the so called Fisher law [11]. It is generally observed that, for percolation models the cluster size distribution function measured at the percolation point follows a power law

$$n_s(c_p)\propto s^{-\tau},$$

where the Fisher exponent is equal [13] to

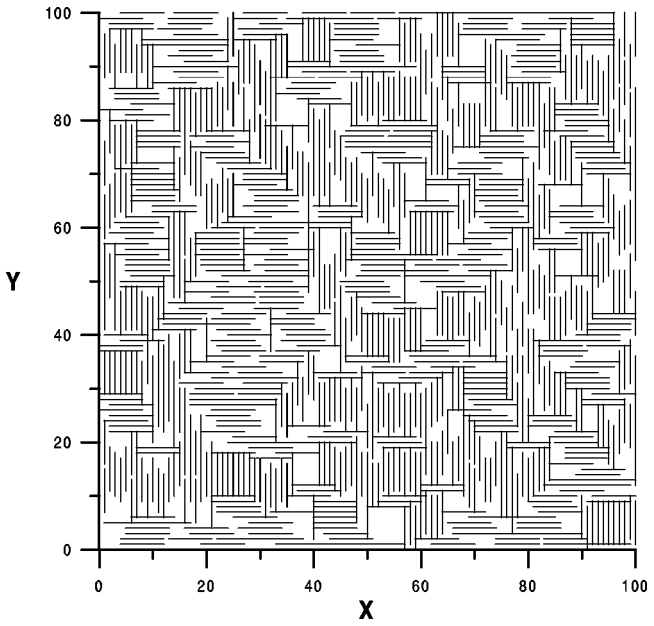

FIG. 3. Snapshot of a spatial distribution of needles at the jamming threshold for $L=100$. The needle length is $a=8$; therefore, no percolation appears.

$$\tau = \frac{187}{91} \approx 2.055,$$

and is a universal quantity throughout many two-dimensional (2D) models. The results of our investigations are presented in Fig. 5, where size distribution functions for clusters at percolation are ploted on a log-log graph for various needle lengths. Averaged over 100 samples on a 1000×1000 lattice, ''experimental'' points follow straight lines with the same slope for all $a=1\ldots6$, determined to be $-\tau=-2.02\pm0.04$. Thus our model ($a>1$) manifests the same characteristic as in standard 2D percolation ($a=1$).

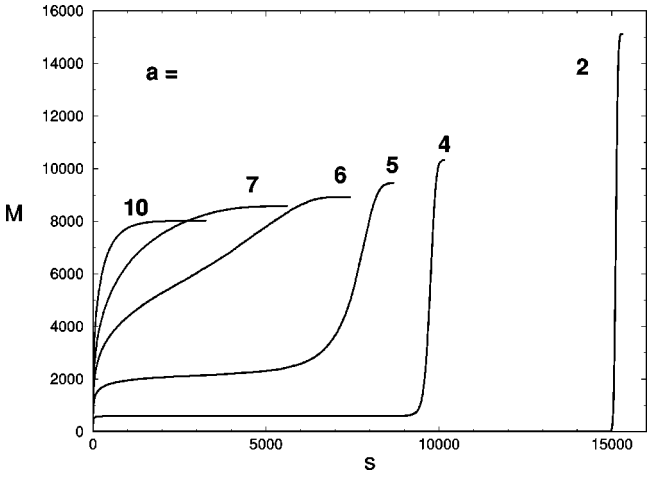

FIG. 4. Plot of $M(s)$, the number of unit bonds in clusters not larger than s vs s, measured at the jamming point. The lattice size is $L=100$, averaged over 10 000 samples. The needle lengths are $a=2$, 4, 5, 6, 7, and 10.

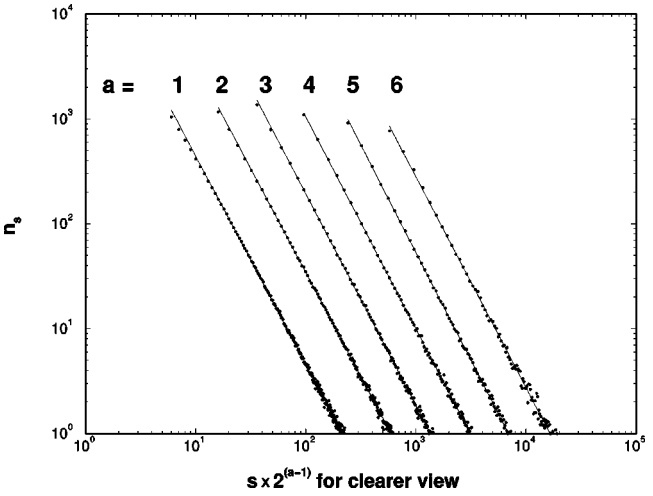

FIG. 5. Cluster size distribution functions n_s for $a=1\ldots6$ at the percolation point, averaged over 100 samples; $L=1000$. Data sets for each a are separated by a factor of 2 for clarity.

Let us now analyze the jamming threshold c_j as a function of the needle length a. It appears that points conform to the following formula with very high accuracy (see Fig. 6):

$$c_j(a) - c_j^* \propto a^{\Delta},$$

where $c_j^*=0.3350\pm0.0025$ and $\Delta=-1.05\pm0.10$ (uncertainties are obtained from graph analysis for various trial values of c_j^* and Δ). The same kind of dependence was found for the site RSA of needles [16], but with $c_j^*(\text{sites})=0.66\pm0.01$. Let us compare the jammed state for both lattices (bonds and sites), especially for very long needles. In both cases needles tend to form domains of parallel alignement, the interdomain space being relatively empty. In domains for sites almost all sites are occupied, but for bonds about 50% of bonds are perpendicular to the needles and are empty. This explains the relation $c_j^*(\text{sites})=2c_j^*(\text{bonds})$.

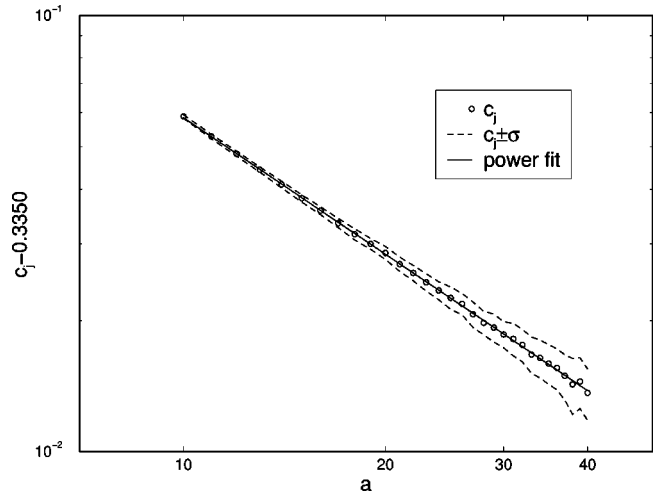

FIG. 6. Power law approach of the $a=\infty$ limit for the jamming threshold. Lattice $L=1000$, averaged over 100 samples, $a=10\ldots40$. A mean standard deviation σ (dotted lines) is also shown.

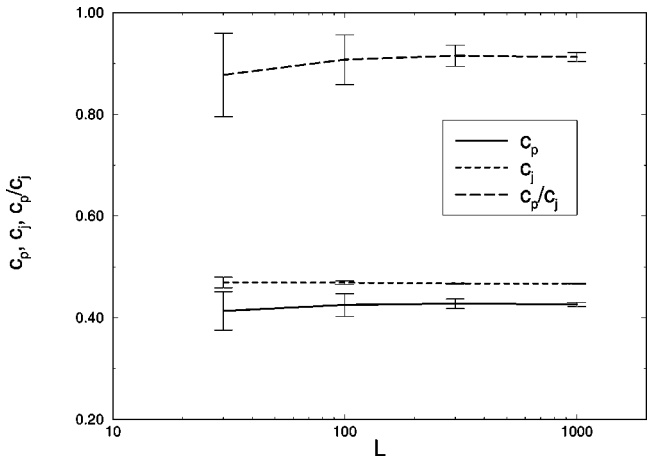

FIG. 7. Convergence analysis. The values of the thresholds c_p, c_j, and c_p/c_j are plotted with error bars against the lattice size L. Here $a=5$, and averaging is over 100 samples.

It should be noted that there were estimates for c_j^*(sites) only (also see Ref. [17]). The dependence of c_j on a is quite different for continuous models of RSA of rectangles (see, e.g., Ref. [15] or [20]): $c_j(a) \propto a^{\Delta}$ with $\Delta=-0.2$ [20] or $\Delta=-0.26$ [15], the threshold tending to zero as $a\to\infty$.

Having determined c_p and c_j we can look at their ratio c_p/c_j carrying some information about the structure of the system (see Fig. 2). One can easily see that c_p/c_j is almost linear with a. Finally, we analyzed the convergence of the thresholds as L tends to infinity. It appears that for $L/a>15$ the values of c_p and c_j do not vary much with increasing L (keeping a constant) while the mean standard deviation σ drops significantly. Thus it is safe to cosider the values of the thresholds obtained for $L=1000$ as the asymptotic (exact) ones—see Fig. 7.

IV. CONCLUSIONS

We have investigated the random deposition of linear segments on the bonds of a square lattice. As in the case investigated earlier [16], we have found a minimum in the percolation threshold dependence on the length of the deposited objects. We believe that the same mechanism is responsible for both results. Unlike the site case, here, for needles longer than $a=6$, the system cannot reach the percolation threshold, since it becomes jammed first. The ratio of the two thresholds shows (till $a=6$) a linear behavior. For the Fisher exponent we obtained the same value as for the standard ($a=1$) 2D percolation problem, which suggests the same universality class.

[1] P.J. Flory, J. Am. Chem. Soc. **61**, 1518 (1939).
[2] A.C. Balazs and I.R. Epstein, Biopolymers **23**, 1249 (1984).
[3] I.R. Epstein, Biophys. Chem. **8**, 327 (1978).
[4] J.J. Ramsden, Phys. Rev. Lett. **71**, 295 (1993).
[5] L. Finegold, and J.T. Donnell, Nature (London) **278**, 443 (1979).
[6] J.W. Evans, D.E. Sanders, P.A. Thiel, and A.E. DePristo, Phys. Rev. B **41**, 5410 (1990).
[7] M. Hasegawa and M. Tanemura, in *Recent Developements in Statistical Interference and Data Analysis*, edited by K. Matusita (North-Holland, Amsterdam 1980).
[8] Y. Itoh and S. Ueda, Ann. Inst. Stat. Math. **31**, 157 (1979).
[9] J.W. Evans, Rev. Mod. Phys. **65**, 1281 (1993).
[10] S.R. Broadbent and J.M. Hammersley, Proc. Cambridge Philos. Soc. **53**, 629 (1957).
[11] D. Stauffer, Physica A **242**, 1 (1997); D. Stauffer and A. Aharony, *Introduction to Percolation Theory* (Taylor & Francis, London, 1994).
[12] J. Kertész, B.K. Chakrabanti, and J.A.M.S. Duarte, J. Phys. A **15**, L13 (1982).
[13] M.B. Isichenko, Rev. Mod. Phys. **64**, 961 (1992).
[14] F. Carmona, F. Barreau, F. Delhaes, and R. Canet J. Phys. (France) Lett. **41**, L534 (1980).
[15] P. Viot, G. Tarjus, S.M. Ricci, and J. Talbot, Physica A **191**, 248 (1992).
[16] G. Kondrat, and A. Pękalski, Phys. Rev. E **63**, 051108 (2001).
[17] B. Bonnier, M. Hontebeyrie, Y. Leroyer, C. Meyers, and E. Pommiers, Phys. Rev. E **49**, 305 (1994).
[18] M. Nakamura, Phys. Rev. A **36**, 2384 (1987).
[19] M. Porto, H.E. Roman, Phys. Rev. E **62**, 100 (2000).
[20] R.D. Vigil, and R.M. Ziff, J. Chem. Phys. **91**, 2599 (1989).

Influence of temperature on percolation in a simple model of flexible chains adsorption

Grzegorz Kondrat
Institute of Theoretical Physics, University of Wroclaw, pl. M. Borna 9, 50-204 Wroclaw, Poland

(Received 5 April 2002; accepted 17 July 2002)

We study random sequential adsorption of flexible chains onto a two-dimensional lattice by computer Monte Carlo simulations. The flexibility of chains is controlled by the temperature of the solution via the Boltzmann factor. We investigate the percolation threshold in the system as a function of chain length and temperature. Several temperature regimes are identified, and respective characteristic types of behavior of the system are discussed. Especially, nonmonotonicity of percolation threshold is observed—there appears a characteristic temperature unique for all chain lengths for which the percolation threshold attains its minimum. © *2002 American Institute of Physics.* [DOI: 10.1063/1.1505866]

I. INTRODUCTION

Recently, there has been still much theoretical and experimental interest in random sequential adsorption (RSA) models. This approach originates from the work of Flory,[1] who studied a cyclization reaction in the polymer chain in which adjacent pendant groups randomly link. In general, in RSA-type models[2–7] we consider objects (e.g., atoms, molecules, or circles, rectangles, ellipsoids, lattice sites, lattice animals) that attach to some substrate (e.g., polymer chain, solid surface, biological membrane or lattice, continuum plane) one by one (sequentially) at a random position provided that there is no overlapping with previously adsorbed objects. Once an object is attached, it will neither move nor desorb back to the solution.

The RSA model finds many application in various fields of physics and chemistry, especially where one deals with irreversible processes. Among important applications are reactions on one-dimensional (1D) polymer chains,[8] chemisorption,[9] adsorption of proteins on solid surfaces,[10] or growth processes in 3D solid-state physics.[11,12] Also, there are models in which objects after being adsorbed are allowed to diffuse on the surface.[13,14] For an extensive overview of the field, see Refs. 15 and 16.

The problem of percolation is an old one,[17] but there are still many questions to be answered.[18] In the simplest formulation on a lattice each site is occupied with probability p (or empty with probability $1-p$). As p increases from 0, occupied sites form clusters (a cluster is a set of occupied sites that are connected via a nearest-neighbor relation). At some threshold concentration c_p of occupied sites there appears a percolating cluster that spans the whole system. There are many applications of percolation theory in physics and chemistry, especially in disordered systems, porous media, and critical phenomena. As percolation is the simplest nontrivial model of phase transitions, it is widely used in describing transition phenomena (e.g., gelation): see, e.g., Ref. 19.

Adsorption and percolation of extended objects belong to standard tools extensively used these days in physics, especially in the quickly evolving area of polymer science. There are many models dealing with conformational changes of polymers due to the presence of an adsorbing surface.[20–24] The behavior of the system is highly influenced by the chain flexibility (or stiffness).[23,25] Also, connectivity plays an important role in the analysis of phase transitions in polymer models.[26,27]

Studying systems of extended flexible objects like polymers from the percolation point of view seems interesting for several reasons. In polymer phase transitions both (temperature-dependent) flexibility of the chains[28] and the percolative character of transitions[29] are important factors being discussed. In physics of colloids[30] and especially in gelation phenomena[31] the basic concept is the emergence of percolation in the system. When adsorbed onto surfaces polymers create some interesting structures[23,32] that can be also analyzed from the percolation point of view. Percolation of perfectly stiff chains (rods) is studied[33,34] in the context of conductivity, where it has applications in material science. The nontrivial effect of relaxing this stiffness condition may be important in studying some composites made from, e.g., semiflexible fibers. This approach may also be useful in investigating the conductivity of materials consisting of tiny metallic structures of various shapes or conducting polymers.[35]

In our paper we analyze the process of adsorbing flexible chains (which can model, e.g., polymers) from a solution onto a solid surface using computer Monte Carlo simulations. We concentrate here on the percolative characteristics of the system and their dependence on temperature, which controls the chain flexibility. Even though our model is relatively simple, it presents a rich behavior that is discussed in detail. The model extends our previous approach[36] in which stiff chains (linear sticks) were considered only.

The organization of the paper is following: Section II describes the model in detail. In Sec. III results of simulations are presented and discussed. Section IV contains the concluding remarks.

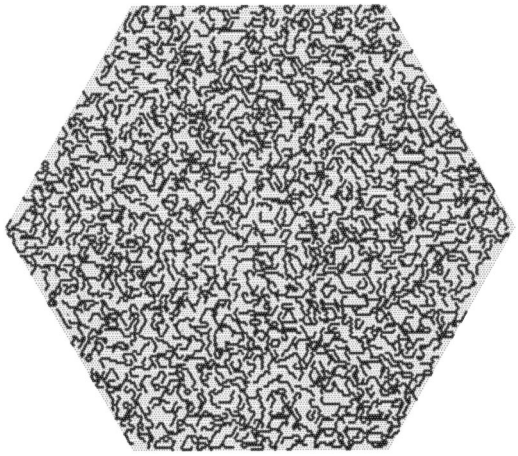

FIG. 1. Snapshot of the system at the end of a simulation (an example). Lattice size $L=100$, chains length $a=10$, and temperature $T=25$.

II. MODEL

Our model describes the process of adsorbing large complex objects (e.g., polymers) onto a solid surface from a solution irreversibly. Within the framework of random sequential adsorption onto the lattice we investigate the percolation characteristics of the system. Namely, we find the dependence of the percolation threshold on the adsorbed object sizes. In this model, which is an extension of the previous model dealing with hard rod (needles) RSA (see Refs. 36 and 37), we investigate the role that chain flexibility and temperature of the solution play in the behavior of the system.

We will be working on a triangular lattice with a marked hexagonal of side size L on it. In a single simulation we perform a number of adsorption trials, each consisting of trying to put a single chain of given length a onto the initially empty hexagonal according to the following rules.

As a chain of size a, we understand a set of a sites of the lattice that are connected by a broken line composed of segments of unit length (i.e., lattice constant). Two adsorbed chains cannot overlap at any point (hard core interaction between the chains), nor can any chain stick out of our hexagonal (hard boundary conditions). We choose a place to start on putting a chain at random. If it is previously occupied, we reject the trial: otherwise, we continue in trying to adsorb consecutive monomers of a given chain. If overlapping occurs at any stage of the process, we reject the whole trial: otherwise, we put the chain onto the lattice and it will remain there forever. We check concurrently with adsorbing the chains whether percolation sets in. Namely, we look for the moment where there appears for the first time a continuous path (a path consisting of nearest neighbors) composed of sites occupied by monomers of adsorbed chains only, which connects two opposite edges of our hexagonal (say, the upper and lower sides). At that moment we find the filling factor—i.e., the ratio of the number of adsorbed monomers to the total number of sites in our hexagonal.

For given chain length a we perform N simulations, each until percolation appears. An example of a chain configuration in the system at the end of a simulation is shown in Fig. 1. We take then the average of the filling factor, approaching now the percolation threshold c_p for a given lattice size L. As L increases to infinity, the results become closer and closer to the exact value of the percolation threshold for an infinite lattice.

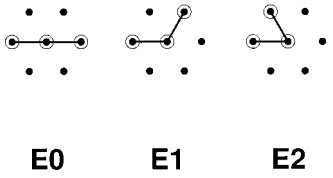

FIG. 2. Possible bendings and their energies.

In order to introduce flexibility of chains into the model (nonflexible straight chains—needles—were studied in detail in Refs. 36 and 37) and let it vary with the temperature of the solution, we invented the following approach.

We assume that monomers interact between themselves via radial force with potential energy $V(\mathbf{r})$. The interaction is restricted only to the monomers that belong to the same chain and are close together (nearest neighbors in the chain or separated at most by one monomer). Then we can attribute to each chain shape (or conformation) a unique potential energy, being the sum of pairwise interaction energies between the monomers. Because we consider the process of adsorbing chains from the solution that is in equilibrium, it is reasonable to claim that the relative probability of coming across a chain of given shape is proportional to the Boltzmann factor $\exp(-E/T)$, where E is total conformation energy and T is the temperature, both measured in the same arbitrary units. As the distance between two consecutive monomers in a chain is always equal to the lattice constant, their contribution to the probability distribution of shapes cancels out. Thus that part of the interaction that matters is the one between next nearest neighbors in a chain—in other words, angles between bonds in a broken line making a chain are only important.

For the sake of simplicity we take here the plain Coulomb potential $V(\mathbf{r})=-c/r$ with some constant c (in fact, the absolute value of this constant cancels out as we have some freedom in rescaling temperature and choosing the lowest-energy level). In the case of a triangular lattice there are only three possible values for bending angles: $\alpha_0=180°$, $\alpha_1=120°$, and $\alpha_2=60°$. Adopting the aforementioned choice of potential (Coulomb repulsion) and rescaling energy-temperature axis to obtain values in the interval $[0,100]$ we arrive at energies corresponding to the angles α_0, α_1, and α_2 equal to $E_0=0$, $E_1=15$, and $E_2=100$, respectively (see Fig. 2). In the zero-temperature limit one can find 0-type bonds only—all chains are straight needles.[36,37] On the other extreme ($T\to\infty$) the model reduces to the self-avoiding random walk approach.[5,24,38] As we can see further, really interesting is some finite-temperature interval, where we can observe some kind of phase transition in the system.

Let us now make a comment on our numerical routine for randomly choosing appropriate chain shapes. At the start we take randomly the position of the first monomer and, randomly, one direction (out of six possible) pointing to the next monomer. If any of them is previously occupied, we

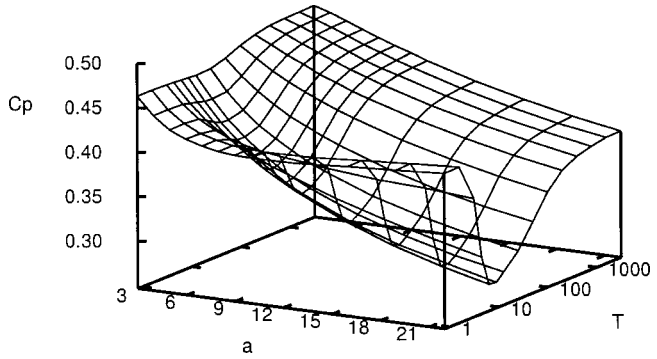

FIG. 3. Percolation threshold c_p as a function of chain length a and temperature T. Lattice size $L=1000$, averaged over $N=100$ samples.

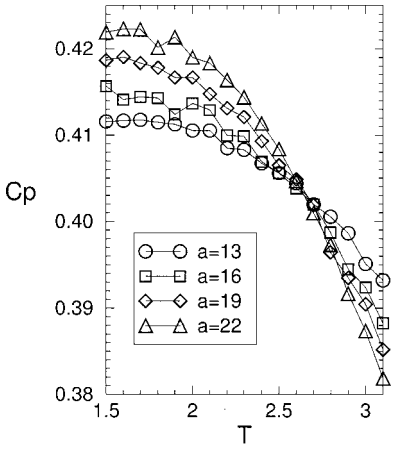

FIG. 4. Behavior of c_p near temperature T_1.

will discard that choice and try again. Otherwise, we choose from the set of five possible bending angles ($-60°$, $-120°$, $\pm 180°$, $+120°$, $+60°$), one according to the probability distribution implied by the Boltzmann factor. This gives the position of the next monomer to be adsorbed. Then we repeat the last step until either all a positions for monomers are empty (so our trial has succeeded and we put the whole chain onto the lattice) or any of them proved to be occupied (and we discard the trial and start again).

There is also another approach—one chooses the position of the next monomer from the set of empty neighbors of the current monomer, which is definitely cheaper with respect to simulation time. Within our model, however, we work with chains that, having one shape, they do not change it. A given chain either fits to the local configuration of empty sites or not, but it does not adjust its shape to a void. This is the case in quick adsorption phenomena, where the time of adsorption of a single chain is much shorter than the time scale of conformational changes.

It could also be possible to use the standard Metropolis algorithm[39] for generating equilibrium configurations of a chain instead of our approach, but giving the same equilibrium probability distributions, it would cost only more computer time.

One could consider in the interaction pairs of monomers farther along the chain than next nearest neighbor. Apart from increasing the computing time and complexity of our program (the need for the Metropolis approach) the only gain we suspect would be possibly some quantitative corrections, like temperature rescaling. It is due to the fact that there is a high correlation between the energy of a chain counted up to next nearest neighbor (as we do here) and one counted over all pairs in the chain.

III. RESULTS

We performed an averaging over a number $N=100$ simulations for each choice of parameters (i.e., the temperature T, the chains length a, and the lattice size L). The analysis of convergence and mean standard deviation proved that the percolation threshold c_p obtained for $L=1000$ can be safely considered as the asymptotic one ($L\to\infty$). Thus we present our results for $L=1000$, which are collected in Fig. 3. We dealt with chain lengths from $a=3$ (for $a=1$ and $a=2$ there is no flexibility—just the known case of monomers and dimers[15,18,36]) up to $a=22$ (for longer chains simulation time grows significantly). We took simulations mainly for temperatures of powers of 2 (up to a constant) in order to cover several orders of magnitude. We choose the limits in such a way that below the lowest temperature investigated, $T_l=0.781\,25=100/2^7$, and above the highest, $T_h=12\,800=100\times 2^7$, nothing interesting happens in the system apparently.

There are several kinds of characteristic behavior in our system for different temperatures. For a temperature small enough ($T\leqslant T_1$) percolation is insensitive to temperature changes. As T approaches temperature T_2, the function $c_p(a)$ becomes flat. For medium temperatures percolation drops to a minimum attained at temperature T_3 unique for all chain lengths. This nonmonotonic behavior of c_p is a novel feature in percolation models. Above T_3 the threshold c_p grows monotonically up to an infinite-temperature limit $c_p(a,T=\infty)$.

For $T\leqslant T_1$ (cold regime) we have the same behavior as described in Ref. 36 for straight needles on a square lattice. In both cases c_p as a function of a attains a minimum. Its existence can be understood in terms of the balance between two mechanisms leading into opposing directions: a decrease of c_p due to increasing of connection range for longer chains and an increase of c_p due to blocking induced by parallel close needles (for details, see Ref. 36). Here a minimum is obtained at $a=10$ instead of $a=13$ in Ref. 36—we attribute this difference to the underlying lattice difference (in Ref. 36 we worked on a square lattice). For low temperatures there are very few bendings in a chain (e.g., for $T\leqslant T_1$ we can expect less than 1.5% of bending angles other than $\alpha_0=180°$) and these do not interfere with the process of percolating cluster formation. At temperature T_1 things start changing. In Fig. 4 we demonstrate $c_p(T)$ for various chain lengths and from the graph we estimate $T_1=2.0\pm 0.2$.

Above temperature T_1 the function $c_p(a)$ starts losing its minimum. For $T=T_2=2.65\pm 0.05$ the threshold becomes constant: $c_p\approx 0.403\pm 0.002$ for longer chains ($a>10$)—see Fig. 4. Increasing the temperature further, c_p becomes a monotonically decreasing function. The reason for this is that

the blocking mechanism no longer works in the system, since chains have more bent shapes and there are more and more possibilities of making a connection between chains. Finally, $c_p(a,T)$, as a function of temperature T, has a minimum at $T \approx T_3 = 7.5$ for all a, so chains connect most easily. Let us note that T_3 is of order of magnitude of E_1—at these energies bending angles of the first kind ($\alpha_1 = 120°$) start to appear widely in the system, while those of the second type ($\alpha_2 = 60°$) are still exceptional (less frequent than $10^{-2}\%$). These minimum phenomena can be explained in terms of an increasing variety of shapes (due to the abundance of first-type bending angles) while still keeping a large extension of the chain. It is also worth mentioning that the minimal value of c_p lies well below the percolation threshold for the ''pure system,'' for which only one type of bending angle is allowed: either 0-type or 1-type (not to say about 2-type, for which c_p is very large). As chains are longer, the discussed effects are more pronounced.

When the temperature grows further, second-type bending angles will appear more frequently and, since they are less suitable for making connections (they cause more compact shapes of the chains), the percolation threshold grows with temperature. For high temperature ($T \gg E$) the system saturates since all Boltzmann factors are very close to unity. The approach to $c_p(a, T \to \infty)$ is roughly a power law: $c_p(a, T=\infty) - c_p(a,T) \propto 1/T$.

During our simulations for each temperature, we also record the mean conformation energy per one adsorbed chain (ME) and we compare it to the mean conformation energy of a solitary chain adsorbed onto an empty lattice ($\mathrm{ME}_{\mathrm{solitary}}$). Those two quantities relate to the true mean energies of the adsorbed surface layer and the solution, respectively. It appears that generally they coinside for all temperatures and chain lengths except for the low-temperature regime. In this case, however ($T<6$), we observe that the adsorbed layer is significantly colder (i.e., has lower energy) than the solution itself. For $T=1.5625$ and $a=22$ we have, for example, $\mathrm{ME}/\mathrm{ME}_{\mathrm{solitary}} = 0.6$. As at these low temperatures chains are mainly linear, so are the holes between closely parallel adsorbed chains. If there appears a chain from the solution that is bent (it sometimes happens for these temperatures), it will likely be rejected (returned to the solution) because it will hardly fit to the linear void. So in our process of adsorption we deal with a kind of filtering—accepted are preferably straight chains which have a lower energy. We found that this phenomenon is again more apparent for longer chains [e.g., $\mathrm{ME}/\mathrm{ME}_{\mathrm{solitary}} = 0.9$ for $T=1.5625$ (as above), but for $a=8$].

As we are convinced that all discussed effects are not just manifestation of a given choice of the lattice, but are of a more general nature, so it would be interesting to compare these results with similar simulations on other lattices. We have performed extensive simulations of a square lattice version of our model. It appeared that the whole landscape of the percolation behavior $c_p(a,T)$ is exactly reproduced on a square lattice. Even the ratio of the characteristic temperatures of the model is the same: $T_1(\mathrm{tri}):T_2(\mathrm{tri}):T_3(\mathrm{tri}) = T_1(\mathrm{sqr}):T_2(\mathrm{sqr}):T_3(\mathrm{sqr})$. Thus the character of discussed phenomena is rather independent of underlying lattice.

Another quantity that is often discussed in RSA-type models is a jamming threshold c_j. It is defined as the final concentration of occupied sites (adsorbed monomers) at the moment when no more objects can be inserted onto the lattice. We have investigated within our model the threshold c_j as a function of the chain length and temperature. It appears that $c_j(a=\mathrm{const},T)$ is insensitive to the temperature changes and drops slowly as the chain length a increases. Thus from a final mass of our adsorbate one can only derive the chain length and not the temperature of the solution.

IV. CONCLUSIONS

In this paper we discussed temperature behavior of the percolation threshold of the system of adsorbed flexible chains. For the cold regime system characteristics coincide with those of straight needles.[36] At moderate temperatures c_p drops significantly, attains a minimum at $T=T_3$, and for high temperatures c_p quickly approaches the infinite-temperature limit self avoiding random walk (SARW case). In our model we assumed some simplifications; e.g., we restricted the interaction between the monomers only up to the second nearest neighbor and we neglected interchain interactions other than hard core. It might be interesting to study more realistic variations of our model, but it seems to us that the overall types of system behavior would not change in that case. Our model could find applications in the study of the deposition of small conducting objects like conducting polymers or tiny metallic structures of various shapes as well as in investigations of the process of gelation.

ACKNOWLEDGMENTS

The author is grateful to Professor Andrzej Pękalski, Professor Joseph Indekeu, Dr. Jan Fransaer, and Dr. Christian Maes for fruitful discussions and helpful comments, and to Professor Joseph Indekeu for his hospitality during his stay in Belgium. This work is supported by KBN Grant No. 5 P03B 013 21.

[1] P. J. Flory, J. Am. Chem. Soc. **61**, 1518 (1939).
[2] M. D. Khandkar and A. V. Limaye, Phys. Rev. Lett. **84**, 570 (2000).
[3] R. S. Ghaskadvi and M. Dennin, Phys. Rev. E **61**, 1232 (2000).
[4] B. Bonnier, Phys. Rev. E **54**, 974 (1996).
[5] J.-S. Wang and R. B. Pandey, Phys. Rev. Lett. **77**, 1773 (1996).
[6] A. Matsuyama, R. Kishimoto, and T. Kato, J. Chem. Phys. **106**, 6744 (1997).
[7] C. K. Gan and J.-S. Wang, J. Chem. Phys. **108**, 3010 (1998).
[8] A. C. Balazs and I. R. Epstein, Biopolymers **23**, 1249 (1984).
[9] A. Cordoba and J. J. Luque, Phys. Rev. B **31**, 8111 (1985).
[10] J. J. Ramsden, Phys. Rev. Lett. **71**, 295 (1993).
[11] J. W. Evans, D. E. Sanders, P. A. Thiel, and A. E. DePristo, Phys. Rev. B **41**, 5410 (1990).
[12] J. Fransaer, Ph.D. thesis, Katholieke Universiteit Leuven, 1994.
[13] C. Fusco and P. Gallo, J. Chem. Phys. **114**, 7563 (2001).
[14] J. J. Gray, D. H. Klein, R. T. Bonnecaze, and B. A. Korgel, Phys. Rev. Lett. **85**, 4430 (2000).
[15] J. W. Evans, Rev. Mod. Phys. **65**, 1281 (1993).
[16] J. Talbot, G. Tarjus, P. R. Van Tassel, and P. Viot, Colloids Surf., A **165**, 287 (2000).
[17] S. R. Broadbent and J. M. Hammersley, Proc. Cambridge Philos. Soc. **53**, 629 (1957).
[18] D. Stauffer and A. Aharony, *Introduction to Percolation Theory* (Taylor & Francis, London, 1994).
[19] M. B. Isichenko, Rev. Mod. Phys. **64**, 961 (1992).
[20] H. S. Chan, M. R. Wattenbarger, D. F. Evans, V. A. Bloomfield, and K. A. Dill, J. Chem. Phys. **94**, 8542 (1991).

[21] Y. Wang and R. Rajagopalan, J. Chem. Phys. **105**, 696 (1996).
[22] K. Sumithra and A. Baumgaertner, J. Chem. Phys. **109**, 1540 (1998).
[23] S. Stepanov, J. Chem. Phys. **115**, 1565 (2001).
[24] K. De'Bell and T. Lookman, Rev. Mod. Phys. **65**, 87 (1993) and references therein.
[25] J. P. K. Doye, R. P. Sear, and D. Frenkel, J. Chem. Phys. **108**, 2134 (1998).
[26] A. P. Chatterjee, J. Chem. Phys. **113**, 9310 (2000).
[27] N. Sushko, P. van der Schoot, and M. A. J. Michels, J. Chem. Phys. **115**, 7744 (2001).
[28] H. Weber, W. Paul, and K. Binder, Phys. Rev. E **59**, 2168 (1999).
[29] P. D. Gujrati, J. Chem. Phys. **98**, 1613 (1993).
[30] S. A. Safran, I. Webman, and G. S. Grest, Phys. Rev. A **32**, 506 (1985).
[31] A. Coniglio, H. E. Stanley, and W. Klein, Phys. Rev. Lett. **42**, 518 (1979).
[32] L. C. Jia and P.-Y. Lai, J. Chem. Phys. **105**, 11319 (1996).
[33] I. Balberg and N. Binenbaum, Phys. Rev. B **28**, 3799 (1983).
[34] J. Boissonade, F. Barreau, and F. Carmona, J. Phys. A **16**, 2777 (1983).
[35] Å. Johansson and S. Stafström, Phys. Rev. Lett. **86**, 3602 (2001).
[36] G. Kondrat and A. Pękalski, Phys. Rev. E **63**, 051108 (2001).
[37] G. Kondrat and A. Pękalski, Phys. Rev. E **64**, 056118 (2001).
[38] R. J. Rubin, J. Chem. Phys. **43**, 2392 (1965).
[39] N. Metropolis, A. W. Rosenbluth, M. N. Rosenbluth, A. H. Teller, and E. Teller, J. Chem. Phys. **21**, 1087 (1953).

The study of percolation with the presence of impurities

Grzegorz Kondrat[a)]
Institute of Theoretical Physics, University of Wrocław, Plac Maxa Borna 9, 50-204 Wrocław, Poland

(Received 17 June 2004; accepted 1 March 2005; published online 12 May 2005)

We consider the process of percolation cluster formation for pointlike conductors subjected to random sequential adsorption onto two-dimensional lattice by computer Monte Carlo simulations. The initial presence of impurities disturbs this phenomenon significantly and we study here how the size and density of impurity particles affect the resulting percolation threshold. Some unexpected features such as the nonmonotonicity of the percolation threshold as a function of impurity concentration are discussed. © *2005 American Institute of Physics*. [DOI: 10.1063/1.1896358]

I. INTRODUCTION

Even though the problem of percolation[1] is known for years[2] and many papers have dealt with its aspects, still there are interesting questions to be answered. In its simplest formulation on a lattice each site is occupied with probability p (or the site is empty with probability $1-p$). As p increases from 0, occupied sites form clusters (a cluster is a set of occupied sites that are connected via nearest-neighbor bonds). At some threshold concentration c_p of occupied sites, there appears a percolating (infinite) cluster that spans the whole system (i.e., there is a path composed of occupied sites that connects opposite edges of the system). Particularly interesting are models in which percolating clusters are formed from extended objects.[3–10] The percolation theory finds many applications in physics and chemistry, especially in disordered systems, porous media, and critical phenomena. As the simplest nontrivial model of phase transition, percolation is widely used in describing transition phenomena (e.g., gelation) (see Ref. 11).

Random sequential adsorption (RSA) models describe the systems that are characterized by implicit randomness and irreversibility. This approach originates from the work of Flory,[12] who studied a cyclization reaction in the polymer chain in which adjacent pendant groups randomly link. In general in RSA-type models[13–18] we consider objects (e.g., atoms, molecules or circles, rectangles, ellipsoids, lattice sites, lattice animals) that attach to some substrate (e.g., polymer chain, solid surface, biological membrane, continuum plane, or lattice) one by one (sequentially) at random position provided that there is no overlapping with previously adsorbed objects (some models allow this constraint to be relaxed). Once an object is attached, it will neither move nor desorb back to the solution.

There are many applications of RSA models in various fields of physics and chemistry, especially where irreversibility of the phenomena is to be considered. Among important applications are the reactions on one-dimensional (1D) polymer chains,[19] chemisorption,[20] adsorption of proteins on solid surfaces,[21] or growth processes in three-dimensional (3D) solid-state physics.[22,23] Also there are models in which objects after being adsorbed are allowed to diffuse on the surface.[24,25] For an extensive overview of the field see Refs. 26 and 27.

In many cases when one investigates the process of percolation [e.g., formation of a network of chemical bonds (gelation) or making a conductive connection between small grains in composites] the presence of impurities must be considered. This is an important factor in studying various characteristics of composites such as conductivity[8,28,29] and structure[8] as well as in other fields like the investigation of random media.[30]

Here we are interested how the presence of impurities itself disturbs the behavior of the system. There are some contributions to this subject,[31,32] but the different points of view (e.g., fluid theory approach versus RSA) make them inadequate for describing phenomena, like the process of sequential adsorption on precontaminated substrate. To deal with this problem we have developed a computer code simulating the behavior of the system using the Monte Carlo method. We concentrate here on 2D systems with pointlike conductors (each conducting particle occupies a single site of the lattice) and more extended impurities (stick-shaped particles of given length). The discussion of more complex case of extended particles of both kinds (conductors and insulators) goes beyond this paper. In the following sections the details of the model (Sec. II) and results with discussion (Sec. III) are described. Concluding remarks are contained in Sec. IV.

II. MODEL

We want to investigate here the process of forming a percolating cluster with the presence of impurities by performing a series of computer simulations. With the absence of imperfections the process of percolation is relatively well studied.[1,11] In real life, however, there is one additional factor that often must be taken into account: impurities. When the surface of interest (in the current paper a 2D lattice) is not ideal initially, but has defects or is covered with obstacles or contamination, the process of growing clusters and making connections between conducting particles is disturbed. One

[a)]Electronic mail: gkon@ift.uni.wroc.pl

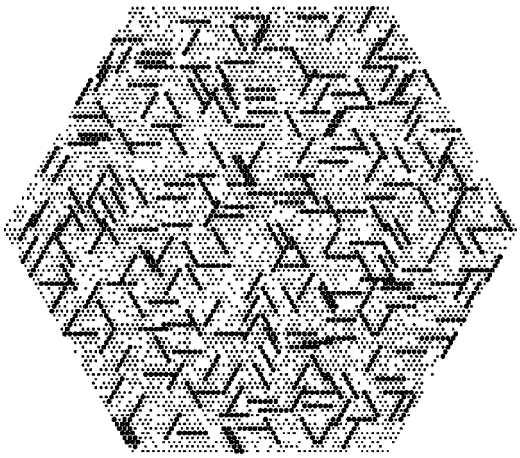

FIG. 1. A typical example of a snapshot of the system at the end of simulation. The size of the insulator particles (full circles) is $ad=6$, its concentration $id=0.2$, and the concentration of conductors (dots) at percolation is $c=0.5572$. The size of the system is $L=50$.

can speak here about either "insulators" or "contaminations," "obstacles," "impurities," etc., depending on the physical context considered.

The simulation setup is as follows. Our surface of interest is modeled on a triangular lattice as a hexagon with sides equal to L lattice constants. Each single computer experiment consists of two steps. Firstly, we cover our sample with particles of impurity up to some concentration id. This concentration is defined as a fraction of sites of the hexagon that are occupied by impurities. Each adsorbed particle of impurity has the shape of a stick consisting of ad consecutive sites ("atoms") in a line. The length ad is the same for all impurity particles in a single simulation. Particles of impurity cannot overlap and their spatial (and orientational) distribution is random with uniform density (generated using the RSA method). After placing impurities up to a desired concentration id we turn to the second step of the experiment—adsorption of the conductors. In this study we consider point-like conducting particles that consist of one lattice site each. We stop the adsorption process when the percolation of conductors sets in the system. This is the case when there exists a set of neighboring conducting particles that connect opposite sites of the lattice. For each simulation a threshold density of adsorbed conducting particles is evaluated. An example snapshot of the system at percolation can be viewed in Fig. 1 (for parameters $L=50$, $ad=6$, and $id=0.2$). For the given set of simulation parameters, size of the lattice (L), length of impurity particles (ad), and density of impurities (id), we perform a series of $N=100$ separate experiments (with various seeds of random number generator) in order to obtain statistical reliability of the results. We derive from each such series a mean value of percolation (c_p) and its mean standard deviation (σ). Continuing this procedure for different choices of parameters' values we obtain the function $c_p=c_p(ad,id;L)$. This function is a starting point for ongoing investigations. The resulting percolation threshold $c_p=c_p(ad,id;L)$ is sensitive to the size of the lattice L, but as $L\to\infty$ the threshold converges to the infinite lattice limit, $c_p^{\infty}(ad,id)=c_p(ad,id;L\to\infty)$. We have worked with L up to 500 and since finite-size effects seem to be very small for $L=500$, we have taken $c_p=c_p(ad,id;L=500)$ for further analysis. Some simulations finished without arriving at percolation, so "no percolation" quantity (NoP) was introduced as a number of such simulations in a series divided by the number of simulations in that series (N).

Here we adopted hard wall boundary conditions (any part of the particle cannot extend beyond the substrate) in order to model the real experiment (no periodic boundary conditions on a single real surface can be observed).

For chosen $L=500$ we measured the value of c_p for values of $ad=1\ldots24$ and for each value of ad we tested the whole range of id for which percolation of conductors appears.

III. RESULTS

The case of point imperfections ($ad=1$) is exceptional (due to no correlation of empty places left after deposition of insulators). Let us look at the following problem of choosing sites of the lattice: "take and mark m sites out of n available." The probability distribution of the possible outcomes will not change if at first we choose at random some $p\leqslant n-m$ sites that will not be marked, and then sites to be marked are chosen out of $n-p$ sites left (here n stands for the total number of sites on the lattice). Let us calculate the appropriate probabilities. Let $P_{\mathrm{I}}(\mathcal{M})$ be the probability that in m trials one has chosen the sites from the set $\mathcal{M}=\{x_1,x_2,\ldots,x_m\}$. Obviously,

$$P_{\mathrm{I}}(\mathcal{M})=\frac{m}{n}\frac{m-1}{n-1}\cdots\frac{1}{n-m+1}=\frac{1}{\binom{n}{m}}.$$

Let $P_{\mathrm{II}}(p,m)$ be the probability that, as above, one has chosen in m trials the sites from the mentioned set $\mathcal{M}$, but previously some p sites had been randomly thrown away from the lattice. The last probability factorizes: $P_{\mathrm{II}}(p,m)=P_{\mathrm{II}A}P_{\mathrm{II}B}$. Here $P_{\mathrm{II}A}$ stands for the probability of choosing these p sites to be thrown away in such a way that none of the thrown away points belongs to the set $\mathcal{M}$,

$$P_{\mathrm{II}A}=\frac{n-m}{n}\frac{n-m-1}{n-1}\cdots\frac{n-m-p+1}{n-p+1}=\frac{\binom{n-m}{p}}{\binom{n}{p}}.$$

The second factor $P_{\mathrm{II}B}$ is the probability of choosing appropriate m sites in m trials, but here one chooses from $n-p$ sites left (p sites had been thrown away),

$$P_{\mathrm{II}B}=\frac{m}{n-p}\frac{m-1}{n-p-1}\cdots\frac{1}{n-p-m+1}=\frac{1}{\binom{n-p}{m}}.$$

One can easily see that indeed $P_{\mathrm{I}}=P_{\mathrm{II}}$, provided that $p\leqslant n-m$. If, however, $p>n-m$, then $P_{\mathrm{II}A}=0$ and the reasoning breaks. This problem is equivalent to the one of generating p impurity positions before adding m conducting particles.

Let us now consider two probabilities: $P(m)$ is the probability that percolating cluster forms just after adsorbing mth

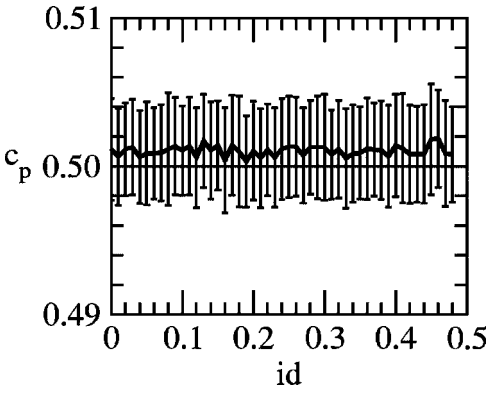

FIG. 2. The percolation threshold $c_p(id)$ for point insulators ($ad=1$). The error bars relate to the mean standard deviation.

conducting particle on n-site lattice (no insulators previously) and $P(m|p)$ is the probability that after adsorbing p insulator particles and the $m-1$ conducting particles, the percolating cluster forms just after adsorbing mth conducting particle. In view of the previous discussion it appears that $P(m)=P(m|p)$ provided that $p \leqslant n-m$, or equivalently $m \leqslant n-p$. The mean value of the percolation threshold reads as

$$c_p(id=0)=\frac{1}{n}\sum_{m=1}^{n} P(m)m$$

and

$$c_p\left(id=\frac{p}{n}\right)=\frac{1}{n}\sum_{m=1}^{n-p} P(m|p)m$$

for pure conducting and insulator contaminated cases, respectively. These two probabilities practically coincide for lattices big enough and p not too big. The only possible difference comes from the set of configurations, for which percolation appears in the system at densities $1-p/n=1-id$ or bigger. And since the percolation transition for large lattices becomes sharp,[1] the probability of attaining percolation at densities well away from the percolation threshold is negligible. Thus we arrive at equality $c_p(id=0)=c_p(id)$ for $id<1-c_p(0)$. In other words the measured percolation threshold for the case of point insulators should not depend on insulator concentration up to $id \lesssim 0.5$. Indeed the above reasoning is in a good agreement with simulations, as one can see on Fig. 2, where $c_p(id)=\text{const}=0.5$ within statistical error. At first glance it may seem contradictory to simple intuition—one can think that "for higher concentration of obstacles percolation clusters should not form easily," but here that is not true. As it was explained above the positions of particles of both kinds are independent (uncorrelated) and formation of percolating cluster of conductors is insensitive to the distributions of impurities (up to $id \lesssim 0.5$).

The analysis is different for bigger impurity particles. As the use of finite-size impurities induces some correlations in the distribution of empty places (and consequently of conductors), the percolation threshold is sensitive to the presence of disturbances (insulators) and increases monotonically with concentration and length of impurity particles (see Fig. 3).

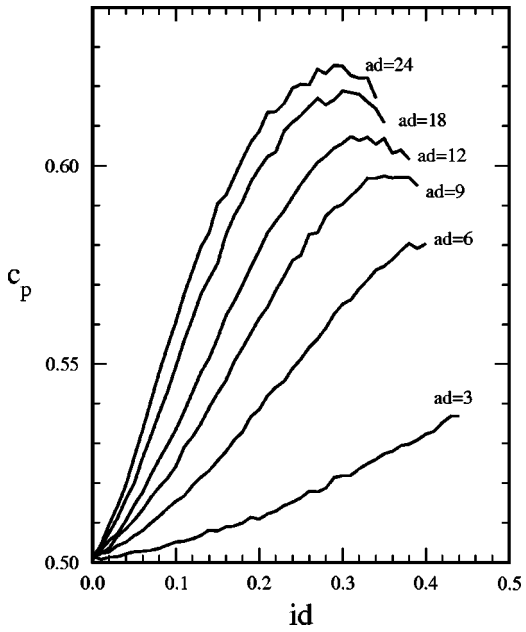

FIG. 3. The percolation threshold $c_p(id)$ for finite-size insulators ($ad=3\cdots24$). The data for which NoP>0 are not shown here.

For a given size of insulators there is an interval $[id^-, id^+]$, where the number of simulations that show no percolation rises from 0% to 100%. Above id^+ there is no percolation at all. Even though the size of conductors $a=1$ implies that these conducting particles can fit the tiniest space free of insulators on a lattice, the absence of percolation results from the formation of an infinite (i.e., percolating) cluster of insulators that limits the connection between conductors. This interval $[id^-, id^+]$ shrinks to a single point id^* as the size of the system rises: $L \to \infty$ (see Fig. 4). The detailed analysis shows that this limiting value id^* is the complement of the percolation threshold c_p^* derived for id infinitesimally below id^*, $id^*=1-c_p^*$. More exactly $id^+=1-c_p(id^-)$ (see curve plotted with circles on Fig. 4). Moreover, this value (id^*) coincides with the percolation threshold of sticks of given length alone [the case of adsorption of linear particles

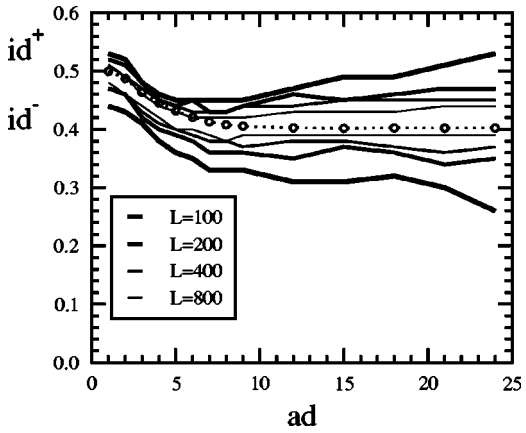

FIG. 4. The specific values of the concentration of insulators id^- (id^+) for which the percolation does not appear at least once (respectively, never) in the number of Monte Carlo runs as a function of ad. The size of the lattice varies here from $L=100$ (thick lines) to $L=800$ (the thinnest lines). The relation $id=1-c_p(id^-)$ is plotted with circles.

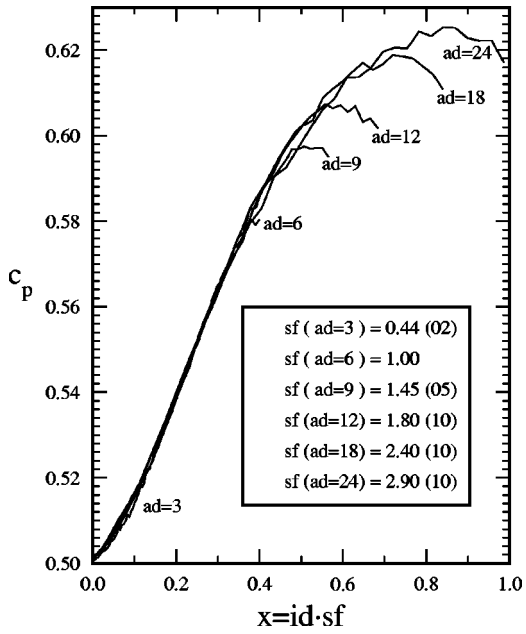

FIG. 5. The rescaled percolation threshold $c_p(x)$ for $ad=1\cdots24$.

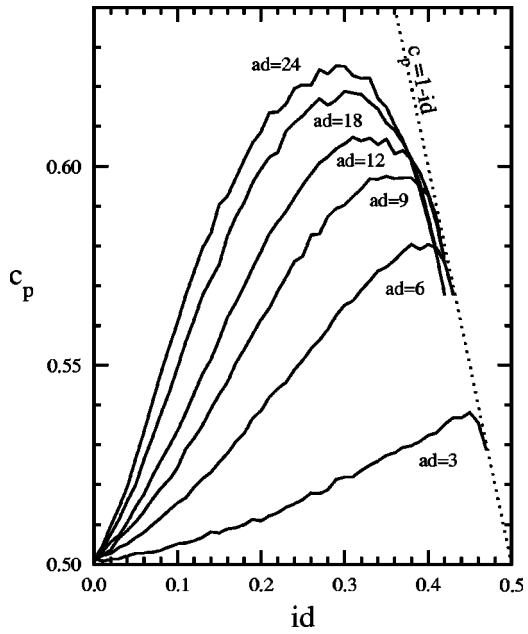

FIG. 6. The percolation threshold $c_p(id)$ for extended insulators ($ad=3\cdots24$). The boundary line $c_p(id)=1-id$ is plotted with dots.

(sticks) with no impurity preadsorbed on a substrate; see Ref. 5 for details], which confirms that the percolation of conductors stops when the percolation of insulators sets in.

Looking at the percolation threshold c_p as a function of insulator concentration id for various sizes of insulator particles, one can observe the shape universality of the curves (at least for id away from id^*). On a single plot one can draw all graphs properly rescaled in abscissa to see this universality (see Fig. 5). The scaling factor $\mathrm{sf}=\mathrm{sf}(ad)$ was determined in such a way that the rescaled functions $c_p(x)$ for $x=id(\mathrm{sf})^{df}$ follow the single (universal) curve. To fix the reference point we arbitrarily chose $\mathrm{sf}(ad=6)^{df}=1$. The consistency is remarkably good on a wide interval of id. Uncertainties of the scaling factor were estimated via graph analysis.

Some deviations are present, especially for insulator concentrations approaching id^* (the effect is more pronounced for higher ad). It should be mentioned that all graphs on Fig. 5 end at id^-, the concentration, for which simulations start to show that it is not possible to reach percolation (at least one simulation out of $N=100$ shows no percolation). The scale factor sf as a function of ad (size of insulator particles) is very smooth and can be fitted with high accuracy by the formula $\mathrm{sf}(ad)=p\ln(qad+r)$ with values $p=2.345$, $q=0.106$, and $r=0.893$.

Let us now discuss the case of high insulator concentrations. It appears (Fig. 6) that after continuous growth, the function $c_p(id)$ reaches a maximum at the concentration of impurities $id=id_M(ad)$ and drops down when id increases further. The reason for the initial increase of the function is rather easy to understand—for bigger amount of long obstacles there are more long barriers that must be gone around to make a connection (or connecting path becomes longer for higher id). This factor is valid, however, only for elongated obstacles ($ad>1$), as we discussed previously. To explain the nonmonotonicity for higher insulator concentration id we have to analyze the structure of the insulating adsorbate and especially the structure of the free space left for adsorption of the conductors. It appears that this remaining free space has, for high impurity concentration, a structure similar to that of the infinite cluster slightly above the percolation threshold, i.e., it consists of blobs, links, and dead ends.[1] A blob is a local region of wide open space where many paths connecting borders of that region can be drawn there. A link is a thin-line-shaped region that connects other parts of the system, otherwise disconnected. A dead end is a region that has no impact on the overall connectivity in the system. Let us concentrate first on the regime of a very high concentration of impurities, where some of the simulations do not end in percolation ($\mathrm{NoP}>0$). This is the case for $id\in[id^-,id^+]$. Then we have the following interesting factor influencing the percolation threshold. The effective insulator distribution is affected by *a posteriori* condition of the appearance of percolation in the system, because only percolating samples are taken into account in calculating the mean value of the percolation threshold c_p. In other words the latest insulator particles are added not uniformly to the empty space, but the addition avoids places that must be occupied by conductors to form the connection (links). Otherwise percolation is blocked and such simulation is discarded when evaluating c_p. So further insulators are adsorbed not to links, but to blobs and dead ends, and this decreases the resulting percolation threshold.

One can assume that a similar mechanism can also work for slightly lower concentrations, for which $\mathrm{NoP}=0$, but still $id>id_M$ (the concentration of impurities, for which the percolation reaches its maximum). Since most of the free space presumably forms dead ends (as does[1] the case of the percolating cluster) the subsequent impurity particles are more likely to adsorb there. So the percolating cluster at the threshold becomes more compact (and smaller).

It is worth noticing (Fig. 6) that all curves $c_p(id)$ for

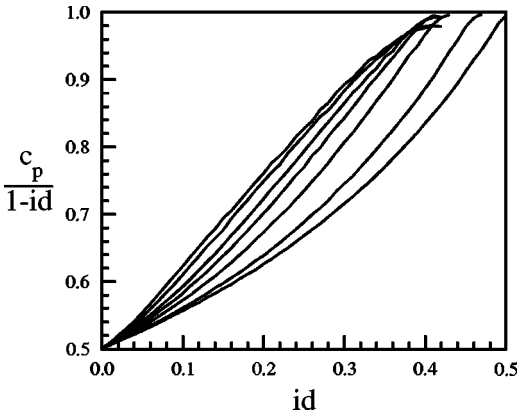

FIG. 7. The relative percolation threshold $c_p^{\mathrm{rel}}(x)=c_p(id)/1-id$. The values of ad are 1, 3, 6, 9, 12, 18, and 24 (starting from the right curve to the left).

$ad=3\cdots24$ lay below the boundary line $c_p(id)=1-id$ of the allowed area, approaching this line as id increases (because always $c_p+id\leqslant 1.0$). Each graph ends here at $id=id^+(ad)$, since beyond this point there is no percolation at all. This value approaches (as $L\to\infty$) the percolation threshold for the pure conducting system (without insulators) of length $a=ad$ (see Ref. 5). The percolation of conductors in the system stops when impurities start to percolate.

Another interesting quantity here is the relative percolation threshold $c_p^{\mathrm{rel}}(id)\overset{df}{=}c_p(id)/(1-id)$, which has the interpretation of the necessary amount of conductors to form an infinite cluster with respect to the volume of free space (not the volume of the whole system). Obviously for low impurity level ($id\approx 0$) we have $c_p^{\mathrm{rel}}\approx 0.5$. On the other extreme ($id\approx id^+$) we can suspect that c_p^{rel} goes to 1.0 because all possible dead ends in the free (left) space has been cut down by impurities, so almost the whole free space becomes the percolating cluster. Assuming the linear increase of c_p^{rel} with id: $c_p^{\mathrm{rel}}(id)=0.5+0.5id/id^+$ one arrives at $c_p(id)=0.5(1-id)(1+id/id^+)$. This dependence reproduces the nonmonotonic character of the function $c_p(id)$ with the maximum at $id_M=0.5(1-id^+)$. As seen in Fig. 7, the measured relative threshold remains increasing function for the whole range of id, as one can expect.[32] Moreover, the character of the increase is in fact linear, at least for longer impurity particles. The questions of justifying with exact arguments the linearity of the relative threshold as well as the deviations from the linear dependence for shorter insulators still remain open.

In the regime of high concentration of impurities ($id>id_M$) even though the percolation threshold decreases, the relative one still increases, according to our intuitive expectations. It should also be noted that the overall effect of the nonmonotonicity of c_p is not very large—the decrease of the threshold is at most of the order of 10%.

IV. CONCLUSIONS

In this paper we discussed how the presence of impurities disturbs the process of forming a percolating cluster of pointlike conductors in the system. In the case of pointlike insulators the percolation process of conductors is insensitive to impurities (at least for impurity concentration below 50%). For finite-size impurities and a small to medium level of impurities the percolation threshold c_p increases with the impurity concentration according to the universal curve (the effect is more apparent for larger size impurities). There exists a characteristic value of impurity concentration (that depends on the size of impurity particles) above which the percolation threshold in the system becomes a decreasing function.

These phenomena relates not only to the case of adsorption of conducting particles onto precontaminated surface (e.g., in preparing conducting composites) but also to other systems where the notion of connectivity plays an important role, e.g., colloids in the process of gelation, filters getting blocked, and in the study of porous materials as well.

ACKNOWLEDGMENTS

The author is grateful to Professor Andrzej Pękalski, Dr. Katarzyna Weron, and Dr. Zbigniew Koza for helpful discussions.

[1] D. Stauffer and A. Aharony, *Introduction to Percolation Theory* (Taylor & Francis, London, 1994).
[2] S. R. Broadbent and J. M. Hammersley, Proc. Cambridge Philos. Soc. **53**, 629 (1957).
[3] N. Provatas, M. Haataja, J. Asikainen, S. Majaniemi, M. Alva, and T. Ala-Nissila, Colloids Surf., A **165**, 209 (2000).
[4] R. Consiglio, D. R. Baker, G. Paul, and H. E. Stanley, Physica A **319**, 49 (2003).
[5] G. Kondrat and A. Pękalski, Phys. Rev. E **63**, 051108 (2001).
[6] G. Kondrat and A. Pękalski, Phys. Rev. E **64**, 056118 (2001).
[7] G. Kondrat, J. Chem. Phys. **117**, 6662 (2002).
[8] E. Kymakis, I. Alexandou, and G. A. J. Amaratunga, Synth. Met. **127**, 59 (2002).
[9] R. E. Amritkar and M. Roy, Phys. Rev. E **57**, 1269 (1998).
[10] J. Carrey and J.-L. Maurice, Phys. Rev. B **65**, 205401 (2002).
[11] M. B. Isichenko, Rev. Mod. Phys. **64**, 961 (1992).
[12] P. J. Flory, J. Am. Chem. Soc. **61**, 1518 (1939).
[13] M. D. Khandkar and A. V. Limaye, Phys. Rev. Lett. **84**, 570 (2000).
[14] R. S. Ghaskadvi and M. Dennin, Phys. Rev. E **61**, 1232 (2000).
[15] B. Bonnier, Phys. Rev. E **54**, 974 (1996).
[16] J.-S. Wang and R. B. Pandey, Phys. Rev. Lett. **77**, 1773 (1996).
[17] A. Matsuyama, R. Kishimoto, and T. Kato, J. Chem. Phys. **106**, 6744 (1997).
[18] C. K. Gan and J.-S. Wang, J. Chem. Phys. **108**, 3010 (1998).
[19] A. C. Balazs and I. R. Epstein, Biopolymers **23**, 1249 (1984).
[20] A. Cordoba and J. J. Luque, Phys. Rev. B **31**, 8111 (1985).
[21] J. J. Ramsden, Phys. Rev. Lett. **71**, 295 (1993).
[22] J. W. Evans, D. E. Sanders, P. A. Thiel, and A. E. DePristo, Phys. Rev. B **41**, 5410 (1990).
[23] J. Fransaer, Ph.D. thesis, Katholieke Universiteit, Leuven, 1994.
[24] C. Fusco and P. Gallo, J. Chem. Phys. **114**, 7563 (2001).
[25] J. J. Gray, D. H. Klein, R. T. Bonnecaze, and B. A. Korgel, Phys. Rev. Lett. **85**, 4430 (2000).
[26] J. W. Evans, Rev. Mod. Phys. **65**, 1281 (1993).
[27] J. Talbot, G. Tarjus, P. R. Van Tassel, and P. Viot, Colloids Surf., A **165**, 287 (2000).
[28] W. J. Kim, M. Taya, K. Yamada, and N. Kamiya, J. Appl. Phys. **83**, 2593 (1998).
[29] D. G. Han and G. M. Choi, Solid State Ionics **106**, 71 (1998).
[30] B. Y. Chen, H. Kim, S. D. Mahanti, T. J. Pinnavaia, and Z. X. Cai, J. Chem. Phys. **100**, 3872 (1994).
[31] A. Zamudio, Y. Duda, and M. Medina-Noyola, Phys. Lett. A **305**, 258 (2002).
[32] S. A. Bagnich and A. V. Konash, J. Phys. A **36**, 1 (2003).

The effect of impurities on jamming in random sequential adsorption of elongated objects

Grzegorz Kondrat[a)]
Institute of Theoretical Physics, University of Wrocław, Plac M. Borna 9, 50-204 Wrocław, Poland

(Received 7 July 2005; accepted 28 November 2005; published online 6 February 2006)

We consider the jamming aspect of random sequential adsorption of extended particles onto two-dimensional lattice by computer Monte Carlo simulations. The initial presence of impurities on the substrate disturbs this phenomenon significantly and we study here how the size and density of impurity particles affect the resulting jamming threshold. We present the formula for jamming threshold as a closed function of all important parameters (the size of primary particles, the size of impurity particles, and the final density of impurities). The fractal dimension of the space free of impurities is also discussed. © *2006 American Institute of Physics*. [DOI: 10.1063/1.2161206]

I. INTRODUCTION

The adsorption of large particles on the surface belongs to one of the most important processes in surface physics and chemistry of many real systems. Random sequential adsorption (RSA) models were used as the simplest approach toward irreversibility.[1] Since a long time ago there has been interest in using RSA in models for reactions on polymer chains,[2,3] chemisorption on crystal surfaces,[4] adsorption in colloidal systems,[5,6] random growth in surface physics,[7] growth processes in three-dimensional (3D) solid-state physics,[8,9] in technology of composites,[10] in granular matter study,[11] in disordered systems,[12] and also in a wider context such as ecology[13] or sociology.[14] The characteristic features important here are (a) irreversibility of deposition (no desorption), (b) randomness of a position (and an orientation) of a particle to be adsorbed, and (c) sequentiality what means that at any time only one particle is being adsorbed, but relaxing of these constraints leads also to interesting models as well.[15,16] There are wide reviews on the topic, see, e.g., Refs. 17–19.

In a large group of RSA models there is one more restriction often considered: no overlapping with previously adsorbed objects is allowed. As a consequence of this the investigated system approaches the jamming state, in which no more objects can be adsorbed (due to absence of free space of appropriate size or shape). In many papers the main concern is focused on the study of a dynamics leading to a such state.[20–23] On the other hand it is also interesting to investigate the structure of the final (jammed) state. One of the basic observations here is that the distribution of adsorbed objects in RSA is different from that obtained at equilibrium[19,24] (in RSA case one has infinite memory of the process and orientational order is purely local, in contrast to the equilibrium case, where there are long-range correlations in a nematic phase).

In studying many systems one often has to consider also some contaminations (impurities) that disturb the act of deposition of primary particles (i.e., that of primary interest) and introduce disorder into the system. It is a very common situation that parts of the system are not perfectly clear, but contaminations have significant effect on the system behavior. This important case, however, is not very well studied and the bibliography on that topic is rather short. In general there are two ways of incorporating the factor of impurity into the model—either competitive adsorption[25–27] (one has an adsorption of particles from a mixture and some probability distribution is used for generating the type of a particle being adsorbed at every time) or preadsorption (covering the surface of interest with impurities up to some level, before the RSA of primary particles starts). It is rather clear that both approaches are not equivalent (the appropriate choice depends on the physical details of the process). We concentrate here on the second possibility (preadsorption), and we want to investigate how the level and size of impurity particles interfere the jamming process of extended primary particles. Both primary and impurity particles considered here are needlelike. We developed a computer code for Monte Carlo simulations of the adsorption process and the analysis of the obtained data constitutes the main body of the paper.

There is a close relation between the present work and Ref. 28, in which we studied the percolation process affected by impurities.

In the following section (Sec. II) we explain the details of the model. Since there appears two different cases, we describe them separately and present the results in two consecutive sections (Secs. III and IV). In the final section (Sec. V) some remarks and conclusions are included.

II. MODEL

In this paper we present conclusions based on extensive Monte Carlo simulations of the system with impurities. The details of this approach are described further in this section. The system of interest consists of two kinds of extended particles (impurities and primary particles) and a substrate on which these particles are being adsorbed. We work here on a triangular lattice and the substrate is a hexagonal of the edge equals L lattice sites. Particles are modeled here as straight

[a)]Electronic mail: gkon@ift.uni.wroc.pl

chains of consecutive lattice sites, with length (defined as the number of sites it covers) depending on their type (throughout the simulations primary particles have length a and impurity particles have length b). In a series of simulations these lengths remain constant. The adsorption is random and sequential what means that at any time we try to put randomly (at random position and orientation) one particle of a given type. The particles cannot overlap (this constraint applies both to particles of the same type and to particles of different types), so in a case of detected overlapping the trial of adsorption of given particle is rejected and the next position and orientation are randomly generated. Once the particle lands in an empty space it stays there forever (no desorption).

One of the main quantities considered in this paper is the jamming threshold for primary particles adsorbed on a substrate previously filled up to some level with impurities. On an empty substrate we adsorb impurities until the coverage c_i (the ratio of the number of lattice sites occupied by impurity particles to the total number of sites in the substrate). Then we adsorb primary particles as long as possible. At some moment, however, there is no empty place that can accommodate a single primary particle—we say that the system is jammed. The jamming threshold $c_j^{\sim}$ is the coverage of primary particles at that moment (the ratio of the number of lattice sites occupied by primary particles to the total number of sites in the substrate). This quantity depends on several parameters: $c_j^{\sim}=c_j^{\sim}(a,b,c_i)$—on the size a of primary particles, the size b of impurity particles, the impurity level c_i, and also on the lattice size L. In order to obtain statistically reliable results we repeat N times the simulations for the same set of parameters' value and we take the average c_j (a wavelet in the symbol $c_j^{\sim}$ denotes the single simulation value in contrast to a value c_j—the mean in a series of simulations). In this paper we took the length of each simulation series $N=100$, what guarantees reasonably good accuracy and low level of fluctuations. The mean standard deviation σ is also calculated and used for controlling statistical errors. In order to get rid of finite-size effects we took for further analysis the simulations done on a substrate as large as $L=500$ lattice units, while we used smaller values L only for comparison. In the study of the pure jamming curve (no impurities added: $c_i=0$), however, we have chosen L as big as 1000 since particles with the length up to $a=50$ were considered. In all simulations hard wall boundary conditions were chosen (they mimic the situation of many real experiments). From the previous study of similar RSA models[18,29,30] it is known that the type of boundary conditions may influence the decay of finite-size effects, but for large enough lattices there have no impact on the results.

The main objective of this study is to discover how the length of impurity particles and the level of impurities in the system influence the jamming threshold of primary particles. It appeared that one can distinguish two separate cases, when the impurity particles are either smaller or larger than the primary particles (either $b<a$ or $b>a$, while the case of $b=a$ is trivial). Because these two possibilities proved so different, we study them in two separate sections.

III. RESULTS: THE CASE OF IMPURITIES SMALLER THAN PRIMARY PARTICLES

At the beginning of our study we need to look at the pure jamming threshold (no impurities at all) as a function of the particles' length: $c_j^0=c_j^0(a)=c_j(a,b,c_i=0)$. This function will be the point of reference for further considerations.

In RSA approach the way that jamming threshold depends on the size of objects being adsorbed on the surface is sensitive to the details of the model. The major factor here is the structure of the substrate: for continuous case it is observed that the function $c_j^0(\alpha)$ has a maximum for aspect ratio α of the objects (rectangles, ellipses) close to 2 and decays to zero with power law.[19,31,32] On the other hand the discrete systems (modeled on a lattice) show different behaviors: the jamming threshold decreases monotonically with size but the infinite limit ($a\to\infty$) remains finite (nonzero). In the literature several forms of this decay are postulated: power law,[29] polynomial in inverses of a,[33,34] inverse of logarithm[35] (for an end-on mechanism of deposition), and exponential[36] (for small values of a). Additionally it appears[29,30,36,37] that the type of underlying lattice has an effect only on numerical constants in the formulas, not on the formulas themselves.

For our data simulated on a triangular lattice with the lattice size $L=1000$ the resulting formula for jamming reads: $c_j^0(a)=c_j^*+\text{const}\,a^{-\Delta}$ with $c_j^*=0.595(5)$, const$=0.54(4)$, and $\Delta=0.75(5)$. The values of a considered here (and in the whole paper) remain in the set $\{1, 2, 3, \ldots, 50\}$.

In the numerical part of our study we obtained the function $c_j(a,b,c_i)$ for fixed a and b while the impurity level c_i ran through the whole admissible interval $[0,\ c_j^0(b)]$, for which one can still adsorb particles. This function is a mean of a series of $N=100$ computer simulations with the same set of parameters. We repeated such series for chosen sizes of particles involved: $a\in\{3,6,9,12,15,18,24\}$ and $b\in\{1,3,6,9,12,15,18,24\}$.

It is obvious that the jamming threshold of longer particles is lower—there are many holes that can accommodate shorter particles but not longer. Contaminating the substrate by impurity particles up to some level c_i in the RSA process makes the surface of the substrate somewhat rough or disordered. The amount of disorder introduced depends on the impurity level c_i as well as the impurity size b. For impurity particles smaller than primary particles ($b<a$) areas forbidden for adsorption of impurities (where these particles cannot fit too small cavities) are also forbidden for primary particles. Thus the resulting jamming threshold c_j will be smaller than the amount of impurities that could be further adsorbed in place of primary particles [up to the jamming of impurities: $c_j(a,b,c_i)<c_j^0(b)-c_i$]. On the other hand in the case when impurity particles are larger than primary particles ($b>a$) there are also areas (holes within impurity structures) that will be covered by primary particles and the final coverage of the substrate by particles (of both kinds) is relatively higher. The difference between these two possibilities seems to be a bit deeper, so each case is described in a separate section. The intermediate case when $b=a$ (particles of both kinds are equal in size) is trivial in the following sense. The

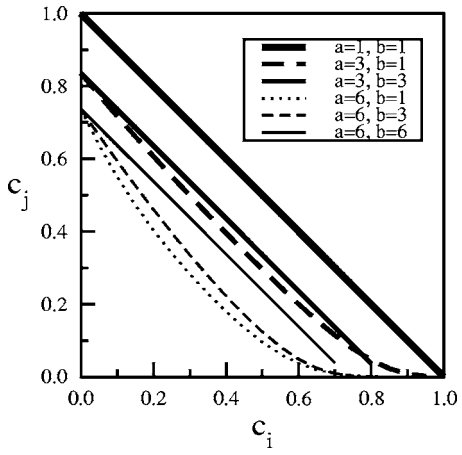

FIG. 1. The case $b \leqslant a$: the jamming threshold $c_j(a,b,c_i)$ for $a=1,3,6$, $b=1,3,6$, and c_i ran through the interval [0.0, 1.0]. The lattice size is $L=500$.

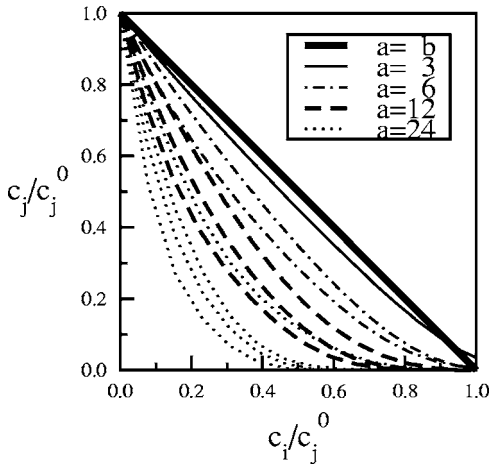

FIG. 2. The jamming threshold after suitable rescaling [dividing both axes by the factor $c_j^0(a)$]. Within the curves of the same type (i.e., the same value of a) lower curves correspond to bigger values of b. For given a the values of b considered on this figure belong to the set {1, 3, 6, 12, 24} providing that $b \leqslant a$.

jamming threshold $c_j(a,b,c_i)$ simply equals the difference between the total jamming threshold $c_j^0(a)$ for one kind of particles only (no impurities) and the impurity level c_i.

In the rest of this section we discuss the first case: $b<a$. In the following we will be aiming at obtaining the functional dependence $c_j=c_j(a,b,c_i)$ in a closed form. As it stands the rough data $c_j(a,b,c_i)$ for only some values of parameters a and b (for clarity) are shown as a function of c_i on Fig. 1. To extract some regularities in this graph we need to do additional operations on the data.

Firstly let us notice that both the function c_j itself and the impurity level c_i practically do not go beyond pure jamming threshold $c_j^0(a)$. We have $c_j(a,b,c_i) \leqslant c_j^0(a)$ since $c_j(a,b,c_i) \leqslant c_j(a,b,c_i=0)=c_j^0(a)$ (the jamming threshold is a decreasing function of c_i). On the other hand for most cases $c_j(a,b,c_i) \approx 0$ for $c_i > c_j^0(a)$ [some minimal deviations can be observed for $b=1\cdots3$ and $a \leqslant 6$ due to the fact that for very small lengths (a,b) there are some elongated holes even for very high level of impurities]. Thus we can normalize both axes by dividing by the factor $c_j^0(a)$.

After this rescaling one can draw the function $c_j(a,b,c_i)/c_j^0(a)$ vs $c_i/c_j^0(a)$ on a single graph for different values of the parameters a and b (see Fig. 2). It appeared that all curves belong to the same family of functions and different curves coincide for some choices of a and b. We discovered that this family can be described by the formula: $y^\beta + x = 1$ [or $y=(1-x)^{1/\beta}$], where $y \equiv c_j(a,b,c_i)/c_j^0(a)$ and $x \equiv c_i/c_j^0(a)$. The exponent $\beta=\beta(a,b)$ does not depend on the impurity level c_i (it has some small deviations from a constant function with respect to c_i, but these are below 0.05 and may be the subject of a finer analysis). This unusually simple formula can be related to some fractality of the area of the substrate that is accessible for primary particles after impurities are deposited. The exponent β may be pertained to the fractal dimension, but here one can rather speak about "relative dimension," because it determines the way how the accessible area (and the process of adsorption itself) can be seen from the point of primary particles. The regular case $\beta=1$ (that is $y+x=1$—all sites that are not impurity are accessible) is reproduced for $b=a$ and especially for $b=a=1$ [for this latter case the scaling factor $c_j^0(a=1)$ is just unity]. Here bigger values of β means more space accessible for the adsorption of the primary particles and the maximum value $\beta=1$ is related to the highest adsorption. The smaller exponent β, the lower jamming threshold (at the same impurity level).

The determination of the functional dependence of β on a and b is the next step of our study. We have observed that the arguments a and b of the exponent function $\beta(a,b)$ enter it via their difference $a-b$: $\beta(a,b)=f(a-b)$. The value of β vs $a-b$ for all a and b investigated is plotted on the Fig. 3. The points follow one function, roughly being $f(x)=5/(4+x)-0.05$. In the case of equal size particles of both kinds (that is the regular case $b=a$) the value $\beta=1$ (as it was discussed above). On the other extreme we have $\beta \to 0$ for big difference in particles' size. The fact that the behavior of the system is governed only by the difference in particle's sizes can be simply explained. In the case of fitting a single pri-

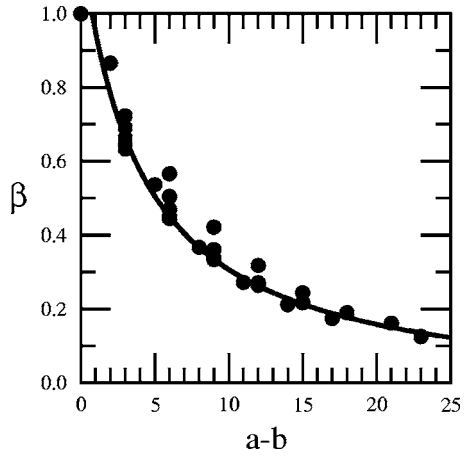

FIG. 3. The values of the exponent β vs the particles' size difference for all possible choices of $a \in \{3,6,9,12,15,18,24\}$ and $b \in \{1,3,6,9,12,15,18,24\}$ such that $b \leqslant a$. The curve is an inverse-type fit $\beta=5/(4+x)-0.05$ with $x=a-b$.

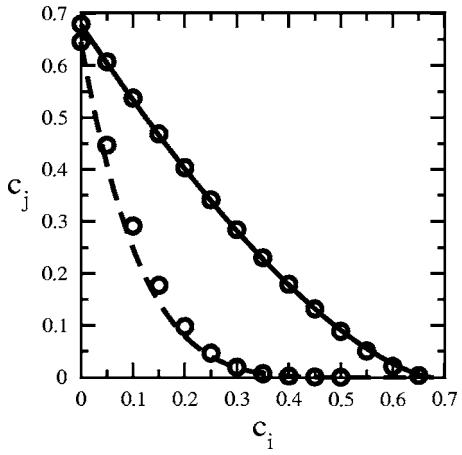

FIG. 4. The illustration of conformity of the formula (1) (lines) to the simulation results (circles) on some examples: the upper solid curve corresponds to the choice $a=12$ and $b=9$ and the lower dashed curve corresponds to $a=24$ and $b=6$.

mary particle to some small hole in the impurity structure this is just that difference which determines the number of possible positions of the particle.

Thus one can describe the jamming threshold in the following closed form:

$$c_j(a,b,c_i) = c_j^0(a)\left(1 - \frac{c_i}{c_j^0(a)}\right)^{g(a-b)}, \tag{1}$$

with

$$g(x) = \frac{80 + 20x}{96 - x},$$

and

$$c_j^0(a) = 0.595 + 0.54a^{-0.75}.$$

It is noteworthy that the function describing such a complicated process can be (at least at the first approximation) expressed in a such compact form. The accuracy of the above formula is for some choice of parameters pretty good (e.g., $a=12$ and $b=9$), for others (e.g., $a=24$ and $b=9$) still satisfactory (see Fig. 4). To get deeper insight into details of the studied phenomenon of interplay between impurity particles and primary particles in the process of adsorption, further study of the subject is needed, however.

IV. RESULTS: THE CASE OF IMPURITIES LARGER THAN PRIMARY PARTICLES

In the case when impurity particles are larger than primary particles the latter can penetrate some internal holes of the impurity adsorbate that cannot be filled up with impurity particles. This can introduce some roughness or fractality of the space not covered by impurities, that is accessible for RSA of primary particles. Let us check that by examining the fluctuation behavior.

In pure RSA (no impurities considered) one can introduce[38] correlation length exponent ν_J for jamming in the form $\sigma \propto L^{-1/\nu_J}$. The correlation length exponent is a standard critical quantity in other critical phenomena, such as percolation.[39,40] It measures the decay of fluctuations σ in the system as the size of the system tends to infinity. This exponent governs also the divergence of correlation length at criticality (as in percolation). In the case of adsorption on heterogenous media one can still introduce this exponent: Loscar *et al.*[41] report that the jamming correlation length exponent ν_J carries information not only about the universality class of the adsorption process itself but also about the fractality of the substrate as well. This is implied by the fact that the fluctuations of the final density of the adsorbate depends not only on the adsorption process of primary particles, but also on the fluctuations introduced by the process of preparing such a heterogeneous medium (i.e., adsorption of impurities). Thus in the RSA processes on heterogeneous media the mean standard deviation of jamming σ_J (which measures the fluctuations in the system) can be decomposed into two terms: σ_{Sub} related to the substrate and σ_{RSA} related to the adsorption process. The RSA part follows usual scaling: $\sigma_{\mathrm{RSA}} \propto L^{-1/\nu_J}$ where the exponent ν_J can be expressed[41] via the fractal dimension of the substrate d_f and the dimensionality of the underlying space D: $\nu_J = 2/(2D - d_f)$, here $D=2$. Thus the exponent ν_J can be equal to unity only for the case of $d_f=2$ (no fractality). In the RSA on clean surface (no impurities) one obviously has[31] $\nu_J=1$.

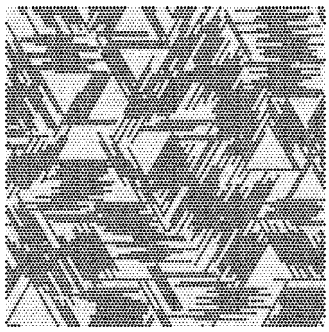

FIG. 5. A typical example of emerging structures at jamming (here no impurities were present: $c_i=0$). The figure shows the central part of a substrate ($L=500$). The adsorbed primary particles of length $a=15$ are plotted in black, left free sites are shown with small dots.

After analyzing fluctuations in the system for $b>a$ and extracting the correlation exponent ν_J from the RSA part of the mean standard deviation σ_{RSA} for various impurity levels c_i we came to the following conclusion. We have the fractal dimension $d_f=2$ for all considered cases (we obtained $\nu_J = 1.00 \pm 0.03$), which means that we have no fractality in the system. After closer inspection (see Fig. 5, on which some part of the system after jamming of impurities with $b=15$ is shown) it appears that the empty space consists of quite regular blocks, on the contrary to the previous suggestions.

V. CONCLUSIONS

In this paper we analyzed the RSA process with two kinds of adsorbed particles: impurity particles that are deposited up to some level in the first stage of the process, and primary particles that are adsorbed on the substrate contaminated by impurities. The resulting jamming threshold of primary particles was investigated and a closed form of its dependence on parameters (size of both kinds of particles and level of contamination) was proposed for impurities smaller

than primary particles. For impurities larger than primary particles the analysis of fluctuations of the jamming threshold indicated that after first stage of the process (adsorption of impurities) the space left for adsorption of primary particles has no fractal properties, but its fractal dimension $d_f=2$.

[1] E. L. Hinrichsen, J. Feder, and T. Jøssang, J. Stat. Phys. **44**, 793 (1986).
[2] P. J. Flory, J. Am. Chem. Soc. **61**, 1518 (1939).
[3] A. C. Balazs and I. R. Epstein, Biopolymers **23**, 1249 (1984).
[4] A. Cordoba and J. J. Luque, Phys. Rev. B **31**, 8111 (1985).
[5] V. Privman, H. L. Frish, N. Ryde, and E. Matijvec, J. Chem. Soc., Faraday Trans. **87**, 1371 (1991).
[6] Z. Adamczyk, T. Babros, J. Czarnecki, and T. G. M. van de Ven, Adv. Colloid Interface Sci. **19**, 183 1983).
[7] L. Finegold and J. T. Donnell, Nature (London) **278**, 443 (1979).
[8] J. W. Evans, D. E. Sanders, P. A. Thiel, and A. E. DePristo, Phys. Rev. B **41**, 5410 (1990).
[9] J. Fransaer, Ph.D. thesis, Katholieke Universiteit Leuven, 1994.
[10] N. Provatas, M. Haataja, E. Seppälä, S. Majaniemi, J. Åström, M. Alava, and T. Ala-Nissila, J. Stat. Phys. **87**, 385 (1997).
[11] K. Trojan and M. Ausloos, Physica A **351**, 332 (2005).
[12] L. Zhang and P. R. Van Tassel, J. Chem. Phys. **112**, 3006 (2000).
[13] M. Hasegawa and M. Tanemura, in *Recent Developements in Statistical Interference and Data Analysis*, edited by K. Matusita (North Holland, Amsterdam, 1980).
[14] Y. Itoh, J. Appl. Probab. **17**, 134 (1980).
[15] G. Tarjus, P. Schaaf, and J. Talbot, J. Chem. Phys. **93**, 8352 (1990).
[16] I. Pagonabarraga, J. Bafaluy, and J. M. Rubí, Phys. Rev. E **59**, 4285 (1999).
[17] N. Provatas, M. Haataja, J. Asikainen, S. Majaniemi, M. Alva, and T. Ala-Nissila, Colloids Surf., A **165**, 209 (2000).
[18] J. W. Evans, Rev. Mod. Phys. **65**, 1281 (1993).
[19] J. Talbot, G. Tarjus, P. R. Van Tassel, and P. Viot, Colloids Surf., A **165**, 287 (2000).
[20] R. H. Swendsen, Phys. Rev. A **24**, 504 (1981).
[21] P. Schaaf and J. Talbot, Phys. Rev. Lett. **62**, 175 (1989).
[22] A. P. Thompson and E. Glandt, Phys. Rev. A **46**, 4639 (1992).
[23] J.-S. Wang and R. B. Pandey, Phys. Rev. Lett. **77**, 1773 (1996).
[24] B. Widom, J. Chem. Phys. **44**, 3888 (1966).
[25] J. W. Evans and R. S. Nord, Phys. Rev. B **31**, 1759 (1985).
[26] J. W. Lee, Colloids Surf., A **165**, 363 (2000).
[27] A. Zamudio, Y. Duda, and M. Medina-Noyola, Phys. Lett. A **305**, 258 (2002).
[28] G. Kondrat, J. Chem. Phys. **122**, 184718 (2005).
[29] G. Kondrat and A. Pękalski, Phys. Rev. E **63**, 051108 (2001).
[30] G. Kondrat and A. Pękalski, Phys. Rev. E **64**, 056118 (2001).
[31] J. D. Sherwood, J. Phys. A **23**, 2827 (1990).
[32] R. D. Vigil and R. M. Ziff, J. Chem. Phys. **91**, 2599 (1989).
[33] B. Bonnier, M. Hontebeyrie, Y. Leroyer, and E. Pommiers, Phys. Rev. E **49**, 305 (1994).
[34] B. Bonnier, Phys. Rev. E **54**, 974 (1996).
[35] S. S. Manna and N. M. Švarkić, J. Phys. A **24**, L671 (1991).
[36] Lj. Budinski-Petković and U. Kozmidis-Luburić, Phys. Rev. E **56**, 6904 (1997).
[37] Lj. Budinski-Petković and U. Kozmidis-Luburić, Physica A **236**, 211 (1997).
[38] N. Vandewalle, S. Galam, and M. Kramer, Eur. Phys. J. B **14**, 407 (2000).
[39] D. Stauffer and A. Aharony, *Introduction to Percolation Theory* (Taylor & Francis, London, 1994).
[40] M. B. Isichenko, Rev. Mod. Phys. **64**, 961 (1992).
[41] E. S. Loscar, R. A. Borzi, and E. V. Albano, Phys. Rev. E **68**, 041106 (2003).

Impact of composition of extended objects on percolation on a lattice

Grzegorz Kondrat*
Institute of Theoretical Physics, University of Wrocław, plac M. Borna 9, 50-204 Wrocław, Poland
(Received 18 January 2008; revised manuscript received 15 May 2008; published 1 July 2008)

We consider the percolation aspect of random sequential adsorption of extended particles onto a two-dimensional lattice using computer Monte Carlo simulations. We investigate how the composition of the particles influences the value of the percolation threshold. Two regimes can be distinguished: one for almost linear particles (with the composition of straight segments reaching 85–100 %) and the second one for more bent (flexible) ones. For more bent particles we found a high correlation between the percolation threshold and the structure of an adsorbate at percolation. We also observe that there is no difference in the conclusions for both kinds of lattice considered (square and triangular).

DOI: 10.1103/PhysRevE.78.011101 PACS number(s): 64.60.ah, 61.46.Bc, 61.43.Hv

I. INTRODUCTION

Even though the problem of percolation [1] has been known for many years [2] and many papers have dealt with its various aspects, there are still many interesting questions to be answered. In a basic lattice formulation, each site is occupied with the probability c or is empty with the complementary probability $1-c$. As c increases from 0, neighboring occupied sites start to form connected clusters with greater and greater size. Eventually, for a certain threshold value c_p, there appears an "infinite" cluster that spans the whole system. The probability threshold depends on the system's size L, but it has a finite limit as $L\to\infty$ (the convergence is a power law [1]). There are many applications of the percolation theory in physics and chemistry, especially in disordered systems, porous media, and critical phenomena. Percolation is the simplest nontrivial model of phase transitions and is widely used in describing transition phenomena [3] (e.g., gelation). Other important applications include resistivity of composites [4,5] and strain behavior of solids [6].

There are several mechanisms of particle deposition onto a surface, but among them random sequential adsorption (RSA) both is relatively simple and has many successful applications in theory and experiment. The starting point in this approach is usually an empty substrate surface. The process of adsorption is sequential, i.e., there is only one particle being adsorbed at a time. The position and orientation of the adsorbed particle at each trial is generated randomly. The result of each trial is determined by a nonoverlapping rule: the trial is accepted (and the particle is adsorbed) if there is no overlapping with the previously adsorbed particles. However, if any part of the particle overlaps with some other particles, the whole trial is rejected and a new position and orientation (in some models also a new shape) is generated again (without any correlation to previous trials). The whole process is irreversible—adsorbed particles stay on the surface forever at the adsorbed positions.

The RSA approach originates from the work of Flory [7], who studied a cyclization reaction in a polymer chain in which adjacent pendant groups link randomly. In general, in RSA-type models [8–13] one usually consider atoms, molecules, or geometric shapes like circles, lines, or ellipses that adsorb on polymer chains, solid surfaces, biological membranes, or lattice or continuum planes. These models are widely used in various fields of physics and chemistry, especially where one deals with irreversible processes. The approach of RSA has been used, among others, in models for reactions on polymer chains [7,14], chemisorption on crystal surfaces [15], adsorption in colloidal systems [16,17], random growth in surface physics [18], growth processes in three-dimensional (3D) solid state physics [19,20], technology of composites [21], granular matter study [22], and disordered systems [23] and also in the wider context of ecology [24] or sociology [25]. For an extensive overview of the field, see Refs. [26–28].

Recently the irreversible adsorption of large particles (polymers, nanoparticles, etc.) has attracted much attention. Among many papers devoted to the subject one can mention Ref. [29], where blocking effects in the adsorption dynamics of linear macromolecules are explored. In Ref. [30] a scale-invariant behavior of the jamming time for linear particles adsorbed on arbitrary finite square lattices is revealed. An analytical derivation of the power law describing the size of jamming fluctuations on homogeneous and inhomogeneous lattices can be found in [31]. The other shapes on a triangular lattice as well as their mixtures were considered in Ref. [32] (see also references therein), where the approach to jamming was investigated. There is an interesting comparison study of lattice adsorption versus continuous adsorption in Ref. [33].

Relatively many papers have been devoted to determining the universality class and the threshold for the percolation of particles modeled by random walks of given length; see Refs. [34–36]. Additional effects connected to nonperiodicity of the substrate (or contamination of the underlying regular lattice) were studied in Refs. [37–39]. Some generalizations of the problem using mixed side-bond percolation can be found in Refs. [40,41]. The interplay between jamming and percolation for monomers, dimers, and square particles at various temperatures was studied in Refs. [42–45]. An interesting model of percolation of very large polymers (with the length of order of the system size) is discussed in Ref [46]. Some aspects of percolation in nanocomposite films were described in Ref. [47].

*gkon@ift.uni.wroc.pl

The solutions of most percolation problems are of mainly approximate nature, since the exact calculations can be done only in very special cases (e.g., c_p for random percolation on a triangular lattice or percolation on Bethe lattices [1]). We decided to perform Monte Carlo simulations of the problem since other approaches did not prove promising.

The paper is organized as follows. In Sec. II we describe the details of the model. A discussion of finite-size scaling and the error bars of the data is included in Sec. III. The main results of the paper are presented in Sec. IV. The reasons for lack of percolation for some sets of parameters are discussed in Sec. V. Additional data on the other (triangular) lattice confirming the previous conclusions (drawn for the square lattice in Sec. IV) are described in Sec. VI. Some additional facts on cluster structure are put forward in Sec. VII. Concluding remarks are included in Sec. VIII.

II. MODEL

In this paper we study adsorption of extended particles of fixed length on a lattice. The coverage of the surface is increased in the process up to the percolation threshold, when there appears a so-called infinite cluster (a cluster that extends through the whole system). The resulting percolation threshold depends on the spatial structure of the particles being adsorbed and their size. We investigate here by means of Monte Carlo simulations how the composition and the size of the particles determine the threshold. Other aspects of a similar model were studied in Ref. [48]. In order to obtain a deeper insight into the problem we carried out simulations on two kinds of 2D lattice: square and triangular.

Each particle is modeled here as a group of a consecutive neighboring sites (monomers) of the lattice (we deal with unbranched polymers). Between successive monomers we have bonds that form a broken line (the backbone of the particle). By the composition of the particle we understand here the fractions of corresponding bending types in a backbone. On a square lattice there are only two types of bending: straight ($S0$) and at right angles ($S1$); on a triangular lattice we have three: straight ($T0$), slightly bent at the angle of 120° ($T1$), and highly bent at the angle of 60° ($T2$); see Fig. 1. For a given particle composition (p_0, p_1) for the square lattice and (p_0, p_1, p_2) for the triangular one, we put particles on a lattice randomly (details below) until percolation appears. Then the resulting density of the particles is calculated (the ratio of occupied sites of the lattice to the number of all sites accessible). To obtain statistically reliable results with a low level of fluctuations we carry on the simulations for a given composition of particles for $N=100$ times. In order to acquire a comprehensive set of data for each considered particle size ($a=3,\ldots,30$), we sample the whole space of compositions with a density step from 0.2 down to 0.01.

A single run for the given composition starts with an empty substrate (a square $L\times L$ on the square lattice, a hexagon with the edge of L lattice units on the triangular one, and hard wall boundary conditions adopted in both cases). The process of adsorption is random and sequential, i.e., at any time we try to put randomly (at random position and orientation) a single particle. Its shape is generated also randomly according to the probability distribution of possible bending types ($p_0{:}p_1$ for the square lattice, $p_0{:}p_1{:}p_2$ for the triangular one). Thus the exact numbers of bending of each type can vary from particle to particle, while the average composition remains constant in a single run. If the particle under consideration overlaps with the particles previously adsorbed, the whole trial is rejected. If there is no overlapping, the particle stays there forever. In each case, we then try to put on the substrate a new particle (with a new shape) at a new position with a new orientation. We repeat this procedure until the percolation cluster arises in the system (i.e., the opposite edges of the system are connected via some path of nearest neighbor sites occupied by the particles). One can consider many definitions of the overall connectivity (e.g., any opposite edges are to be connected, given opposite edges are to be connected, all opposite edges are to be connected, etc.), but asymptotically all are equivalent [49]. Here we check the connectivity between upper and lower edges of the system. It appeared that for some values of the simulation parameters we cannot observe percolation, especially for long particles and p_2 very close to 1. In this case particles tend to form compact, isolated islands, so the connectivity in the system is poor. Jamming in the system sets in before percolation can appear (no more particles can be added due to a lack of free space of appropriate shape). More detailed discussion of this effect is postponed to Sec. V. For reliability of the results it is important to keep finite-size effects within reasonable limits. For bigger lattices the statistical fluctuations of the threshold obtained are smaller. Also the difference between the limiting ("exact") value of the threshold (size of the lattice $L\to\infty$) and the values obtained for a given size L drops down to zero with increasing L. Thus it is desirable to use as large latices as possible. We carry out our simulations on lattices as big as $L=1000$ for a square lattice and $L=300$ for a triangular one. Extensive discussion of finite-size effects (scaling), statistical deviations, and errors is included in the following section.

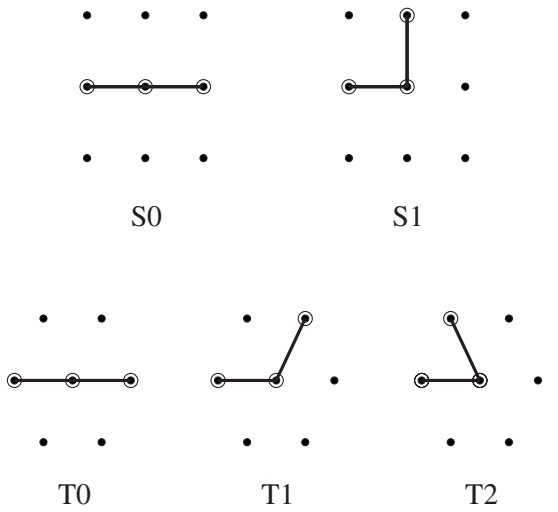

FIG. 1. Possible types of backbone bending on a square (top) and a triangular lattice (bottom).

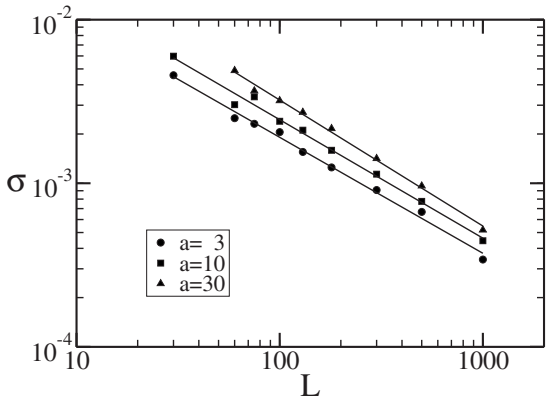

FIG. 2. Standard deviations σ of the square lattice threshold for $a=3$, 10, and 30 as a function of the lattice size L. The composition parameters are $p_0=0.80$, $p_1=0.20$. Straight lines represent power law fits with exponents −0.770(21), −0.724(25), and −0.770(22) for $a=3$, 10, and 30, respectively.

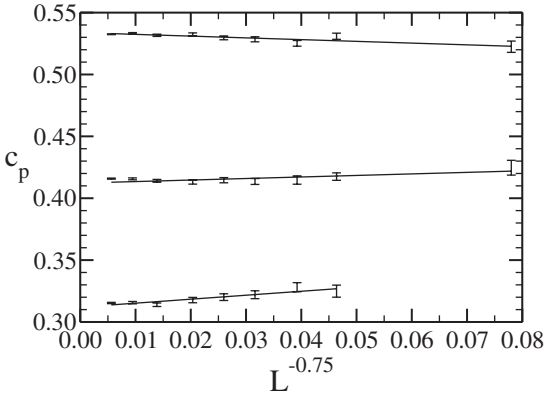

FIG. 3. Finite-size scaling of the square lattice threshold c_p against $L^{-1/\nu}$ for $\nu=4/3$, particles with $a=3$, 10, and 30, and lattice size $L=30,\ldots,1000$. The composition parameters are $p_0=0.80$, $p_1=0.20$.

III. DISCUSSION OF FINITE-SIZE SCALING

For percolation-type systems on finite lattices, it is known [1] that finite-size scaling theory describes correctly the dependence of the average threshold and its standard deviation on the size of the lattice L. In such systems one assumes that the probability Π that a lattice of linear size L percolates at concentration p has the form $\Pi(p,L)=\Phi[(p-p^*)L^{1/\nu}]$. The scaling function $\Phi(x)$ increases from 0 to 1 as its argument x increases from $-\infty$ to $+\infty$. Here p^* is the infinite (exact) percolation threshold (as $L\to\infty$) and the constant ν is the critical exponent (4/3 for simple site percolation in two-dimensional systems). It appears from the scaling theory that (a) the standard deviation σ of the threshold ($\sigma=\langle p^2\rangle-\langle p\rangle^2$) measured for a finite lattice L satisfies the power law

$$\sigma \propto L^{-1/\nu}, \tag{1}$$

and (b) the effective percolation threshold c_p (the mean value measured for a finite lattice) approaches the exact value p^* also via power law

$$c_p - p^* \propto L^{-1/\nu}. \tag{2}$$

To check the validity of relation (1) we collected data for various sizes of the particles ($a=3,\ldots,30$), various compositions ($p_1=0,0.2,0.4,0.7,0.9$), and square lattices of various sizes ($L=30$, 60, 75, 100, 130, 180, 300, 500, and 1000). Obviously, for long particles ($a\approx 30$) we omit the lattice size $L=30$ due to extremely high finite-size effects. For all data we obtained the confirmation of Eq. (1) with the value of the exponent $1/\nu$ ranging from 0.69 ± 0.02 to 0.77 ± 0.02. This coincides with the theoretical value for two-dimensional percolation $1/\nu=0.75$. A typical log-log plot of σ vs L is given in Fig. 2. Numerical points follow the power law within reasonable accuracy.

In the following we will analyze the percolation threshold c_p for $L=1000$ as a function of composition in more detail, but now we estimate the differences in the threshold value between the finite ($L=1000$) and infinite (exact) cases: $\Delta=|c_p(L=1000)-p^*|$. Plotting the mean value c_p of the threshold for various lattice sizes L against $L^{-1/\nu}$, we confirm the validity of the finite-size scaling in the system. From the plots we estimate the difference $\Delta\leq 0.004$ for all parameters, except for very long straight particles ($a\approx 30$ and $p_0\approx 1.00$), where $\Delta\leq 0.01$. An example of such a plot is given in Fig. 3. Our Δ stands here for the error we make taking thresholds for $L=1000$ instead of the exact ($L\to\infty$) value.

We can also ask about the statistical fluctuations and uncertainty for the chosen $L=1000$. We obtain the mean value of c_p in a series of $N=100$ simulations. The statistical error of the mean is $\sqrt{N}$ times smaller than the standard deviation σ. The numerical values of this error are well below 10^{-3} for all parameters of the model and do not exceed 2×10^{-4} for $L=1000$.

IV. RESULTS FOR SQUARE LATTICE

In the case of the square lattice we analyzed particles of sizes between 3 and 30. We skipped the case $a<3$ (monomers and dimers), as one cannot speak about the composition of such small particles. We chose the sampling step of p as 0.1, but additionally we considered a more refined grid for sufficiently small p_1, where the percolation threshold as a function of a composition changes more quickly (small p_1 implies $p_0\approx 1.0$, i.e., straight particles). The considered value of p_1 belongs to the set $\{0,0.01,0.02,\ldots,0,05,0.010,0.15,0.2,0.3,\ldots,1.0\}$ and the complement $p_0=1-p_1$. The percolation threshold c_p is shown in Fig. 4. For all lengths and compositions of the particles we plot the resulting percolation threshold (lines are guides for the eye only), obtaining a two-dimensional surface. The sections of this surface for constant values of the length a are the main point of interest in this work, since they show the composition dependence of the percolation threshold. Examples for some chosen lengths ($a=5$, 10, and 20) are shown in Fig. 5. It can be seen that the variation of composition dependence is larger for longer particles, while for the smallest ones ($a=3$) the threshold remains a nearly constant function. For all lengths, however, we observe a common qualitative behavior as p_1 increases from zero. For $p_1=0.0$ (thus $p_0=1-p_1=1.0$ and the particles form straight

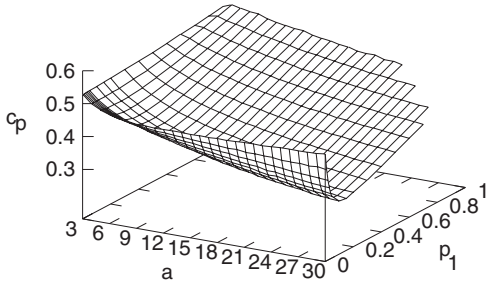

FIG. 4. Percolation threshold c_p as a function of the particle size a and its composition on a square lattice (p_1 is the relative amount of bendings of type $S1$). Here the size of the system $L=1000$. Lines are guides for the eye only.

needles) we have a local maximum; then the threshold sharply decreases as p_1 approaches a particular value of 0.15, for which we have a minimum. Then the function increases in a linear manner in the rest of the interval [0,1].

The fact that for higher values of p_1 the threshold is larger comes from the smaller diameters of such particles (to make up a percolating cluster one needs more particles, when they are more compact). In contrast, the straightest shapes (with $p_1 \approx 0.0$) do not mean the easiest way of making connections in the system (or the lowest value of the percolation threshold). This is because needlelike particles in the process of adsorption make domains of common alignment. When a linear particle is adsorbed close to another particle with the same orientation, they will be likely connected by other parallel particles. The density of a system composed of such domains is higher than for more flexible (bent) particles, where the particles have more possibilities of touching each other and the clusters have a sparser structure. It should be noticed that the changes of the threshold c_p are large in the vicinity of $p_1=0$. From the experimental point of view, this means that the system is very sensitive to small deviations from linearity of the particles (in the case of less straight particles, variation of their composition results in smaller changes of the percolation threshold).

With the two above-mentioned mechanisms of increasing the threshold for either small or large values of the parameter p_1, one expects a minimum at some intermediate value of p_1.

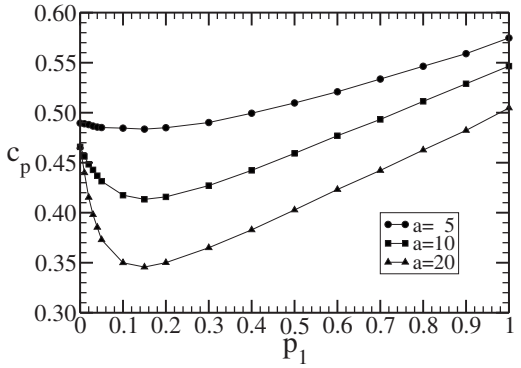

FIG. 5. Percolation threshold as a function of the particles' composition only. Each line represents a section of the surface of Fig. 4 for the given particle length (here $a=5$, 10, and 20). The size of the system $L=1000$. Lines are guides for the eye only.

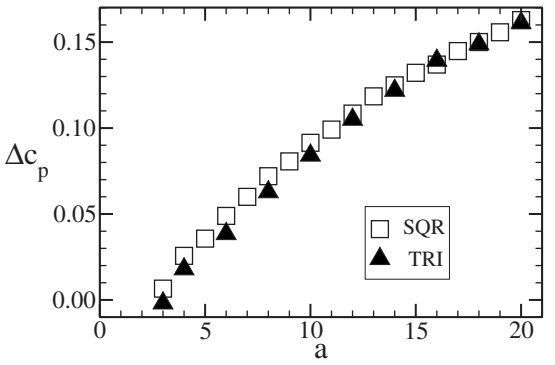

FIG. 6. Comparison of the relative height Δc_p of the maximum of the percolation threshold for linear particles as a function of the particle length a for two kinds of lattice: square (squares) and triangular (triangles). This height is measured against the reference level; see text for details. Uncertainties are smaller than the size of the symbols.

The localization of this minimum can in general depend on the size of the particles. We found, however, that it is not the case here—the value of $p_1=0.15$ is universal for particles of all sizes. That means that this specific composition ($p_0=0.85, p_1=0.15$) is the most favorable one for percolation on a square lattice. Unfortunately, a theoretical determination of that value is difficult and still needs further investigation.

We consider now the threshold $c_p(p_0,p_1)$ as a sum of a linear part (the main component) and a function with a peak around $p_1=0$ (the domain component). In particular, we measure the height of the peak of the latter in the following way. We take the difference Δc_p between the value of c_p obtained in simulations for $p_1=0$ and the linear dependence extrapolated to $p_1=0$ (we draw an extrapolation line through two points for $p_1=0.4$ and 0.7, since in that interval we have very well-pronounced linear behavior of c_p). The resulting height of the peak accounting for domains of parallel alignment is presented in Fig. 6. The results for the square lattice are plotted as squares. The triangles on the plot correspond to a similarly defined Δc_p on a triangular lattice; see the detailed discussion in Sec. VI. The uncertainties of the data shown are smaller than the size of the symbols.

V. NO-PERCOLATION REGIME

For large values of $p_1 \geq 0.8$ and for long particles ($a > 23$) there are problems in reaching percolation. For such compositions the particles are quite compact and connectivity between them is rather low. The interparticle space is narrow, so it is difficult to adsorb another big compact particle. Owing to the statistical algorithm used for generating the shape of the particles (each next bond is chosen according to probability), it is often possible to fill such a narrow-shaped space with a big particle; however, one needs an extremely large number of trials (very long expected values of adsorption times). In order to avoid waiting for practically infinite time to end a simulation, we introduced in our computer code a maximum number of allowed unsuccessful adsorption trials in a row. After reaching this limit a current run is qualified as "no-percolation" case and stopped. In Fig. 4

only such sets of parameters are taken into account, for which in all $N=100$ runs percolation was reached. For each series of simulations we introduce the quantity N^{NOP}, the ratio of the number of no-percolation cases to all cases in a series (N). For $L=1000$ we obtained $N^{\mathrm{NOP}}>0$ for $a=30$ ($p_1=0.8$), $a>26$ ($p_1=0.9$), and $a>23$ ($p_1=1.0$). The finite-size scaling of N^{NOP} done for $L=30,\ldots,1000$ divided the considered set of parameters (a, p_0, and p_1) into two categories: (a) those for which $N^{\mathrm{NOP}}\to 0.0$ as L increases, and (b) those for which $N^{\mathrm{NOP}}\to 1.0$ as L increases. In other words, the transient set of parameters for which neither $N^{\mathrm{NOP}}\neq 0$ nor $N^{\mathrm{NOP}}\neq 1$ is shrinking as we go to larger lattices. Thus the no-percolation characteristics can be attributed to the given particles' parameters (namely, their size and composition) rather than stemming from computational limitations and finite-size effects. A similar absence of percolation in adsorption models was reported in the study of adsorption of big squares on a lattice [50,51], where no percolation was found for the size of the squares $a>3$.

VI. RESULTS FOR TRIANGULAR LATTICE

We carried out the simulations also on the triangular lattice in order to check the universality of the studied dependencies. Indeed, the whole behavior is confirmed. The details of the triangular version of the simulations do not differ distinctly from the square case. Here we considered particles of size $a=3,\ldots,20$ and the substrate size L as large as 300. These values are smaller than those for the square case mainly due to the much larger computational costs of simulations on the triangular lattice. For example, the time for$N=100$ simulations for $(p_0,p_1)=(0.2,0.8)$ and $L=300$ was about 31 000 s (nearly 9 h), while for $(p_0,p_1,p_2)=(0.2,0.4,0.4)$ and the same values of L and N the simulations on the triangular lattice lasted 81 000 s (22.5 h).

The typical landscape of dependence of the percolation threshold on the composition is given in Fig. 7, where c_p is plotted against p_1 and p_2 (probabilities of bending types $T1$ and $T2$ of Fig. 1, respectively) for particles of size $a=10$. The three vertices of the plot, left, right, and rear, correspond to straight linear particles ($p_0=1$, $p_1=0$, and $p_2=0$), particles with bonds of type $T1$ ($p_0=0$, $p_1=1$, and $p_2=0$), and most bent particles with bonds of type $T2$ ($p_0=0$, $p_1=0$, and $p_2=1$), respectively. The arrows on the plot point to isolines of constant level of p_1 or p_2. It can be clearly seen that the behavior of the threshold is dominated by the linear part (flat surface), above which there is a peak around the leftmost vertex that corresponds to the linear straight particles.

Finite-size scaling was checked also for these data and we obtain confirmation of Eq. (1) with the value of the exponent $1/\nu$ ranging from 0.68 to 0.81 with errors ≤ 0.05. Again this coincides with the theoretical value for two-dimensional percolation, $1/\nu=0.75$. As before, we estimate the difference in the threshold value between the finite ($L=300$) and infinite (exact) cases: $\Delta=|c_p(L=300)-p^*|$. From the plots of the mean value c_p of the threshold against $L^{-1/\nu}$, we obtained the difference $\Delta\leq 0.004$ for all parameters, except for long straight particles ($a=20$ and $p_0\approx 1.00$), where $\Delta\leq 0.012$. Again the value of Δ is considered as giving the accuracy of Fig. 7.

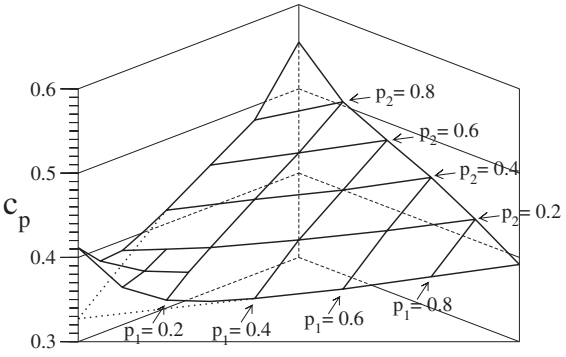

FIG. 7. Percolation threshold c_p on the triangular lattice for particles of length $a=10$ as a function of their composition (p_1,p_2). The arrows point to isolines of constant level of p_1 or p_2. The leftmost vertex (with $c_p\approx 0.41$) corresponds to strictly linear particles $(p_0,p_1,p_2)=(1,0,0)$; the rightmost one with $c_p\approx 0.39$ corresponds to particles made of $T1$-type bending only [composition (0,1,0)] while the rear one describes the most compact case of $c_p\approx 0.55$ and composition (0,0,1). The dotted lines approaching the value $c_p\approx 0.33$ represent the reference level, from which the height Δc_p of the peak is measured (see more details in the text).

We now determine the height of the peak rising above the plane of Fig. 7, as it is a measure of deviation from linear behavior for straight particles. We took three representative points on the flat (linear) part of the plot, $(p_0,p_1,p_2)=(0.6,0.4,0.0)$, (0.6,0.0,0.4), and (0.2,0.4,0.4), and we extrapolate this plane to the composition of linear particles (1.0,0.0,0.0) (see the dotted lines on Fig. 7). The height of that peak, Δc_p, is plotted on Fig. 6 with triangles. One can see that the data for square and triangular lattices coincide. Here the error bars do not exceed the size of the symbols.

The most favorable composition (for which the percolation threshold acquires its minimal value) is located for all particle sizes at $p_2=0$ and p_1 between 0.2 and 0.3 (thus p_0 lies between 0.7 and 0.8). The more exact estimation of that point needs further study, however.

On the triangular lattice there are also simulations where no percolation was reached (see more detailed discussion of this effect in Sec. V). For relatively small particles ($a<14$), we arrive at percolation at every run for all compositions (p_0,p_1,p_2). When we consider larger particles, more bent shapes cease to percolate while straight ones still form percolating clusters. Here the value of the percentage p_2 of most bent segments is crucial. For example, percolating particles for the most bent shape $(p_0=0,p_1=0,p_2=1)$ have the maximum size $a=13$, for lower p_2 $(p_0=0,p_1=0.4,p_2=0.6)$ the maximum size is $a=22$, but for $p_2=0$ all considered particles (up to $a=30$) percolate. The exact finite-size scaling of N^{NOP} in the triangular case was not done, however, due to very long times of simulations for high values of lattice size L and particle size a.

VII. CLUSTER STRUCTURE ANALYSIS

In order to verify the possibility of correlation between the percolation threshold and some single-particle characteristics, we checked also how the composition of the particles

affects the mean square radius of gyration and the mean end-to-end distance. It turned out that there is no sharp transition for any composition of a single particle, so the appearance of different regimes of percolation (high value of the threshold for almost straight particles, no percolation for very compact particles, mild linear dependence for the other cases) can be attributed only to collective interaction of the particles.

On the other hand, the composition of the particles influences the structure of the percolating cluster. We investigated this relation further and looked at the percentage of sites having a given number of neighbors. We found a strong correlation between the relative number of sites with exactly two neighbors (for the square lattice) and the percolation threshold. For the linear part (away from the peak for $p_0 \geq 0.8$ and no-percolation regime) the equation $c_p = 0.897(1 - R_2)$ is satisfied within an accuracy of 0.03. The quantity R_2 is defined as the mean ratio of a number of adsorbed sites with exactly two neighbors to the total adsorbed number of sites (monomers of the particles) at percolation, averaged over N simulation runs. The collected data (for $p_0 \in [0.1, 0.8]$ in the square case) as well as the linear relation postulated above are presented in Fig. 8. The statistical errors of the points are of order $\sigma(R_2) \leq 0.02$ and $\sigma(c_p) \leq 0.015$. All data presented in Fig. 8 are obtained for lattice size $L = 300$.

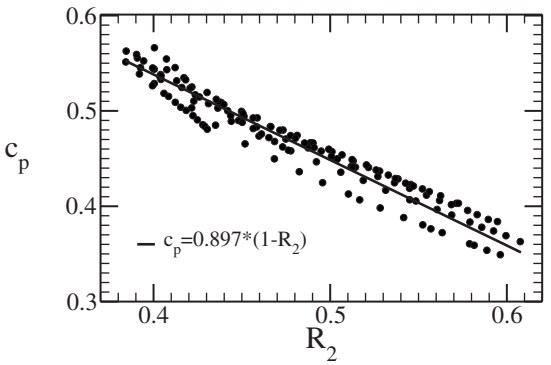

FIG. 8. Correlation between the percolation threshold c_p and the percentage R_2 of monomers with exactly two nearest neighbors at percolation for various compositions ($p_1 = 0.2, \ldots, 0.9$) and sizes ($a = 3, \ldots, 20$) of the particles (for the square lattice). The line $c_p = 0.897(1 - R_2)$ is also shown. Statistical errors are smaller than 0.015 for c_p and smaller than 0.02 for R_2.

VIII. CONCLUSIONS

We analyzed the random sequential adsorption of extended particles with a given size and composition of the shape on square and triangular lattices. The shape variables on the square lattice p_0, p_1 (defined as the percentage of a given kind of bending in a chain) influence the percolation threshold c_p in such a way that one can look at the whole landscape of the function $c_p(p_0, p_1)$ as a sum of a mildly linear part for $p_1 \geq 0.4$ and sharp peak around $p_1 = 0$. The overall behavior of the threshold c_p is common on both lattices considered. In particular, the height of the peak as a function of the particle size coincides for both cases.

A linear correlation between the percolation threshold and cluster structure (more precisely, the relative amount of monomers with exactly two neighbors at percolation) was observed for particles with $0.2 \leq p_1 \leq 0.9$ (on a square lattice).

[1] D. Stauffer and A. Aharony, *Introduction to Percolation Theory* (Taylor & Francis, London, 1994).
[2] S. R. Broadbent and J. M. Hammersley, Proc. Cambridge Philos. Soc. **53**, 629 (1957).
[3] M. B. Isichenko, Rev. Mod. Phys. **64**, 961 (1992).
[4] F. Carmona, P. Prudhon, and F. Barreau, Solid State Commun. **51**, 255 (1984).
[5] A. Bunde, W. Dieterich, and E. Roman, Phys. Rev. Lett. **55**, 5 (1985).
[6] P. C. Robinson, J. Phys. A **16**, 605 (1983).
[7] P. J. Flory, J. Am. Chem. Soc. **61**, 1518 (1939).
[8] M. D. Khandkar, A. V. Limaye, and S. B. Ogale, Phys. Rev. Lett. **84**, 570 (2000).
[9] R. S. Ghaskadvi and M. Dennin, Phys. Rev. E **61**, 1232 (2000).
[10] B. Bonnier, Phys. Rev. E **54**, 974 (1996).
[11] J.-S. Wang and R. B. Pandey, Phys. Rev. Lett. **77**, 1773 (1996).
[12] A. Matsuyama, R. Kishimoto, and T. Kato, J. Chem. Phys. **106**, 6744 (1997).
[13] C. K. Gan and J.-S. Wang, J. Chem. Phys. **108**, 3010 (1998).
[14] A. C. Balazs and I. R. Epstein, Biopolymers **23**, 1249 (1984).
[15] A. Cordoba and J. J. Luque, Phys. Rev. B **31**, 8111 (1985).
[16] V. Privman, H. L. Frish, N. Ryde, and E. Matijvec, J. Chem. Soc., Faraday Trans. **87**, 1371 (1991).
[17] Z. Adamczyk, T. Babros, J. Czarnecki, and T. G. M. van de Ven, Adv. Colloid Interface Sci. **19**, 183 (1983).
[18] L. Finegold and J. T. Donnell, Nature (London) **278**, 443 (1979).
[19] J. W. Evans, D. E. Sanders, P. A. Thiel, and A. E. DePristo, Phys. Rev. B **41**, 5410 (1990).
[20] J. Fransaer, Ph.D. thesis, Katholieke Universiteit Leuven, 1994.
[21] N. Provatas, M. Haataja, E. Seppälä, S. Majaniemi, J. Åström, M. Alava, and T. Ala-Nissila, J. Stat. Phys. **87**, 385 (1997).
[22] K. Trojan and M. Ausloos, Physica A **351**, 332 (2005).
[23] L. Zhang and P. R. Van Tassel, J. Chem. Phys. **112**, 3006 (2000).
[24] M. Hasegawa and M. Tanemura, in *Recent Developements in Statistical Inference and Data Analysis*, edited by K. Matusita (North-Holland, Amsterdam, 1980).
[25] Y. Itoh, J. Appl. Probab. **17**, 134 (1980).
[26] N. Provatas, M. Haataja, J. Asikainen, S. Majaniemi, M. Alva, and T. Ala-Nissila, Colloids Surf., A **165**, 209 (2000).
[27] J. W. Evans, Rev. Mod. Phys. **65**, 1281 (1993).
[28] J. Talbot, G. Tarjus, P. R. Van Tassel, and P. Viot, Colloids Surf., A **165**, 287 (2000).
[29] P. B. Shelke, A. G. Banpurkar, S. B. Ogale, and A. V. Limaye,

Surf. Sci. **601**, 274 (2007).
[30] A. E. Bea, I. M. Irurzun, and E. E. Mola, Phys. Rev. E **73**, 051604 (2006).
[31] E. S. Loscar, R. A. Borzi, and E. V. Albano, Phys. Rev. E **68**, 041106 (2003).
[32] I. Lončarević, Lj. Budinski-Petković, and S. B. Vrhovac, Eur. Phys. J. E **24**, 19 (2007).
[33] A. Cadilhe, N. A. M. Araújo, and V. Privman, J. Phys.: Condens. Matter **19**, 065124 (2007).
[34] Y. Wu, B. Schmittmann, and R. K. P. Zia, J. Phys. A **41**, 025004 (2008).
[35] V. Cornette, A. J. Ramirez-Pastor, and F. Nieto, Physica A **327**, 71 (2003).
[36] V. Cornette, A. J. Ramirez-Pastor, and F. Nieto, Eur. Phys. J. B **36**, 391 (2003).
[37] G. Kondrat, J. Chem. Phys. **122**, 184718 (2005).
[38] G. Kondrat, J. Chem. Phys. **124**, 054713 (2006).
[39] V. Cornette, A. J. Ramirez-Pastor, and F. Nieto, J. Chem. Phys. **125**, 204702 (2006).
[40] M. Dolz, F. Nieto, and A. J. Ramirez-Pastor, Eur. Phys. J. B **43**, 363 (2005).
[41] M. Quintana, I. Kornhauser, R. López, A. J. Ramirez-Pastor, and G. Zgrablich, Physica A **361**, 195 (2006).
[42] F. Rampf and E. V. Albano, Phys. Rev. E **66**, 061106 (2002).
[43] E. S. Loscar, R. A. Borzi, and E. V. Albano, Phys. Rev. E **74**, 051601 (2006).
[44] M. C. Gimenez, F. Nieto, and A. J. Ramirez-Pastor, J. Chem. Phys. **125**, 184707 (2006).
[45] N. I. Lebovka, N. V. Vygornitskii, and A. V. Palikhov, J. Mol. Liq. **127**, 93 (2006).
[46] M. Gopalakrishnan, B. Schmittman, and R. K. P. Zia, J. Phys. A **37**, L337 (2004).
[47] T. K. H. Starke, C. Johnston, and P. S. Grant, Scr. Mater. **56**, 425 (2007).
[48] G. Kondrat, J. Chem. Phys. **117**, 6662 (2002).
[49] F. Yonezawa, S. Sakamoto, and M. Hori, Phys. Rev. B **40**, 636 (1989).
[50] M. Nakamura, Phys. Rev. A **36**, 2384 (1987).
[51] M. Porto and H. E. Roman, Phys. Rev. E **62**, 100 (2000).